MASS SPECTROMETRY-BASED ANALYSIS OF THE HLA-LIGANDOMES OF RENAL CELL CARCINOMA AND BENIGN RENAL TISSUE

MASSENSPEKTROMETRISCHE ANALYSE DER HLA-LIGANDOME DES NIERENZELLKARZINOMS UND DES BENIGNEN NIERENGEWEBES

DISSERTATION

DER MATHEMATISCH-NATURWISSENSCHAFTLICHEN FAKULTÄT
DER EBERHARD KARLS UNIVERSITÄT TÜBINGEN
ZUR ERLANGUNG DES AKADEMISCHEN GRADES EINES
DOKTORS DER NATURWISSENSCHAFTEN
(DR. RER. NAT.)

VORGELEGT VON
DIPL. BIOL. ARMIN RABSTEYN
AUS STUTTGART

TÜBINGEN
2018

Gedruckt mit Genehmigung der Mathematisch-Naturwissenschaftlichen Fakultät der Eberhard Karls Universität Tübingen.

Tag der mündlichen Qualifikation:	28.03.2018
Dekan:	Prof. Dr. Wolfgang Rosenstiel
1. Berichterstatter:	Prof. Dr. Stefan Stevanović
2. Berichterstatter:	Prof. Dr. Hans-Georg Rammensee

Die vorliegende Dissertation wurde unter der Leitung von

Herrn Prof. Dr. Stefan Stevanović

In der Zeit von November 2011 bis März 2015 am Interfakultären Institut für Zellbiologie, in der Abteilung Immunologie der Eberhard-Karls-Universität Tübingen durchgeführt.

Ich versichere, dass ich die Dissertation selbstständig und ohne unerlaubte Hilfsmittel angefertigt habe. Von anderen Personen übernommene Daten oder durchgeführte Arbeiten sind als solche gekennzeichnet.

Tübingen, den 10.04.2018 Armin Rabsteyn

Abstract

Peptide vaccination is a promising immunotherapeutic approach for the treatment of malignancies. In this project, the unique opportunity to analyze HLA ligandomes of samples from tumor and adjacent benign tissue of renal cell carcinoma (RCC) patients by mass spectrometry was given. This allowed for the establishment of a novel approach of antigen definition by comparative profiling of malignant and benign HLA ligandomes. Analyses were performed for HLA class I and II of tumor and benign tissue sample pairs in a cohort of 33 RCC patients. Altogether, the acquired dataset includes 35.543 unique HLA class I ligand identifications derived from 11.279 unique source proteins and 8.344 unique HLA class II ligand identifications derived from 2.199 unique source proteins. Comparative analysis revealed a new class of tumor antigens based on tumor-exclusive representation of HLA ligand source proteins, termed ligandome-derived tumor-associated antigens (LiTAAs). A selection of LiTAA-derived HLA ligands (ligandome-derived tumor-associated peptides, LiTAPs) were tested for immunogenicity in high-throughput priming experiments using artificial antigen-presenting cells (aAPCs). Immunogenic LiTAPs will eventually provide a 'warehouse' of suitable vaccination peptides and allow for a personalized vaccination approach based on individual HLA typing and actual target expression on tumor cells. Furthermore, analysis of healthy (benign) tissue HLA ligandomes is a step towards a comprehensive map of the healthy human immunopeptidome, an important prerequisite for the definition of tumor-specific immunotherapy targets.

In a second project, naturally presented HLA ligands derived from *mycobacterium tuberculosis* (*Mtb*) were identified by infection experiments. HLA ligands derived from *Mtb* antigens encoded in a viral vector could be identified, whereas analysis of macrophages infected with live *Mtb* did not reveal any new *Mtb*-derived HLA ligands. Such HLA ligands may provide the basis for the design of more efficient subunit vaccines against tuberculosis as well as development of enhanced infection screening assays.

Zusammenfassung

Die Peptidimpfung ist ein vielversprechender immuntherapeutischer Ansatz für die Behandlung maligner Erkrankungen. In diesem Projekt bestand die einmalige Möglichkeit, die HLA-Ligandome von Proben aus Tumor und benignem Gewebe am Nierenzellkarzinom erkrankter Patienten massenspektrometrisch zu analysieren. So konnte ein neuer Ansatz zur Antigendefinition durch vergleichende Analyse maligner und benigner HLA-Ligandome entwickelt werden. Die Analysen wurden für HLA Klasse I und II in Probenpaaren von Tumor und benignem Gewebe einer Kohorte von 33 Nierenzellkarzinom-Patienten durchgeführt. Insgesamt umfasst der erhaltene Datensatz 35.543 identifizierte unterschiedliche HLA Klasse I-Liganden die 11.279 verschiedenen Quellproteinen entstammen, sowie 8.344 unterschiedliche HLA Klasse II-Liganden, die 2.199 verschiedenen Quellproteinen entstammen. Die vergleichende Analyse offenbarte eine neue Klasse von Tumorantigenen, basierend auf einer Tumor-exklusiven Repräsentation der Quellproteine der HLA-Liganden, genannt Ligandom-abgeleitete Tumor-assoziierte Antigene (LiTAAs). Eine Auswahl von LiTAA-entstammenden HLA-Liganden (Ligandom-abgeleitete Tumor-assoziierte Peptide, LiTAPs) wurden auf ihre Immunogenität in hochdurchsatz-*priming* Experimenten mit künstlichen antigenpräsentierenden Zellen (aAPCs) untersucht. Immunogene LiTAPs werden letztendlich eine ‚Lagerhalle' mit geeigneten Impfpeptiden bilden und eine personalisierte Impfung basierend auf HLA-Typisierung und tatsächlicher Expression der Zielstrukturen auf Tumorzellen ermöglichen. Weiterhin ist die Analyse gesunder (benigner) HLA-Ligandome ein Schritt Richtung einer umfassenden Karte des gesunden humanen Immunpeptidoms, eine wichtige Voraussetzung für die Definition tumorspezifischer immuntherapeutischer Zielstrukturen.

In einem zweiten Projekt wurden natürlich präsentierte HLA-Liganden aus *Mycobacterium tuberculosis* (*Mtb*) in Infektionsexperimenten identifiziert. HLA-Liganden aus in einem viralen Vektor codierten *Mtb*-Antigenen konnten identifiziert werden, während die Analyse mit lebenden *Mtb* infizierter Makrophagen keine neuen HLA-Liganden aus *Mtb* ergab. Solche HLA-Liganden können sowohl die Basis für das Design effizienterer *subunit*-Impfungen gegen Tuberkulose als auch für die Entwicklung verbesserter Infektions-Überprüfungen bilden.

Table of contents

Abbreviations

AICD	Activation induced cell death
AC	Alternating current
ADCC	Antibody dependent cellular cytotoxicity
AIRE	Autoimmune regulator
APC	Antigen presenting cell
aAPC	Artificial antigen presenting cell
BCG	Bacillus Calmette-Guérin
BCR	B cell receptor
B-LCL	B-lymphoblastoid cell line
BSA	Bovine serum albumin
β-ME	β-mercaptoethanol
β_2m	β_2 microglobulin
CAR	Chimeric antigen receptor
ccRCC	Clear cell renal cell carcinoma
CDR	Complementary determining region
CID	Collision-induced dissociation
CLIP	Class II-associated invariant chain peptide
CRM	Charged residue model
CTL	Cytotoxic T-lymphocyte
CTLA-4	Cytotoxic T-lymphocyte antigen 4
Da	Dalton
DAMP	Danger-associated molecular pattern
DC	Dendritic cell
DC	Direct current
DDA	Data-dependent acquisition
DMSO	Dimethyl sulfoxide
DRIP	Defective ribosomal product
EBV	Epstein-Barr virus
EDTA	Ethylenediaminetetraacetic acid
ER	Endoplasmatic reticulum
ERAAP	Endoplasmatic reticulum aminopeptidase associated with antigen processing
ESI	Electrospray ionization
FACS	Fluorescence activated cell sorting
FCS	Fetal calf serum
FDR	False discovery rate
FOXP3	Forkhead box P3

FPKM	Fragments per kilobase per million reads
FPR	Formyl peptide receptor
FSC	Forward scatter
GM-CSF	Granulocyte-macrophage colony-stimulating factor
GvHD	Graft-versus-host disease
GvL	Graft-versus-leukemia
HBV	Hepatitis B virus
HCl	Hydrochloric acid
HCV	Hepatitis C virus
HEPES	2-(4-(2-hydroxyethyl)-1-piperazineethanesulfonic acid
HLA	Human leukocyte antigen
HPLC	High performance liquid chromatography
HPV	Human papilloma virus
HSA	Human serum albumin
HSCT	Hematopoietic stem cell transplantation
ICAM-1	Intercellular adhesion molecule 1
IDO	Indolamine-2,3-dioxygenase
IEM	Ion evaporation model
IFN-α	Interferon α
IFN-γ	Interferon γ
ILC	Innate lymphoid cell
IL-10	Interleukin 10
IL-12	Interleukin 12
IL-13	Interleukin 13
IL-17	Interleukin 17
IL-2	Interleukin 2
IL-21	Interleukin 21
IL-22	Interleukin 22
IL-4	Interleukin 4
IL-5	Interleukin 5
IL-6	Interleukin 6
IL-7	Interleukin 7
IMDM	Icove’s Mofified Dulbecco’s Medium
ITAM	Immunoreceptor tyrosine-based activation motif
kDa	Kilodalton
LC-MS/MS	Liquid chromatography-coupled tandem mass spectrometry
LFA-1	Lymphocyte function-associated antigen 1
LFQ	Label-free quantification
li	Invariant chain / CD74
LTQ	Linear ion trap

MACS	Magnetic activated cell sorting
MDM	Monocyte-derived macrophage
MDR-TB	Multi-drug-resistant tuberculosis
MDSC	Myeloid-derived suppressor cell
mHA	Minor histocompatibility antigen
MHC	Major histocompatibility complex
MOI	Multiplicity of infection
mRCC	Metastatic renal cell carcinoma
mRNA	Messenger ribonucleic acid
MS	Mass spectrometry
Mtb	Mycobacterium tuberculosis
mTOR	Mammalian target of rapamycin
MVA	Modified vaccinia Ankara
MIIC	MHC II loading complex
NK cell	Natural killer cell
PAMP	Pathogen-associated molecular pattern
PAP	Prostatic acid phosphatase
PBMC	Peripheral blood mononuclear cell
PBS	Phosphate buffered saline
PD-1	Programmed cell death protein 1
PD-2	Programmed cell death protein 2
PE	Phycoerythrin
PEG	Polyethylene glycol
PerCP	Peridinin-chlorophyll-protein complex
PLC	Peptide loading complex
PMEL	Premelanosome protein
PMSF	Phenylmethylsulfonylfluoride
PPG	Polypropylene glycol
ppm	Parts per million
PRR	Pattern recognition receptor
PSM	Peptide spectrum match
RAG	Recombination activating gene
RCC	Renal cell carcinoma
RSS	Recombination signal sequence
SAPE	Streptavidine-conjugated phycoerythrin
scFv	Single-chain variable fragment
SSC	Side scatter
TAA	Tumor-associated antigen
TAP	Transporter associated with antigen processing
TB	Tuberculosis

TBS	Tris buffered saline
TCM	T cell medium
TCR	T cell receptor
TdT	Terminal deoxynucleotidyl transferase
TGF-β	Transforming growth factor β
TFA	Trifluoroacetic acid
T_{fh} cell	Follicular T helper cell
T_h cell	T helper cell
TIL	Tumor-infiltrating lymphocyte
TKI	Tyrosine kinase inhibitor
TLR	Toll-like receptor
TNF-α	Tumor necrosis factor α
TNF-β	Tumor necrosis factor β
T_{reg} cell	Regulatory T cell
TSA	Tumor-specific antigen
TSB	Tetramer staining buffer
uHPLC	Ultra high performance liquid chromatography
VCAM-1	Vascular cell adhesion protein 1
VEGF	Vascular endothelial growth factor
VLA-4	Integrin α4β1
XDR-TB	Extensively drug-resistant tuberculosis

Tables

Figures

1 Introduction

1.1 The immune system

The immune system has evolved as a protection mechanism of organisms against the invasion by other organisms. It is therefore in general a system of discrimination of ‘self’ and ‘non-self’ components within an organism. The evolution of complex life itself is thought to have been dependent on such invasion events. Eukaryotic cells probably evolved by symbiogenesis of unicellular prokaryotes. Cell organelles of eukaryotic cells such as mitochondria or chloroplasts are most likely of bacterial origin [1]. However, the evolution of multicellular eukaryotic organisms was dependent on the ability to exclude external organisms from their interior life. In the course of evolution of complex life, a multitude of mechanisms have evolved to achieve distinction of ‘self’ and ‘non-self’. These range from simple physical barriers, enzymes, enzyme cascades and proteins to highly sophisticated immune cells. In higher organisms, the immune system constitutes the defense against a whole array of invasive organisms called pathogens, involving many bacteria, viruses, fungi and parasites. The immune system’s task is to recognize pathogens as extrinsic intruders and clear them from the host organism. To accomplish this duty, two distinct systems have developed. The innate immune system is evolutionarily older and is present in all plants and animals. Innate immune responses are immediate and strong however they rely on the detection of conserved danger signals and are therefore rather unspecific. The adaptive immune system has developed later and can only be found in jawed vertebrates. Adaptive immune responses are delayed, but highly specific and establish an immunological memory to a particular pathogen after its clearance. The activation and induction of adaptive responses depends on the interplay with innate immunity.

1.1.1 The human innate immune system

The innate immune system is the first line of defense of the human body against infections. It is a compendium of physical, biological and chemical barriers as well as humoral and cellular defense mechanisms. All contact surfaces of the human body with

the environment constitute barriers. The largest surface is the skin, being not only a physical barrier but also a biological and chemical one: intruding pathogens are repelled by the stratum corneum and the epidermis [2]. Colonialization of pathogens is further aggravated by commensal bacteria. Those commensals compete with pathogens for space and nutrients and furthermore metabolize lipids to fatty acids. The resulting acidic pH value of the skin is hostile to many pathogens [3]. Additionally, the skin can produce and secrete antimicrobial peptides like β-defensins [4]. These basic mechanisms are also present at the more vulnerable barriers like intestine, genitourinary tract and lungs. Furthermore, antimicrobial enzymes like lysozyme can be secreted in bodily fluids [5].

In case pathogens manage to breach these barriers, the body reacts with inflammation. Infected cells and immune cells can recognize pathogens by detection of unique molecular structures. These molecules are referred to as pathogen-associated molecular patterns (PAMPs). PAMPs are widely conserved between groups of microorganisms and therefore represent a distinguishing feature for the immune system. The molecular patterns range from bacterial cell wall components such as peptidoglycan, lipopolysaccharides and flagellins to viral nucleic acids [6].

PAMPs are recognized by pattern recognition receptors (PRRs). These receptors can be expressed intracellularly as well as on the cell surface. The most prominent representatives of PRRs are the toll-like receptors (TLRs), which were originally discovered in *drosophila* [7] and later shown to play a role in the activation of the immune system in *drosophila* [8] and in humans [9]. Upon recognition of a cognate ligand, signaling cascades, mainly the NF-κB and AP-1 pathways are induced to promote expression of inflammatory genes like pro-inflammatory cytokines and type I interferons. The initial local inflammation reaction has several purposes: the release of prostaglandins permeabilizes blood vessels to facilitate extravasation of immune cells into the surrounding tissue. Additionally, leukotrienes and chemokines exert attractant effects on leukocytes. These leukocytes represent the cellular defense of the innate immune system. It consists of cells from the myeloid lineage like eosinophils, basophils, mast cells and specialized phagocytes like monocytes, macrophages, dendritic cells (DCs) and neutrophils. Natural killer cells (NK cells) and innate lymphoid cells (ILCs) are cells of the lymphoid lineage and complement the innate cellular defense. While most innate immune mechanisms rely on direct recognition and elimination of pathogens, NK cells can

detect and kill infected cells. The activation and triggering of NK cells is controlled by a delicate balance of activating and inhibitory signals [10, 11]. Of note, the strongest inhibitory signal for NK cells is the surface expression of MHC molecules on target cells. MHC expression is altered in some viral and bacterial infections and in certain tumors, whereby NK cell inhibition gets attenuated enabling the recognition and lysis of target cells [12]. A second cytotoxic feature of NK cells is antibody-dependent cellular cytotoxicity (ADCC). Antibody-marked cells are recognized by binding of the Fc-part of antibodies to the activating Fc-Receptor CD16 on NK cells and thereby mediate cytotoxicity [13].

While NK cells serve as direct cytotoxic killers of infected cells, phagocytes recognize free pathogens, particles and cell debris. Several modes of recognition of pathogens have been described for phagocytes: first, conventional receptor-ligand interactions via formyl-peptide receptors (FPRs) [14] or TLRs can direct phagocytes to pathogens by chemotaxis and induce an activated phenotype. Second, pathogens can be opsonized for phagocytosis by complement proteins or antibodies. Binding of these immune complexes to complement receptors and Fc receptors expressed on phagocytes induces phagocytosis [15]. The resulting phagosomes or endosomes merge with lysosomes within the cell, thereby destroying the contained pathogens by acidification, enzymatic digestion and reactive oxygen species (respiratory burst) [16, 17]. Furthermore, phagocytes are responsible for the clearance of dead host cells and cell debris.

While neutrophils are the most prominent representatives and mainly have scavenging function in the circulation, macrophages and dendritic cells are highly specialized phagocytes with important additional features. These cells express an array of PRRs and other receptors for sensing of pathogens and danger signals [18]. They orchestrate the initial immune response by amplification of danger signals and represent the interface between innate and adaptive immune response [19]. These cells are therefore termed antigen-presenting cells (APCs). They have the ability to process antigens and (cross-) present peptides in the context of MHC on the cell surface. Upon activation by recognition of pathogen- or danger-associated molecular patterns (PAMPs or DAMPs), especially DCs become highly efficient in priming of naïve T cells [20]. The activation leads to increased antigen processing properties, as well as to the expression of costimulatory molecules and cytokines necessary for efficient T cell priming.

1.1.2 The human adaptive immune system

In contrast to the innate immune system with its reliance on germline encoded receptors and recognition of conserved pathogenic structures, adaptive immune responses are antigen-specific and develop within the course of an infection. Adaptive immunity is constituted of two major components, a humoral and a cellular response. The humoral response is mediated by antibody-producing B cells, while the cellular response is mediated by T cells. Both cell types belong to the lymphoid line and originate from hematopoietic stem cells. The induction of adaptive immune responses is always dependent on precedent innate immune responses. Hence, adaptive responses are delayed in comparison to immediate innate responses. In the course of an infection, antigens are taken up by APCs and these cells become activated and mature. They migrate from peripheral tissues to lymphoid organs where they present antigenic peptides in the context of MHC to T cells. This process of priming of naïve T cells involves three major signals: First, the T cell needs to express a cognate T cell receptor (TCR) for the respective MHC:peptide complex [21]. Second, a costimulatory signal is necessary. This is provided by the expression of CD80 and CD86 on activated APCs and the interaction of these molecules with CD28 on the T cell [22]. Of note, a lack of the co-stimulus leads to T cell anergy [23]. Third, activated APCs produce an array of cytokines that can bind to respective receptors on the T cell. The most important one for general priming of T cells seems to be interleukin 12 (IL-12) [24]. For CD8+ T cells, the priming process results in differentiation into mature cytotoxic T lymphocytes (CTL), whereas for CD4+ T cells the situation is more complex. CD4+ T cells can differentiate into several subsets of T helper cells (T_h cells) and the composition of APC-derived cytokines during priming seems to influence this [25]. There are at least three types of T_h cells and regulatory T cells (T_{reg}):

- **T_h1 cells** are polarized mainly by IL-12 and promote cell-mediated immunity against intracellular pathogens via the effector cytokines interleukin 2 (IL-2), interferon γ (IFN-γ), CD154 and tumor necrosis factor α (TNF-α) [26, 27].

- **T_h2 cells** are polarized mainly by interleukin 4 (IL-4) and promote humoral immunity against extracellular parasites, pathogens and toxins via the effector cytokines IL-4, interleukin 5 (IL-5) and interleukin 13 (IL-13) [26, 28, 29].

- **T_h17 cells** are polarized by transforming growth factor β (TGF-β) and interleukin 6 (IL-6) and promote cell-mediated inflammation against extracellular pathogens and fungi via interleukin 17 (IL-17) and interleukin 22 (IL-22). They might also play a role in autoimmune diseases [30].

- **T_{reg} cells** are polarized by TGF-β and promote regulation of immune responses in the periphery via TGF-β and interleukin 10 (IL-10). They are further characterized by the expression of the transcription factor forkhead box p3 (FOXP3) [31]. T_{reg} cells have immunosuppressive capabilities and maintain pheripheral tolerance to avoid autoimmune reactions [32].

After initial priming, T cells become highly activated, produce and secrete large amounts of IL-2 and additionally express the α-chain of the IL-2 receptor. Together with the constitutively expressed β- and γ-chain, the receptor becomes highly affine for the cytokine. Signaling of the IL-2 receptor triggers the entry of T cells into the cell cycle, promoting massive clonal expansion of the primed T cell. Clonal expansion produces huge amounts of T cells with identical TCRs which differentiate to effector cells within several days. Mature effector T cells can exert their functions upon recognition of their cognate antigen without co-stimulation.

The function of CD8+ CTLs is detection and lysis of infected cells. CTLs express an altered array of adhesion molecules guiding them to activated endothelial cells at inflammation sites. Interaction of lymphocyte function-associated antigen 1 (LFA-1) and integrin α4β1 (VLA-4) on CTLs with their respective ligands intercellular adhesion molecule 1 (ICAM-1) and vascular cell adhesion protein 1 (VCAM-1) on activated endothelium promotes extravasation of CTLs at inflammation sites. The same interaction of these unspecific adhesion molecules mediates contact of CTLs with target cells. This interaction is strengthened if the TCR of the CTL binds to its cognate MHC:peptide complex on the target cell. An immunological synapse forms at the contact area of effector and target cell with TCRs, co-receptors and MHC:peptide complexes clustering in the center and adhesion molecules in the periphery [33]. Aggregation of TCRs leads to activation of signaling pathways that polarize the CTL towards the target cell by reorganization of the cytoskeleton. The effector molecules granzyme B and perforin are stored in cytotoxic granules of the CTL and released specifically at the immunological synapse to take effect

on the target cell. Perforin binds to the plasma membrane of target cells and oligomerizes by establishment of disulfide bonds to form a pore [34] through which the pro-apoptotic serine protease granzyme B can enter the target cell. Granzyme B unleashes programmed cell death by activation of caspase cascades [35]. Additionally, CTLs can induce apoptosis by expression of CD95L (Fas ligand) and engagement of CD95 (Fas receptor) on target cells [36]. Apart from these direct mechanisms, CTLs are able to release cytokines after antigen encounter: members of the tumor necrosis factor (TNF) superfamily like TNF-α and TNF-β can elicit apoptosis in TNF receptor-expressing target cells [37]. IFN-γ has anti-viral properties, induces upregulation of MHC expression and can activate other immune cells like macrophages and NK cells [38]. A distinct subset of cytotoxic CD4+ CTLs has also been reported [39].

The function of CD4+ T_h cells differs from that of CD8+ CTLs as described above. While some subtypes leave the lymphatic tissue after priming to exert their effector function, others remain within those tissues. The TCR of CD4+ T cells recognizes peptides in the context of MHC class II, which is mainly present on APCs. T_h1 cells have three major functions: first, they can activate macrophages in the periphery by secretion of IFN-γ and members of the TNF family [40]. Macrophages that have taken up pathogens or are infected need activation by T_h1 cells to enhance their ability to neutralize intracellular pathogens by production of reactive oxygen species. In some cases, T_h1 cells provide granulocyte-macrophage colony-stimulating factor (GM-CSF) which can induce differentiation of macrophages into DCs. The second function is to provide help for T cell priming. A lack of sufficient activation of an APC to prime CD8+ CTLs may be substituted by additional binding of an effector T_h1 cell to the same APC. Upon recognition of the cognate MHC:peptide complex, the activated T_h1 cell produces CD154 (CD40L), a membrane-bound member of the TNF family. The interaction of CD154 with its receptor CD40 on the APC induces a higher expression of costimulatory molecules by the APC which facilitates priming of CD8+ CTLs [41]. The third function is the interaction with B cells causing these cells to produce certain opsonizing isotypes of antibodies (IgG1 and IgG3) [42]. The main objective of T_h2 cells and follicular T helper cells (T_{fh} cells) is to activate B cells to induce antibody production. B cells are responsible for the humoral arm of the adaptive immune response. Naïve B cells mainly reside in lymphatic tissues and in the blood where they encounter antigens that are transported from infection sites to

lymphatic tissues by enhanced lymph flow. Soluble antigens like bacterial toxins but also cell surface antigens of pathogens can be bound by the B cell receptor (BCR). In contrast to the TCR, the BCR binds antigens in their native (unprocessed) form. The BCR of naïve B cells is membrane bound and upon binding of a cognate antigen, internalization of the complex is induced (receptor-mediated endocytosis). The antigen is processed within the B cell and peptide fragments are presented on the cell surface in the context of MHC class II molecules. These peptides can be recognized by antigen-specific T_h2 and T_{fh} cells which in turn activate the B cell by expression of CD154, IL-4 and IL-21 [43]. Activated B cells and antigen-specific T_h cells form germinal centers in primary lymph follicles where they proliferate extensively. With the help of T_h cells, B cells undergo several modifications: the affinity of the BCR for its antigen is enhanced by somatic hypermutation, a process in which point mutations are introduced in the genes encoding for the variable regions of the heavy and light chains (V_H and V_L) of the BCR [44]. B cell clones with enhanced BCR affinity for the respective antigen receive survival signals through BCR signaling while reduced antigen recognition leads to cell death. In a repetitive cycle B cells undergo this process of affinity maturation. A second modification is the switch of isotype classes to produce soluble BCRs (antibodies) with high affinity and variable effector functions. The main functions of the different Isotype classes are neutralization of extracellular pathogens and toxins (IgG and IgA), opsonization for phagocytosis or ADCC (IgG1 and IgG3), sensitization of mast cells (IgE) and activation of the complement system (IgM) [45]. After completion of affinity maturation and isotype switch, B cells differentiate to antibody-producing plasma cells which leave the lymphatic tissues and migrate to the bone marrow.

Both humoral and cellular adaptive responses are highly antigen-specific and the generation of these responses takes time, however after clearance of the initial infection an immunologic memory develops. While most effector cells undergo apoptosis due to absence of their recognized antigens, some B- and T cells differentiate to long-lived memory cells. These cells are resting in lymphoid tissues and the bone marrow and can mount immediate and strong immune responses upon re-infection with the same pathogen. This immunological memory is the basis for the concept of vaccination.

1.1.3 The T cell receptor

The T cell receptor (TCR) mediates recognition of peptide antigens presented on MHC molecules on the surface of nucleated cells [46]. The molecule is a heterodimer that belongs to the immunoglobulin superfamily and consists of a TCR α- and β-chain in approximately 95 % of all T lymphocytes (αβ T cells). The α- and β-chains consist of variable (V) regions at the N-terminus and the constant (C) regions at the C-terminus of the molecule. The V regions of the α- and β-chain are responsible for the interaction with MHC:peptide complexes and are therefore determining for the antigen specificity of a T cell. Antigen recognition is mediated by complementary determining regions (CDRs), of which each of the receptor chains possesses three (CDR1-3). The CDRs are hypervariable loops that originate from gene rearrangements of TCR genes during T cell development. The TCRα locus is located on chromosome 14 and consists of about 70-80 different V_α (variable) gene segments, 61 different J_α (joining) gene segments and a C segment. The TCRβ locus is located on chromosome 7 and consists of 52 different V_β gene segments and two gene clusters that contain one $D_{\beta(1/2)}$ (diversity) gene segment, 6-7 $J_{\beta(1/2)}$ gene segments and one $C_{\beta(1/2)}$ gene segment each [47]. The V- (D-) and J gene segments are rearranged to a complete V-domain exon by somatic recombination. The combinatorial possibilities enhance the diversity of the TCR repertoire. However, somatic V(D)J recombination in lymphocytes is potentiated by a second unique mechanism: the individual gene segments are flanked by recombination signal sequences (RSSs) that can be recognized and bound by RAG proteins (recombination activating genes 1 and 2). These proteins are part of an enzyme complex called V(D)J recombinase [48]. Upon binding of the complex, recombination is initiated by a single strand DNA break between the RSS and the coding segment. Subsequently, the second strand is broken up and two DNA ends form, a blunt end at the RSS end and a hairpin at the coding end. In a second step, the coding ends of the gene segments are ligated. A complex of enzymes including DNA polymerases and DNA repair enzymes catalyzes the ligation process. In a crucial first step, hairpin DNA ends are opened by the enzyme artemis [49] resulting in blunt or sticky ends, depending on the site of strand break. The overhanging nucleotides are termed P-nucleotides due to their palindromic nature. In a second step, the enzyme TdT (terminal deoxynucleotidyl transferase) adds random nucleotides to the single strand ends which are called N-nucleotides (non-templated) [50]. Finally, the two single strands pair by

addition of nucleotides or removal of P- and N-nucleotides mediated by DNA polymerases and exonucleases, respectively. The two strands are then ligated by DNA ligase IV to complete the recombination process. The random nucleotides at the junction sites of the gene segments lead to an almost infinite number of possible unique TCR genes although diversity is restricted by reading frame shifts. The whole process is called junctional diversity and is mostly similar for the B cell receptor (BCR) – where it was first described [51, 52]. Functional V(D)J exons are transcribed and spliced to the C segments which encode for the constant regions of the TCR chains, the linker site for bisulfide bonding of the α- and β-chains, the transmembrane domain and the cytoplasmic domain. They are not affected by gene rearrangement. The resulting mRNAs are subsequently translated to proteins and the α- and β-chains pair to form the TCR. In theory, about 10^{18} different TCR variants may arise by junctional diversity [45], a number that is only restricted by the T cell count of about $3x10^{11}$ in the human body [53]. As described, antigen recognition is mediated by the CDR regions. The CDR1 and 2 loops originate mainly from germline parts of the V-gene segments and have limited diversity. Thus, they mainly interact with the less variable parts of the MHC molecule. The CDR3 loop however has its origin in the highly variable junctional regions and constitutes the center of the antigen receptor and the contact surface with MHC peptide ligands [54, 55]. A small amount of T lymphocytes (about 5 %) express TCR γ- and δ-chains instead of α- and β-chains (γδ T cells). The process of gene rearrangement is similar for those cells however the amount of gene segments is smaller leading to reduced combinatorial variance. The γδ TCRs do not recognize MHC:peptide complexes and their CDR regions rather resemble those of antibodies [56]. The recognized antigens are subject of ongoing investigations and are diverse, including lipids in complex with CD1 molecules, phosphoantigens and stress-induced cell surface molecules [57, 58].

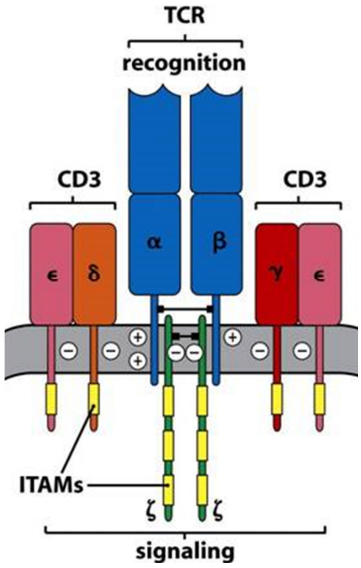

Figure 1: Schematic structure of T cell receptor complex components. The heterodimer of TCR α- and β-chain is located in the center and is associated with six invariant accessory chains (γ-, δ- and ε-chains of the CD3 complex and the ζ-chain homodimer. ITAMs are necessary for the induction of signal cascades upon receptor engagement. Figure from [45].

The molecular weights of the TCR α- and β-chain are 50 and 38 kDa, respectively [59]. The chains are linked at the linker region by a disulfide bond to form the heterodimer. Together with additional proteins, the TCR forms the TCR complex: two ε-chains and one γ- and δ- chain associate to the CD3 complex. The CD3 complex stabilizes surface expression of the TCR and partakes in intracellular signaling. A second accessory molecule is a homodimer of ζ-chains located at the intracellular site of the TCR complex [60]. CD3 and ζ-chains carry ITAMs (immunoreceptor tyrosine-based activation motif) at their cytoplasmic tails that mediate signal transduction within the cell upon receptor engagement through activation of an (auto-) phosphorylation cascade (see figure 1) [61]. Furthermore, proper T cell activation depends on signaling via co-receptors: CD4 is expressed on T_h cells and T_{reg} cells and is a monomer that binds to MHC class II molecules [62]. CD8 is expressed on CTLs and is a heterodimer that binds to MHC class I molecules [63, 64]. The co-receptors recruit important signaling molecules such as Src family kinases and phosphatases at their cytoplasmic residues. Signal transduction and activation of the TCR signal cascade is amplified massively by these molecules [65].

1.1.4 The major histocompatibility complex

The major histocompatibility complex (MHC) is a gene cluster present in the genome of almost all vertebrates. It was named after its function was first discovered in transplantation experiments. The MHC genes encode for proteins relevant for histocompatibility and immune recognition [66, 67]. The most important proteins are the MHC molecules which mediate antigen presentation to T cells. MHC molecules are membrane-bound proteins and are divided into two classes: MHC class I molecules are present on almost all nucleated cells and present peptide antigens to CTLs. MHC class II molecules are almost exclusively expressed on APCs and present peptide antigens to T_h cells. In humans, the MHC is located on chromosome 6 and MHC molecules are referred to as HLA molecules (human leukocyte antigen, HLA) due to their discovery on leukocytes [68, 69]. Both classes of HLA molecules are polygenes that are further divided into major and minor subtypes: for class I, the major molecules are HLA-A, HLA-B and HLA-C, while minor molecules are HLA-E, HLA-F and HLA-G. For class II, the major molecules are HLA-DP, HLA-DQ and HLA-DR and the minor ones are HLA-DM and HLA-DO. Thus, every human individual has six gene loci for HLA class I molecules (α-chains) and ten to twelve gene loci for HLA class II molecules (α- and β-chains). Major HLA genes are highly polymorphic (see table 1) while minor HLA genes (and the gene for the α-chain of HLA-DR) show only few polymorphisms [70, 71].

Table 1: Statistics on major HLA class I and II gene polymorphism. Amount of known alleles for each of the different major HLA genes is listed (IMGT/HLA 10/2017).

	HLA class I			HLA class II					
	A	B	C	DRA	DRB	DQA1	DQB1	DPA1	DPB1
Alleles	3997	4859	3605	7	2395	92	1152	56	942
Proteins	2792	3518	2497	2	1751	35	779	26	655

The high genetic polymorphism of HLA genes within the human population increases the likelihood of inheritance of different alleles for each of the major HLA genes. The genes are expressed codominantly, therefore the cells of an individual can express up to six different major HLA class I molecules. Expression of different major HLA class II molecules is more variable due to combinatorial pairing of the different α- and β-chains. The genetic

polymorphism of HLA genes does not affect gene regions encoding for the backbone of HLA molecules but rather for those encoding for the peptide binding cleft. This leads to altered peptide binding capabilities of different HLA allotypes. Thus, variance of HLA allotypes within a population potentiates the amount of presentable peptides from each protein, which enables efficient defense against pathogens on population level. Immune evasion of pathogens by mutation and sequence alteration of antigens is counteracted by the ability of variable peptide presentation on HLA molecules within a population.

1.1.5 MHC structure and antigen processing

MHC class I molecules are membrane-bound surface proteins consisting of a variable α-chain (43 kDa) and β_2-microglobulin (12 kDa). The α-chain is composed of three protein domains (α_1, α_2 and α_3). The α_3 domain is invariant and harbors a transmembrane region while the α_1 and α_2 domains are the highly variable parts and form the peptide binding cleft [72]. The cleft is formed by several protein folds with β-sheets at the basis and α-helices at the sides (see figure 2) [73]. The conformation of the binding cleft restricts the length of peptide binders to eight to twelve amino acids. The N- and C-termini of bound peptides interact with conserved amino acids of the binding cleft forcing a linear conformation of the bound peptides [74]. The variable parts of distinct MHC allotypes add another prerequisite for peptide binding: diversity in the amino acid sequences leads to the formation of distinct protein pockets alongside the peptide binding groove. Amino acid side chains of the ligand need to interact with these pockets by formation of hydrogen bonds and hydrophobic interactions. Thus, each allotype preferentially binds peptides containing specified amino acids. These specified amino acids are termed anchor residues (mostly at position two and at the C-terminus of the peptide) which are specific for each MHC allotype and restrict peptide binding [75]. The combination of length, spacing and nature of anchor residues of a peptide required for binding to a specific MHC allotype is called peptide motif [76]. The knowledge of these peptide motifs allows for the *in silico* prediction of peptide binders for defined MHC allotypes from protein sequences with tools like SYFPEITHI [77] and NetMHC [78].

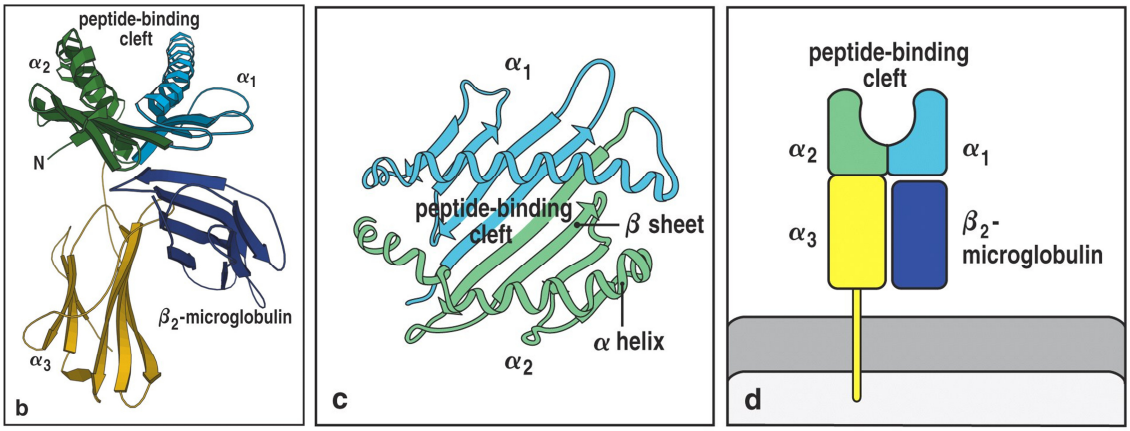

Figure 2: Structure of MHC class I molecules. The α-chain with its three domains and the non-covalently bound β_2-microglobulin are depicted. Unique secondary structures are visible in the band model (b). The peptide binding cleft is formed by the α_1 and α_2 domains (c). Schematic of the MHC molecule shows the transmembrane domain of the α_3 domain (d). Figure adapted from [45].

MHC class I molecules preferentially present peptides derived from cytosolic proteins [79]. The protein repertoire of a cell underlies a constant turnover: proteins are synthesized, degraded and recycled with various turnover times for different protein species. Degradation is executed by the proteasome, a large protein complex (1700 kDa). It is built up of two subunits: the 20S subunit consists of four stacked rings that form a barrel-like structure. The outer rings have seven α-subunits (α_1-α_7) and mediate recognition and uptake of substrates, while the inner rings have seven β-subunits (β_1-β_7) and possess proteolytic capacities. The subunits β_1, β_2 and β_5 are threonine proteases and cleave polypeptides after acidic, basic or hydrophobic amino acids forming the C-termini of MHC ligands. The 19S subunit forms a 'lid' for the barrel-like structure and mediates recognition of ubiquitinated proteins and protein unfolding, thereby regulating the activity of the proteasome [80]. Proteins are tagged for degradation by ubiquitination during the regular protein turnover or in case of erroneous protein synthesis or folding (defective ribosomal products, DRIPS). The resulting peptides have a length of about 25 amino acids and are released into the cytosol, where they are further processed N-terminally by cytosolic proteases [81, 82]. The cytosolic peptides are eventually transported into the endoplasmatic reticulum (ER) by the transporter associated with antigen processing (TAP) [83], where further processing by several peptidases such as the endoplasmatic reticulum aminopeptidase associated with antigen processing (ERAAP) may take place [84, 85]. Newly synthesized MHC class I α-chains get translocated to the

ER where they are held partly folded by the chaperone calnexin. Upon binding of β_2-microglobulin to the α-chain, calnexin dissociates and the MHC molecule binds to the PLC (peptide loading complex). The PLC consists of several proteins, including the chaperone calreticulin and tapasin, which directs the PLC to the TAP transporter. Binding of a peptide to the binding cleft of an MHC molecule stabilizes the MHC:peptide complex and it dissociates from the PLC. Peptide-loaded MHC class I molecules enter the secretory pathway and are transported in vesicles from the ER *via* the golgi apparatus to the cell surface (see figure 3) [86].

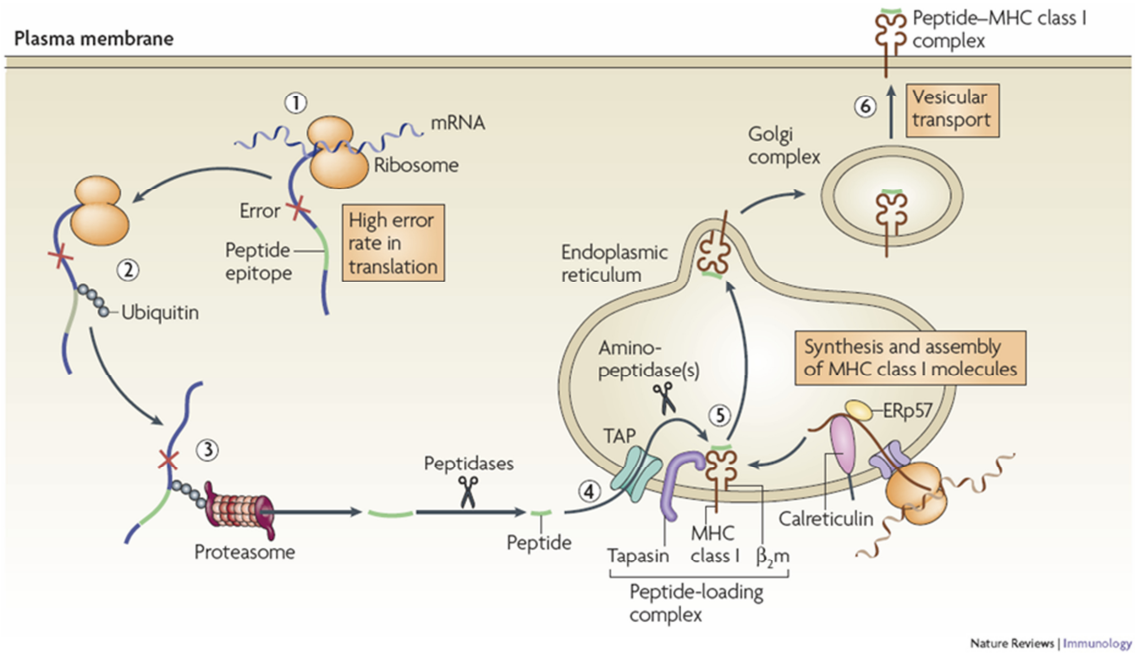

Figure 3: Antigen processing pathway for MHC class I peptide ligands. Ubiquitinated proteins are tagged for degradation by the proteasome (3). The resulting peptides are released into the cytosol and further processed before translocation to the ER by TAP (4). Empty MHC class I molecules are directed to TAP by the PLC and peptides bind to the empty binding clefts (5). The MHC:peptide complexes are stabilized and translocate to the cell surface by vesicular transport (6). Figure from [87].

MHC class II molecules are membrane-bound surface proteins like MHC class I molecules. They are heterodimers consisting of an α-chain (34 kDa) and a β-chain (29 kDa). Both chains are composed of two protein domains: while the α_2 and β_2 domains are invariant and possess transmembrane domains, the α_1 and β_1 domains are highly variable and form the peptide binding cleft [88, 89]. The binding cleft architecture is relatively similar to that of MHC class I molecules, however it is not completely closed at the edges (see figure 4). This more ‘open’ conformation allows binding of longer peptides with lengths from nine

to 25 amino acids [90]. As a result, the unspecific interactions that hold the peptide in place do not establish between peptide N- and C-termini and the edges of the binding cleft, but rather between the peptide backbone and the α-helices forming the binding cleft. Although peptide length is far more variable than for MHC class I molecules, MHC class II ligands harbor core sequences that exhibit similar binding motifs. The anchor residues are often located in positions one, four, six and nine of the core sequence [91]. The presence of a core sequence binding motif can lead to length variants of MHC class II peptide ligands. Furthermore, the specificity of the binding pockets for the anchor residues is far less restrictive, leading to promiscuous ligands (peptides may bind to various allotypes) [92].

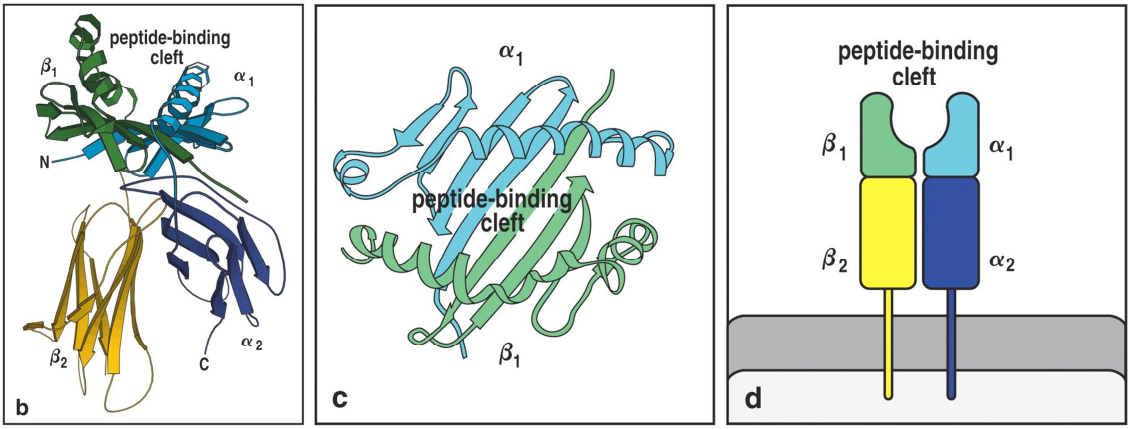

Figure 4: Structure of MHC class II molecules. The α-chain and β-chain with their two respective domains are depicted. Unique secondary structures are visible in the band model (b). The peptide binding cleft is formed by the α_1 and β_1 domains and has an open conformation (c). Schematic of the MHC molecule shows the transmembrane domain of the α_2 and β_2 domains (d). Figure adapted from [45].

MHC class II molecules preferentially present peptides derived from exogenous proteins. Phagocytes like DCs, macrophages or B cells take up exogenous proteins by phagocytosis, pinocytosis or receptor-mediated endocytosis. The resulting endosomes fuse with lysosomes, which carry proteases and lower the pH of the merged vesicle. The exogenous proteins get unfolded by thiol reductases and degraded to peptides by proteases, mainly of the group of cathepsins [93]. MHC class II molecules are translocated to the ER after synthesis. The invariant chain (Ii, CD74) forms a homotrimer and binds to the peptide binding clefts of three MHC class II molecules to stabilize the proteins and avoid premature peptide loading within the ER. The invariant chain further acts as a sorting signal to guide the nonameric complexes from the ER to the endosomes. Fusion of an

endosome containing MHC class II molecules with a lysosomal vesicle generates a special compartment, the MHC II loading complex (MIIC) [94]. The lowered pH activates cathepsins that cleave the Ii leaving only the class II-associated invariant chain peptide (CLIP) within the peptide binding cleft. The minor MHC class II molecules HLA-DM and HLA-DO catalyze exchange of the CLIP with peptides contained in the MIIC. By fusion of the MIIC with the cell membrane, MHC class II molecules are translocated to the cell surface (see figure 5).

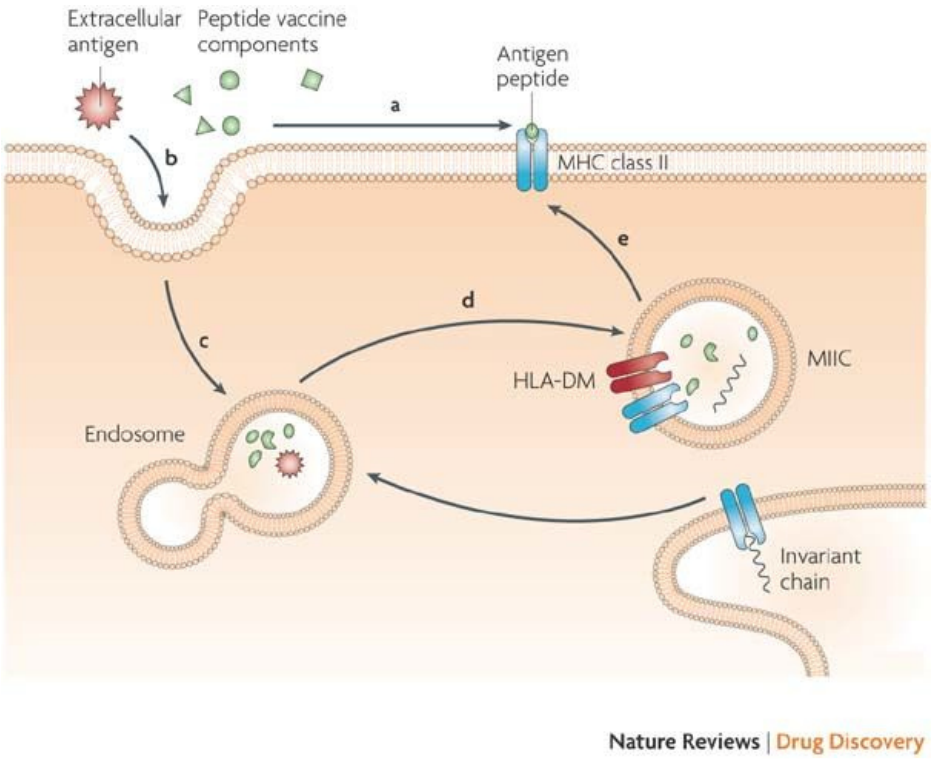

Figure 5: Antigen processing pathway for MHC class II peptide ligands. Extracellular peptides, proteins and pathogens are taken up by phagocytosis, pinocytosis or receptor-mediated endocytosis (b). Phagosomes fuse with lysosomes and antigens get degraded by proteases to produce peptides (c). Fusion of this vesicle with a MHC class II-containing endosome generates the MIIC (d). Peptides are loaded onto MHC class II molecules by exchange of CLIPs with the help of HLA-DM and HLA-DO within the MIIC. Fusion of the MIIC with the cell membrane translocates MHC class II molecules to the cell surface. Figure from [95].

The classical ways of antigen processing for MHC class I and II molecules separates the origin of antigens into intracellular for MHC class I and extracellular for MHC class II. The origin of antigens correlates with the types of T cells that recognize those antigens. MHC class I molecules are present on all cells to showcase infection, cell stress or malignant transformation to CTLs and allow recognition and clearance of such cells [96]. MHC class II molecules on the other hand, mainly present extracellular antigens on APCs

to induce T_h cell responses that help mounting antibody responses or support cellular immune responses. However, the separation of antigenic origin is circumvented by several alternative mechanisms. Antigen processing is influenced by the presence of pro-inflammatory cytokines like IFN γ: the proteasome is activated by the expression of the activator PA28 and some of the proteasomal subunits are exchanged, changing the cleavage specificity. The immune proteasome alters the repertoire of presented peptides during inflammatory reactions [97, 98]. Intracellular proteins may enter the endosomal and lysosomal compartments through autophagy leading to presentation of peptides derived from these proteins on MHC class II molecules [99]. Furthermore, APCs are capable of cross presentation of peptides derived from exogenous antigens on MHC class I molecules [100].

1.1.6 Selection and development of T lymphocytes

T cells originate from common lymphatic progenitor cells of the bone marrow. After initial differentiation steps, the early progenitor cells migrate *via* the bloodstream from the bone marrow to the thymus. The thymus is the most important organ in the development of mature T cells. It is located above the heart and is predominantly active during childhood and adolescence and degenerates with increasing age. It consists of numerous thymic lobules which are separated in two distinct regions, the outer cortex and the inner medulla. Within the cortex, thymocytes are tightly packed, while the medulla shows a more loose arrangement of cells intersected with Hassall's corpuscles (see figure 6).

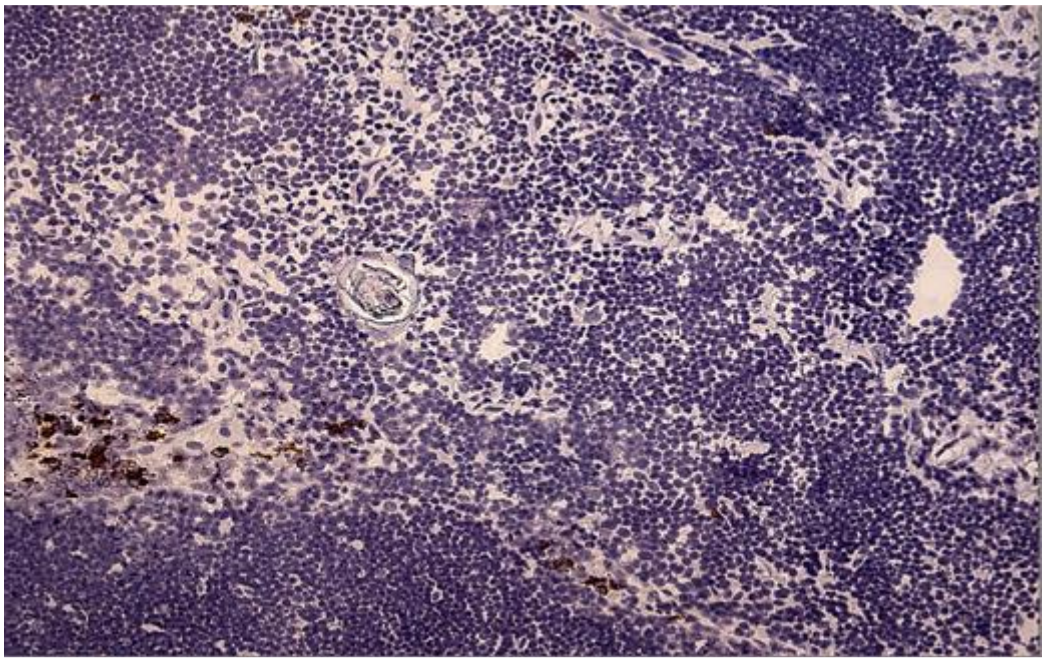

Figure 6: Tissue section of a thymic lobule. The cortex with tightly packed thymocytes is visible at the bottom and right side. The medulla is visible in the center with loosely packed cells and a Hassall's corpuscle. Figure from [101].

Within the thymus stroma, progenitor cells start maturation to T lymphocytes by engagement of Notch-1 receptors [102]. The cells undergo a proliferation phase with gene rearrangement of the TCR β-chain and expression of lineage-specific proteins. The cells do not express the co-receptors CD4 and CD8, wherefore this development stadium is called "double negative thymocyte". In case of successful gene rearrangement for the TCR β-chain, the cells express a pre-TCR, a heterodimer formed of the TCR β-chain and a pre-α-chain, together with CD3 and both co-receptors CD4 and CD8 [103]. During this "double positive thymocyte" stage gene rearrangement for the TCR α-chain ensues and the mature α:β TCR is expressed. Failed receptor chain pairing leads to apoptosis of the cells but may be rescued by additional recombination events using remaining V_α and J_α genes. At this developmental stage the thymocytes are located in the cortex of the thymus, where they undergo a positive selection procedure: the TCRs of the cells need the ability to bind to MHC molecules which provides survival signals to the cell by the TCR signaling cascade [104]. After positive selection, expression of the TCR is enforced, while expression of the co-receptors is suppressed and the thymocytes migrate to the thymic medulla. Here, a second, negative selection process takes place. The thymocytes interact with APCs like DCs and macrophages and thymic stromal cells which express MHC class I

and II molecules and the transcription factor AIRE (autoimmune regulator). AIRE enforces ectopic transcription and expression of almost all genes and thereby generates a projection of the peripheral tissues on MHC ligandome level of the APCs [105]. During negative selection, thymocytes first express CD4 and interaction of the TCR with MHC class II molecules is screened. If the interaction is too weak, CD4 is downregulated and CD8 is expressed and the TCR is screened for interaction with MHC class I molecules. Thus, by interaction of their TCRs and co-receptors with MHC class I or II molecules, thymocytes are destined to CD4+ or CD8+ lineages [106]. T cells expressing TCRs that bind MHC molecules with bound self-antigens with high avidity become apoptotic in this selection stage [107]. Negative selection prevents the release of autoreactive T cells into the periphery however the selection is not entirely exhaustive. Only about 2 % of initial precursor cells pass the thymic selection processes and leave the thymus as naïve T cells [108]. These cells circulate in the bloodstream and the lymphatic system until they encounter an APC presenting the cognate MHC:peptide complex for their TCR. After priming of a naïve T cell, it expands clonally and matures to an effector phenotype that can exert its effector function upon antigen encounter. To avoid autoimmunity, T cells are further regulated by peripheral tolerance mechanisms: naïve T cells that recognize their cognate MHC:peptide complex in the periphery without adequate costimulatory signals become anergic or undergo activation induced cell death (AICD) [109]. A second mechanism of peripheral tolerance is suppression of T cell activity by T_{reg} cells or myeloid derived suppressor cells (MDSCs).

1.2 Cancer immunotherapy

Cancer is the second leading cause of death with about 14 million new cases in 2012 and about 8.8 million cancer-related deaths in 2015 [110]. In most cases, cancer is a disease that develops in elderly people due to a lifelong exposition to certain risk factors, such as radiation, chemical carcinogens and chronic infections [111]. The WHO estimates that the prevalence of cancer will rise by about 70 % in the next two decades due to the increase in life expectancy of the world population. Therapy of cancer usually includes surgical resection of the tumor and chemo- or radiotherapy to target residual tumor cells and undetectable micro-metastases. Chemotherapies are rather unspecific medications

targeting cell division which can cause severe side effects leading to high numbers of treatment-associated deaths. Nevertheless, treatment protocols for the various cancer types are continuously improved and higher standards of medical care facilitate early detection of tumors thereby increasing favorable treatment outcomes [112]. After decades of improvements on standard therapy protocols, the concept of cancer immunotherapy has become one of the most promising new treatment approaches. However, the idea that the immune system can recognize and eliminate tumor cells is not a new one. Already in 1893, the American surgeon William Coley observed remissions of cancer patients after acute bacterial infections. He started to treat sarcoma patients with his “Coley toxin”, in fact attenuated *Streptococcus pyogenes* cultures, which nowadays is considered as what has been the first cancer immunotherapy [113]. In 1909, Paul Ehrlich postulated the theory that the immune system is capable of tumor cell recognition and control of tumor growth [114]. In the late 1950s those early theories were adopted and further developed by Lewis Thomas and later by Frank Burnet leading to the immunosurveillance theory in 1967: cells of the immune system are constantly surveying host tissues and are capable to recognize tumor-associated antigens or neo-antigens that tumor cells acquire during malignant transformation [115, 116]. The theory of immunosurveillance is nowadays substantially acknowledged and is the foundation for the development of modern immunotherapies [117]. A prerequisite for the development of effective cancer immunotherapies is the understanding of the underlying mechanisms that lead to immune surveillance failure and tumor outgrowth.

1.2.1 Tumor biology

Malignant transformation of healthy cells is mainly caused by mutations in genes that regulate cell division and cell growth. Some groups of these genes were even named after their association with cancer, like (proto-) oncogenes or tumor suppressor genes [118]. Mutation of transcription regulators or molecules of certain signaling pathways likewise may induce malignant transformation. Furthermore, loss or impairment of DNA repair mechanisms can lead to accumulation of mutations and thereby to transformation of cells. For a minority of cancer cases, causative mutations are inherited and germline encoded, while for the majority of cases these mutations are acquired during lifetime by exposition to risk factors. The genetic instability of malignant cells fosters the

accumulation of mutations and alteration and deregulation of the DNA causes changes in the proteome of those cells. These alterations are showcased by MHC molecules on the cell surface and can be recognized by T cells. Antigens of tumor cells that can be recognized by T cells are termed tumor antigens and are subdivided into different classes:

- **Differentiation antigens:** tissue-specific antigens only expressed in the tumor and the corresponding healthy tissue the tumor originates from. An example is the premelanosome protein (PMEL, gp100), which is almost exclusively expressed in melanocytes and plays an essential role in melanin production. The protein serves as target for immunotherapies against melanoma as this tumor originates from melanocytes. T cell responses against this antigen may also target healthy melanocytes inducing a vitiligo phenotype [119-121].

- **Overexpressed antigens:** proteins present in healthy tissues that are overrepresented in the tumor by altered gene expression. An example is VEGF, a protein that is overexpressed in a variety of tumors. It promotes tumor vascularization to counteract hypoxia and nutrient deficiency in solid tumors and serves as target for antibody- and kinase inhibitor-based therapies [122-124].

- **Oncoviral antigens:** some tumors originate from virus-infected cells. Viruses like the human papilloma virus (HPV) or the Epstein-Barr virus (EBV) can induce malignant transformation of infected cells [125-127]. Chronic infection with hepatitis B or C virus (HBV, HCV) is suspected as one cause of liver cancer. The antigens originate from the viral proteome and can act as oncogenes. The discovery that HPV infection is causative for cervical cancer was awarded with the nobel prize for medicine in 2008 for Harald zur Hausen and led to the first approved preventive anti-cancer vaccine in 2006 [128, 129].

- **Cancer/testis antigens:** expression is usually restricted to immune-privileged tissues of the reproduction apparatus like ovaries or testicular germ cells and is aberrantly reactivated in tumor cells. Proteins of the MAGE family for example are expressed in a variety of tumors and high expression usually correlates with poor prognosis. However, MAGE-specific T cells were described to be present in many cancer patients in peripheral blood as well as in TILs [130, 131].

- **Oncofetal antigens:** expression is restricted to prenatal development and is aberrantly (re-) activated in tumor cells. The protein Six1 is a member of the homeoprotein family, a group of transcription regulators that control organogenesis and polarization during embryogenesis. Thus, expression of these proteins has pleiotropic effects and modulates the transcription of a wide range of target genes. Dysregulation of the developmental functions of such proteins in mature organs may initiate and/or promote tumorigenesis [132].

- **Mutated antigens:** the amino acid sequence of antigens is changed by nonsynonymous mutations. These antigens are highly tumor-specific and unique for individual tumors. Targeting of such antigens by immunotherapy is a promising approach of highly individualized tumor therapy [133]. Interestingly, one single mutated antigen may suffice as rejection antigen if antigen-specific T cells are present [134].

The antigen classes are characterized by different levels of tumor specificity. While less specific antigens are referred to as tumor-associated antigens (TAAs), the ones with high specificity are termed tumor-specific antigens (TSA). Examples of antigens from the different classes are listed in table 2.

Table 2: Classification of tumor antigens with examples. Modified from [135].

Classification	Antigen	Specificity
Differentiation	MELAN A/MART1 TYROSINASE GP100 NY-BR1	TAA
Overexpressed	HER2/NEU P53 MUC-1 EpCAM VEGF	TAA
Oncoviral	HPV E6 and E7	TAA/TSA
Cancer/testis	MAGE BAGE NY-ESO-1 SPAG9	TAA/TSA
Oncofetal	SIX1 HOX	TSA
Mutated	CDK4 P53 RAS	TSA

The antigenic signature of individual tumors is probably composed of antigens derived from different antigen classes and is dependent on individual genetic alterations. In general, development of a tumor can be understood as a failure of immunosurveillance or a lack or loss of immunogenic antigens expressed on tumor cells. This led to the expansion of the theory of immunosurveillance by Robert Schreiber, who postulated that tumors undergo selective pressure by the immune system and develop in a co-evolutionary manner [117]. The process of cancer immunoediting has three stages:

- **Elimination:** Malignant cells are recognized and eliminated by the immune system
- **Equilibrium:** Malignant cells that survive the elimination stage persist in a latent or dormant stage. Further genetic alterations are acquired that lead to differentiated clones that are either immunologically rejected or ignored. The cellular composition of tumors is edited by this process.
- **Escape:** Tumor cells that evade control by the immune system grow out to form established tumors.

While immunogenic tumor cells are prone to elimination, those that avoid immune recognition have a selective advantage and continue to grow. The mechanisms that lead to immunologic ignorance of tumors are manifold. One escape mechanism is antigen loss, which is probably induced by selection through the immune system [136]. In some cases, tumors are dependent on single altered antigens that promote malignant transformation [137], however more often a multitude of alterations is causative. In those cases, selection against one antigen is compensated by usage of several altered signaling pathways (and other genetic alterations) maintaining the malignant phenotype of a cell. A second possibility for antigen loss is complete loss of MHC expression [138] or TAP deficiency, albeit making those cells targets for elimination by NK cells [139, 140]. Another tumor escape mechanism is the formation of a distinct tumor microenvironment. The microenvironment consists of normal cells that are recruited by tumor cells or by chronic inflammation processes at the tumor site and has direct effects on immunologic surveillance. The immune suppressive functions of the tumor microenvironment include formation of physical barriers by stromal cells, preventing the infiltration of tumors by immune cells [141] as well as the accumulation of regulatory cells like T_{regs} and MDSCs. Those cells produce anti-inflammatory cytokines like TGF-β [142] and IL-10 and other growth factors which impair T cell priming and function [143, 144]. Additionally, T_{regs} express cytotoxic T-lymphocyte antigen 4 (CTLA-4), a molecule that competes with CD28 for the binding of the co-stimulatory molecules CD80 and CD86 [145] thereby preventing efficient priming of T cells. Several other molecules within the tumor microenvironment have direct effects on infiltrating T cells: proliferation is inhibited in the presence of indolamine-2,3-dioxygenase (IDO) [146] while constant activation of T cells leads to the expression of exhaustion markers like the Fas receptor or the programmed cell death proteins 1 and 2 (PD-1 and PD-2). Interaction of Fas with its receptor FasL induces AICD in T cells [147]. Engagement of PD-1 and PD-2 with their receptors (PD-L1 and PD-L2) leads to anergy of antigen-specific T cells [148, 149]. Immune evasion is acknowledged as a critical hallmark of cancer [150] and the composition of the tumor microenvironment in general and the infiltration of T cells in particular has significant influence on therapy outcomes [151]. As T cells are the key players in immunologic cancer recognition and rejection, most immunotherapeutic approaches aim at activating or restoring T cell activity against tumor cells.

1.2.2 Immunotherapeutic approaches

Immunotherapies can be divided into active and passive approaches. The mode of action of passive immunotherapies in general is administration of immune cells or molecules that possess anti-tumoral properties while active immunotherapies aim at the *in vivo* (re-) activation of the patient's own immune system. One of the first passive immunotherapeutic approaches was hematopoietic allogeneic stem cell transplantation (HSCT) for the treatment of leukemias and lymphomas [152]. During the therapy, stem cells of an HLA-matched donor are transferred into a conditioned patient (myeloablation by chemotherapy). T cells that originate from donor stem cells exert strong immune responses against leukemic blasts by recognition of tumor antigens and minor histocompatibility antigens (mHAs) [153]. This favorable graft-versus-leukemia effect (GvL) makes HSCT a powerful treatment opportunity however T cell reactivities often are not restricted to tumor cells but also target benign healthy tissues. The phenomenon of graft-versus-host disease (GvHD) can lead to severe side effects and is a major drawback of HSCT. Modern protocols for transplant generation therefore include T cell elimination to minimize alloreactive T cell contents and GvHD risk. Another passive approach is adoptive T cell transfer, where antigen-specific T cells are isolated directly from the patients' tumor (tumor-infiltrating lymphocytes, TILs) or blood or from blood of an unrelated donor [154]. The isolated T cells are screened for tumor (antigen) reactivity *in vitro* and reactive cells are rapidly expanded using high amounts of IL-2, unspecific stimulation of CD3 and CD28 and sometimes irradiated feeder cells. The cell products are then (re-) infused into patients at high cell numbers. To enable engraftment and persistence of the cells, conditioning of patients by lymphodepletion and continuous IL-2 administration is required [155, 156]. A more sophisticated form of adoptive cell transfer is the administration of genetically engineered T cells. These cells are modified by lentiviral transduction to express chimeric antigen receptors (CARs) [157] or TCRs [158]. CARs are constructs of an antibody single-chain variable fragment (scFv) for surface antigen recognition coupled to intracellular signaling domains that activate the effector cell for elimination of the target cell upon antigen encounter. The CAR approach is dependent on highly specific surface tumor antigens, currently limiting implementation to few cancer entities like B cell leukemias (CD19 as target is exclusively expressed on B cells) [159, 160]. Therapeutic monoclonal antibody technology is the most advanced

branch of passive immunotherapy. Antibodies against several tumor-associated surface antigens are approved for clinical application [161]. Classical antibody-mediated effector mechanisms like opsonization, receptor blockade, ADCC and complement activation provide anti-tumoral efficacy [162-164]. The development of bispecific antibody constructs of various formats further enhances the cytotoxic potential by recruitment of T cells as effector cells [165].

Active immunotherapy aims at the activation of a patient's own immune system to recognize and eradicate tumors. A rather unspecific approach is cytokine therapy. Interferons like Interferon α (IFN-α) have anti-proliferative properties and thereby can inhibit tumor growth if applied systemically [166] while on the other hand, it has beneficial effects on T cell priming [167]. IFN-γ has pro-inflammatory properties and stimulates antigen processing and presentation. Immune recognition of tumor cells by CTLs is thereby enhanced [168]. Finally, IL-2 stimulates proliferation of T cells and NK cells [169]. Systemic administration of immune-stimulatory cytokines however also leads to severe side effects that originate from unspecific immune cell activation.

Another systemic active immunotherapy is the application of checkpoint-inhibitory antibodies. Checkpoint molecules are natural components of peripheral tolerance and can shut down T cell responses or prevent efficient priming of T cells. In the tumor microenvironment however, beneficial anti-tumor T cell responses are inhibited by an excessive expression of checkpoint molecules. The first checkpoint blockade antibody that was approved for clinical application was Ipilimumab in 2011 for treatment of metastatic melanoma [170]. It binds to CTLA-4 on T cells and blocks the interaction with CD80 and CD86 on APCs, which leads to more efficient T cell priming and less transduction of inhibitory signals within T cells [171]. In 2014, two additional checkpoint-blocking antibodies against PD-1, Pembrolizumab and Nivolumab, were approved for second-line melanoma therapy. PD-1 is expressed on T cells and is upregulated in the context of constant inflammation through high levels of IFN-γ [172, 173]. Engagement of PD-1 with one of its ligands, PD-L1 or PD-L2, leads to T cell anergy. PD-1 ligands are expressed to high extent within the tumor microenvironment and by tumor cells themselves, rendering TILs unresponsive and thereby evading immune recognition and elimination [174, 175]. Blockade of PD-1 interaction with its ligands can restore T cell activity leading to tumor elimination. Combination therapy with anti-CTLA-4 and anti-PD-

1 seems to have synergistic effects showing unprecedented efficacy in melanoma patients [176]. However, as checkpoint blockade antibodies are administered systemically and interfere with central tolerance mechanisms, the side effects can be severe [177]. Melanoma was the first indication in which checkpoint blockade was tested and showed good responses. It is also one of the malignancies with the highest mutation count [178], possibly harboring the highest amounts of mutated or neo-antigens [179]. In the meantime, it has become apparent that the presence of T cells specific for those mutated antigens is a significant predictor for success of checkpoint therapy [180]. Restoration of T cell activity against such antigens improves the chance of tumor rejection [181, 182]. Thus, in tumor types with lower mutational burden checkpoint inhibition has heuristically lower prospects of therapy success [183].

Active tumor vaccination is the most diversified approach of active immunotherapy aiming to induce specific T cell responses against tumor antigens *in vivo*. First attempts were made to vaccinate with autologous tumor cells or tumor lysates in combination with immune-stimulatory cytokines [184, 185]. Direct delivery of antigens to APCs is used to enhance T cell priming. For this purpose, DCs are generated from autologous cells and loaded with tumor lysates, peptide pools or transfected with expression vectors coding for tumor antigens [186-188]. The first clinically approved immunotherapy of this kind was Sipuleucel-T in 2010 for treatment of metastatic prostate cancer. Here, DCs are generated from patient PBMCs, loaded with a fusion protein consisting of the tumor antigen prostatic acid phosphatase (PAP) and the immune modulator GM-CSF *ex vivo*, before re-infusion into the patient [189]. Major disadvantages of approaches involving the *ex vivo* or *in vitro* manipulation of cells are high costs and regulatory concerns, facts that often prevent clinical testing of such approaches (also true for adoptive cell transfer and CAR-T cell therapies). These drawbacks can be avoided by direct immunization with defined tumor antigens. A prerequisite for this approach is the knowledge of the actual tumor antigens of interest. Apart from whole proteins, peptides of various lengths derived from tumor antigens have been used for vaccination approaches. While longer peptide sequences of about 25 amino acids length can bind to MHC class II molecules, they may get processed by APCs at the vaccination site for presentation of embedded MHC class I ligands [190]. Additionally, overlapping peptides covering the complete sequence of a tumor antigen can be used for vaccination. The advantage of this approach

is that one does not necessarily need to know the exact determinants of immunogenicity of a tumor antigen. However, if the exact sequence of immunogenic HLA ligands is known, those peptides can be used for vaccination and constitute a defined drug that is relatively easy to produce [191]. Peptide vaccines have been tested extensively in a multitude of cancers however the results were quite disillusioning despite of single treatment successes [192-194]. The efficacy of peptide vaccines is dependent on several factors: first, most tumor antigens are of relatively low immunogenic nature, i.e. the frequencies of antigen-specific naïve T cells as well as TCR avidities are rather low. For the induction of strong antigen-specific T cell responses efficient adjuvant agents are therefore indispensable [195]. Unfortunately, availability of clinically approved substances is limited to a few agents, which restricts the possibilities for the design of peptide vaccine applications. Second, the selection of tumor antigens has enormous impact on the efficacy of peptide vaccines. Classical tumor-antigens are used for peptide vaccination based on expression analysis of tumor tissues however this does not take into account HLA polymorphism and actual HLA presentation. Careful selection and validation of targets can enhance immunogenicity and efficacy of peptide vaccines [196, 197]. Only recently, a highly personalized peptide vaccine against neo-epitopes in melanoma patients showed promising results in a phase I clinical trial [198]. Of note, vaccination against neo-epitopes was also successfully conducted by administration of RNAs coding for 27mer peptides harboring individual amino acid mutations. The RNAs were designed for each patient based on identified tumor-specific mutations and were administered directly to lymph nodes to target APCs [199]. Thus, selection of suitable antigens and higher levels of personalization have the potential to significantly improve the outcomes of active tumor vaccination in the future. Additionally, combination of different (immuno-) therapeutic approaches is envisioned to further advance cancer therapies by synergistic effects [200-202].

1.3 Renal cell carcinoma

Renal cancer is the twelfth most common cancer in the western world accounting for about around 3 % of all newly diagnosed malignancies [203]. The incidence rate in men is about twice as high as in women (16.9 vs. 8.0 cases per 100.000 individuals) and the

median 5-year survival rate was 76 % in men and 78 % in women in 2012 in Germany [204]. About 90 % of all renal cancers are renal cell carcinomas (RCC) and among RCCs, clear cell RCC (ccRCC) is the most common subtype accounting for about 75 % of cases. Papillary (15 %) and chromophobe (5 %) RCCs are two less frequent subtypes, as well as nephroblastoma [205]. RCCs are often diagnosed by chance as symptoms only develop in late stages of the disease. In cases of metastatic disease (mRCC), the median survival rate is poor with only about 22 months and the 5-year survival rate is less than 10 % [206]. RCCs originate from cells of the proximal renal tubular epithelium and are mostly resistant to chemotherapy and radiotherapy [207]. Thus, surgery is the most commonly applied first treatment. During complete (radical) or partial nephrectomy the tumor tissue as well as benign, unaffected renal tissue is removed. The fact that benign tissue is available for almost all tumor samples allowed for the conduction of this study with the unique possibility of a comparative analysis of benign and malignant sample pairs. RCC is regarded as a highly immunogenic tumor based on the observation of high amounts of tumor-infiltrating lymphocytes (TILs) [208] and spontaneous disease regressions [209]. Thus, RCC was one of the first cancer entities where unspecific immunotherapy with cytokines (IFN-α and IL-2) showed clinical benefit and was approved for first-line treatment of advanced disease [210]. Although since then a multitude of more specific immunotherapy approaches were tested in RCC patients, treatment modalities were solely changed by the introduction of small molecules and monoclonal antibodies with various targets: tyrosine kinase inhibitors (TKIs) like Sunitinib target vascular endothelial growth factor (VEGF) but also exhibit off-target effects and are prone to resistance development of tumors [211-213]. Inhibition of VEGF is thought to prevent tumor angiogenesis and metastatic transition of tumor cells. Other VEGF-targeting agents approved for the treatment of mRCC are Sorafenib [214], Pazopanib [215] and Bevacizumab in combination with IFN-α [216]. The other target is mammalian target of rapamycin (mTOR), a kinase that regulates cell growth and proliferation. The approved mTOR inhibitors Temsirolimus [217] and Everolimus [218] similarly show off-target effects and resistance development. Clinical studies testing more advanced treatment approaches were only recently conducted: Cabozantinib is a multikinase inhibitor targeting VEGFR, MET, RET and AXL [219] and Nivolumab is a checkpoint blockade antibody against PD-1 [220]. Both treatments outcompeted standard therapies by far:

Cabozantinib showed a 42 % reduction in the risk of progression or death and higher response rates (21 % vs. 5 %) compared to Everolimus. Nivolumab showed a reduction of 27 % in the risk of death and higher tumor response rates (25 % vs. 5 %), as well as improved overall survival (OS) compared to Everolimus. Thus, the treatment modalities of mRCC are about to change in the near future [221]. However, complete remissions remained rare in these clinical trials, showing the medical need for innovative therapeutic options.

1.4 Tuberculosis

Tuberculosis (TB) is the infectious disease with the highest prevalence in the human population. About one-third of the world's population is currently infected with *Mycobacterium tuberculosis* (*Mtb*), the germ causing the disease. Every year, about 9 million new infections and 1.7 million deaths due to tuberculosis worldwide are estimated [222]. Infection rates and mortality are significantly increased in immunocompromised individuals, especially in HIV-infected patients, making tuberculosis a major health threat in developing and third-world countries.

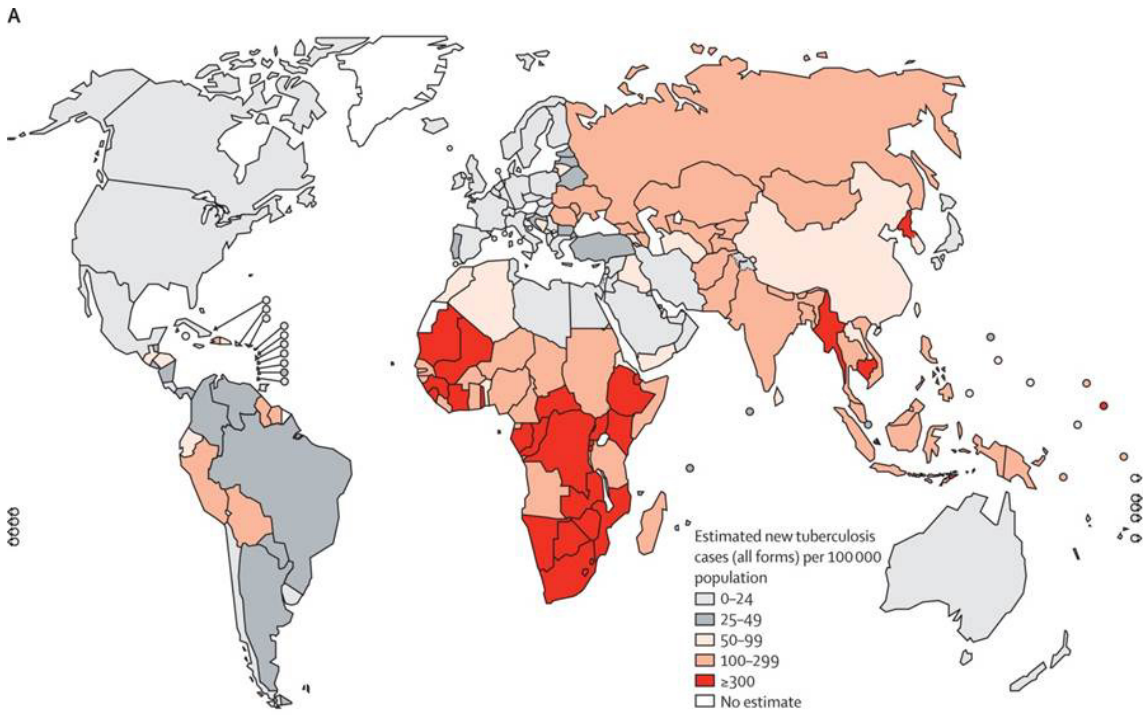

Figure 7: Estimated tuberculosis incidence rates in 2009. Figure adapted from [222].

Infection is transmitted by *Mtb*-containing aerosol droplets that are produced by coughing, spitting or sneezing of infected individuals with an active disease state. *Mtb* is (depending on virulence of the strain) highly infective so that inhalation of only few of such droplets with low amounts of germs can cause transmission [223]. The majority of infections however (90-95 %) do not progress to cause active tuberculosis but remain asymptomatic (latent TB). The lifetime chance for latently infected individuals to develop active disease is about 10 % and untreated active disease has mortality rates above 50 % [224].

The cause of TB is infection with *Mtb*, an aerobic, non-motile bacillus that was first discovered by Robert Koch in 1882. It cannot be characterized by Gram staining as the cell wall is impermeable for basic dyes but instead is described as acid-fast since it withstands decolourisation with acidic organic solvents. *Mtb* has some unique features: first, it is characterized by very slow cell division cycles of 16-20 hours. Second, the cell wall contains high levels of mycolic acids and lipids, conferring resistance to hostile environments and antibiotics, but probably also to immune recognition and eradication [225-227]. Mycobacteria that enter the respiratory system infect macrophages present in pulmonary alveoli [228]. Macrophages recognize mycobacteria as foreign by engagement of scavenger and complement receptors leading to phagocytosis of the bacteria [229]. Under normal circumstances phagosomes mature and fuse with lysosomes, leading to digestion of phagosome content. However, *Mtb* has evolved strategies to circumvent destruction by interfering with normal vesicle trafficking within macrophages and developing resistance against reactive oxygen species and acidic environments [230-233]. Instead, *Mtb* uses macrophages as primary host cells and replicates within the cells, eventually leading to cell death. Infected macrophages provoke an innate and adaptive immune response however in most cases the immune system is not able to eradicate the pathogen. Immune recognition leads to the formation of caseous granulomas, the typical manifestation of latent TB. Necrotic infected macrophages at the center are surrounded by T cells, fibroblasts, neutrophils and giant cells. Thus, latent TB is characterized by an equilibrium state between immune response and immune evasion [234]. Disturbance of this delicate balance may lead to dissemination and active TB [235, 236].

Diagnosis of active TB requires a lung X-ray and sputum cultures for verification. The slow cell division of *Mtb* prolongs time to diagnosis therefore antibiotic treatment is indicated

prior to definitive diagnosis. Diagnosis of latent TB is even more difficult. The classical tuberculin skin test has limited reliability and newly developed IFN-γ release assays did not meet expectations in sensitivity and reliability either. Thus, a "gold standard" diagnosis tool for latent TB remains elusive [237]. Treatment of active TB involves a combination therapy with the antibiotics isoniazid, rifampicin, pyrazinamide and ethambutol for two months followed by another four months of a combination of rifampicin and isoniazid [222]. The emergence of strains with primary or acquired antibiotic resistance aggravates treatment. Multi-drug-resistant TB strains (MDR-TB) are resistant to the first-line drugs rifampicin and isoniazid, while extensively drug-resistant TB strains (XDR-TB) are additionally resistant to at least three of the second-line drug classes. Cases of totally drug-resistant TB strains have also been reported [238].

The only vaccine available against TB is Bacillus Calmette-Guérin (BCG), an avirulent strain that was isolated from *Mycobacterium bovis* cultures developed by subsequent subculturing by Albert Calmette and Camille Guérin in the early 20th century. The vaccine was first used in 1921 in children and is until now the most widely used vaccine worldwide. However, it only decreases the risk of infection by about 20 % and the risk of developing active disease by about 60 % [239, 240]. BCG is also used as an immunotherapeutic agent for the treatment of bladder cancer [241]. The BCG vaccine is not successful in containing the TB pandemic, and with the rise of antibiotic resistant strains there is an immanent need for effective preventive and therapeutic vaccines for TB. The two main strategies pursued in TB vaccine research are either replacement of BCG with an improved (genetically engineered) whole-organism priming vaccine or the use of BCG in combination with a boosting subunit vaccine [242, 243]. Both concepts are currently under investigation in clinical trials [244]. Better understanding of interactions of *Mtb* and the immune system and delineation of the *Mtb* genome pave the road for new approaches in the design of genetically engineered avirulent or attenuated strains for vaccination and subunit vaccines [245-248]. One additional approach emerging from recent studies is host-directed therapy. Fine-tuning of the cellular immune response to *Mtb* infection in combination with first-line therapies showed promising first results, even in MDR- and XDR-TB [249, 250].

1.5 Aim of the study

Peptide vaccination is a promising immunotherapeutic approach not only for treatment of malignancies but also for infectious diseases. Until now, selection of targets for peptide vaccination greatly relied on classical tumor-associated antigens that are thought to play substantial roles in tumor biology and development. Only few studies used naturally presented HLA ligands as targets for vaccination in humans, thus the selection criteria for suitable targets require research-based improvements to better exploit the potential of peptide vaccines. The availability of tumor and benign tissues from RCC specimens allows for the development of a comparative approach for the selection of suitable HLA ligands for peptide vaccination. Technical improvements in mass-spectrometric analysis of HLA-binding peptides facilitate exhaustive analysis of HLA ligandomes not only of tumor but also benign tissue. HLA ligandomes could be profiled on single-patient level as well as on the level of a whole cohort of RCC patients. This may lead to a complete newly defined class of antigens, solely based on tumor-exclusive HLA presentation and irrespective of antigen function in tumorigenesis or (over-) expression in RNA profiles of tumor samples. Additionally, individual profiling might enhance possibilities of personalization of vaccine constituents based on individual tumor HLA ligandome profiles. For this purpose, HLA ligandomes of sample pairs of RCC patient tumor and benign tissues should be characterized by mass spectrometry. One special focus was on the improvement of peptide isolation and identification from normal tissues, as this objective was hampered in the past by smaller sample sizes, more difficult sample preparation and technical limitations of the mass spectrometry setup. An additional benefit of identification of HLA ligandomes of healthy tissues is that this will provide a database of the human HLA ligandome of healthy tissues in the future. This database will be of use for selection of ligandome-based peptide vaccine candidates for virtually any tumor entity, as antigens that are presented in a healthy state would represent negative selection criteria. To investigate the validity of antigen selection based on comparative profiling, a selection of peptide candidates should be tested for immunogenicity in *in vitro* priming experiments. Immunogenicity is a major hallmark for promising peptide vaccine candidates and describes the presence of antigen-specific naïve T cells in the T cell repertoire. The presence of such T cells should be verified by priming with artificial antigen-presenting

cells (aAPCS) followed by subsequent clonal expansion and detection using HLA tetramer staining and FACS analysis.

The second part of this study dealt with the identification of naturally presented HLA ligands derived from mycobacterial antigens. For this purpose, two different approaches should be applied: first, a viral vector encoding for a set of mycobacterial antigens should be used to infect a B-lymphoblastoid cell line (B-LCL). Second, monocyte-derived macrophages should be generated from PBMCs of healthy individuals for infection with a live *Mtb* strain. Knowledge of naturally presented HLA ligands derived from mycobacterial antigens might not only provide evidence for the design of peptide vaccines or subunit booster vaccines against TB, but might furthermore provide the basis for the development of TB infection screening assays with superior sensitivity and specificity.

2 Materials and methods

2.1 Materials

2.1.1 Renal cell carcinoma tissue samples

Patient tissue samples were deployed by the University's clinic for Urology Tübingen (head of department Prof. Dr. med. Arnulf Stenzl). All patients gave written informed consent for the scientific usage of resected tissues. This work is approved by the Ethics committee of the University Hospital Tübingen (Project number 27/2009BO2).Tissue samples were snap frozen in liquid nitrogen directly after surgery and stored at -80°C until further use. For each patient, malignant and benign tissue was deployed and analyzed. HLA typing was performed either by the Blood Bank Tübingen or the Section for Transplantation Immunology and Immune Hematology of the University Hospital Tübingen.

Table 3: Analyzed tissue samples of RCC patients. Listed are patient's pseudonyms, masses of malignant and benign tissue samples and HLA typing of the patients. For reasons of clarity and comprehensibility, HLA-typings with a maximum of four digits are depicted.

Sample ID	tumor mass [g]	benign mass [g]	HLA class I		HLA class II		
RCC301	2.5	2.4	A*23:01, B*14:02, C*04:01,	A*33:01, B*44:03, C*08:02	DRB1*01,	DRB1*07,	DRB4
RCC302	3.0	2.4	A*03, B*07,	A*32, B*15	DRB1*04, DRB4	DRB1*11,	DRB3,
RCC310	5.2	1.1	A*03:01, B*13:02, C*03:03,	A*30:01, B*15:01, C*06:02	DRB1*03, DRB4	DRB1*07,	DRB3,
RCC318	7.3	2.2	A*02:01, B*08:01, C*02:02,	A*24:02, B*51:01, C*07:01	DRB1*03,	DRB1*11,	DRB3
RCC330	9.0	1.6	A*03:01, B*38:01, C*12:03,	A*26:01, B*51:01, C*14:02	DRB1*04, DRB5	DRB1*16,	DRB4,
RCC352	8.5	3.3	A*24, B*35,	A*68, B*55	DRB1*12,	DRB1*13,	DRB3
RCC358	3.0	1.5	A*03:01, B*07:05, C*12:03,	A*31:01, B*18:01, C*15:05	n.a.		

Sample ID	tumor mass [g]	benign mass [g]	HLA class I		HLA class II		
RCC370	5.3	3.0	A*02, B*07	A*24,	DRB1*08,	DRB1*13,	DRB3
RCC376	16.8	4.5	A*02:01, B*44:03, C*16:01	A*03:01, C*04:01,	DRB1*07,	DRB4	
RCC385	3.0	2.0	A*01:01, B*27:05, C*03:02,	A*32:01, B*58:01, C*05:01	DRB1*13, DRB5	DRB1*15,	DRB3,
RCC792	3.1	1.4	A*02, B*15,	A*03, B*27	n.a.		
RCC349	3.0	2.0	A*24:02 B*35:08 C*03:04	B*40:01 C*04:01	DRB1*03:01, DRB4*01:01, DQA1*03:01, DPB1*14:01	DRB1*04:03, DQB1*02:01, DQA1*05:01,	DRB3*02:02, DQB1*03:02, DPB1*02:01,
RCC200	5.1	2.1	A*02:01, B*40:01, C*03:04,	A*66:01, B*41:02, C*17:01	DRB1*13:02, DRB3*03:01, DQA1*01:02, DPB1*03:01	DRB1*13:03, DQB1*03:01, DQA1*05:01,	DRB3*01:01, DQB1*06:04, DPB1*04:02,
RCC227	7.1	6.1	A*02, B*07,	A*03, B*41	DRB1*01,	DRB1*15,	DRB5
RCC441	1.0	0.2	A*01:01, B*08:01, C*04:01,	A*03:26, B*35:01, C*07:01	DRB1*03:01, DQB1*02:01, DQA1*05:01,	DRB1*13:01, DQB1*06:03, DPB1*01:01,	DRB3*01:01, DQA1*01:03, DPB1*04:01
RCC299	1.7	1.0	A*02, B*44:03,	A*26, B*49:01	DRB1*07, DRB4	DRB1*14,	DRB3,
RCC287	2.9	2.9	A*02, B*27,	A*32, B*40	DRB1*01,	DRB1*04,	DRB4
RCC1138	6.0	5.5	A*02:01, B*40:01, C*03:04,	A*68:01, B*47:01, C*06:02	DRB1*07:01, DRB4*01:01, DQA1*02:01, DPB1*15:01	DRB1*11:03, DQB1*02:02, DQA1*05:01,	DRB3*02:02, DQB1*03:01, DPB1*04:01,
RCC1147	2.5	1.2	A*02:01, B*40:01, C*02:01,	A*24:02, B*40:02, C*03:04	DRB1*13:02, DRB4*01:01, DQA1*02:01, DPB1*11:01	DRB1*07:01, DQB1*06:04, DQA1*01:02,	DRB3*03:01, DQB1*02:10, DPB1*03:01,
RCC1131	2.8	0.6	A*02:01, B*07:02, C*03:04,	A*03:01, B*40:01, C*07:02	DRB1*15:01, DRB5*02:02, DQA1*01:02,	DRB1*16:01, DQB1*05:02, DPB1*04:01	DRB5*01:01, DQB1*06:02,
RCC1148	5.6	0.4	A*01:01, B*07:02, C*07:02,	A*11:01, B*44:03, C*16:01	DRB1*07:01, DRB4*01:01, DQA1*01:02, DPB1*11:01	DRB1*13:02, DQB1*02:10, DQA1*02:01,	DRB3*03:01, DQB1*06:04, DPB1*03:01,
RCC245	1.5	1.5	A*24, B*37,	B*44:03	DRB1*08		
RCC247	5.0	3.0	A*11, B*13,	A*30, B*15	DRB1*01,	DRB1*07,	DRB4
RCC251	3.0	1.0	A*02:01, B*15:01, C*03:04,	A*03:01, B*35:01, C*04:01	DRB1*04:01, DQB1*02:02, DQA1*03:01,	DRB1*07:01, DQB1*03:02, DPB1*04:01,	DRB4*01:01, DQA1*02:01, DPB1*11:01
RCC286	5.1	2.7	A*03, B*13,	A*30, B*18	DRB1*07, DRB5	DRB1*15,	DRB4,
RCC291	8.0	1.2	A*02, B*18,	A*03, B*44:02	DRB1*13,	DRB3	
RCC1157	1.8	1.4	A*02:01,	A*24:02,	DRB1*11:01,	DRB1*15:01,	DRB3*02:02,

Sample ID	tumor mass [g]	benign mass [g]	HLA class I		HLA class II		
			B*07:02, C*02:02,	B*51:01, C*07:02	DRB5*01:01, DQA1*01:02,	DQB1*03:01, DQA1*05:01,	DQB1*06:02, DPB1*04:01
RCC381	6.5	4.1	A*02, B*39,	A*26, B*57	DRB1*07,	DRB1*08,	DRB4
RCC1154	1.6	1.4	A*01:01, B*08:01, C*02:02,	A*02:01, B*27:05, C*07:01	DRB1*03:01, DQB1*02:01, DQA1*01:01,	DRB1*01:01, DQB1*05:01, DPB1*03:01,	DRB3*01:01, DQA1*05:01, DPB1*04:02
RCC1187	2.5	2.1	A*24:02, B*18:01, C*07:01,	A*68:01, B*51:01, C*14:02	DRB1*13:01, DRB4*01:01, DQA1*01:03, DPB1*04:02	DRB1*07:01, DQB1*02:02, DQA1*02:01,	DRB3*01:01, DQB1*06:03, DPB1*02:01,
RCC1188	2.9	2.0	A*11:01, B*14:07N, C*07:01,	A*24:02, B*18:01, C*08:02	DRB1*11:01, DRB4*01:01, DQA1*05:01, DPB1*04:01	DRB1*07:01, DQB1*02:02, DQA1*02:01,	DRB3*02:02, DQB1*03:01, DPB1*03:01,
RCC1203	5.0	1.0	A*02:01, B*40:01, C*03:04,	A*68:02, B*53:01, C*04:01	DRB1*13:02, DRB3*03:01, DQA1*01:02, DPB1*04:01	DRB1*13:01, DQB1*06:04, DQA1*01:03,	DRB3*01:01, DQB1*06:03, DPB1*13:01,
RCC1223	3.7	1.9	A*02:01, B*39:01, C*03:03,	B*15:01, C*12:03	DRB1*13:01, DQB1*06:03, DQA1*01:03,	DRB1*01:01, DQB1*05:01, DPB1*04:02,	DRB3*02:02, DQA1*01:01, DPB1*03:01
RCC1248	4.2	2.6	A*03:01, B*27:05, C*01:02,	A*31:01, B*35:01, C*04:01	DRB1*11:01, DQB1*03:01, DQA1*05:01,	DRB1*01:01, DQB1*05:01, DPB1*04:02,	DRB3*02:02, DQA1*01:01, DPB1*02:01
RCC1238	1.5	1.5	A*68:01, B*44:02, C*07:04,	B*51:01, C*15:02	DRB1*13:01, DQB1*06:03, DQA1*01:03,	DRB1*01:01, DQB1*05:01, DPB1*06:01,	DRB3*02:02, DQA1*01:02, DPB1*02:01
RCC1192	2.5	2.5	A*03:01, B*08:01, C*07:01,	A*11:01, B*51:01, C*15:02	DRB1*11:01, DRB3*02:02, DQA1*05:01,	DRB1*03:01, DQB1*02:01, DPB1*02:01,	DRB3*01:01, DQB1*03:01, DPB1*09:01
RCC1198	2.4	1.8	A*02:01, B*27:05, C*01:02,	A*26:01, B*57:02, C*04:01	DRB1*01:01, DQB1*02:02, DQA1*01:01,	DRB1*07:01, DQB1*05:01, DPB1*01:01,	DRB4*01:01, DQA1*02:01, DPB1*04:01
RCC1170	2.3	1.6	A*24:02, B*35:02, C*04:01	A*68:02, B*53:01,	DRB1*13:02, DRB3*02:02, DQA1*01:02,	DRB1*11:04, DQB1*03:01, DQA1*05:01,	DRB3*03:01, DQB1*06:04, DPB1*04:01
RCC1152	5.0	2.0	A*25:01, B*07:05, C*05:01,	A*29:01, B*44:02, C*15:05	DRB1*04:01, DRB4*01:01, DQA1*05:01, DPB1*04:02	DRB1*11:01, DQB1*03:02, DQA1*03:01,	DRB3*02:02, DQB1*03:01, DPB1*04:01,

2.1.2 Healthy blood donors

Leukapheresis products (Leuka xx) and whole blood samples (J xxx) were provided by the transfusion medicine of the University Hospital Tübingen.

Table 4: Leukapheresis and whole blood samples. Leukapheresis samples were used for macrophage generation. Whole blood samples were used for CD8+ T-cell priming assays.

Sample ID	Cell count	Monocyte count	HLA class I
Leuka 03	$3.3*10^9$	$3.0*10^8$	A*02, A*03, B*35, B*44, C*04
Leuka 04	$3.5*10^9$	$3.7*10^8$	A*03, A*26, B*51, B*57, C*01, C*06
Leuka 05	$1.7*10^9$	$1.7*10^8$	A*02, A*03, B*35, C*04
Leuka 06	$5.2*10^9$	$6.0*10^8$	A*03, A*26, B*51, B*57, C*01, C*06
Leuka 07	$4.9*10^9$	$6.2*10^8$	A*02, A*28, B*51, C*01, C*02
Leuka 08	$2.8*10^9$	$2.6*10^8$	A*02, A*03, B*07, B*51
J 136	n.a.	n.a.	A*02
J 147	n.a.	n.a.	A*02, B*07
J 154	n.a.	n.a.	A*02
J 164	n.a.	n.a.	B*07
J 171	n.a.	n.a.	A*02, B*07
J 174	n.a.	n.a.	A*03, B*07
J 185	n.a.	n.a.	B*44
J 193	n.a.	n.a.	A*02

2.1.3 B-LCL cell line JY

The cell line JY originates from an Amish boy with pediatric B-cell leukemia. It was immortalized by infection with Epstein-Barr virus (EBV) and is therefore referenced as B-lymphoblastoid cell line (B-LCL). JY is homozygous for the HLA class I genes and expresses high amounts of HLA class I molecules on the cell surface. The HLA class I typing is A*02:01, B*07:02 and C*07:02. These HLA class I alleles represent some of the most common alleles in the Caucasian population. These features make this cell line a valuable *in vitro* model for HLA ligandome analysis studies. JY is cultured as suspension cell line.

2.1.4 Mycobacterium tuberculosis strain H37Rv

H37Rv is the most commonly used pathogenic laboratory strain of mycobacteria. It was first isolated in 1905 and showed high pathogenicity in guinea pig models. In 1934, the strain H37 was separated in a pathogenic ‘Rv’-strain and an avirulent ‘Ra’-strain [251]. The H37 strains have since become the reference strains for studies in the field of mycobacteria and tuberculosis. Handling of H37Rv requires a qualified laboratory of security stage 3 (S3) after Infection Protection Act. Therefore, all work with pathogenic H37Rv was performed by Stephanie Kallert of the working group of Prof. Steffen Stengert at the University Hospital Ulm in an appropriate S3 laboratory. H37Rv is cultured on Lowenstein-Jenson or Middlebrock 7H10 medium.

2.1.5 Modified vaccinia Ankara (MVA) strain MVA-TBF

MVA-TBF is a viral vector subunit-vaccine, developed to boost immune responses after BCG vaccination. MVA is an infectious living *vaccinia* strain which is unable to replicate in infected cells. It therefore can be used as a vector to vaccinate against various antigens. Since infected cells show classical behavior of virus infection, the vector itself serves as adjuvant in vaccination approaches. MVA-TBF encodes for four mycobacterial antigens:

Ag85A	mycobacterial mycol-transferase A; Rv3804c
TB9.8	ESAT-6 like protein ESXG; Rv0287
TB10.4	low molecular weight protein antigen 7 ESXH; Rv0288
Acr2	heat stress induced ribosome binding protein A; Rv0251c

A predecessor of MVA-TBF, MVA-Ag85A [252] is currently under investigation in clinical trials [253, 254]. MVA-Ag85A contains only one mycobacterial antigen (Ag85A) and was shown to be highly immunogenic [255, 256]. It was also shown to be a safe and immunogenic booster vaccine in humans in clinical phase I trials [257]. MVA-TBF was kindly provided by Helen McShane from the University of Oxford. It was stored in 10 mM Tris pH 9.0 at -80°C until use.

2.1.6 Devices

Agitator with pestle RZR 2020	Heidolph Instruments
Analytical balance AC 211 S	Sartorius
Autosampler Micro AS	Thermo Scientific
C18 Nano-LC column Acclaim PepMap RSLC, 2 µm 100 Å, 75 µm I.D. x 25 cm	Dionex
C18 Nano-LC column Acclaim PepMap RSLC, 2 µm 100 Å, 75 µm I.D. x 50 cm	Dionex
C18 Nano-LC trap column, Acclaim PepMap100, 5 µm 100 Å, 300 µm I.D. x 5 mm	Dionex
Cell culture hood	Technoflow, Integra Biosciences
Centrifuge 5415R	Eppendorf
Cold trap KF-2-110	H. Saur Laborbedarf
Cryo freezing container	Nalgene

Cryotome	Leica Biosystems
ELISA reader Spectramax 340	Molecular Devices
Flow cytometer FACS-Canto II	Becton Dickinson
FPLC system ÄKTA prime	Amersham Biosciences
Freezer -20°C	Liebherr
Freezer -80°C	Forma
Glass Econo-Columns 0.5 – 5 cm diameter for affinity chromatography	BioRad Laboratories
Incubator for agar plates	Heraeus
Incubator for cell cultures Heraeus BB 6220 CU with 5 % CO_2 gas supply	Heraeus
Light microscope	Zeiss
MACS columns and magnet	Miltenyi Biotech
Magnetic stirrer RCT basic	IKA Labortechnik
Mass spectrometer LTQ Orbitrap XL	Thermo Scientific
Mass spectrometer Q-Tof 2	Waters
Multichannel pipette 200 µl	Abimed
Nano uHPLC Ultimate 3000 RSLC nano	Dionex
Nano HPLC NanoLC 2D	Eksigent
Neubauer counting chamber, 0.1 mm depth	LO Laboroptik
Peptide synthesizer EPS 221	Abimed
pH-meter 765	Knick
Pipettes 1, 10, 20, 100, 1000 µl	Gilson
Pipettor Pipetboy acu	Integra Biosciences
Peristaltic pump LKB P-1	Pharmacia
Potter glass tubes 2, 5, 10, 20 ml	Novodirect
Precision balance	Sartorius
Quartz cuvette 10 mm layer thickness	Hellma
Refrigerator	Liebherr
Shaking incubator OMV-ROM	Infors Multitron
Small shaker Vibrax VXR	IKA
Spectrophotometer NanoDrop 1000	Thermo Scientific
Speed vac vacuum concentrator	Bachofer
Spinning wheel	Bachofer
Stirring cell system Amicon	Millipore
Tabletop centrifuge Heraeus Biofuge fresco	Heraeus
Tabletop centrifuge Heraeus Biofuge pico	Heraeus
Tabletop centrifuge Megafuge 1.0	Heraeus
Ultracentrifuge RC 5C Plus	Sorvall
Ultracentrifuge L-80	Beckman Coulter

Ultracentrifuge rotor Ti70	Beckman Coulter
Ultrasonic cell disruptor Sonifier 250	Branson Ultrasonic
UV-Vis-spectrometer Ultraspec 3000	Pharmacia
Vortex Minishaker MS 2	IKA Labortechnik
Water bath	GFL
Water distiller	Heraeus

2.1.7 Consumables

26G Needle Microlance	Becton Dickinson
50 ml reagent reservoir	Corning
96-well plates U-bottom, F-bottom	Corning
Cell culture flask 75 cm^2, 175 cm^2	Greiner bio-one
Cell scraper	Greiner bio-one
Compensation beads	Invitrogen (Life technologies)
Cryotubes 2 ml	Greiner bio-one
Cryotubes dark	Biozym
FACS tubes 5 ml	Becton Dickinson
Filter top Stericup & Steritop	Millipore
Glass bottles & beakers	Schott
Low-bind tubes 0.5, 1.5, 2 ml	Eppendorf
MACS columns LS	Miltenyi Biotec
Nano-ESI Emitter PicoTip 360/20 µm	New Objective
Parafilm	Pechiney Plastic Packaging
Petri dish	Greiner Bio-one
Pipette tips 10, 200, 1000 µl	Starlab
Pipette tips PEG-reduced Diamond, 10, 200, 1000 µl	Gilson
Reservoirs 50 ml, 100 ml	Corning Incorporated
Safe-lock tubes 0.5, 1.5, 2 ml	Eppendorf
Serological pipettes 2, 5, 10, 25, 50 ml	Becton Dickinson
Surgical disposable scalpel	Braun
Sterile filter 0.20 µm	Sartorius
Streptavidin-coated microspheres	Bangs Laboratories
Syringe-driven filter unit	Millipore
Syringe luer-lock 5 ml, 30 ml, 50 ml	Beckton Dickinson
Three-way valve for medical applications, Discofix C3	B. Braun Melsungen AG
Tubes 15, 50 ml	Greiner bio-one
Ultrafiltration unit Amicon Ultra, 10 kDa NMWL, 0.5, 4, 15 ml	Millipore

ZipTip µ-C_{18}, 10 µl	Millipore

2.1.8 Chemicals

2-(4-(2-hydroxyethyl)-1-piperazineethanesulfonic acid (HEPES)	Gibco Life Technologies
2-propanol (Isopropanol)	Merck
Acetonitrile (MS-Grade)	Thermo Scientific
Ampicillin sulfate	Roth
ATP	Sigma-Aldrich
Bacto Tryptin	Difco
Bacto Yeast Extract	Difco
Bovine serum albumin, BSA	Sigma-Aldrich
Bradford reagent, Roti Nanoquant	Roth
CD8 MicroBeads, human (130-045-201)	Miltenyi
CHAPS	AppliChem
Chloramphenicol	Sigma-Aldrich
CNBr-activated sepharose	GE Healthcare
Complete Protease Inhibitor tablet	Roche
Cyclosporin A (Sandimmun)	Novartis
D-Biotin	Sigma-Aldrich
Descosept AF	Dr. Schuhmacher GmbH
Dimethyl sulfoxide (DMSO)	WAK-Chemie
DNAse	Roche
Ethanol	SAV LP
Ethylenediaminetetraacetic acid, EDTA	Roth
FCS (fetal calf serum)	PAA Laboratories
Ficoll (Biocoll)	Millipore
Formaldehyde	Fluka
Formic acid	Merck
Gentamycin	Gibco
Glycerol	Roth
Glycine	Roth
HSA (human serum albumin)	Biotest
Hydrochloric acid (HCl)	Roth
IMDM (Icove's Modified Dulbecco's Medium)	Lonza
Ionomycin	Sigma-Aldrich
L-arginine	Sigma-Aldrich
Leupeptin	Roche
L-glutamine	Gibco (Life technologies)

LIVE/DEAD Fixable Dead Cell Stain	Invitrogen (Life technologies)
Methanol	Merck
Monosodium phosphate, NaH_2PO_4	Merck
Oxidized glutathione	Sigma-Aldrich
PBS (Phosphate buffered saline)	Gibco (Life technologies)
Penicillin (10^3 x U/ml)/Streptomycin (10 g/ml), Pen/Strep	Sigma-Aldrich
Pepstatin	Roche
PMSF (Phenylmethylsulfonylfluoride)	Roche
Reduced glutathione	Sigma-Aldrich
RPMI 1640 + 25 mM HEPES + L-Glutamax	Gibco (Life technologies)
Sodium acetate, CH_3COONa	Roth
Sodium azide, NaN_3	Merck
Sodium bicarbonate, $NaHCO_3$	Sigma-Aldrich
Sodium chloride, NaCl	VWR Chemicals
β-mercaptoethanol, β-ME	Roth
Streptavidin-PE (SAPE)	Invitrogen (Life technologies)
Trifluoroacetic acid, TFA	Applied Biosystems
Trypan blue	Gibco (Life technologies)
Trypsin/EDTA	PAA Laboratories
Urea	Roth
Water (MS-Grade)	Baker

2.1.9 Cytokines and growth factors

GM-CSF, human recombinant	R&D Systems
IL-12, human recombinant	PromoKine
IL-2, human recombinant	R&D Systems
IL-4, human recombinant	R&D Systems
IL-7, human recombinant	PromoKine
IFN-γ, human recombinant	R&D Systems
TNF-α, human recombinant	R&D Systems

2.1.10 Media, buffers and solutions

Coupling buffer	0.1 M $NaHCO_3$, 0.5 M NaCl in ddH_2O (pH 8.3)
Desalting solution	1 % (v/v) FA in H_2O (MS-Grade)
Elution solution	1 % (v/v) FA, 50 % (v/v) AcN in H_2O (MS-Grade)
FACS buffer	0.01 % NaN_3, 2 mM EDTA, 2 % FCS in PBS
Freezing medium	10 % DMSO in FCS
Injection buffer	10 mM Sodium acetate, 3 M Guanidinium chloride in

	ddH_2O
LB medium	0.5 % NaCl, 0.5 % Bacto Yeast, 1 % Bacto Trypton in ddH_2O
LB – Amp/Cam agar plate	1.5 % agar, 100 µg/ml ampicillin sulfate, 50 µg/ml chloramphenicol in LB medium
Loading solvent	0.05 % TFA, 1 % AcN in H_2O (MS-Grade)
Lysis buffer (2x)	1 tablet Roche Complete Protease Inhibitor, 400 mg CHAPS in 33 ml PBS
MACS buffer	0.5 % BSA, 2 mM EDTA in PBS
Macrophage differentiation medium	1 % Pen/Strep, 10 ng/ml GM-CSF, 5 % HS in RPMI 1640
PBS-BSA	0.5 % BSA in PBS
PBSE	1 mM EDTA in PBS
PBS-Tween	0.05 % Tween in PBS
Permwash buffer	0.01 % NaN_3, 0.1 % Saponin, 0.5 % BSA in PBS
Refolding buffer	6.97 % L-arginine in ddH_2O; pH 7.76
Resuspension buffer	0.1 % NaN_3, 1 mM EDTA, 1 mM DDT, 100 mM NaCl, 50 mM Tris in ddH_2O
Solvent A	0.1 % TFA in H_2O (MS-Grade)
Solvent B	0.05 % TFA, 80 % AcN in H_2O (MS-Grade)
TBS (Tris buffered saline)	20 mM Tris, 150 mM NaCl in ddH_2O; pH 8
TCM (T cell medium)	50 µM β-ME, 1 % Pen/Strep, 10 % HS in IMDM
Tetramer freezing buffer	48 % glycerol, 1.5 % HAS, 0.06 % NaN_3, 1x protease inhibitor in 20 mM Tris
Thawing medium	3 µg/ml DNAse, 50 µM β-ME, 1 % Pen/Strep, 10 % human plasma in IMDM
Triton buffer	0.1 % NaN_3, 1 mM EDTA, 1 mM DDT, 0.5 % Triton X 100, 100 mM NaCl, 50 mM Tris in ddH_2O
TSB (tetramer staining buffer)	50 % FCS in PBS
Urea buffer	8 M Urea, 10 mM Tris (pH 8.0), 10 mM NaH_2PO_4, 0.1 mM EDTA, 0.1 mM DDT

2.1.11 Antibodies

Anti-human CD8, mouse, clone RPA-T8, PerCP conjugated	Becton Dickinson
Anti-human CD28, mouse, clone 9.3	In house production by C. Falkenburger
Anti-human HLA class I, mouse, clone W6/32	In house production by C. Falkenburger
Anti-human HLA-DR, mouse, clone L243	In house production by C. Falkenburger

Anti-human HLA class II, mouse, clone Tü39	In house production by C. Falkenburger

2.1.12 Software

FACSDiva 6.1.3	Becton Dickinson
FlowJo v.10	Miltenyi Biotech / TreeStar
MASCOT Server 2.2.04	Matrix Science
Office 2010	Microsoft
Proteome Discoverer 1.3 / 1.4	Thermo Fisher Scientific
Qual Browser	Thermo Fisher Scientific
XCalibur 2.0.7	Thermo Fisher Scientific
GraphPad Prism 7	GraphPad Software

2.2 Protein biochemical methods

2.2.1 Synthesis of recombinant MHC class I heavy chains

HLA allele DNA sequences were modified by addition of a BirA biotinylation sequence at the C-Terminus and deletion of the transmembrane domain. The modified DNA sequences were cloned into the expression vector pET-3d. 50 µl of BL21(DE3) E. coli cells were transformed with the plasmid pLysS and co-incubated with 0.2 µl of the respective vector for 20 min on ice. Afterwards, heat shock transformation was induced by incubation in a 42°C water bath for 90 s. After transformation, samples were chilled briefly on ice before addition of 1 ml of LB medium and further incubation for 30 min in a water bath at 37°C. 100 µl of the sample were transferred onto a LB-Amp/Cam agar plate and incubated overnight at 37°C. Growing colonies were picked the next day and inoculated into 5 ml LB-Amp/Cam medium. Cultures were incubated in the shaker for 8 h at 250 rpm and 37°C. Expanded Cultures were transferred into 100 or 200 ml LB-Amp/Cam and further expanded overnight in the shaker at 180 rpm at 37°C. At the next day, ten 2 l Erlenmeyer flasks were filled with 1 l LB medium each, 1 ml ampicillin 1000x and 1 ml chloramphenicol 1000x were added and temperature was adjusted to 37°C. 15 ml of the overnight cultures were inoculated into each of the flasks and cultures were incubated in the shaker at 180 rpm and 37°C. The OD600 was measured continuously until it reached a target value between 0.4 and 0.6. Expression of recombinant proteins

was induced by subsequent addition of 0.5 µl of a 1 M IPTG solution to each flask. Cultures were incubated for 4 h before collection and centrifugation in an ultracentrifuge SLA 3000 rotor for 20 min at 5000 rpm and 4°C. Supernatants were discarded and pellets were resuspended in 180 ml of PBS and stored in six aliquots of 30 ml at -80°C. Aliquots were thawed in a water bath at RT and treated with ultrasound three times for 2 min (output 5, 50 % duty cycle). DNA was digested by addition of 150 µl of 10 mg/ml DNAse I and 300 µl of 1 M $MgCl_2$ and incubation for 20 min at 37°C. Lysates were centrifuged in an ultracentrifuge SS34 rotor for 20 min at 15000 rpm and 4°C. Supernatants were discarded, the pellets consisted of two distinct layers, the lighter, upper grey-brown layer consisting of cell debris and the denser, lower white layer consisting of inclusion bodies. The upper layer was discarded carefully by abrasion. Triton buffer was added to the inclusion bodies and the suspension was homogenized. The solution was centrifuged in an ultracentrifuge SS34 rotor for 20 min at 15000 rpm at 4°C. The washing step with triton buffer was repeated for at least three times until the inclusion body pellets became completely white. After another washing step with resuspension buffer, pellets were taken up in 20 – 40 ml of urea buffer, depending on the respective pellet size. The solution was rotated on a spinning wheel overnight at 4°C. Remaining insoluble parts were removed by another ultracentrifugation step in a SS34 rotor for 20 min at 15000 rpm and 4°C. The purity of the protein solution was determined by comparison of the OD260 and OD280 values by nanodrop measurement. The ratio had to be below 0.6 to suffice quality standards. Protein concentration was determined by Bradford assay (2.2.3) and adjusted to 2 mg/ml in urea buffer. Aliquots of 8 mg of protein were stored in cryotubes at -80°C.

2.2.2 MHC:peptide complex refolding (monomer generation)

Stable Monomers were generated by refolding of peptides to the respective recombinant HLA heavy chain and β_2-microglobulin (β_2m). Synthetic peptides were used in amounts of 2.5 – 7.5 mg at a concentration of 10 mg/ml in DMSO. Peptide solutions, 385 mg of reduced glutathione, 77.5 mg of oxidized glutathione and 250 µl of PMSF 1000x were resolved in 250 ml of refolding buffer. An aliquot (8 mg) of the respective HLA heavy chain was thawed at RT, resolved in 780 µl of injection buffer and loaded into a 1 ml syringe equipped with a 26 G needle. An aliquot (7 mg) of recombinant β_2m was resolved in

700 µl of injection buffer and loaded into another 1 ml syringe equipped with a 26 G needle. The refolding buffer solution was stirred at high speed and HLA heavy chains and β_2m were forcefully injected consecutively. Refolding solutions were incubated for 12 h at 10°C on a slow shaker. After 12 and 24 h incubation, another aliquot of the respective HLA heavy chain was added as described above. On day three, refolding solutions were filtered through a 0.22 µm membrane vacuum filter to remove protein aggregates. Afterwards, refolding solutions were transferred into a stirring cell and processed through a NMWL 30000 filter membrane under a nitrogen atmosphere with 4 bar pressure. The solutions were concentrated to approx. 25 ml volume. The retentates were stored at 4°C while the permeates were used for a second refolding process. Peptides and glutathione remain in sufficient amounts in the permeates, only PMSF 1000x, HLA heavy chains and β_2m need to be added again. Refolding and stirring cell processes were repeated as described above and the retentates were pooled. Retentates were further concentrated in a NMWL 10000 filtration tube (Amicon) at 4000 rpm and 4°C to a final volume of 5 ml. The concentrated retentates were subjected to a size exclusion chromatography on a Superdex 75 column at a flow rate of 3 ml/min of TBS. Eluates were collected in fractions of 4 ml and UV absorption at 280 nm was measured. Fractions of the monomer peak were pooled and PMSF 1000x, Leupeptin 1000x and Pepstatin 1000x were added immediately to generate a 1x final concentration. The solutions were again concentrated in a NMWL 10000 filtration tube (Amicon) at 4000 rpm and 4°C to a final volume of 5 ml. 400 µl of 1 M Tris pH 8, 25 µl of 1 M $MgCl_2$ and 250 µl of 100 mM ATP were added to the solutions and mixed by inversion. In the next step, monomers were biotinylated by addition of 10 – 20 µg BirA enzyme and 28.5 µl of 100 mM biotin to the solutions and incubation in a 27°C water bath for 12 – 16 h. After biotinylation a second size exclusion chromatography was performed as described above. Fractions from the biotinylated monomer peak were collected, pooled and PMSF, Leupeptin and Pepstatin were added to a final 1x concentration. The solutions were finally concentrated in a NMWL 10000 filtration tube (Amicon) at 4000 rpm and 4°C to a final volume of 250 – 350 µl. Protein concentration was determined by Bradford assay (2.2.3) and adjusted to 2 mg/ml with TBS. Aliquots of 50 µg Monomer were stored at -80°C until use. A sample of the biotinylated monomer product was taken for mass spectrometric analysis to ensure

peptide content of the monomers. The analysis was performed on a QTof mass spectrometer by Claudia Falkenburger.

2.2.3 Bradford assay

The Bradford assay is a colorimetric assay and one of many assays to determine protein concentrations. The advantages of the assay are high sensitivity and simplicity. Like most assays for experimental protein concentration measurement, it is rather imprecise with deviations of up to 30 % from the actual values. The accuracy of the Bradford assay depends on the content of arginine, histidine, phenylalanine, tyrosine and tryptophan of the measured proteins, as the detection reagent binds to the cationic and unpolar aromatic residues of these amino acids. The assay is based on an absorbance shift of the dye Coomassie Brilliant Blue G-250. The cationic form is red and has its absorption maximum at 465 nm, while the anionic form is blue and has its absorption maximum at 595 nm. Under acidic conditions, the dye converts to the anionic form and can bind to proteins by forming noncovalent complexes. Thus, the absorbance at 595 nm is proportional to the amount of protein in the sample. The protein concentration of a sample is determined by comparison of the measured OD595/OD465 ratio to a standard curve derived from standard protein solutions (BSA).

The assay was used to determine protein concentrations of recombinant MHC heavy chains and biotinylated monomers. Calibration curves were generated with standard solutions of BSA with concentrations of 0 µg/ml, 20 µg/ml, 40 µg/ml, 60 µg/ml, 80 µg/ml and 100 µg/ml. BSA solutions were generated using the corresponding buffers of the samples (8 M Urea for recombinant MHC heavy chains and TBS for monomers). Samples had to be diluted to generate concentrations and values that lie within the range of the calibration curve (between 1:50 and 1:400). Assays were performed in a flat-bottom 96-well plate. Measurements were performed in triplicate for each sample dilution. 5x Bradford reagent was diluted with ddH_2O to a 1x concentration and 200 µl of the solution was mixed with 50 µl of sample in each well. Assays were incubated for 5 min at RT in the dark before measurement of the OD595/OD465 ratios in an ELISA reader. Protein concentrations were calculated by comparison to the calibration curve.

2.2.4 Tetramerization of biotinylated MHC:peptide monomers

Tetramers can be used to detect T cells that express TCRs specific for a given MHC:peptide complex. Tetramers are generated by binding of biotinylated MHC:peptide complexes to streptavidin, a protein with four binding sites for biotin. Streptavidin can further be coupled to a fluorochrome, enabling its detection by flow cytometry. Tetramerization is necessary, as MHC:peptide monomers alone were shown to bind only weakly to TCRs [258]. The binding affinity is enhanced by the ability of tetramers to crosslink specific TCRs, thereby stabilizing the binding and the enhancing the staining intensity [259]. Tetramerization of biotinylated MHC:peptide complexes was achieved by conjugation with fluorochrome PE (R-phycoerithrin)-labeled streptavidin (SAPE). Since one molecule streptavidin can bind four monomers, the stoichiometric ratio for the reaction was 1:4. For one aliquot of 50 µg of a given monomer, 78.5 µl of the SAPE reagent were used to obtain the correct ratio of reactants. For maximum efficiency of the tetramerization reaction, SAPE was added in ten steps of 7.85 µl each. After each SAPE addition, samples were rotated on a spinning wheel in the dark for 30 min at 4°C. Tetramers were stored for up to eight weeks in the dark at 4°C. For longer storage times, tetramers had to be frozen in tetramer freezing buffer at -80°C. Tetramers were mixed with tetramer freezing buffer in a 3:1 ratio and aliquots of 10 – 20 µl were generated. Final concentration was 483 µg/ml for fresh tetramers and 322 µg/ml for frozen tetramers, respectively.

2.2.5 Peptide synthesis

All synthetic peptides were synthesized in-house by Patricia Hrstic, Nicole Bauer and Stefan Stevanović. Peptides were synthesized using the 9-fluorenylmethyl-oxycarbonyl/tert-butyl (Fmoc/tBu) method as described before [260]. All peptides were synthesized on the automated peptide synthesizer EPS221 (Abimed) by solid-phase peptide synthesis [261]. All peptides were qualified for purity by HPLC analysis and for identity by mass spectrometry. Peptides were stored as lyophilisates at 4°C until further use.

2.2.6 Isolation of HLA ligands from primary tissues

Isolation of HLA ligands from tissue samples is a multi-step protocol: First, tissue samples were homogenized by cutting, treatment with a tissue homogenizer and sonification. Membrane proteins were then isolated from tissue lysates by ultracentrifugation and sterile filtration. The solubilized protein fraction was subsequently processed through an immunoaffinity column to isolate MHC molecules. By acidic elution, Peptide:MHC complexes are destroyed and released from the column. The eluate was further processed through a 10 kDa filter to retain MHC chains and purify MHC ligands. MHC precipitation was performed on two subsequent days. On day one, tissue was homogenized and the immunoaffinity columns were prepared. Affinity chromatography was performed overnight. On day two, acidic elution of MHC:peptide complexes and sample preparation for LC/MS analysis were conducted. The general workflow for isolation of HLA ligands is demonstrated in figure 8.

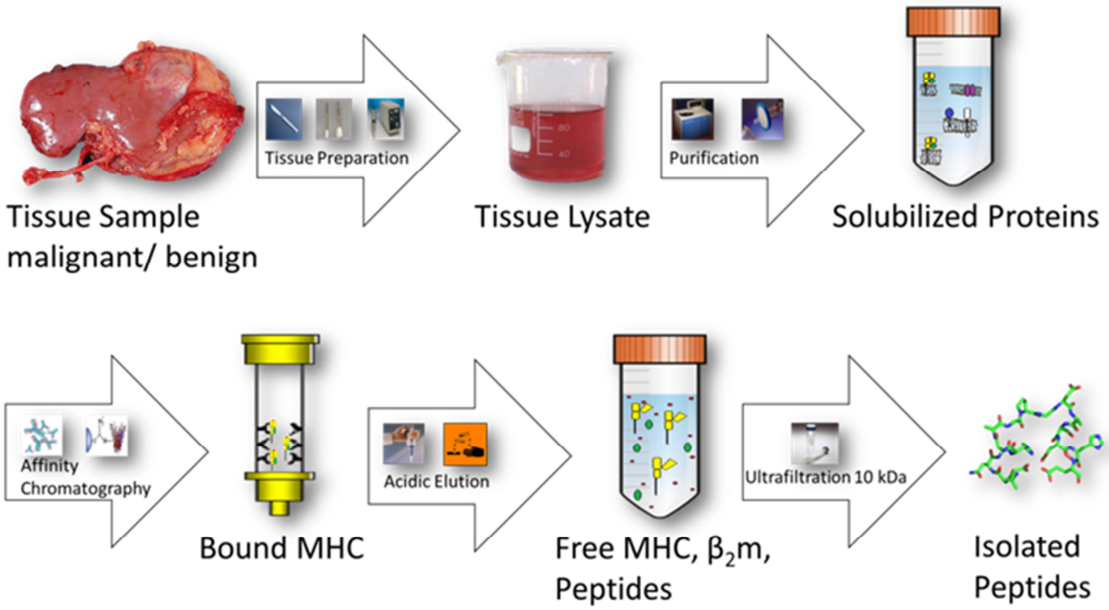

Figure 8: Workflow for the isolation of HLA ligands from primary tissue samples. Tissue samples are prepared to produce a homogenous tissue lysate. Solubilized proteins are purified by centrifugation and filtration. MHC:peptide complexes are isolated by affinity chromatography. HLA ligands and protein chains are eluted from the columns by acid addition. In a final step, HLA ligands are separated from MHC chains by size exclusion filtering. Figure from [101].

2.2.7 Manufacture of HLA affinity chromatography columns

HLA affinity chromatography columns consist of a stationary phase of CNBr-activated sepharose coupled to specific antibodies for HLA molecules of interest [262]. All steps were performed at room temperature. Centrifuge settings were 300 rpm for 5 min at RT. The ratio for coupling was 40 mg of CNBr-activated sepharose per 1 mg of antibody. CNBr-activated sepharose was weighed into a 50 ml tube, dissolved in 45 ml 1 mM HCl (in ddH_2O) and rotated for 30 min for activation of binding sites. Activated sepharose was centrifuged and supernatant was discarded carefully by pipetting. The respective volume of antibody was dissolved in coupling buffer to a total volume of 45 ml and added to the sepharose. The mixture was rotated for 2 h for coupling of antibodies to the activated sepharose. Antibody-coupled sepharose was centrifuged and supernatant was discarded carefully by pipetting. 45 ml of 0.2 M Glycine (in ddH_2O) was added to the antybody-coupled sepharose and the mixture was rotated for 1 h for blockage of remaining binding sites. After another centrifugation, removal of the supernatant and two washing steps with PBS, antibody-coupled sepharose was resuspended in the respective volume (1 ml per 1 mg of antibody) of 0.02 % NaN_3 (in PBS). Antibody-coupled sepharose was stored at 4°C for up to two months.

2.2.8 Preparation of tissue samples

The preparation of tissue samples is a crucial step for successful MHC-precipitation. It is important to produce a homogenous tissue lysate to ensure high yields of MHC ligands by precipitation. All steps were carried out in a cooling chamber at 4°C. Reaction tubes and beakers were rinsed with 1x lysis buffer every time tissue lysate was transferred to prevent loss of material. Tissue samples were directly taken from -80°C storage on dry ice to processing in the cooling chamber. Tissue samples were put into a petri dish and covered with 2x lysis buffer to prevent proteolytic reactions. Samples were cut into small pieces using forceps and scalpel. In some experiments, the cutting process was performed in a cryotome. Temperature was set to -20°C and samples were cut into slices of 10 µm thickness. The slices were directly transferred to 2x lysis buffer. Tissue pieces were then transferred to a custom glass tube. Tissue was homogenized by shearing force by a fitting pestle that is agitated by a tissue homogenizer (Potter-Elvehjem method).

Homogenization was performed with samples on ice and for several intervals to prevent heating of samples. Tissue lysate was transferred to an appropriate glass beaker. Tissue lysate was stirred for 1 h on a magnetic stirrer. Next, tissue lysate was transferred to a 50 ml tube and further homogenized by ultrasound treatment. Sonification was carried out on ice for 3 min at 150 W (medium power) and 33 % pulse frequency. Tissue lysate was transferred back to glass beakers and stirred for another 1 h. To remove cell debris, centrifugation steps were performed, depending on sample volumes:

- for volumes ≤ 20 ml, lysate was apportioned into 2 ml reaction tubes and centrifuged at 13000 rpm for 99 min at 4°C;
- for volumes ≥ 20 ml, lysate was first transferred to 50 ml reaction tubes and centrifuged at 4000 rpm for 20 min at 4°C. Supernatants were transferred to ultracentrifugation tubes and centrifuged at 40000 rpm for 70 min at 4°C.

Supernatants of the centrifugation steps were processed through a 0.2 µm sterile filter to produce final lysate for affinity chromatography.

2.2.9 Preparation of cell pellets

Preparation of cell pellets was performed according to the protocol for tissue samples however the cutting and homogenization steps are not necessary. Cell pellets were washed with PBS twice before lysis. Single cells were lysed by adding lysis buffer to the cells and shaking of lysates for 1 h on a shaker. All further steps were performed similar to the protocol for tissues (2.2.8). For *Mtb*-infected Macrophages, all steps were performed in a qualified S3 laboratory at the University Hospital Ulm. The generated lysates were subjected to a sterility test and were stored at -20°C for the duration of the test (2 weeks). As soon as sterility was verified, lysates were released for shipment on dry ice from the University Hospital Ulm to the Department of Immunology Tübingen. Here, lysates were thawed and processed to HLA affinity chromatography.

2.2.10 HLA affinity chromatography

Affinity chromatography of MHC molecules was performed overnight at 4°C in a cooling chamber. Columns were filled with appropriate amounts of antibody-coupled sepharose.

For this purpose, stored coupled sepharose was resuspended and transferred to the columns. 1 ml of the solution is equivalent to 1 mg of antibody and 1 mg of antibody was used per 1 mg of tissue or 1 ml of cell pellet, respectively. Affinity columns with different HLA specificities were connected in series by tubings with luer-lock connections. The column series was connected to a peristaltic pump and the system was washed for at least 30 min linearly with PBS. This step is also useful to detect leakages in the system. The system was then equilibrated with 1x lysis buffer before injection of the lysate. The system was closed to a circular system by placement of the suction and outlet tubes in the tissue lysate reaction tubes. Tissue lysate was circulating through the column system overnight at a low flowrate between 1 – 3 ml/min. At the next day, the system was rebuilt from circular to linear and lysate was washed out by injection of PBS. Lysate was collected and stored at 4°C until final assessment of results of the respective samples. The system was purged linearly with PBS for at least 30 min and afterwards with ddH_2O for at least 60 min. After the washing steps, columns were let run dry and collected for acidic elution.

2.2.11 Elution of HLA affinity chromatography columns

MHC:peptide complexes were eluted from the columns by addition of trifluoroacetic acid (TFA). Noncovalent bonds between antibodies and MHC molecules and between MHC molecules and bound peptide ligands are disrupted by lowering of the pH value. All steps were performed at 4°C in a cooling chamber. Column matrices were covered with 0.2 % TFA (approximately 40 µl per 1 mg of antibody). For the first elution, the pH value was further lowered by addition of 1 µl of 10 % TFA per 1 mg of antibody. Columns were incubated for 20 min on a shaker. Eluate was recovered from the columns by applying air pressure through a tubing-connected 50 ml syringe. The elution step was repeated for eight times to maximize recovery of MHC ligands from the columns. Eluates were collected in NMWL 10000 ultrafiltration units (Amicon) and centrifuged at highest speed for at least 30 min at 4°C. Amicons were washed three times with 3 ml of solvent A before usage (4000 rpm, 15 min at RT). Peptide ligands pass the molecular sieve whereas MHC chains and antibodies are retained. Retentates were stored for further experiments at -80°C. The flowthroughs were frozen at -80°C and lyophilized. Lyophilisates were taken up in 250 – 500 µl of solvent A and transferred to low-bind Eppendorf tubes (1.5 ml volume). Samples were concentrated by vacuum centrifugation to volumes between 10 and 30 µl.

2.2.12 Sample preparation for LC-MS/MS

Samples had to be cleaned and desalted prior to LC-MS/MS measurement. For this purpose, ZipTip$_{\mu\text{-}C18}$ columns were used. These 10 µl pipette tips contain a C_{18}-matrix with a capacity of 2 µg to bind peptides by hydrophobic interactions. ZipTips were washed 10 times with 10 µl elution solution and equilibrated 10 times with desalting solution. Peptides were loaded onto the ZipTip by pipetting samples up and down 10 times. Samples on ZipTip columns were desalted 5 times with 10 µl desalting solution. For elution of peptides, 25 µl of elution solution were put into an autosampler vial and elution solution was pipetted 10 times through the ZipTip columns. For each sample, the whole ZipTip procedure was repeated for 10 times. Samples were then concentrated in a vacuum centrifuge to a volume of 5 µl and resolved in appropriate volumes (depending on quantity of planned measurements) of loading solution.

2.3 Mass spectrometry

Mass spectrometry is an analytical method to determine mass-to-charge ratios of ionized molecules. Technical improvements have made it the technique of choice for the analysis of samples with high complexity. The combination of features like high mass accuracy, speed and sensitivity is superior to any other analytical method for complex mixtures of biomolecules. Modern LC-MS experiment setups reduce the complexity of samples by on-line coupling of a high performance liquid chromatography (HPLC) to the mass spectrometer. Molecules are separated on a column by hydrophobicity and delivered to the mass spectrometer in a continuous nanoflow. Identical molecules are thereby focused and can be measured at the same time, which increases the identification probability. The detection limit of modern instruments for peptides lies in the sub-femtomolar range.

2.3.1 Nanoflow reversed-phase (u)HPLC

Two different RP-HPLC systems were used for this work: a Nano-LC 2D-HPLC (Eksigent) and an UltiMate 3000 RSLC Nano-uHPLC (Dionex). The principle of analyte separation by hydrophobic properties of the peptides is similar for both systems: the setup consists of a sample loop for acquisition, a precolumn for concentration and a C_{18} stationary phase

column for separation of the samples. Peptides bind to the stationary phase by hydrophobic interactions. They are eluted by continuously increasing proportions of non-polar solvents in the mobile phase. Thus, peptides with higher hydrophobicity elute later from the column than hydrophilic peptides. This leads to considerations for the gradient settings: a steep gradient can lead to the co-elution of peptide fractions, while a flat gradient might broaden peptide peaks. The first could overload the mass spectrometer with too many peptide species at a time, while the latter might cause undercut of the detection threshold. Both events can lead to a decrease of identified peptide species in the sample. One way to increase separation performance is the reduction of particle size of the matrix within the separation column. Another possibility is to increase the theoretical floor count by extension of the column length. This leads to higher peak capacity and better separation of co-eluting peaks. However, both measures also increase the backpressure of the system, making more powerful pumps for the delivery of the mobile phase a requisite. The UltiMate 3000 RSLC Nano-uHPLC is the superior system with supported pressures of > 800 bar and columns with particle sizes ≤ 2 µm and lengths ≥ 50 cm. Due to the low flowrates in nanoflow HPLC systems, equilibration of the separation column during gradient operation takes time. As a consequence, peptide fractions are focused and take more time to pass through the separation column than the actual flowrate, whereby retention times are delayed. Another variable influencing retention times is temperature. Therefore, most modern systems are equipped with a column oven to ensure retention time reproducibility. Eluting peptide fractions are transferred through a capillary from the separation column to the PicoTip, an accurately extended capillary. The PicoTip is faced towards the interface of the mass spectrometer. Here, the mobile phase leaves the HPLC system and solved peptide fractions are ionized for measurement.

2.3.2 Electrospray ionization

Electrospray ionization (ESI) is a gentle ionization technique which is most suitable for the analysis of biomolecules [263, 264]. Mass spectrometers can only measure charged molecules, therefore peptides have to be ionized prior to measurement. For this purpose the solvent needs to be electrically conductive and contain acid. Biomolecules are protonated by the acidic solvent and thereby gain positive charges. To guide ions into the

mass spectrometer, a high voltage from 1.6 – 2.2 kV is applied between the PicoTip and the interface plate of the mass spectrometer. As the analyte solvent enters this electric field, cations become accelerated towards the negative counter pole at the mass spectrometer interface. This leads to an excess of positively charged molecules at the tip of the emitter, producing a fine aerosol by charge repulsion, the Taylor cone. The ESI source of most mass spectrometers further support the application of sheath gas (nitrogen) in coaxial direction to the electrospray emitter to facilitate formation of droplets and curtain gas (heated nitrogen) in vertical direction to the electrospray emitter to support evaporation of the solvent and prevent entrance of neutral particles. The MS interface and the transfer capillary are heated to 200°C to aid solvent evaporation, whereby charged droplets become smaller in size but maintain the same amount of charged molecules. The droplets eventually reach their Rayleigh limit, a point at which the electrostatic repulsion of the cations becomes stronger than the surface tension of the droplets. At this point, the droplets become instable and a process known as Coulomb fission occurs, in which the droplets explode into many smaller and more stable droplets. Repetitive Coulomb fissions further reduce the size of the droplets. The production of single gas-phase analyte ions is described by two controversial models [265]:

- The ion evaporation model (IEM) proposes emission of single ions from small droplets by increasing charge density at the surface [266].
- The charged residue model (CRM) proposes continuous evaporation and Coulomb fission cycles, until droplets with single ions emerge [267].

Smaller molecules form single analyte ions in the gas-phase more likely by IEM, while larger molecules produce these ions by CRM. ESI mostly produces multiply charged ions $[M+nH^+]^{n+}$, charge states are dependent on molecule size. For MHC-bound peptides with masses between 800 and 2000 Da, charge states usually range from 2+ to 4+.

2.3.3 Tandem mass spectrometry

All measurements in this work were performed on a LTQ Orbitrap XL. The machine consists of five main parts, as shown in figure 9. The unique advantage of the machine is its feature to perform tandem mass spectrometry [268]. This is possible due to the fact

that two distinct mass analyzers are integrated in one machine: the linear ion trap (LTQ) with relatively low mass accuracy but high sensitivity and the Orbitrap with superior mass accuracy. These features qualify the LTQ Orbitrap XL for the discovery of thousands of unique peptide species from a complex mixture. In the following paragraph, the duty cycle for measurements in this instrument is explained.

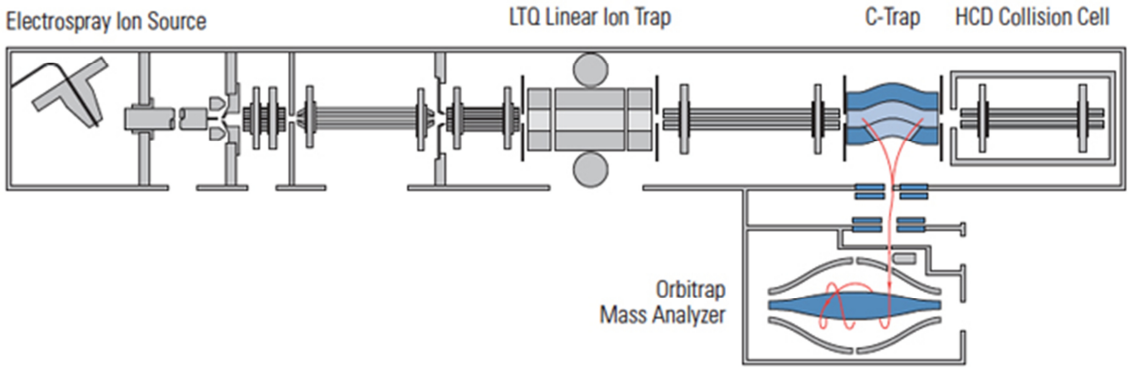

Figure 9: Schematic depiction of the LTQ Orbitrap XL. The five main parts of the machine are depicted. The ion current is produced by the ESI source and enters the mass spectrometer through the transfer capillary. It passes the first two quadrupoles and enters the LTQ. Here, it is accelerated into the C-Trap. In the C-Trap, ions are decelerated and collected. The focused ion cloud is injected into the Orbitrap mass analyzer to perform high resolution survey scans with high mass accuracy. The most intense precursor ions detected in the survey scan are selected for further analysis in the LTQ. The selected precursor ion species are consecutively collected in the LTQ for fragmentation and measurement of fragment ions. Survey scans and measurements in the LTQ can be performed simultaneously. Analysis of fragment ions with high mass accuracy can be performed by fragmentation of ions in the HCD collision cell and subsequent measurement in the Orbitrap mass analyzer. Source: http://planetorbitrap.com/data/fe/image/LTQXL_Schema(1).png (figure adapted from [269]).

The ESI source creates a continuous ion current that enters the mass spectrometer through the transfer capillary. From this point on, a high vacuum (< 10^{-5} Torr) is applied. The ions are focused by a system of electromagnetic lenses and pass through two quadrupoles to enter the LTQ. The ion current passes the LTQ in axial direction and is transferred through another quadrupole into the second ion trap, the C-Trap. Ion traps can trap ions in electric fields created by superposition of a direct current (DC) voltage and a high-frequency alternating current (AC) voltage. The C-Trap functions as an ion distributor between the LTQ, the HCD collision cell and the Orbitrap. Deceleration of ions is achieved by the electric trap field and the collision with N_2 dampening gas within the trap. Thereby, focused ion packages form and are subsequently injected into the Orbitrap mass analyzer. The Orbitrap consists of a spindle-shaped central electrode and an outer

electrode with two bell-shaped parts that are connected by a ceramic ring (figure 10). The analyte ions are injected orthogonally to the central electrode and start to constantly orbit it within the electric field. Eccentric introduction causes them to oscillate orthogonally to the inner electrode along the z-axis (figure 10).

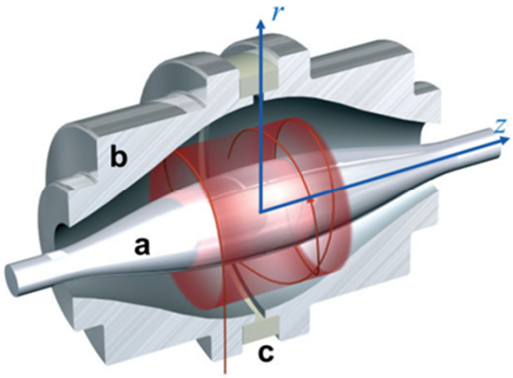

Figure 10: Cut-away model of the Orbitrap mass analyzer. The Orbitrap is built of an inner spindle-shaped electrode (a) and an outer barrel-shaped electrode (b). The outer electrode consists of two parts, connected by an isolating ceramic ring (c). Analyte ions are injected orthogonally to the z-axis and decentrally. The central electrode (a) produces an electric field, causing the ions to constantly orbit the electrode (r = constant). The oscillation frequencies of the ions along the z-axis correlate with their respective m/z values. THhe oscillations cause an image current at the outer electrode (b). Figure from [269].

The oscillating ions generate a measureable image current at the outer electrodes. This current is produced by all ion species present in the Orbitrap at a given time point, thus the signal needs to be decomposed by Fourier transformation. The frequency of harmonic oscillations of an orbital trapped ion correlates directly with its m/z value: $\omega = \sqrt{\left(\frac{z}{m}\right) * k}$ (where ω is the angular velocity, z is the charge, m is the mass and k is the curvature of the field, a device constant) [270]. The identification of m/z values with this technique has two major advantages: first, the high mass accuracy for exact determination of m/z values of analyte ions. Second, the extremely high resolution allows differentiation of ions with almost similar m/z values. The mass accuracy of the Orbitrap is 3 ppm (parts per million), meaning for the measurement of a molecule with 1 kDa molecular weight, the deviation would not exceed 0.003 Da. The resolution is 60000 at an m/z value of 400, meaning the differentiation of two ions with m/z values differing in $\frac{1}{60000}$ is possible. The “survey scan” performed in the Orbitrap identifies the m/z values of all ion species present at a given time point. However, absolute molecular masses of peptides are not sufficient for

unambiguous identification of peptide sequences. For this purpose, peptides have to be fragmented and mass spectra of the fragments need to be measured. Precursor ions for fragmentation are selected according to the settings of the instrument software (data dependent acquisition, DDA). Selection of ions with defined m/z values for measurement in the LTQ is achieved by a quadrupole. It consists of 4 parallel rod electrodes with opposite electrodes charged identically to apply an alternating electric field (see figure 11). The voltage between neighboring electrodes consists of direct current and high frequency alternating current. By adjustment of the voltages, the alternating electric field is influenced to grant passage to ions with defined m/z values on a stable trajectory. Ions with differing m/z values have an instable trajectory, collide with the electrodes and are discharged [271].

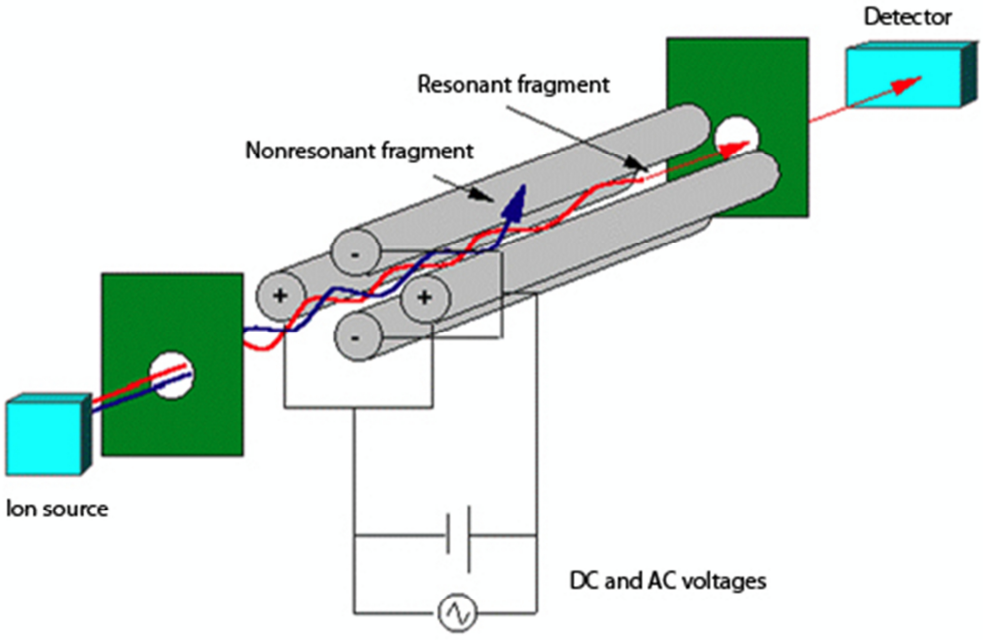

Figure 11: Schematic of a quadrupole mass analyzer. Voltages can set stable trajectories for ions with defined m/z values. Source: https://www.chromservis.eu/i/gc-ms-tof-description?lang=EN, 16.02.2018.

Selected ions pass the quadrupole and are decelerated and trapped in the LTQ. The linear ion trap consists of a quadrupole and two end electrodes. The ions get trapped in a potential well between the two-dimensional electric field of the quadrupole and the static potentials of the end electrodes. Undesired ions are removed by application of multi-frequency resonance ejection waveforms. These ions get resonantly activated, start to

oscillate and are ejected from the LTQ [272]. The energy of the selected precursor ions is subsequently increased by application of their respective resonance excitation voltage. This causes oscillation and, by collision with inert gas atoms, dissociation (fragmentation) of the ions, a process called collision-induced dissociation (CID) [273]. Fragment ions are maintained within the ion trap. Measurement of the fragment ions is accomplished by linear increase of the RF voltage, whereby ions become instable and are ejected from the trapping field. The m/z values of ejected ions increase with increasing RF voltage. The ejected ions reach the detector: two conversion dynodes, where they produce secondary electrons. These electrons are detected by two secondary electron multipliers to generate an amplified signal.

The strategy of identification of precursor masses with high mass accuracy and resolution and of fragment ions with lower mass accuracy but high sensitivity is referenced as the "high-low-strategy" [274]. In combination with dynamic exclusion, it is the superior method for the identification of HLA ligands from complex mixtures. The dynamic exclusion excludes precursor ions from measurement for a specified time after their first selection/measurement. In this way, less abundant co-eluting ions can be measured. The high sensitivity of the LTQ enables the generation of fragment spectra from low ion counts.

2.3.4 Experimental setup

In this passage, the settings for the performed LC-MS/MS measurements are elucidated. Samples were taken up in appropriate volumes of loading solution in an autosampler vial. One acquisition consumed 5 µl of sample, usually 20 % sample shares were measured (i.e. samples were taken up in 25 µl of loading solution). The autosampler vials were put into a tempered autosampler in a defined position. Samples were aspired by a needle into a 10 µl sample loop using the "sandwich method": prior and after the sample volume, loading buffer was aspired into the sample loop.

For the Eksigent nanoLC 2D, samples were loaded for 30 min with a high flowrate of 20 µl/min (solvent A) from the sample loop onto a 5 mm PepMap 100 C_{18} Nanotrap column. Peptides were subsequently loaded and separated on a 25 cm PepMap C_{18} column with 3 µm particle size. Separation was performed at RT. The

isocratic gradient ranged from 0–55 % of solvent B within 120 min at a flow rate of 300 nl/min.

For the Dionex UltiMate3000 RSLCnano, samples were loaded for 5.75 min with a high flowrate of 4 µl/min (3 % solvent B) from the sample loop onto a 2 cm PepMap 100 C_{18} Nanotrap column. Peptides were subsequently loaded and separated on a 25 or 50 cm PepMap C_{18} column with 2 µm particle size. Separation was performed at 50°C. The isocratic gradient ranged from 2.4-32 % of solvent B within 140 min at flow rates of 175 - 300 nl/min.

For the LTQ Orbitrap XL, DDA mode was used. Survey scans were performed with 1 s scan time in the Orbitrap mass analyzer. Ions were collected for 500 ms in the C-Trap before injection. Survey scans were conducted with a resolution of 60000 and a range of 400–650 m/z for class I peptides and 300–1500 m/z for class II peptides. The five most intense mass peaks with a charge between 2^+ and 3^+ (for class I peptides) and ≥ 2^+ (for class II peptides) from each survey scan were selected as precursor masses for subsequent fragmentation and measurement of fragment spectra in the LTQ (top five method [275]). Ions of each of the top five peptide species were collected for 200 ms. Peptides were fragmented by CID (normalized collision energy 35 %, activation time 30 ms, isolation width 1.3 m/z). Dynamic exclusion was enabled (exclusion list size 500) and set to values between 3–5 s.

2.3.5 Computational processing of raw data

Mass spectrometry data is stored in RAW-files, all information obtained in one measurement is contained in the file. The dataset covers information of all survey scans, selected precursor masses with respective retention times and all fragment scans. Thousands of fragment spectra are usually generated in one MS-run, therefore software-based evaluation of the raw data is indispensable. The software ProteomeDiscoverer 1.4 (Thermo Fisher Scientific) was used for processing of raw data. MS^1 spectra and corresponding fragment spectra were transmitted to a local MASCOT server (MASCOT 2.2.04, Matrix Science) and compared to theoretical fragment spectra of the entire proteome. A probability-based algorithm annotates experimental spectra to theoretical spectra [276]. The algorithm MOWSE (molecular weight search) was initially programmed

for processing of mass spectrometry data of proteolytic protein digests [277]. The 'SWISS-PROT' database (www.uniprot.org, release date 27.09.2013) [278] was used for generation of theoretical precursor and fragment spectra of the respective taxonomy (*homo sapiens*, *vaccinia virus* and *mycobacterium sp*.). Data of technical replicates was combined for processing. Further settings for data processing were:

1. Precursor mass tolerance 5 ppm
2. Fragment mass tolerance 0.5 Da
3. Signal-to-noise ration ≥ 3
4. No enzymatic cleavage specificity
5. Oxidized methionine allowed as dynamic modification
6. Protein grouping disabled
7. Rank 1 peptides only

The quality of the resulting peptide sequences was assessed by two computational parameters, the false discovery rate (FDR) and the Ion Score. The FDR was determined by the percolator algorithm [279] by processing of data against a decoy database that consisted of a shuffled version of the target database. All peptide identifications with a value of $q \geq 0.05$ were discarded from the result lists (5 % FDR). The IonScore S (or MASCOT score) is another parameter indicating the probability P that the matching of a theoretical and an experimental fragment spectrum is a stochastic event:

$$S = -10 * \log P$$

The IonScore inversely correlates with a high error probability of spectrum annotation, therefore all peptide identifications with $S \leq 20$ were discarded from the result lists. Precursor ions of HLA peptide ligands are usually charged 2^+, fragmentation of these ions results in two 1^+ charged ions or one 2^+ charged ion and one neutral fragment (neutral loss, not measureable). Ions with a charge at the N-terminus are termed a-, b- and c-ions, while ions with a charge at the C-terminus are termed x-, y-, and z-ions. The index indicates the number of remaining amino acid residues of the fragment. An ion may break at two sites, resulting in internal fragments. Further breaks include loss of H_2O (indicated

by ^{0}) or NH_3 (indicated by *) [280, 281].The nomenclature of peptide fragments is depicted in figure 12.

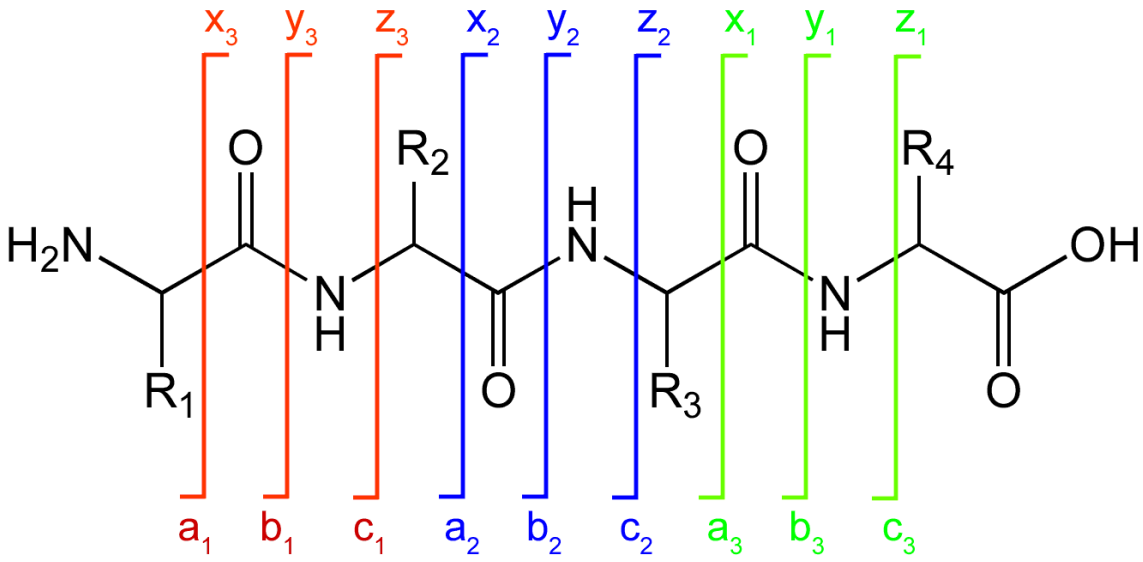

Figure 12: Peptide fragmentation and nomenclature of fragment ions. Ions with a charge at the N-terminus are termed a-, b- and c-ions, while ions with a charge at the C-terminus are termed x-, y-, and z-ions. Source: http://upload.wikimedia.org/wikipedia/commons/f/fb/Peptide_fragmentation.gif, 16.02.2018.

Collision induced fragmentation preferentially induces breaks at the peptide bond, resulting in b- and y-ions. Thus, a more or less complete series of b- and y-ions within an experimental spectrum will result in a lower probability of false annotation and therefore in a high IonScore. However, since processing algorithms were initially programmed for the identification of proteolytic peptides (with tryptic digest motif R or K at the C-terminus), several drawbacks for the identification of HLA ligands are inherent. CID induces breaks at the weakest molecular bonds, resulting in preferential fragmentation prior to proline, aspartate and glutamate. This may lead to low intensities or complete loss of other ions resulting in lower IonScores. Additionally, internal fragments may occur in peptides with hydrophobic amino acid residues at the C- or N-terminus with adjacent charged amino acids, which is the case for some HLA binding motifs. Molecular masses and m/z values of internal fragments can be calculated by *in silico* fragmentation using the software ProteinProspector (http://prospector.ucsf.edu/prospector/mshome.htm). However, internal fragments are not considered for annotation by the ProteomeDiscoverer software. These remaining “unexplained” peaks in the fragment

spectrum lead to decreased IonScores. Other sources of unexplainable peaks may be interference with ions originating from other precursors or from ubiquitous contaminants like polyethylene glycol (PEG), polypropylene glycol (PPG), polysiloxanes and detergents (CHAPS, Triton). Those contaminant peaks can be identified by comparison with a list of ubiquitous contaminants in mass spectrometry [282]. False negative peptide identifications could be verified by manual validation using those information however this was not possible given the size of the datasets.

Further filters were applied to the processed datasets: Peptide length was limited to 8–12 amino acids for MHC class I ligands and 12–25 amino acids for MHC class II ligands. Finally, HLA annotation of MHC class I ligands was performed using SYFPEITHI [77]. Peptides that could not be assigned to a given HLA typing of the respective sample were discarded.

2.4 Cell biological methods

All steps for cell culture experiments were conducted under sterile conditions. Cells were cultured in incubators with constant parameters: a humidified atmosphere with 7.5 % CO_2 at 37°C. Culturing of *Mtb*-infected macrophages was performed in an approved S3 laboratory at the University Hospital Ulm.

2.4.1 Isolation of PBMCs from leukapheresis products and whole blood samples

Peripheral blood mononuclear cells (PBMCs) consist of cells of the lymphoid line (T cells, NK cells, B cells) and monocytes. PBMCs can be isolated from peripheral blood by density gradient centrifugation. To achieve separation of PBMCs, blood is layered over a dense sugar solution (Ficoll-Hypaque). During centrifugation, the more dense blood components pass the sugar solution, while the more lightweight ones remain on the top. This leads to separation of blood plasma and thrombocytes (top), PBMCs (intermediate) and granulocytes and erythrocytes (bottom). Whole blood samples were transferred to 50 ml tubes and centrifuged for 20 min at 2000 rpm and RT w/o brake to separate blood plasma. Plasma (top layer) was carefully taken off and transferred to 50 ml tubes. Plasma samples were heat-inactivated for 30 min in a 56°C water bath. Plasma samples were

subsequently centrifuged twice for 15 min at 2500 rpm and RT. The pellets were discarded (denatured proteins and complement factors). The serum samples were frozen at -20°C and later used in T cell priming experiments as autologous cell culture supplement. The remaining phase of PBMC, erythrocytes and granulocytes, as well as leukapheresis products were diluted 1:2 with PBS prior to PBMC isolation. 50 ml tubes were prepared with 15 ml of Ficoll and 35 ml of the diluted blood samples were carefully layered over the Ficoll solution. Tubes were centrifuged for 30 min at 2000 rpm and RT w/o brake. After centrifugation, the intermediate PBMC layers were collected and pooled in 50 ml tubes. PBMCs were washed three times with PBS with intermittent centrifugation steps with decreasing speed (10 min at 1500 rpm, 1300 rpm, 1100 rpm and RT). Cells were counted after isolation and could be used for further experiments.

2.4.2 Cell counting

Cells were counted microscopically in a glass Neubauer cell counting chamber with 0.1 mm depth. Counting chamber and cover glass were cleaned and dried prior to counting. The chamber was assembled by moisturizing the chamber and application of the cover glass with pressure until formation of Newton rings at the contact surfaces could be observed. This ensured the correct volume of the counting chamber. Cell suspensions were diluted with PBS to concentrations eligible for manual counting. Cell dilutions were then mixed 1:1 or 1:10 (depending on cell concentration) with 0.05 % trypan blue (in PBS) for staining of dead cells. 10 µl of the mixture were pipetted into the counting chamber and cells were counted manually in two opposite large squares (each 1 mm^2) under the microscope. Cell count was determined by the formula:

$$\text{cell count} = \frac{\text{cell count total}}{\text{\# of counted large squares}} * \text{dilution factor} * \text{chamber factor } (10^4) * \text{volume cell suspension}$$

2.4.3 Cell freezing and thawing

Cells were harvested by centrifugation for 5 min at 1300 rpm and RT. Pellets were resuspended in appropriate volumes of cold freezing medium (5–10*10^6 cells/ml) stored in aliquots of 1–2 ml in cryotubes. Tubes were transferred into a cryo freezing container

with isopropanol isolation to provide a constant temperature decline of ~1°C/min. Freezing containers were stored at -80°C.

For thawing of cells, aliquots were taken from -80°C and thawed slowly until a visible frozen ice core remained in the tubes. Aliquots were then taken up in 10 ml of thawing medium and centrifuged for 5 min at 1500 rpm and 4°C. These steps were performed quickly to avoid cell damage by freezing medium components (DMSO). The supernatants were discarded and cell pellets were washed in 10 ml of thawing medium and centrifuged again for 5 min at 1500 rpm and 4°C. Cell pellets were then resuspended in the respective culture medium at appropriate culturing densities.

2.4.4 Infection of B-LCL with MVA-TBF

The cell line JY was cultured as suspension culture in RPMI 1640 supplemented with 10 % heat-inactivated FCS and 1 % Penicillin/Streptomycin (P/S). Medium was changed after two days and cultures were split once a week. For infection, cells were harvested and washed twice with PBS (centrifugation for 10 min at 1300 rpm and RT). Cells were counted and adjusted to $1*10^9$ cells/ml of PBS. Cell suspensions were mixed with respective amounts of MVA-TBF to achieve a MOI (multiplicity of infection) of 5. The suspensions were incubated gently shaking for 1 h at 37°C. Afterwards, suspensions were supplemented with warm culture medium ($1*10^8$ cells/ml) and incubated for 12 h. Cells were then harvested and washed twice with PBS (centrifugation for 10 min at 1300 rpm and RT). The cell pellets were either directly subjected to lysate generation for HLA affinity chromatography or snap frozen at -80°C until further use. For the “starvation experiment”, the aim was to induce autophagy and thereby cross presentation of *MVA*-derived peptides on MHC class II. For this experiment, JY cells were incubated prior (3 d) and after infection in medium w/o FCS supplement.

2.4.5 Generation of macrophages from PBMC

Macrophages were generated from PBMC of leukapheresis products derived from healthy blood donors. Macrophages can be generated by differentiation of monocytes (monocyte-derived macrophages, MDM). PBMCs of healthy individuals consist to 10-15 %

of monocytes. Monocytes were isolated from PBMC by an adherence step. PBMCs were adjusted to $1*10^7$ cells/ml of culture medium (RPMI 1640, supplemented with 5 % HS) and transferred to 250 cm^2 cell culture flasks. The adherence step was performed for 90 min with 20 ml of cell solution per culture flask and horizontal (maximum adherence surface) incubation. Non-adherent cells were removed, washed twice with PBS (centrifugation for 10 min at 1300 rpm and RT) and cryopreserved. The remaining adherent cells were rinsed twice with PBS in the culture flasks before 30 ml of macrophage differentiation medium was applied. Monocytes were differentiated into macrophages by culturing the cells for 5±1 days in the presence of 10 ng/ml GM-CSF.

2.4.6 Infection of macrophages with H37Rv

The macrophage cultures were transported to the University Hospital Ulm for infection with mycobacteria in an appropriate S3 laboratory. Here, cells were harvested using a cell scraper and counted. Cells were adjusted to a concentration of $1*10^7$ /ml in culture medium w/o GM-CSF and antibiotics (RPMI 1640 with 10 % HS). Bacteria were thawed and incubated for 10 min in an ultrasound bath. Afterwards, bacteria were added to the cell culture with a MOI of 5 and cultures were incubated for 1-3 days. After infection, cells were harvested and processed for lysate generation (2.2.9).

2.4.7 Magnetic activated cell sorting (MACS) of CD8+ T cells

Cell sorting by MACS relies on surface expression of protein markers on target cell populations. In most cases these are CD molecules however techniques for activation markers and cytokines are also available. Superparamagnetic nanoparticles coated with antibodies against the desired surface markers are used for cell labelling. After incubation of the cells with the magnetic particles, the solution is loaded onto a column that is placed in a strong magnetic field. Labelled cells are retained in the column by magnetic attraction, while all other cells pass through. The sorted cells can then be recovered from the column by removal of the magnetic field. Cell separation was performed according to the manufacturers' protocol. All steps were performed under sterile conditions on ice or at 4°C, using cold buffers. PBMCs were harvested in a 50 ml tube and washed in cold MACS buffer and centrifuged for 10 min at 1300 rpm and 4°C. Cell pellet was resuspended

in 80 µl of MACS buffer per 10^7 cells. 20 µl of CD8 MicroBeads were added per 10^7 cells and the mixture was incubated for 15 min at 4°C for cell labelling. Afterwards, cells were washed by addition of MACS buffer to a total volume of 50 ml. Cells were centrifuged for 10 min at 1300 rpm and 4°C. The pellets were resuspended in in 500 µl of MACS buffer per 10^8 cells. Depending on cell counts, variable amounts of separation columns were used, as the LS column has a maximum capacity of $2*10^9$ cells. LS columns were placed in a MACS separator and rinsed with 3 ml of MACS buffer. After rinsing, cell suspensions were applied to the columns. Flow through was collected separately and the columns were washed trice by addition of 3 ml of MACS buffer. Columns were subsequently removed from the magnetic separator and placed on a collection tube. Sorted cells were flushed from the column by addition of 5 ml of MACS buffer and firmly pushing the plunger into the column. After cell counting, cells were harvested for further experiments.

2.4.8 *In vitro* priming of CD8+ T cells with artificial APCs

The immunogenicity of HLA peptide ligands can be assessed by T cell priming experiments. Briefly, immunogenicity describes the presence of naïve T cells expressing a T cell receptor complementary for a certain HLA:peptide complex in the T cell repertoire and the ability of these naïve T cells to clonally expand and mature upon recognition of their cognate antigen. The process of antigen recognition, T cell activation and induction of clonal expansion is called T cell priming. It is usually mediated by professional APCs like DCs. These professional APCs express high amounts of MHC molecules on their cell surface, as well as costimulatory molecules like CD80 and CD86. Furthermore, they are characterized by the ability of antigen uptake (by phagocytosis) and antigen processing and (cross-) presentation. A third feature is the production of pro-inflammatory cytokines in response to activation by danger signals. The priming process is classically defined as a composition of three main signals:

- Signal 1: Interaction of a T cell receptor with a cognate MHC:peptide complex.
- Signal 2: Binding of the costimulatory molecule CD28 to its ligand CD80.
- Signal 3: Engagement of cytokine receptors with pro-inflammatory cytokines.

After priming, the activated T cells produce IL-2 and promote their clonal expansion. The process of T cell priming by autologous APCs can be recapitulated *in vitro* however the process of DC generation from PBMCs is very time consuming and cost intensive. Further drawbacks are a broad range of donor variance in efficacy of DC generation and the inapplicability for high throughput screenings due to the needed cell counts. To circumvent these drawbacks, a priming technique using aAPCs was used to assess the immunogenicity of potential tumor-associated peptides. This approach enables for high throughput priming experiments. APCs are substituted by special streptavidin-coated polystyrene microspheres. These microspheres have the size of a natural cell and can be loaded with biotinylated molecules by binding to streptavidin. By loading of the beads with biotinylated HLA:peptide complexes (monomers) and a biotinylated stimulatory α-CD28 antibody, signal 1 and 2 for T cell priming can be provided by the aAPCs. Signal 3 can be provided by addition of the respective cytokines to the cell culture. The composition of the aAPCs is illustrated in figure 13.

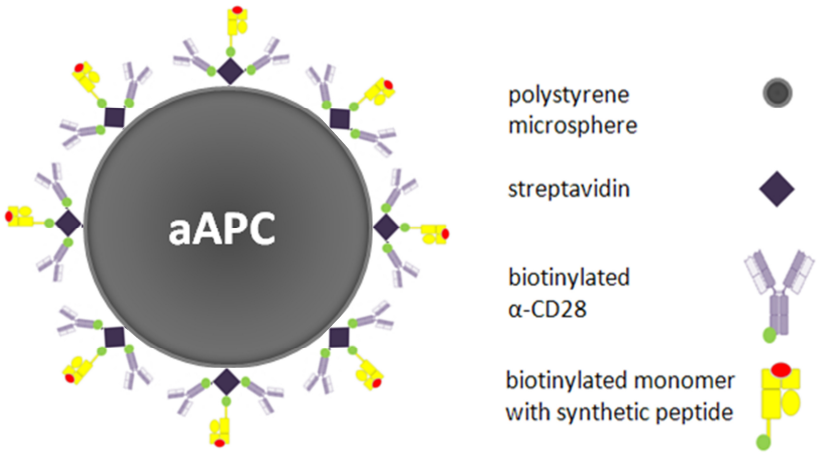

Figure 13: Schematic of an artificial antigen presenting cell. Polystyrene microspheres are customized to the size of a natural cell and coated with streptavidin. This enables binding of biotinylated molecules to the microspheres. To generate aAPCs, biotinylated HLA:peptide monomers and a stimulatory α-CD28 antibody were bound onto the microspheres. Figure from [283].

For priming experiments, freshly isolated PBMCs from whole blood samples of healthy donors were used (2.4.1). All steps were conducted under sterile conditions. PBMCs were cultured over night at a density of $1*10^7$ cells/ml in TCM supplemented with 2.5 ng/ml IL-7 and 10 U/ml IL-2 in 75 cm^2 cell culture flasks in standing position. On day two, CD8+ T cells were isolated by MACS (2.4.7) and cultured over night at a density of $1*10^7$cells/ml

in TCM supplemented with 2.5 ng/ml IL-7 and 10 U/ml IL-2 in 75 cm^2 cell culture flasks in standing position. On day three, CD8+ T cells were harvested, counted and adjusted to $1*10^7$ cells/ml in TCM. $1*10^6$ cells (100 µl) were seeded into each well of a 96-well plate with round bottoms (only the inner 60 wells were used per plate, the outer rows were filled with 200 µl PBS for evaporation protection). For each cell plate, a mirror plate (bead stock plate) containing the aAPCs was produced. All steps of the aAPC manufacture were performed on ice. The amount of produced aAPCs was sufficient for four restimulation cycles to compensate for pipetting losses. For each well (priming experiment), 800000 beads were needed. The respective amount of beads was transferred into a 50 ml tube and washed twice with MACS buffer (centrifugation for 10 min at 2500 rpm and 4°C). After washing, beads were resuspended in appropriate amounts of MACS buffer (100 µl for each well/priming experiment) and seeded into a 96-well plate. The respective biotinylated HLA:peptide monomers were diluted to 200 ng/ml in MACS buffer and 50 µl/well were added to the beads. The plates were incubated gently shaking for 30 min at RT. Next, the biotinylated stimulatory α-CD28 antibody was diluted to 600 ng/ml in MACS buffer and 50 µl/well were added. The plates were again incubated gently shaking for 30 min at RT. Afterwards, aAPC plates were washed four times with MACS buffer (centrifugation for 2 min at 2500 rpm and 4°C) to remove remaining unbound molecules. The aAPCs were resuspended in 200 µl of MACS buffer per well and the plates were covered in tin foil and stored at 4°C. For T cell stimulation, aAPCs were resuspended and 50 µl of each well were transferred to a new 96-well plate. The aAPCs were washed twice with 150 µl of cold TCM w/o HS (centrifugation for 2 min at 2500 rpm and 4°C) and taken up in 100 µl of warm TCM supplemented with 5 ng/ml IL-12. Finally, the bead solution was transferred to the T-cell plate and mixed with the T cells. Every 2-3 days after stimulation, 100 µl of medium were substituted by fresh TCM supplemented with 40 U/ml IL-2 to support T cell expansion. The aAPC stimulation was repeated every 7 days to a total of three stimulation cycles. The time schedule for the aAPC priming is depicted in figure 14. After 3 cycles of stimulation, T cells were rested for another week without cytokine supplements before flow cytometric analysis.

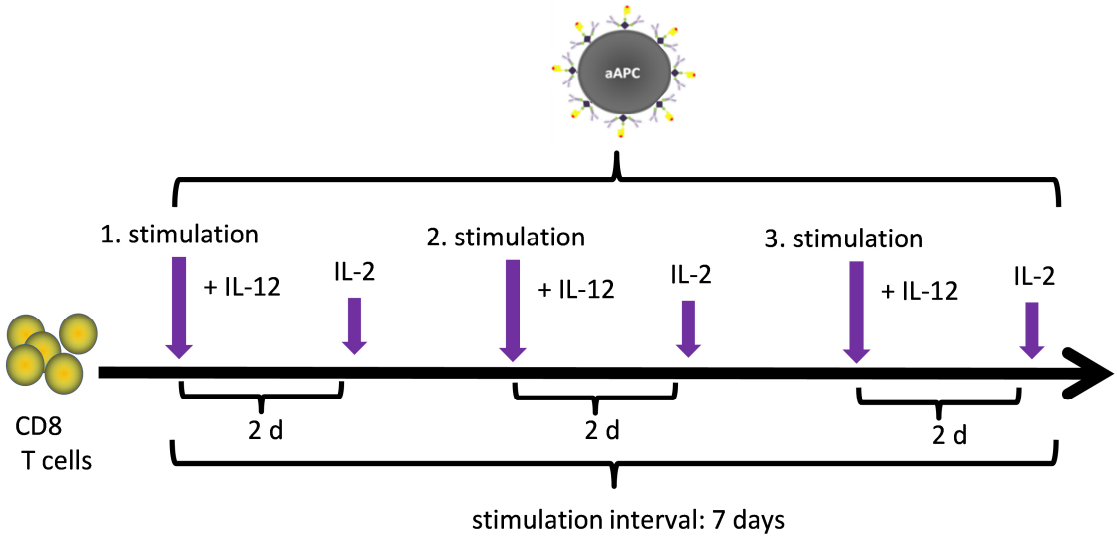

Figure 14: Schematic time schedule of the aAPC T-cell priming protocol. CD8+ T cells were stimulated once a week with aAPCs and IL-12 for a total time of three weeks. Medium was exchanged every 2-3 days after aAPC stimulation with supplement IL-2. After three stimulation cycles, T cells were analyzed by flow cytometry. Figure from [283].

2.5 Flow cytometry

Flow cytometry is an analytical method for the characterization of single cells based on cell intrinsic properties like size, granularity and expression of distinct extra- and intracellular markers. The first devices were based on impedance [284] however modern devices are based on optical detection mechanisms. Today, flow cytometry is based on excitation of fluorochromes by light with defined wavelengths (lasers) and detection of light emissions of the fluorochromes. Several thousand cells can be analyzed per second on multiple parameters in a flow cytometer. The cell suspension is focused to a fine and constant stream of droplets each containing one cell by hydrodynamic focusing within the flow cell. The droplet stream passes on through the flow cell where focused laser beams cross the cell stream. Depending on the setup of the flow cytometer, different amounts of lasers and detection channels are available. A basic feature of all cytometers however, is the detection of light scattering by the individual cells when passing the laser beam. The forward scatter (FSC) is measured directly opposite to the light source and indicates cell size. The side scatter (SSC) is measured orthogonally to the light source and indicates cell granularity. These two features enable discrimination of cell populations like lymphocytes, monocytes, granulocytes and other cell types. For further discrimination of

subtypes, cells have to be labelled with fluorochrome-labelled antibodies specific for the cell markers of interest. The amount of emitted fluorescence correlates with the amount of bound antibody and thus with the marker density of the cell. Each fluorochrome has an excitation maximum and an emission maximum at defined wavelengths. Thus, the more lasers with different wavelengths a flow cytometer has, a greater variety of fluorochromes can be used for labelling and the greater the amount of markers that can be analyzed in a single experiment. After excitation, the light emissions are detected by photomultipliers and translated into digital signals. Flow cytometry is often referenced as FACS (fluorescence activated cell sorting), a technique for sorting of cells based on one or multiple markers. While flow cytometers are used for solely for cell analysis, cell sorters additionally provide the possibility to sort cell according to the analyzed markers. A schematic of a flow cytometer is depicted in figure 15.

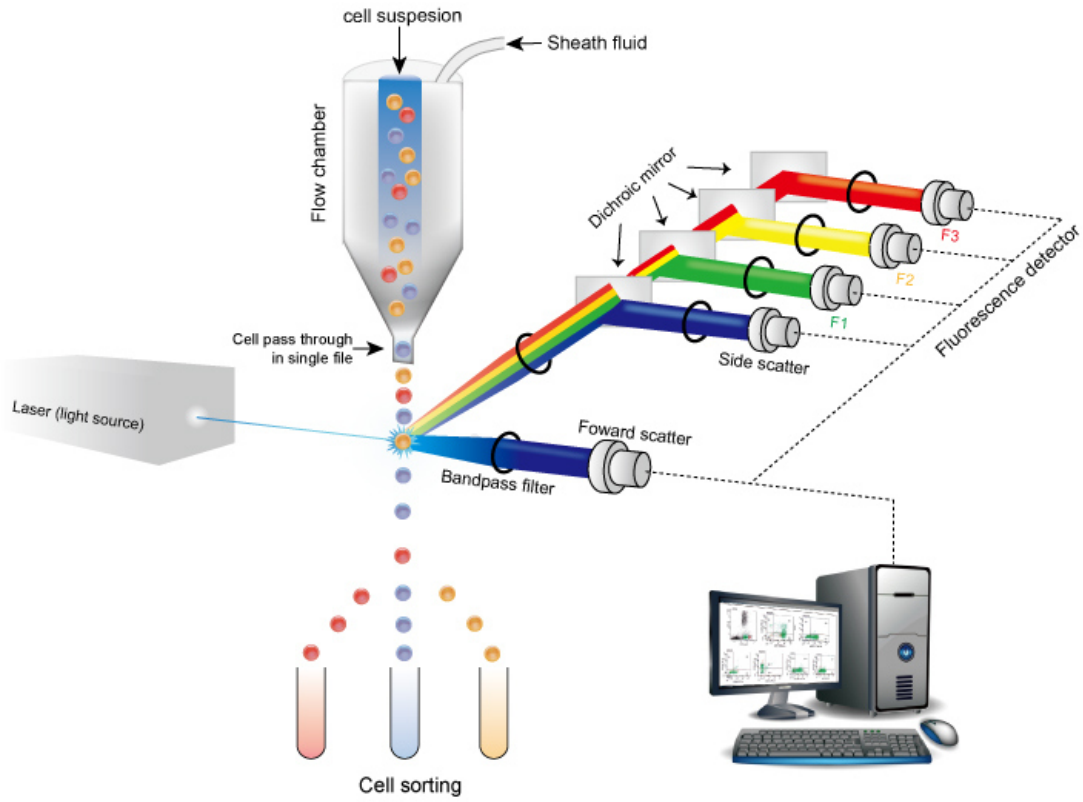

Figure 15: Schematic of a FACS machine. The cell stream passes the laser beam, FSC and SSC are detected and fluorescent labels are excited at different wavelenghts. The light emission of the fluorescents are detected by photomultipliers (F1-3) and translated into digital signals. Figure from https://www.creative-diagnostics.com/flow-cytometry-guide.htm, 18.02.2018.

2.5.1 Tetramer staining of CD8+ T cells

T cells from priming experiments (2.4.8) were analyzed by tetramer (2.2.4) staining. Cell culture plates were centrifuged for 2 min at 1800 rpm and 4°C. The supernatants were discarded by inverting the plates and flicking downwards. Remaining drops were removed by pressing the plate onto a towel. Cells were washed with PBSE (centrifugation for 2 min at 1800 rpm and 4°C) and supernatants were discarded as described above. During the centrifugation step, the live/dead staining was prepared. A stock solution of PBSE with diluted Aqua LiveDead (1:200-400) was prepared to provide 50 µl of staining solution per well. After addition of the staining solution, plates were incubated for 20 min at 4°C in the dark. Cells were washed with TSB as described above. During the centrifugation step, tetramer staining was prepared. Tetramers were centrifuged for 5 min at 13000 rpm and 4°C to remove protein aggregates. Stock solutions of the respective tetramers were prepared in TSB with tetramer concentrations of 5 µg/ml to provide 50 µl of staining solution per well. After addition of the staining solution, plates were incubated for 30 min at RT in the dark. Cells were washed with FACS buffer as described above. During the centrifugation step, CD8 staining was prepared. A stock solution of FACS buffer with diluted α-CD8-PerCP (1:200) was prepared to provide 50 µl of staining solution per well. After addition of the staining solution, plates were incubated for 20 min at 4°C in the dark. Cells were washed with FACS buffer as described above. Cells were then resuspended in 200 µl of FACS buffer and subjected to flow cytometry. Cells were fixed by resuspension in FACS buffer with 1 % formaldehyde if flow cytometry was not performed at the same day. After incubation for 20 min at 4°C in the dark, cells were washed with FACS buffer as described above and could be stored at 4°C in the dark for up to three days prior to analysis.

2.5.2 Analysis of Tetramer staining by flow cytometry

All tetramer stainings were analyzed on a BD FACSCanto II flow cytometer. The setup of the machine contains three lasers (violet 405 nm, blue 488 nm and red 633 nm) and eight detection channels (two for violet, three for blue and red) plus the FSC/SSC laser and detectors. Emission spectra of fluorochromes may overlap, therefore compensation measurements have to be performed to calculate signal spillover of each fluorochrome to

the other detection channels. To perform compensation measurements, compensation beads were labelled with the respective fluorochrome-labelled antibodies used for cell staining. During measurement of the beads, the voltages of the detectors were adjusted to produce reasonable signals for the respective fluorochromes. After measurement of all compensation controls, the software FACS Diva calculated the compensation matrix. Cells were measured at 2,000-4,000 Events per second and about 200,000 events were recorded per sample. Data analysis of the raw data (FCS files) was performed with the software FlowJo v.10. The gating strategy was as follows: first, lymphocytes were gated using the FSC(A) and SSC(A) parameters (A=area). Next, cells from the lymphocyte gate were gated for single cells using the FSC(A) versus the FSC(H) (H=height). Single cells were further gated for viability using the Aqua LiveDead marker (dead cells were stained by the marker). Finally, viable cells were analyzed for simultaneous staining of CD8::PerCP and the Tetramer::PE.

3 Results

The results part is subdivided into several parts. First, results obtained during an attempt to improve peptide isolation from primary tissues are described. Second, results of HLA ligandome analysis of RCC specimen samples pairs (tumor/benign) are ensuing. In this context, the definition of RCC tumor antigens based on comparative HLA ligandome profiling for HLA class I and II is shown, as well as factors that influence antigen selection. In a third part, immunogenicity assays of selected peptides derived from ligandome-defined tumor-associated antigens are described. In the last part, results of the approaches for identification of *Mtb*-derived HLA ligands are listed.

3.1 Improvement of tissue preparation for HLA ligandomics

Tissue preparation prior to isolation of HLA molecules is a crucial step influencing the exhaustive analysis of HLA ligandomes by mass spectrometry. To improve tissue preparation, the standard preparation method was compared to a method where a cryotome was used for primary tissue disintegration. Cryotomes produce thin slices of a snap-frozen tissue sample for microscopy or histology purposes. Here, it was used to cut whole samples into 10 µm slices to improve cellular disruption and accessibility. The tissue slices were subsequently transferred into lysis buffer and treated similarly for the following steps of tissue preparation and HLA isolation. Equivalent tumor and benign tissue samples from the same RCC specimen were used and isolated HLA ligands were identified by mass spectrometry. Five replicates of each sample were measured, each containing a 20 % sample share of the whole sample. The results are depicted in table 5.

Table 5: Results of cryotome preparation and standard preparation of HLA ligands. Equivalent shares of tumor and benign tissue samples from specimen RCC302 were prepared using either a cryotome or standard protocols. Results of five replicate measurements from each sample. Peptides: Identified unique peptide sequences, PSMs: peptide spectrum matches, Proteins: source proteins of peptides.

	Cryotome			Standard Preparation		
Sample	**Peptides**	**PSMs**	**Proteins**	**Peptides**	**PSMs**	**Proteins**
RCC302 Benign W6/32 Rep#1	278	717	549	127	292	163
RCC302 Benign W6/32 Rep#2	25	63	36	99	238	148
RCC302 Benign W6/32 Rep#3	283	722	487	95	221	134
RCC302 Benign W6/32 Rep#4	294	726	515	161	395	209
RCC302 Benign W6/32 Rep#5	259	602	485	139	368	183
RCC302 Benign W6/32 5 Replicates CoProcessed	**478**	**3091**	**688**	**262**	**1864**	**335**
RCC302 Tumor W6/32 Rep#1	1317	5232	1256	408	1313	489
RCC302 Tumor W6/32 Rep#2	1299	5303	1272	448	1449	516
RCC302 Tumor W6/32 Rep#3	1331	5414	1290	424	1238	498
RCC302 Tumor W6/32 Rep#4	1298	5154	1260	400	1249	484
RCC302 Tumor W6/32 Rep#5	1296	5356	1271	468	1409	560
RCC302 Tumor W6/32 5 Replicates CoProcessed	**1830**	**26473**	**1662**	**641**	**5859**	**726**

Inter-replicate variance was relatively low except for replicate #2 of benign tissue of the cryotome preparation, probably due to technical issues of the LC-MS system. The results were filtered according to the established criteria for HLA ligandomics (see 2.3.5). Unique peptide identifications were consistently higher in the cryotome preparation MS runs for benign and tumor samples when compared to standard preparation. The same holds true for the amount of peptide spectrum matches (PSMs), an additive value counting all spectra in one run that were assigned to one of the unique peptide sequences. Along with higher peptide identifications, the number of peptide source proteins was elevated in cryotome preparation MS runs (see figure 16).

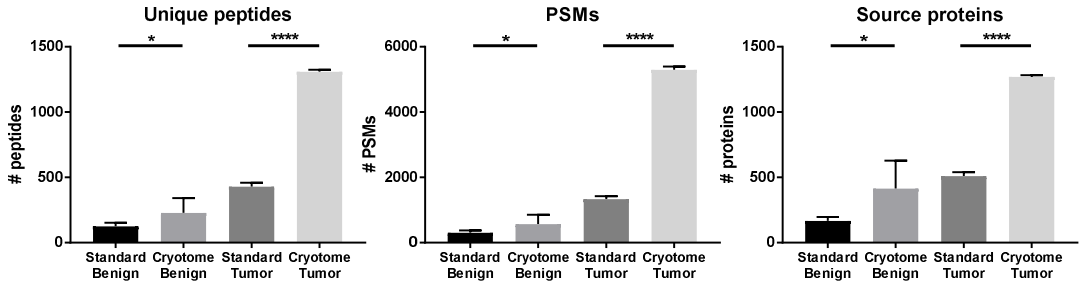

Figure 16: Comparison of standard tissue preparation and cryotome preparation. Means of 5 replicate measurements of each sample with standard deviations. Unique peptide, PSM and peptide source protein values are given. Unpaired t-test was performed to assess significant differences between samples.

To assess the actual impact of cryotome preparation on exhaustive HLA ligandome analysis, data of the replicates was co-processed and differences in identification counts were analyzed (see figure 17).

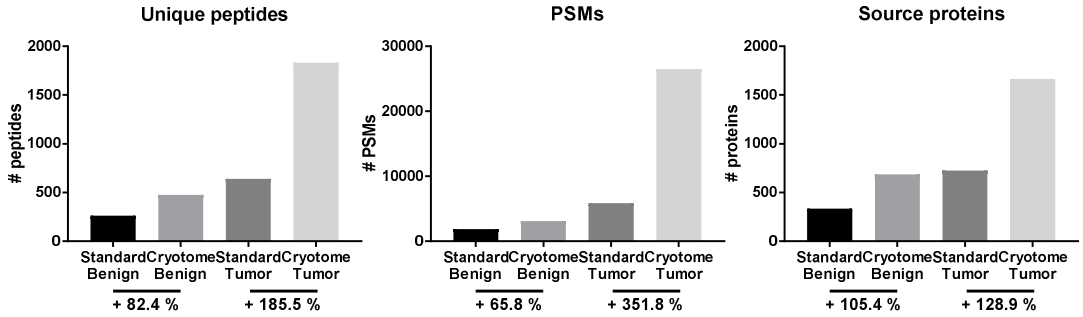

Figure 17: Identifications from co-processed replicates. Complete values of unique peptide identifications, PSMs and unique peptide source protein identifications from standard preparation and cryotome preparation samples after combination of replicate data.

Cryotome preparation yielded superior results in terms of unique peptide identifications, PSMs and unique source protein identifications. Proportional gains were higher in tumor samples than in benign samples with the highest increase in PSMs in the tumor sample. Nevertheless, cryotome preparation had a substantial beneficial impact on identifications in all perspectives and could improve exhaustive HLA ligandome analysis. To compare the entireties of identified peptides, overlap analyses were performed (see figure 18).

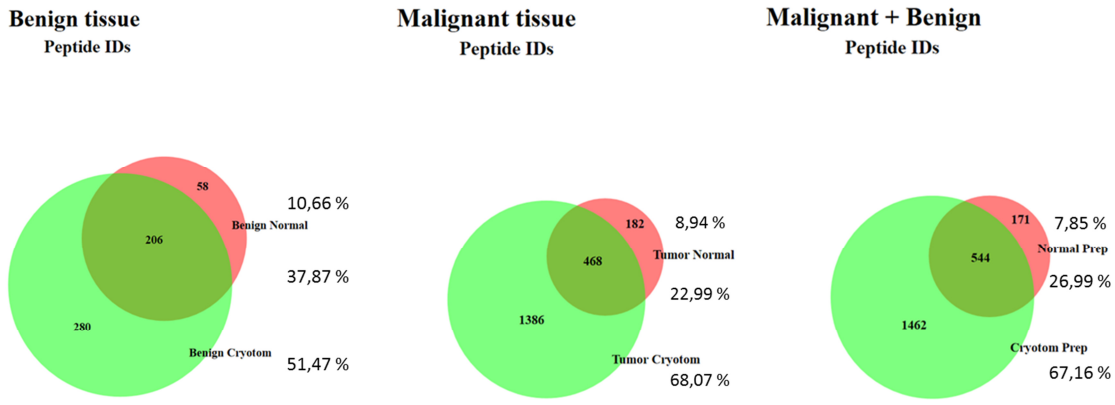

Figure 18: Overlap analyses of peptide identifications from standard and cryotome preparation. Entireties of identified peptides in standard preparation samples are depicted in red, entireties of identified peptides in cryotome preparations are depicted in green.

A minority of peptide identifications were only present in standard preparation samples. About 90 % of total peptide identifications were covered by the cryotome preparation samples. The loss of peptide identifications may be explainable by inherent reproducibility infirmities of mass spec replicate measurements.

3.2 Exhaustive HLA class I ligandome analysis of RCC samples

Technical improvements in HLA ligand isolation were not the only improvements to enhance immunopeptidome analysis. Upgrading the technical setup primarily boosted peptide identifications and allowed for reliable and more reproducible MS measurements. Implementation of a uHPLC system to the LC-MS setup allowed application of separation columns with superior peptide fractionation capabilities. Enhanced peptide peak focusing and reduced co-elution of peptide peaks contributed to an enormous increase in peptide identifications. The gradient settings of the uHPLC for peptide separation as well as the MS settings were adjusted and optimized for HLA ligand identification [285]. These technological advances for the first time enabled an exhaustive analysis of HLA ligandomes of tumor and benign tissues. However, the huge datasets also demanded new evaluation strategies to identify tumor-associated peptides and antigens. In the past, tumor-associated peptides were selected by validation of MS spectra and published tumor-association of the peptide source proteins. This strategy was not applicable for primary antigen selection from exhaustive HLA ligandomics and was replaced by comparative profiling. In this approach, tumor-associated antigens are defined solely on their representation in HLA ligandomes of tumor tissues and their absence in benign and normal tissues. Such antigens may be defined for individual patients as well as within a cohort of RCC patients.

3.2.1 Peptide identifications in HLA class I preparations from RCC tumor and benign samples

HLA preparation and characterization of HLA class I ligands was performed for tumor and benign tissue samples from 38 RCC specimen in total (see table 3). Raw data was processed and filtered according to the established standard criteria (see 2.3.5) to obtain high-confidence HLA ligands. The results are listed in table 6.

Table 6: Peptide identifications for HLA class I from the RCC cohort. Tumor and benign tissue samples of 38 RCC specimen were analyzed. Unique peptide identifications (peptides), total peptide spectrum matches (PSMs) and peptide source protein identifications (Proteins) are listed for each sample. Samples with less than 200 peptide IDs are marked in grey and were excluded from further analyses.

	Tumor			Benign		
Sample	**Peptides**	**PSMs**	**Proteins**	**Peptides**	**PSMs**	**Proteins**
RCC301	2140	22124	1973	1172	8109	1195
RCC302	1915	30804	1732	541	5165	796
RCC310	1674	14379	1584	817	4158	905
RCC318	1722	21887	1653	211	2213	298
RCC330	2854	37997	2453	1172	11486	1183
RCC352	1262	7197	1272	856	10084	912
RCC358	2756	8573	2399	494	1074	644
RCC370	1224	3341	1215	451	850	541
RCC376	4911	22291	3476	2511	12392	2202
RCC385	2238	6517	2050	1176	3256	1284
RCC792	1297	19687	1297	165	1322	268
RCC200	1901	22662	1721	957	5961	1014
RCC227	1088	7246	1123	1577	11518	1500
RCC441	1224	8370	1232	97	398	160
RCC299	34	58	36	19	36	62
RCC287	Failed	Failed	Failed	Failed	Failed	Failed
RCC1138	2977	35737	2319	1037	7457	1039
RCC1147	799	4039	841	511	2831	606
RCC1131	1175	5563	1189	38	83	115
RCC1148	2382	19232	1982	1760	10290	1688
RCC245	122	255	151	56	110	129
RCC247	1446	7318	1382	423	1297	504
RCC251	95	211	120	1304	6574	1179
RCC286	443	2543	480	673	4391	791
RCC291	1362	5507	1267	105	319	127
RCC1157	782	3884	825	16	29	20
RCC381	1658	24089	1549	1005	15642	1025
RCC1154	936	16704	947	548	6235	744
RCC1187	767	5357	800	960	6229	972
RCC1188	2079	17968	1920	1337	10698	1305
RCC1203	1399	33014	1349	809	9553	927
RCC1223	3432	30910	3155	655	4244	807
RCC1248	2020	14254	1782	1535	9569	1435
RCC1238	1801	12282	1687	1918	12366	1811
RCC1192	1427	13282	1202	1298	9275	1390
RCC1198	1156	8307	1254	716	5458	891
RCC1170	1150	8676	1146	990	4698	1066
RCC1152	3069	37097	2715	1394	11229	1424
Median	1641	14577	1494	846	5854	891

Unique peptide IDs, PSMs and source protein IDs varied substantially between different samples. In general, identification rates were higher in tumor samples than in benign samples for all parameters. Median peptide IDs were approximately doubled in tumor samples when compared to benign samples. This might at least partly be accounted to higher sample masses of tumor samples. Samples in which unique peptide IDs did not exceed 200 identifications were excluded from further analysis to avoid artefacts from failed HLA preparations/MS measurements (marked grey in table 6).

3.2.2 Exhaustive HLA ligandome analysis identifies tumor-exclusive HLA class I ligands for individual RCC patients

HLA ligandomes of tumor and benign samples from individual patients were analyzed on the level of HLA ligands to identify tumor-associated peptides (TUMAPs). As this was done on the basis of naturally presented peptides and comparison of the HLA ligandomes of malignant and benign samples, the identified peptides are termed ligandome-derived tumor-associated peptides (LiTAPs). The data evaluation strategy is depicted in figure 19.

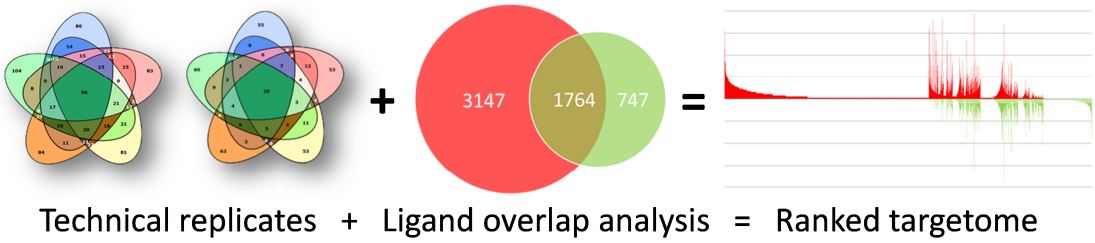

Figure 19: Strategy for identification of LiTAPs. Tumor and benign samples are measured in replicates to perform exhaustive HLA ligandome analysis. The peptide identifications are subsequently compared in an overlap analysis. HLA ligands with high presentation frequencies (i.e. high PSM counts) in tumor tissue (red, left side of waterfall plot) and absent presentation in benign tissue (green, right side of waterfall plot) are defined as LiTAPs.

To perform comparative analysis of tumor and benign HLA ligandomes for individual patients, peptide IDs were ranked based on the corresponding PSM values. PSM values indicate how many spectra that match to a unique peptide sequence were acquired during MS measurements. The values are therefore an indicator for the abundance of individual peptide species in the samples. Peptides that are highly abundant in tumor

samples and absent in benign samples were regarded as LiTAPs, which might be suitable targets for peptide vaccination approaches in individual patients.

3.2.3 Population-specific antigen identification for HLA class I

In a next step, ligandome-derived tumor-associated antigens (LiTAAs) were identified for RCC. For this purpose, data from the remaining 29 RCC specimen with high quality in tumor and benign samples were subjected to comparative analysis. To account for different HLA allotypes within the cohort and resulting peptide varieties, analysis was performed on the level of HLA ligand source proteins. This allowed for a population-wide analysis based on the frequency of HLA presentation of unique source proteins. The total values of identifications that were used for this analysis are listed in table 7.

Table 7: HLA class I identification values for population-based comparative analysis. Combined values for the cohort of 29 RCC specimen of which appropriate data from tumor and benign tissue was available.

	Unique peptide IDs	PSMs	Unique protein IDs	Total Protein IDs
Tumor	31601	508268	10616	49395
Benign	15124	197532	7070	29667
Total	35543	705800	11279	79062

Comparative profiling altogether identified 4209 HLA class I ligand source proteins that were exclusively identified in tumor samples. Of those, 811 had a presentation frequency of over 10 %, i.e. they were identified in at least 3 out of 29 tumor samples. The top 115 LiTAAs for HLA class I from this analysis have presentation frequencies of over 20 %, meaning they were identified in at least 6 out of 29 tumor samples (see figures 20 and 21).

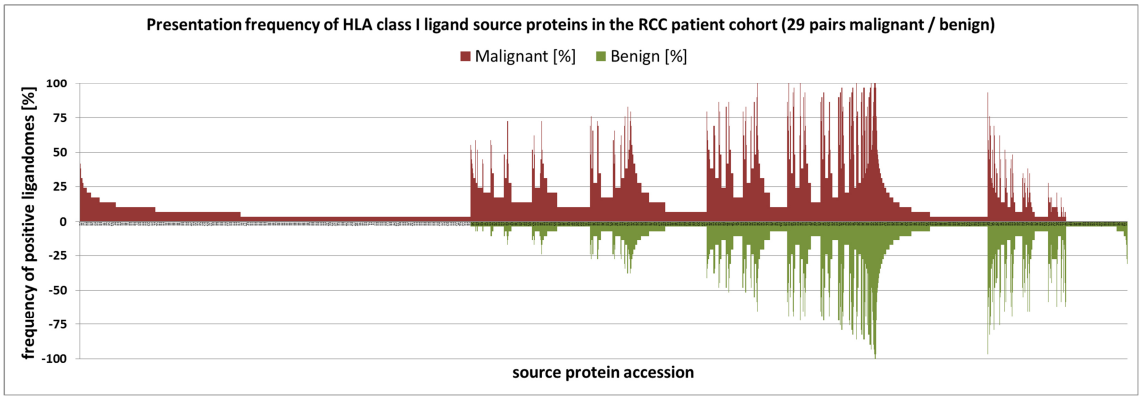

Figure 20: Presentation frequencies of HLA class I ligand source proteins in the RCC cohort. Protein accessions of each of the 11279 identified source proteins are displayed on the x-axis. Frequencies of detection of HLA ligands for each source protein are displayed on the y-axis. Identifications from tumor samples are displayed in the positive range above the x-axis in red, identifications from benign samples are displayed in the negative range below the x-axis in green. Source proteins on the far left were defined as LiTAAs.

Figure 21: Word cloud of the top 115 HLA class I LiTAAs for RCC. Font size represents presentation frequency. Presentation frequencies ranged between 20.7 % and 41.4 % of all tumor samples (i.e. between 6 and 12 of all 29 tumor samples).

The top 11 LiTAAs are listed in table 8 with corresponding presentation frequencies and numbers of different identified HLA class I ligands.

Table 8: The top 11 HLA class I LiTAAs for RCC as defined by comparative profiling. Gene and protein names as well as presentation frequencies in tumor samples of the RCC cohort and numbers of different corresponding identified HLA ligands are listed.

Rank	Gene	Protein	Presentation frequency [%]	# of different HLA ligands
1	PLOD2	Procollagen-lysine,2-oxoglutarate 5-dioxygenase 2	41.4	14
1	FCGR3A	Low affinity immunoglobulin gamma Fc region receptor III-A	41.4	5
1	ATP5C1	ATP synthase subunit gamma, mitochondrial	41.4	7
1	PHKA2	Phosphorylase b kinase regulatory subunit alpha, liver isoform	41.4	10
2	SLC16A3	Monocarboxylate transporter 4	37.9	9
2	RPLP0	60S acidic ribosomal protein P0	37.9	9
2	CTSD	Cathepsin D	37.9	17
2	HIPK3	Homeodomain-interacting protein kinase 3	37.9	12
3	ALOX5	Arachidonate 5-lipoxygenase	34.5	9
3	COMT	Catechol O-methyltransferase	34.5	6
3	ANP32A	Acidic leucine-rich nuclear phosphoprotein 32 family member A	34.5	6

3.2.4 Coverage estimations for the HLA class I ligandome of RCC

Ligandome-based identification of suitable antigens for peptide vaccination is dependent on an exhaustive analysis of HLA ligandomes. To estimate the level of exhaustion that was achieved with the current cohort and technical setup, cumulative analyses on identified HLA class I ligands and respective source proteins for tumor and benign RCC samples were performed (see figure 22).

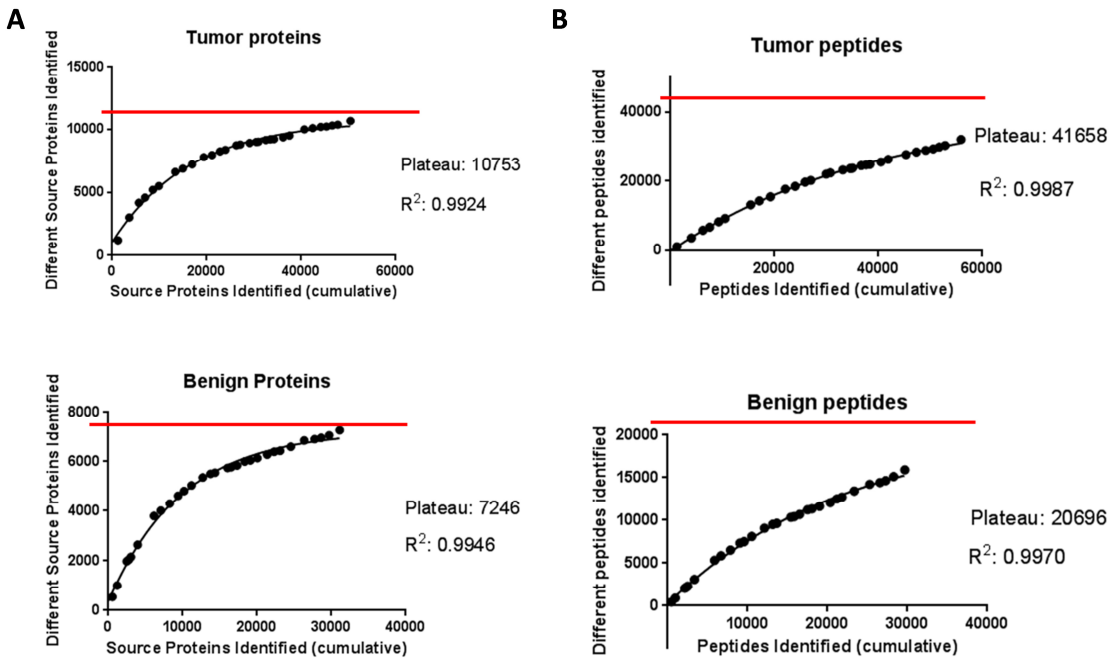

Figure 22: Estimations for the degree of exhaustion of HLA class I ligandome analysis in RCC. Nonlinear one-phase associations between cumulative numbers of identified source proteins and numbers of unique identified source proteins (A) and between cumulative numbers of identified peptides and numbers of unique identified peptides (B) in 29 RCC tumor and benign sample pairs. Red lines indicate calculated plateaus. R^2 value indicates goodness of fit.

On the level of HLA ligand source proteins, the estimated achievable plateaus for tumor and benign samples were almost reached with the analyzed cohort of 29 RCC sample pairs. The calculated plateau for HLA ligand source proteins was higher for tumor samples (10753) than for benign samples (7246), probably reflecting a more heterogeneous cell composition and aberrant protein expression in tumors. On the level of identified HLA ligands, the estimated plateaus were by far not reached for tumor and benign samples in the RCC cohort, reflecting HLA allotype heterogeneity and the affiliated peptide binding specificities. Thus, exhaustive analysis of HLA class I source protein level provides a reliable data basis for definition of LiTAAs, whereas exhaustive mapping of actual HLA class I ligands would demand for extension of the RCC cohort to account for HLA heterogeneity.

3.2.5 Enhanced LiTAA definition for RCC based on additional normal tissue HLA class I ligandomes

The availability of tumor and benign tissue from RCC patients enabled the development of a novel approach for antigen definition, but only HLA ligandomes of kidney malignant and healthy tissues were taken into account so far. Immunization against the newly defined potential tumor-associated antigens (for example by peptide vaccination) however might induce a systemic T cell response against these antigens. In principle, selected antigens for vaccination should be as tumor-exclusive as possible. It was therefore necessary to define additional exclusion criteria for antigen selection, i.e. delineate the HLA ligandomes of any human tissue to exclude HLA ligands that are presented elsewhere in the body apart from the tumor. A database of such experimentally defined, naturally expressed HLA ligands of the human body demands huge efforts and its' setup was initiated in a collaborative approach at the Department of Immunology. At the time of analysis, this database contained HLA ligands derived from 138 normal tissues, including kidney, PBMC, bone marrow, liver, colon, ovary, bladder, heart, lung, small intestine, thyroid, spleen, brain and muscle. The input data for normal tissues contained 40172 unique HLA ligands derived from 11642 source proteins. People involved in the generation of this database were Daniel Kowalewski, Heiko Schuster, Nico Trautwein and Claudia Berlin. Comparative profiling was performed using all RCC datasets that passed quality criteria (see table 6) resulting in comparison of HLA ligandomes of 33 RCC tumor samples to those of the 138 normal samples. Data analysis identified 14455 unique HLA ligands originating from 1785 source proteins that were exclusively identified in tumor samples. Of those source proteins, 58 had a presentation frequency of over 10 %, i.e. they were identified in at least 4 out of 33 tumor samples. Only the top 5 LiTAAs for HLA class I from this analysis had presentation frequencies of over 20 %, meaning they were identified in at least 7 out of 33 tumor samples (see figures 23 and 24). The total number of identified LiTAAs was greatly reduced when compared to the analysis of RCC samples alone as described in chapter 3.2.3, underlining the potential of the normal tissue database as exclusion criterion for antigen selection.

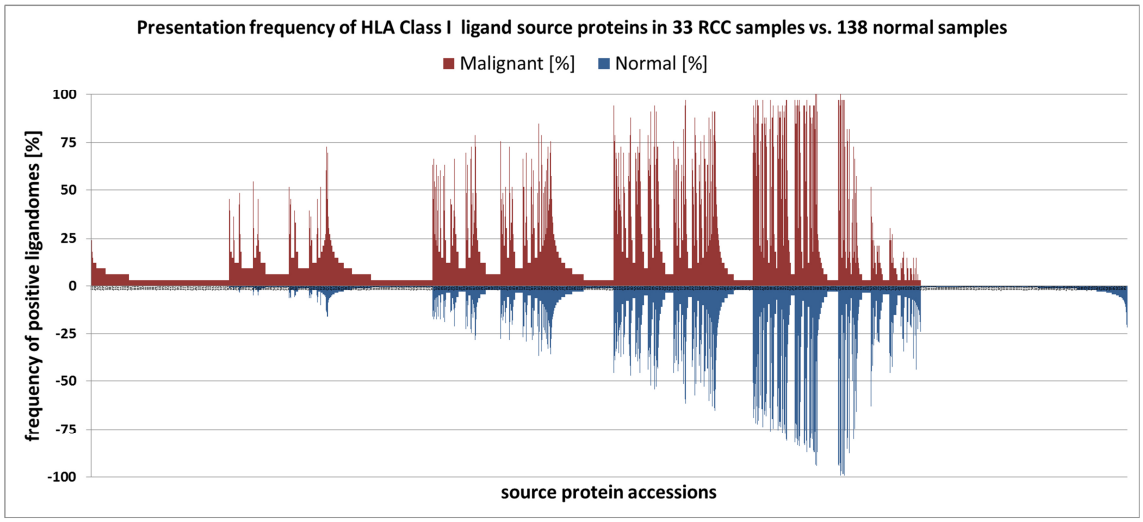

Figure 23: Presentation frequencies of HLA class I ligand source proteins of RCC samples compared to normal tissue samples. Protein accessions of each of the 13427 identified source proteins are displayed on the x-axis. Frequencies of detection of HLA ligands for each source protein are displayed on the y-axis. Identifications from tumor samples are displayed in the positive range above the x-axis in red, identifications from normal samples are displayed in the negative range below the x-axis in blue. Source proteins on the far left were defined as LiTAAs.

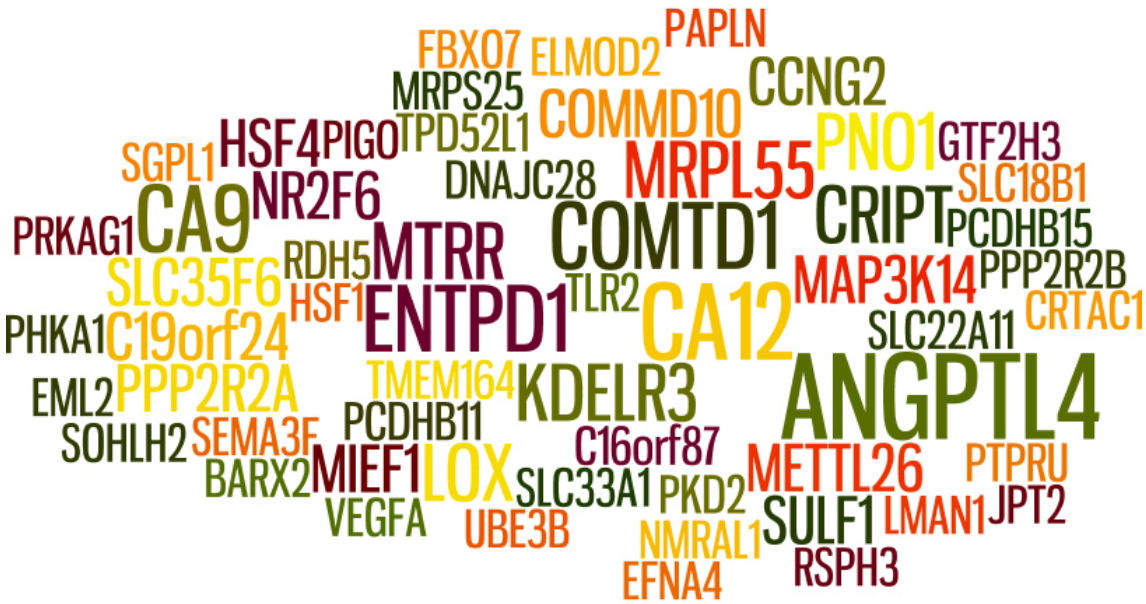

Figure 24: Word cloud of the top 58 HLA class I LiTAAs for RCC based on comparative profiling with 138 normal tissues. Font size represents presentation frequency. Presentation frequencies ranged between 12.1 % and 27.3 % of all tumor samples (i.e. between 4 and 9 of all 33 tumor samples).

The Top 11 LiTAAs are listed in table 9 with corresponding presentation frequencies and numbers of different HLA class I ligands.

Table 9: The top 11 HLA class I LiTAAs for RCC as defined by comparative profiling with 138 normal tissues. Gene and protein names, as well as presentation frequencies in tumor samples of the RCC cohort and numbers of different corresponding identified HLA ligands are listed.

Rank	Gene	Protein	Presentation frequency [%]	# of different HLA ligands
1	ANGPTL4	Angiopoietin-related protein 4	27.3	7
2	CA12	Carbonic anhydrase 12	24.2	6
3	ENTPD1	Ectonucleoside triphosphate diphosphohydrolase 1	21.2	6
3	CA9	Carbonic anhydrase 9	21.2	6
3	COMTD1	Catechol O-methyltransferase domain-containing protein 1	21.2	4
4	KDELR3	ER lumen protein-retaining receptor 3	18.2	6
4	LOX	Protein-lysine 6-oxidase	18.2	4
4	MRPL55	39S ribosomal protein L55, mitochondrial	18.2	3
4	PNO1	RNA-binding protein PNO1	18.2	6
4	CRIPT	Cysteine-rich PDZ-binding protein	18.2	2
4	MTRR	Methionine synthase reductase	18.2	7

3.3 Exhaustive HLA class II ligandome analysis of RCC samples

HLA class II ligandomes were analyzed and evaluated analogous to HLA class I albeit several restrictions are inherent to HLA class II ligands. First, peptide binding to HLA class II molecules is not as restrictive as it is for HLA class I as ligands are more promiscuous and may bind to different allotypes. Second, peptide length is not restricted, resulting in length variants of peptides with a shared core sequence and different N- and C-termini. Third, expression of HLA class II is more variable in RCC samples than expression of MHC class I, which influences the experimental outcome of HLA class II preparation and ligandome analysis. Owing to these constraints, data analysis was limited to HLA class II ligand source proteins and their tumor association.

3.3.1 Peptide identifications in HLA class II preparations from RCC tumor and benign samples

HLA preparation and characterization of HLA class II ligands was performed for tumor and benign tissue samples from almost the entire RCC cohort (see table 3). Raw data was processed and filtered according to the established standard criteria (see 2.3.5) to obtain high-confidence HLA ligands. The results are listed in table 10.

Table 10: Peptide identifications for HLA class II from the RCC cohort. Tumor and benign tissue samples of 38 RCC specimen were analyzed. Unique peptide identifications (Peptides), total peptide spectrum matches (PSMs) and peptide source protein identifications (Proteins) are listed for each sample. Samples with less than 100 peptide IDs are marked in grey and were excluded from further analyses.

	Tumor			Benign		
Sample	**Peptides**	**PSMs**	**Proteins**	**Peptides**	**PSMs**	**Proteins**
RCC301	744	7418	217	16	96	11
RCC302	443	10695	222	421	7108	267
RCC310	577	5523	284	652	7377	373
RCC318	Failed	Failed	Failed	Failed	Failed	Failed
RCC330	1471	17998	653	250	2024	207
RCC352	Failed	Failed	Failed	Failed	Failed	Failed
RCC358	Failed	Failed	Failed	Failed	Failed	Failed
RCC370	Failed	Failed	Failed	Failed	Failed	Failed
RCC376	1076	8442	511	702	5292	422
RCC385	Failed	Failed	Failed	Failed	Failed	Failed
RCC792	246	5071	120	291	4594	163
RCC200	53	322	56	36	136	45
RCC227	233	1981	251	452	3902	326
RCC441	417	3071	280	Failed	Failed	Failed
RCC299	7	13	39	1	3	21
RCC287	Failed	Failed	Failed	Failed	Failed	Failed
RCC1138	562	5848	371	24	129	14
RCC1147	8	19	14	25	103	72
RCC1131	272	2013	247	Failed	Failed	Failed
RCC1148	319	2075	175	9	21	13
RCC245	2	2	2	9	16	77
RCC247	539	2819	339	131	420	104
RCC251	328	2152	267	33	81	78
RCC286	70	235	50	508	4683	334
RCC291	851	6737	395	220	1327	110
RCC1157	55	266	55	3	5	20
RCC381	495	7787	269	479	7452	263
RCC1154	Failed	Failed	Failed	Failed	Failed	Failed
RCC1187	Failed	Failed	Failed	Failed	Failed	Failed
RCC1188	490	4093	326	274	2632	220
RCC1203	727	7690	346	256	1005	133
RCC1223	391	5368	234	432	5945	310
RCC1248	354	5966	208	276	2968	159
RCC1238	415	3428	216	448	3537	234
RCC1192	431	7077	212	511	6056	281
RCC1198	375	5828	357	256	213	2724
RCC1170	490	2983	274	433	1931	213
RCC1152	1151	17226	524	641	6115	398
Median	453	5005	250	278	2685	271

As for HLA class I, unique peptide IDs, PSMs and source protein IDs also varied substantially between different samples and identification rates were higher in tumor samples than in benign samples for HLA class II. Median peptide IDs were as well approximately doubled in tumor samples when compared to benign samples. As preparations were performed from the same samples as for HLA class I analysis, higher masses of tumor samples in general may have influenced results. Differential or absent expression of HLA class II in some of the samples (especially the benign ones) may have been another influencing factor. Samples in which unique peptide IDs did not exceed 100 identifications were excluded from further analysis to avoid artefacts from failed HLA preparations/MS measurements (marked grey in table 10).

3.3.2 Population-specific antigen identification for HLA class II

Comparative analysis was performed analogous for HLA class II to define LiTAAs for RCC. The amount of samples that had to be excluded from analysis was higher than for HLA class I: data from 18 RCC specimen with high quality in tumor and benign samples remained and was subjected to comparative analysis. The total values of identifications that were used for this analysis are listed in table 11.

Table 11: HLA class II identification values for population-based comparative analysis. Combined values for the cohort of 18 RCC specimen of which appropriate data from tumor and benign tissue was available.

	Unique peptide IDs	PSMs	Unique protein IDs	Total Protein IDs
Tumor	6553	120052	1793	5290
Benign	4221	72411	1377	4043
Total	8344	192463	2199	9333

Comparative profiling altogether identified 822 HLA class II ligand source proteins that were exclusively identified in tumor samples. Of those, 159 had a presentation frequency of over 10 %, i.e. they were identified in at least 2 out of 18 tumor samples. The top 61 LiTAAs for HLA class II from this analysis have presentation frequencies of over 15 %, meaning they were identified in at least 3 out of 18 tumor samples (see figures 25 and 26).

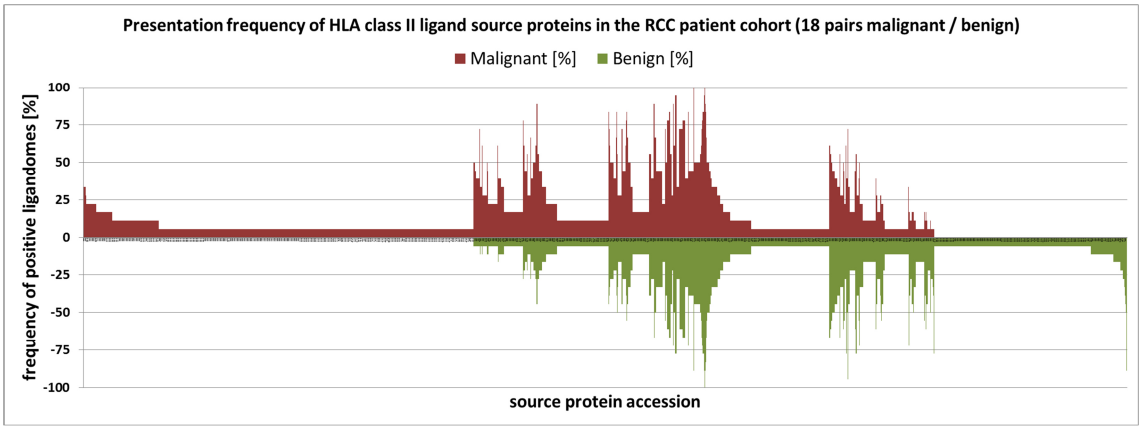

Figure 25: Presentation frequencies of HLA class II ligand source proteins in the RCC cohort. Protein accessions of each of the 2199 identified source proteins are displayed on the x-axis. Frequencies of detection of HLA ligands for each source protein are displayed on the y-axis. Identifications from tumor samples are displayed in the positive range above the x-axis in red, identifications from benign samples are displayed in the negative range below the x-axis in green. Source proteins on the far left were defined as LiTAAs.

Figure 26: Word cloud of the top 62 HLA class II LiTAAs for RCC. Font size represents presentation frequency. Presentation frequencies ranged between 16.6 % and 33.3 % of all tumor samples (i.e. between 2 and 6 of all 18 evaluable tumor samples).

The top 6 LiTAAs are listed in table 12 with corresponding presentation frequencies and numbers of different identified HLA class II ligands.

Table 12: The top 6 HLA class II LiTAAs for RCC as defined by comparative profiling. Gene and protein names, as well as presentation frequencies in tumor samples of the RCC cohort, numbers of different corresponding identified HLA ligands and core sequences are listed.

Rank	Gene	Protein	Presentation frequency [%]	# of different HLA ligands/core sequences
1	IGHG1	Immunoglobulin heavy constant gamma 1	33.3	16/5
1	ENO1	Alpha-enolase	33.3	7/6
1	GAA	Lysosomal alpha-glucosidase	33.3	5/4
1	EZR	Ezrin	33.3	13/5
1	HTRA1	Serine protease HTRA1	33.3	12/5
2	LGALS3BP	Galectin-3-binding protein	27.8	6/3

At the time of analysis, no or only few data of HLA class II ligand preparations from other normal tissues were available. Thus, an enhanced LiTAA analysis based on additional normal tissue data was not feasible.

3.3.3 Coverage estimations for the HLA class II ligandome of RCC

To estimate the level of exhaustion that was achieved for HLA class II with the current cohort and technical setup, cumulative analyses on identified HLA class II ligands and respective source proteins for tumor and benign RCC samples were performed (see figure 27).

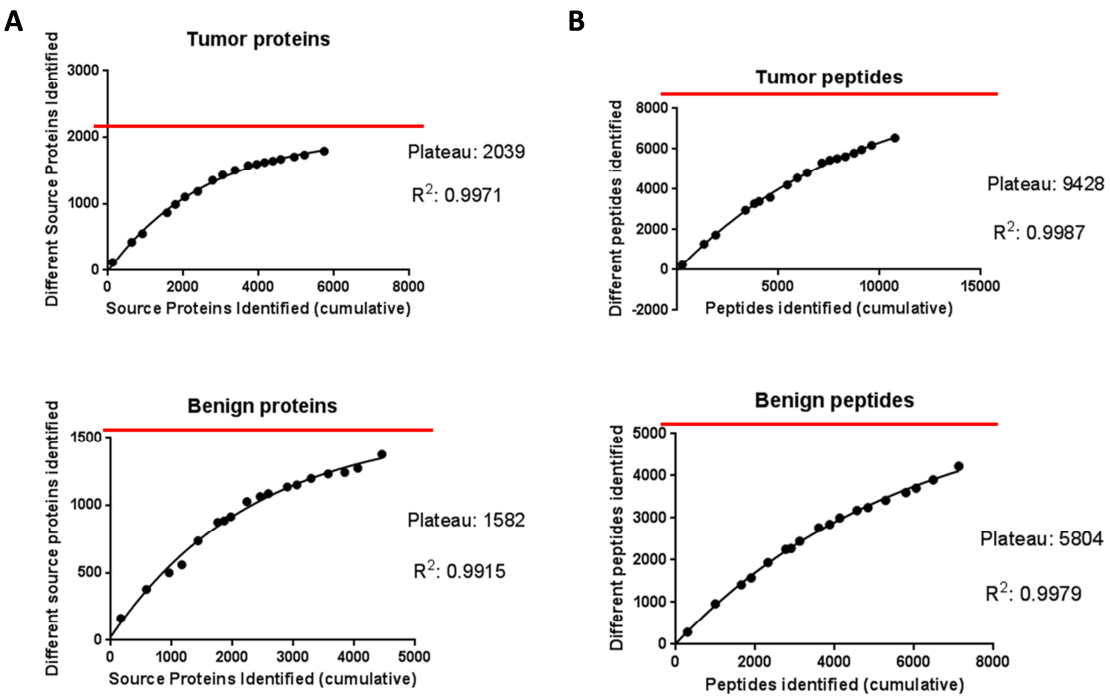

Figure 27: Estimations for the degree of exhaustion of HLA class II ligandome analysis in RCC. Nonlinear one-phase associations between cumulative numbers of identified source proteins and numbers of unique identified source proteins (A) and between cumulative numbers of identified peptides and numbers of unique identified peptides (B) in 18 RCC tumor and benign sample pairs. Red lines indicate calculated plateaus. R^2 value indicates goodness of fit.

Due to the lower sample number with evaluable data for HLA class II, the general degree of exhaustion is lower when compared to HLA class I. Another observation is that numbers of unique source proteins as well as numbers of unique peptides are substantially lower in HLA class II ligandomes. On the level of HLA ligand source proteins, the estimated achievable plateaus for tumor and benign samples were approximated to a lesser extent than for HLA class I with the analyzed cohort of 18 RCC sample pairs. The calculated plateau for HLA ligand source proteins was higher for tumor samples (2039) than for benign samples (1582), as it was the case for HLA class I ligandomes. On the level of identified HLA ligands, the estimated plateaus were approached to a greater extent than in HLA class I for tumor and benign samples, reflecting promiscuous and less restrictive peptide binding. Thus, extensive measurements of further RCC samples will reveal additional source protein identifications that are necessary to amend LiTAA definition for HLA class II.

3.4 Immunogenicity testing of LiTAA-derived peptides

In the course of development of the comparative approach, suitability of LiTAA-derived peptides for peptide vaccination have to be verified. The ability to induce peptide-specific T cell responses *de novo* is the most important requirement for peptide vaccines, indicating their immunogenicity. To test immunogenicity of LiTAA-derived HLA ligands, an interim analysis was performed and peptides were chosen to perform proof-of-principle priming experiments.

3.4.1 Selected HLA ligands for immunogenicity testing

Eleven peptides derived from various antigens that were identified as LiTAAs were selected and synthesized. The fragment spectra of synthetic peptides were compared to those of the naturally identified peptides for verification. Peptides were subsequently refolded to MHC monomers to perform priming experiments. The selected peptides are listed in table 13.

Table 13: Selected LiTAA-derived HLA ligands for immunogenicity testing. Internal peptide ID, peptide sequence, peptide mass, protein source, isotope labelling of the synthetic peptide and HLA restriction are listed. After final analysis of comparative profiling, source proteins were checked for tumor-exclusive representation again, since antigens were selected from an interim analysis (-: antigen is not defined as LiTAA any more, +: antigen is still defined as LiTAA in final analysis of RCC tumor/benign pairs, ++: antigen is still defined as LiTAA in final analysis of RCC tumor vs. normal tissues).

Peptide ID	Sequence	Mass	Source	LiTAA	Isotope	HLA
130543	SLDVSAPKV	915.5073	AHNK2	+	*V4	A*02
130544	AEIEIVKDL	1029.5754	P4HA1	+	*V6	B*44:03
141031	GLADASLLKKV	1113.6758	ATX10	-	-	A*02
141032	MPSASMTRL	992.4784	NDRG1	-	-	B*07/B*35
141034	SMTLAIHEI	1013.5216	DEGS1	-	-	A*02
140037	APGVGKSAL	799.4600	RAD	+	*V4	B*07
141007	RTAFTLKQK	1091.6452	SLN13	-	-	A*03
141012	IQAKKALDL	998.6125	COMTD1	++	-	A*03/A*33
141018	NPNLRIISL	1038.6186	ASM3A	+	-	B*07/B*14
141019	KIKSPAKMAEK	1229.7166	RGS5	-	-	A*03
141025	MPLLRQEEL	1127.6009	EHD2	-	-	B*07/B*08/B*14

All selected peptide sequences were verified by comparison of fragment spectra of synthetic peptides and naturally presented peptides (see Annex A). However, since the peptides were selected from an interim analysis, not all of the source proteins can still be

regarded as LiTAAs after final data evaluation. Several of the antigens were excluded as LiTAAs by final analysis of the RCC tumor/benign cohort (indicated with "-" in the LiTAA column in table 13). Others were still identified as LiTAAs in the RCC cohort but were excluded by comparative analysis with the complete normal tissue database (indicated with "+" in the LiTAA column in table 13). Of note, two of those antigens, AHNK2 and P4HA1, each had a single identification in the complete normal tissue database: the AHNK2-derived peptide ALEIPSGSQA was identified once (with one PSM) in a granulocyte sample but HLA typing of the sample (A*01, A*02, B*44, B*57) does not qualify this peptide as a binder. The P4HA1-derived peptide STIDKVSVL was identified once (with one PSM) in a benign liver sample but in this case also, HLA typing of the sample (A*03, A*68, B*15, B*40) does not qualify this peptide as a binder. Thus, these single identifications are probably false-positive identifications. The only LiTAA that was confirmed by comparative profiling with the normal tissue database was COMTD1 (marked with "++" in table 13). Despite neglection of the source proteins as LiTAAs, some of the used peptides remained tumor-exclusive (i.e. other peptides derived from their source proteins were identified in normal tissues). Those peptides might represent another class of tumor antigens that originate from differential antigen processing in malignant cells. This was the case for the peptides SLDVSAPKV, AEIEIVKDL, MPSASMTRL, IQAKKALDL and KIKSPAKMAEK. In fact, KIKSPAKMAEK is the highest-ranking tumor-exclusive peptide in the whole RCC cohort. It was identified in 10 different RCC samples (representing 30.3 % of all samples) and never on any of the 138 normal tissues used for exclusion in comparative profiling.

3.4.2 Immunogenicity testing by aAPC priming experiments

Synthetic peptides were refolded into HLA monomers as described in 2.2.2. This was successful for all but one peptide (IQAKKALDL). After biotinylation, HLA monomers were used to generate artificial antigen presenting cells for *in vitro* T cell priming and tetramers for experiment readout by FACS analysis. CD8+ T cells were isolated from whole blood samples of donors with matched HLA typings. For each donor, at least 24 priming experiments (wells) were conducted for each tested peptide to facilitate priming of low-frequent, peptide-specific naïve T cells. Frequencies of peptide-specific naïve T cells are estimated to range between 10^{-5} to 10^{-7} [286, 287]. Hence, input of 24 million CD8+ T cells

should be sufficient for priming of low-frequent peptide-specific naïve precursors. After T cell priming, cells were analyzed by staining with respective tetramers to identify peptide-specific T cells. An example for FACS analysis is depicted in figure 28.

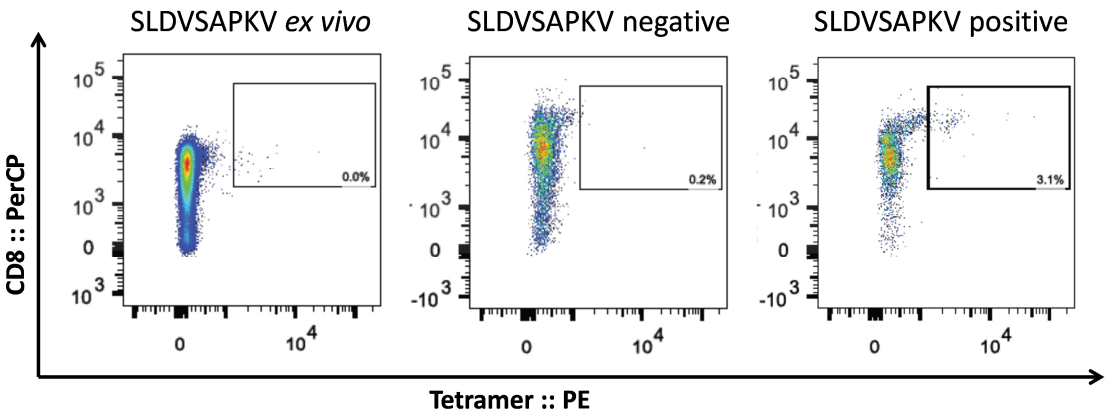

Figure 28: Representative example of tetramer staining after aAPC priming. Cells were pre-gated for lymphocytes, single cells and viable cells. CD8 was stained with PerCP, the tetramer dye was PE. Tetramers were used to stain T cells *ex vivo* to exclude existing memory T cell responses in blood donors (left). Tetramers were used to stain T cells that were primed with an irrelevant peptide to exclude unspecific binding (middle). Cells that were CD8::PerCP and Tetramer::PE double-positive cells were regarded as peptide-specific CD8+ T cells (right).

For each priming experiment, *ex vivo* stainings of PBMC with the corresponding tetramers were conducted to exclude existing memory T cell responses in blood donors. As a negative control, T cells from the same donor that were primed with an irrelevant peptide were tetramer stained to exclude unspecific binding of the tetramer. Cells that were stained double-positive for CD8 and tetramer were regarded as peptide-specific. Data was evaluated based on following criteria: the tetramer-positive population had to contain at least 0.2 % of all CD8+ T cells to be considered as positive priming result. Additionally, the percentage of tetramer-positive cells at least had to be doubled when compared to the negative control. The results of the priming experiments are summarized in table 14.

Table 14: Summary of aAPC T cell priming results. Immunogenicity testing was performed with T cells from eight whole blood samples (see table 4). Peptides were tested for immunogenicity in HLA matched donors. Priming results of tested peptides are indicated in the matrix below blood donor IDs. Red fields indicate negative priming results. Green fields indicate positive priming results.

Sequence	HLA	# Tests	# Positive	# Positive wells	Frequency [%]	J136	J147	J154	J164	J171	J174	J185	J193
SLDVSAPKV	A*02	4	3	34	75	0	1	1					1
AEIEIVKDL	B*44	1	0	0	0							0	
GLADASLLKKV	A*02	5	4	11	80	0	1	1		1			1
MPSASMTRL	B*07	3	1	1	33		1			0	0		
SMTLAIHEI	A*02	3	2	18	67			0		1			1
APGVGKSAL	B*07	2	2	2	100		1		1				
RTAFTLKQK	A*03	2	0	0	0				0		0		
NPNLRIISL	B*07	2	1	3	50					0	1		
KIKSPAKMAEK	A*03	2	0	0	0				0		0		
MPLLRQEEL	B*07	1	1	3	100				1				

All HLA-A*02 and –B*07-restricted peptides were proven to be immunogenic by *in vitro* aAPC primings. The HLA-B*44:03-restricted peptide could only be tested once, due to relatively low allele frequency of B*44 less blood donors were available. A second problem was the missing subtyping of HLA-B*44 positive donors. Subtypes of HLA-B*44 exhibit different peptide binding restrictions, which could influence peptide recognition by T cells in case of a mismatch. Both HLA-A*03-restricted peptides were tested twice and immunogenicity could not be evidenced. This might partly have been due to bad quality of the HLA monomers, as elevated tetramer signals were also detectable in the negative controls. In general, immunogenicity testing should include at least five different blood donors for any peptide, so that no final conclusion could be made on the immunogenicity of those peptides that did not yield positive results yet.

3.5 Identification of mycobacterial HLA ligands

To identify HLA ligands derived from mycobacterial antigens, two approaches were employed. First, the B-LCL cell line JY was infected with a viral vector encoding for several mycobacterial antigens and HLA preparation was performed. Second, monocyte-derived macrophages were generated from healthy blood donors and subsequently infected with live mycobacteria, followed by HLA preparation. Analysis of MS data generated from

these samples was challenging since data had to be processed against *Mtb* (and *Vaccinia*) protein databases in addition to the human proteome. Fragment spectra had to be evaluated with focus on which suggested peptide sequence annotation was best fitting.

3.5.1 HLA class I-presented peptides from B-LCL after infection with MVA-TBF

The B-LCL cell line JY was infected with MVA-TBF with a MOI of 5 as described in 2.4.4. The use of this infection model had several advantages: JY is homozygous for HLA-A, -B and –C, thus possible binding motifs of identified HLA ligands were reduced. In addition JY has extraordinarily high expression of HLA molecules which facilitated HLA ligandome analysis. The viral vector MVA-TBF on the other hand encodes only for few antigens but possesses extreme virulence, which increased the probability of antigen expression. Furthermore, immune evasion mechanisms of live mycobacteria were circumvented by this approach. After HLA preparation and MS analysis, raw data was processed against three distinct protein databases containing human, mycobacterial and viral protein sequences. The software ProteomeDiscoverer gave out ranks indicating the probability for a fragment spectrum to match to each of the suggested peptide sequences from the three databases. These ranks, in combination with manual interpretation of fragment spectra and consideration of HLA ligand motifs, allowed for the assignment of fragment spectra to a suggested peptide sequence from one of the databases. As a proof for a working infection system many HLA ligands derived from *MVA* proteins were identified (see table 15).

Table 15: Identified *MVA*-derived HLA class I ligands. Suggested peptide identifications with matching HLA binding motifs and superior fragment spectrum annotation for *MVA*-derived peptide sequences.

Sequence	HLA	# PSMs	Protein
IVIEAIHTV	A*02	51	Thymidilate kinase
GLNDYLHSV	A*02	13	Protein O1
SLKDVLVSV	A*02	13	DNA-directed RNA polymerase 7 kDa subunit
ALDEKLFLI	A*02	11	Intermediate transcription factor 3 large subunit
KLFSDISAI	A*02	11	Protein E5
KLIIHNPEL	A*02	8	Surface antigen S
ILDDNLYKV	A*02	6	Putative nuclease G5
ILSLPRIAL	A*02	5	RNA helicase NPH-II
KVDDTFYYV	A*02	4	Interferon antagonist C7
AAKGASMTL	A*02	3	Thymidilate kinase
DMMSLNLTI	A*02	1	Interleukin-1-binding protein
FVKFKLTL	A*02	1	Protein B17
ILSDENYLL	A*02	1	Protein A6
IVQEAILSL	A*02	1	RNA helicase NPH-II
KISNTTFEV	A*02	1	3 beta-hydroxysteroid dehydrogenase/Delta 5→4-isomerase
VMKANNSVI	A*02	1	3 beta-hydroxysteroid dehydrogenase/Delta 5→4-isomerase
YIIGNIKTV	A*02	1	Protein A35
APRSGLSL	B*07	10	Deoxyuridine 5'-triphosphate nucleotidohydrolase
SPRPTASSDSL	B*07	7	Protein I3
HPTSNSLNAL	B*07	3	Protein B14
IPSPGIML	B*07	3	Pro-vaccinia growth factor
SPRIGDQL	B*07	1	Major core protein 4b
IFLDYKKY	C*07	1	mRNA-capping enzyme catalytic subunit

Processing against the *Mtb* database revealed HLA-presented peptides from two of the four vector-encoded mycobacterial antigens (see table 16). The validity of identifications was verified by comparison of fragment spectra from naturally presented peptides and synthetic peptides. Spectral validation of the peptides was already performed prior to this work [288], as this was not the first infection experiment with MVA-TBF. First results were confirmed by this experiment, with additional identification of the TB9.8-derived peptide AAKVNTLLDV. The synthetic peptide was not available to perform spectral validation.

Table 16: Identified *Mtb*-derived HLA class I ligands. Suggested peptide identifications with matching HLA binding motifs and superior fragment spectrum annotation for *Mtb*-derived peptide sequences.

Sequence	HLA	# PSMs	Protein
LLDAHIPQL	A*02	18	Esat-6 like protein esxG
RVRGAVTGM	A*02	6	Diacylglycerol acyltransferase/mycolyltransferase Ag85A
HVKPTGSAV	A*02	3	Diacylglycerol acyltransferase/mycolyltransferase Ag85A
AAKVNTLLDV	A*02	2	Esat-6 like protein esxG
IYHPQQFVY	C*07	9	Diacylglycerol acyltransferase/mycolyltransferase Ag85A

In an attempt to identify HLA class II ligands of viral and mycobacterial origin, autophagy and mutual cross-presentation of cytoplasmic proteins to MHC class II was induced. For this purpose, cells were “starved” in FCS-free medium after infection with MVA-TBF and prior to HLA ligand preparation. HLA class II ligands derived from viral proteins could be identified, however no ligands of mycobacterial origin were detected (see table 17).

Table 17: Identified *MVA*-derived HLA class II ligands. Peptide identifications show length variants typical for HLA class II binders. Core sequences are indicated in red.

Sequence	Protein
DKNDVYSMATARSLD DKNDVYSMATARSLDA DKNDVYSMATARSLDAL DVYSMATARSLDA DVYSMATARSLDAL	Envelope protein F13
QLKNLLAQIGGDAA LKNLLAQIGGDAA NLLAQIGGDAA	25kDa core protein A12L
LCYFILIFNIIVP LCYFILIFNIIVPA	Virion membrane protein A21
AKRMLFTSTNDKI KRMLFTSTNDKI	Protein L1

3.5.2 HLA class I-presented peptides from macrophages infected with live *Mtb*

Monocyte-derived macrophages were generated from leukapheresis products from healthy donors. After maturation, the cells were transported to the University Hospital Ulm for infection with the live mycobacterial laboratory strain H37Rv in an appropriate S3 laboratory (see 2.4.6). After production of the cell lysate and sterility testing, cell lysates were transferred back to Tübingen to perform HLA preparation and MS analysis. As described in 3.5.1, raw data had to be processed against distinct databases for human and *Mtb* proteins. Assignment of fragment spectra to suggested peptide sequences was similarly conducted by manual interpretation and consideration of HLA binding motifs. Candidate *Mtb*-derived HLA ligands should furthermore be validated by comparison of fragment spectra of naturally presented and synthetic peptides. If cell counts were high, a control HLA preparation with uninfected macrophages was performed. Results of the infection experiments for HLA class I and II are listed in tables 18 and 19.

Table 18: Identified peptides from HLA class I preparations of *Mtb*-infected macrophages. Uninfected controls were performed for samples with high cell counts. N.d.: not done.

Sample	Human Peptide IDs	Human PSMs	MTB Peptide IDs	MTB PSMs	Uninfected Control Peptides	Uninfected Control PSMs
Leuka04	609	2547	13	27	n.d.	n.d.
Leuka05	0	0	0	0	n.d.	n.d.
Leuka06	22	41	0	0	180	544
Leuka07	18	45	1	1	106	421
Leuka08	217	785	57	57	n.d.	n.d.

Table 19: Identified peptides from HLA class II preparations of *Mtb*-infected macrophages. Uninfected controls were performed for samples with high cell counts. N.d.: not done.

Sample	Human Peptide IDs	Human PSMs	MTB Peptide IDs	MTB PSMs	Uninfected Control Peptides	Uninfected Control PSMs
Leuka04	348	1027	4	24	n.d.	n.d.
Leuka05	43	266	0	0	n.d.	n.d.
Leuka06	10	34	0	0	35	251
Leuka07	27	172	0	0	41	328
Leuka08	9	35	0	0	n.d.	n.d.

A selection of candidate *Mtb*-derived peptides identified from these experiments was subjected to spectral validation by comparison to spectra of synthetic peptides. The selected peptides are listed in table 20.

Table 20: Putative *Mtb*-derived HLA ligands selected for spectral validation. Peptides with HLA binding motif and highest rank for a fragment spectrum match to the *Mtb* protein database were selected for spectral validation. Possible HLA restrictions and PSMs are indicated.

Sequence	HLA	# PSMs	Gene	Protein	Spectral validation
LIAVPTGIK	A*03	4	ctaD	Probable cytochrome c oxidase subunit 1	ambiguous
KTTTAEALGK	A*03	2	eccA2	ESX-2 secretion system protein EccA2	ambiguous
TMEIVGRLR	A*03	1	ispH1	4-hydroxy-3-methylbut-2-enyl diphosphate reductase 1	no
LVDAAVHSY	A*26	3	hemC	Porphobilinogen deaminase	no
DVLGLLRDAY	A*26	1	kgd	Multifunctional 2-oxoglutarate metabolism enzyme	no
MVASGVVSVY	A*26	1	plsB1	Putative acyltransferase plsB1	no
LPPGVVNVV	B*51	7	n.a.	Probable aldehyde dehydrogenase	no
DARNELAPV	B*51	2	pknK	Serine/threonine-protein kinase PknK	no
EALVRTDI	B*51	1	n.a.	Uncharacterized RNA pseudouridine synthase Rv1711/MT1751.1	no
LAQLPITI	B*51	1	qcrA	Ubiquinol-cytochrome c reductase iron-sulfur subunit	no
DAIRSAAL	B*51	1	rpsB	30S ribosomal protein S2	ambiguous
FSISEGLEEY	B*57	1	ctpG	Probable cation-transporting ATPase G	no
ALTDRVAGTLREW	Cl. II	1	recB	RecBCD enzyme subunit RecB	no
KSASTMLMVDNATGVKAL	Cl. II	2	Rv0945	Uncharacterized oxidoreductase Rv0945	no

Spectral validation of the candidate peptides did not result in clearly confirmed *Mtb*-derived HLA ligands (see Annex B). Further peptide candidates were selected from more recent experiments but peptide synthesis and spectral validation was not yet performed by the time this work was finished. New candidates for *Mtb*-derived HLA ligands are listed in table 21.

Table 21: Candidate peptide list for *Mtb*-derived HLA ligands. Putative HLA ligands awaiting verification by spectral comparison. Possible HLA restriction, PSMs and IonScores are indicated.

Sequence	HLA	# PSMs	Ion Score	Gene	Protein
AATVRDAL	B*51	1	25	hemC	Porphobilinogen deaminase
TAAGSAVSAL	B*51	1	21	smc	Chromosome partition protein Smc
PGSVLSAAGV	B*51	2	22	PPE3	Uncharacterized PPE family protein PPE3
LAKKAESL	B*51	2	26	atpD	ATP synthase subunit beta
ALGAKLSSL	A*02	1	32	eccC4	ESX-4 secretion system protein EccC4
YGPGLGTSL	B*51	1	20	rmlA	Glucose-1-phosphate thymidylyltransferase
RMSAVTAI	A*02	1	22	Rv1486c	Uncharacterized protein Rv1486c
MVTAAYVL	A*02	1	20	mraY	Phospho-N-acetylmuramoyl-pentapeptide-transferase
VGPVARGDV	B*51	2	22	Rv2468c	Uncharacterized protein Rv2468c
RPQDGAII	B*07	1	23	dnaE1	DNA polymerase III subunit alpha
LVAGGPFVL	A*02	1	26	egtB	Hercynine oxygenase
TGQIDRAL	B*51	1	20	mazE6	Antitoxin MazE6
LPPGVVNVV	B*51	5	22	Rv0458	Probable aldehyde dehydrogenase
RVPDVDSL	A*02	1	23	Rv1375	Uncharacterized protein Rv1375
MLRDLAAL	A*02	1	29	Rv3427c	Putative ATP-binding protein Rv3427c in insertion sequence
IPIALTEM	B*07/ B*51	2	23	PPE68	PPE family immunomodulator PPE68
LLALLQQL	A*02	10	27	PPE4	PPE family protein PPE4
GLPAATVQR	A*03	1	24	ligB	DNA ligase B
VAGAVLREV	B*51	1	20	devS	Redox sensor histidine kinase response regulator DevS
SLVAGGSLVL	A*02	1	23	dxr	1-deoxy-D-xylulose 5-phosphate reductoisomerase
VAGRNVGAAI	B*51	1	21	pdtaS	Probable sensor histidine kinase pdtaS
LASDRGAGAL	B*51	1	25	PPE46	Uncharacterized PPE family protein PPE46
AFAKTPPTV	B*51	1	24	ffh	Signal recognition particle protein
LLNNPHRL	A*02	7	25	relE	Toxin RelE
RLAAIPILL	A*02	1	21	mmpL9	Probable transport protein MmpL9
VGRVPLLLL	B*51	2	23	glgP	Glycogen phosphorylase
IAQQRAIIV	B*51	4	32	secA2	Protein translocase subunit SecA 2
LVEQAQAQK	A*03	1	21	ctpA	Copper-exporting P-type ATPase
KVQGSAFNSV	A*02	1	21	eccC3	ESX-3 secretion system protein EccC3
LAQGAEIHVM	B*51	1	23	adhA	Probable alcohol dehydrogenase AdhA

4 Discussion

The data produced during this work will be part of a superior effort to define the human immunopeptidome in its entirety. Only recently, mapping of the human proteome was achieved in a joint effort [289, 290]. Experimental evidence for quantitative protein expression in human organs based on direct identification of the proteins by shotgun mass spectrometry approaches rather than by RNA expression profiling will support immunotherapeutic advances. Mapping the human immunopeptidome in health and disease will be the next big step towards efficient immunotherapeutic approaches [291-295]. Mapping the human proteome became feasible due to technical improvements of mass spectrometers and enhanced peptide separation capabilities by uHPLC, as well as improved data analysis algorithms. The entire human transcriptome is estimated to contain 20,000 to 25,000 genes and the amount of unique proteins will not greatly exceed this number [296, 297], constituting a limited source protein range. Furthermore, tryptic digestion of proteins produces equal (and predictable) peptide species independent of the individual tissue donor. Such invariable conditions facilitated mapping of the human proteome. Mapping of the complete human immunopeptidome however, will be an unequally more difficult enterprise. While the protein sources remain the same as for proteome mapping, the variety of peptide species will multiply considerably due to HLA polymorphisms and distinct HLA binding motifs. A concomitant effect is variety in detection opportunities by mass spectrometry of such peptides. While tryptic peptides show good ionization properties, HLA ligands vary greatly in this aspect, depending on the actual peptide sequence. Additional hurdles are isolation of HLA ligands from tissues as a prerequisite for identification compared to simple cell or tissue lysis and subsequent proteolytic digestion. In addition, HLA ligand presentation is not solely dependent on protein expression but also on protein turnover and antigen processing. Thus, the range of actual amounts of molecules of unique peptide species in complex samples is probably higher than the dynamic range that modern mass spectrometers can employ, so that low-abundant peptide species are not detectable. To build a comprehensive map of the immunopeptidome, those issues have to be tackled. Technological progress will facilitate measurement of complex samples with high dynamic ranges, so that the other tasks are at hand. One is improvement of HLA ligand isolation and analysis settings, another is HLA

preparation and measurement of healthy and malignant (or infected) human tissues. In the meantime, interim analyses may provide interesting new targets for immunotherapeutic approaches albeit these targets may be falsified at any time until the complete immunopeptidome was mapped. For the RCC cohort at least, saturation of the estimated total identifiable HLA class I ligand source proteome was almost reached, as described in 3.2.4. It may therefore serve as a relatively robust antigen definition database.

4.1 Improvement of HLA preparation for HLA ligandomics

HLA preparation is still a bottleneck for exhaustive HLA ligandome analysis. The estimated amount of HLA molecules on renal cells is 40,000 [298]. The median number of HLA class I ligands that was identified on RCC tumors was 1,641 unique peptides. This would imply (if all cells from a sample were uniformly concerning their HLA ligandome) that the median peptide copy number presented on single cells would calculate to 24 molecules. This estimation lies close to an optimal median value, as peptide-specific T cells were described to be reactive to as few as 2-10 MHC:peptide molecules on a single cell [299]. However, the dynamic range for peptide amounts is not taken into account in this equation. Furthermore, the cell composition of tumor tissues is not uniform and consequently the HLA ligandome of single cells is not either. Thus, the detection threshold at the moment is probably higher (also reflected by generally lower peptide yields in more uniform benign tissues, where the median of identifications was 846 calculating to a median peptide copy number of 47 per cell). The estimations of peptide copy numbers between 24 and 47 per cell based on the experimental datasets obtained during this work are in line with earlier calculations regarding this issue [300]. Another observation is that peptide yields are highly dependent on the sample mass used for HLA preparation. For cryotome preparation, samples of 1 g were used and cryotome preparation significantly outperformed standard preparation. The strongest increase was seen in PSM values of cryotome preparations. This might indicate that either the analysis reached an exhaustive level or that MS settings should be tweaked to identify less abundant peptides. In samples with high complexity and dynamic range, co-eluting highly abundant peptides produce multiple fragment spectra whereby co-eluting less abundant

peptides are not selected for fragmentation and will not be identified. Therefore, increasing the dynamic exclusion time for measurements of such exhaustive samples may result in enhanced peptide identifications.

A second aspect is data evaluation of exhaustive HLA ligandomics. Technical improvements and the resulting large datasets were accompanied by the necessity for definition and application of filter criteria. While the application of filters for FDR and ion score produces a dataset with high confidence, a large amount of peptide identifications is discarded as false negative. This issue could be tackled by generation of a spectral database from existing peptide identifications for raw MS data processing. This would also remove a data processing bias concerning ion scores and FDR values, as the used software tools were originally programmed for the identification of tryptic peptides. Furthermore, a valid HLA annotation tool for identified peptides could serve as an additional data filtering tool.

4.2 Exhaustive HLA ligandome analysis for RCC

The average amount of identified HLA class I ligands was approximately doubled in tumor samples when compared to benign samples (see table 6). This may be only partly explained by samples sizes, which were usually larger for tumor than for benign tissues. Comparisons of bulk RCC tumors and autologous benign renal tissue revealed an elevated HLA class I expression in bulk tumors [301, 302]. These analyses however were based on bulk tumor tissues and did not account for tissue heterogeneity: intra-tumoral presence of distinct tumor cells like tumor stem cells and branches of different malignant cell clones may enhance the HLA ligand repertoire [303]. Additionally, other cell types within the tumor mass like endothelial and stromal cells and most importantly, infiltrating immune cells probably contribute to the entirety of the HLA ligandome of bulk tumor samples [304, 305]. Hence, the amount of obtained HLA ligands from a given tumor sample may reflect the degree of immune cell infiltration within this tumor and HLA ligands derived from immune cells need to be identified as such to eliminate them from tumor antigen definition. Analysis of PBMC HLA ligandomes at least partly accounts for this issue, reflecting the antigens that were defined as LiTAAs in the RCC-exclusive analysis (see 3.2.3) but were later rejected when PBMC and other healthy tissue HLA

ligandomes where added to comparative analysis (see 3.2.5). Exhaustive HLA ligandomics enabled the implementation of a new approach to identify tumor-associated antigens by comparative profiling. The advantage of this approach is that target selection solely relies on experimentally identified antigens and comparison of HLA ligandomes of healthy and malignant tissues. These antigens may prove to be superior targets compared to classically defined tumor antigens in immunotherapeutic approaches. One drawback of those classical tumor antigens is that most of them were identified by RNA expression profiling. However, HLA peptide presentation and RNA expression were shown to correlate only poorly [306]. This is consistent with our own data: we performed RNA expression analysis for three RCC tumor and benign sample pairs and calculated differential expression values (FPKM tumor/benign). HLA ligandome analysis was performed for the same samples and unique HLA ligand representation was estimated by intensities of precursor ions (label-free quantification, LFQ). Correlation analysis was performed for the set of HLA ligand source proteins that was detectable in both RNAseq and MS experiments (see figure 29).

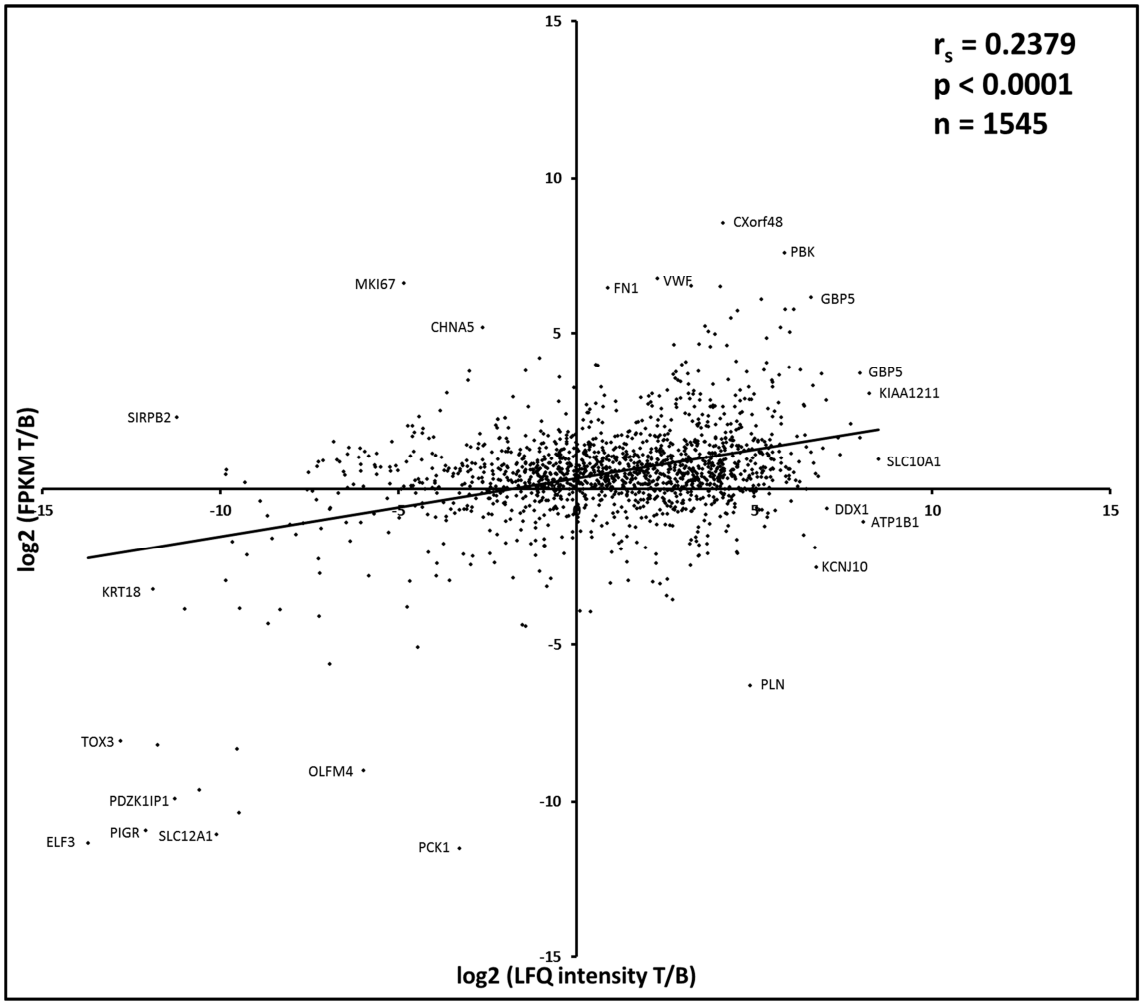

Figure 29: Correlation analysis of RNA expression and HLA ligand representation. Scatterplot of relative mRNA expression compared to relative representation of source proteins in the HLA ligandomes of 3 paired RCC patient samples (tumor/benign). Only proteins with values for FPKM and LFQ intensity in paired tumor and benign samples were included for analysis. Correlation was calculated with Spearman r test.

In addition, we compared the overlap of the top 100 overexpressed gene products (RNAseq) with the top 100 overrepresented HLA ligand source proteins identified in the three individual RCC tumor samples. Again, the overlap was poor in all cases (see figure 30). Hence, RNA expression is no indicator for HLA presentation, which disqualifies this analysis for selection of suitable target antigens for T cell-based immunotherapeutic approaches.

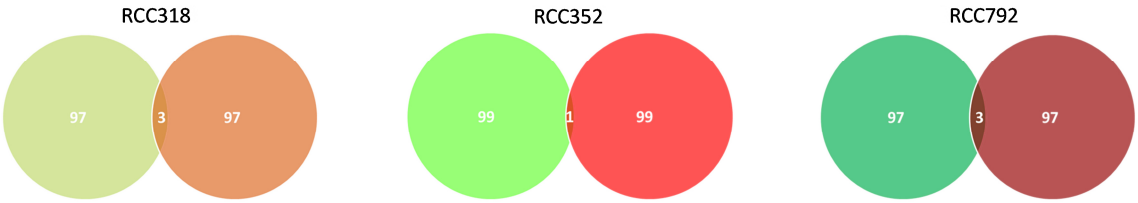

Figure 30: Overlap analysis of the Top 100 RNAseq and LFQ MS identifications. The Top 100 overexpressed gene products as identified by RNAseq (green) were compared to the Top 100 overrepresented HLA ligand source proteins as identified by LFQ MS (red) in three individual RCC tumor samples.

Comparative profiling identifies a new class of tumor antigens based on tumor-exclusive HLA representation of source proteins (LiTAAs). Those antigens should provide superior targets for T cell-based immunotherapies such as peptide vaccination. The identified top RCC antigens for HLA class I are partly already linked to RCC or cancer in general in the literature, while others were never associated with RCC before. ANGPTL4 is discussed as a biomarker for RCC as serum levels are elevated in RCC patients [307]. It is also one of the HIF-responsive genes, like many other proteins in the LiTAA lists for RCC [308]. CA12 was shown to be overexpressed in RCC [309]. Inhibition of ENTPD1 is discussed as a general cancer treatment as it produces extracellular adenosine that inhibits immune effector cells [310]. CA9 is the classical RCC tumor antigen and was already used in clinical studies [311]. LOX is discussed as a target for small molecule inhibitors in RCC and is associated with tumor progression [312]. COMTD1, KDELR3, MRPL55, PNO1, CRIPT and MTRR on the other hand were not linked to RCC or cancer in general so far. For the identified HLA class II antigens, the situation is quite similar. ENO1 is a tumor suppressor and shows increased expression in RCC [313]. EZR is implicated in various human cancers [314], as well as HTRA1 [315]. LGALS3BP was shown to be overexpressed in RCC [316] and is discussed as a serum biomarker for various cancers. IGHG1 and GAA were not linked to cancer or RCC in the literature so far. The fact that several of the identified LiTAAs are already associated with RCC or cancer in general in the literature may serve as an indicator that antigen discovery by comparative profiling is a suitable approach. The strategy needs further improvements, as some antigens may be discarded due to false positive identifications emerging only once in a benign or healthy sample (as described in 3.4.1). LiTAAs may also be suitable to delineate specificities of tumor-infiltrating T cells. Until now, only few of these specificities are known and insights into the targetome of TILs may pave the way for new immunotherapeutic treatment approaches such as

adoptive cell transfer with antigen-specific T cells. Additionally, a second class of antigens could be defined, based on actual tumor-exclusive HLA ligands rather than on HLA ligand source protein presentation frequency. Some of the identified antigens are discarded in LiTAA analysis however on the level of HLA ligands certain peptides may remain tumor-exclusive. This is the case for the peptide KIKSPAKMAEK (derived from the protein regulator of G-protein signaling 5, RGS5). While the source protein is represented with many other HLA ligands in the dataset of healthy tissues, this peptide was never found in any of the healthy tissues whereas it is the highest-ranking peptide in RCC tumor samples with identifications in 10 out of 33 tumor samples. Taking into consideration that this peptide is a binder for HLA-A*03 and HLA-A*11, it was found in 100 % of patient samples with a respective HLA typing. Such peptides might emerge exclusively in tumors due to differential antigen expression and might constitute a second class of valuable targets for T cell-based immunotherapies.

4.3 Design of peptide vaccines based on LiTAAs

A first approach to peptide vaccine design based on LiTAAs would be to select HLA-matched peptides from the highest-ranking LiTAAs for each individual patient based on the individual HLA typing. Such an approach would demand for a “warehouse” of suitable peptides that have been checked for immunogenicity. The ability to induce a specific T cell response is an important prerequisite for the selection of vaccine candidates. However, heterogeneity in RCC tumors seems to be extremely high. This could be observed in LiTAA analyses, where the highest-ranking antigen only had a presentation frequency of 27.3 %. Additionally, when comparing the top 100 antigens from three individual RCC tumor samples as identified by RNA expression analysis and LFQ MS, the overlaps are extremely low (see figure 31). Thus, HLA ligandome analysis of individual tumor samples should be performed prior to peptide vaccine design. The analysis does not take long and the educational benefit would greatly enhance vaccine design for individual patients. Individual expression of LiTAA-derived HLA ligands could be taken into account, adding an additional degree of personalization to the vaccine design (see figure 32). Furthermore, vaccination with peptides that are not expressed in the individual tumor would be avoided.

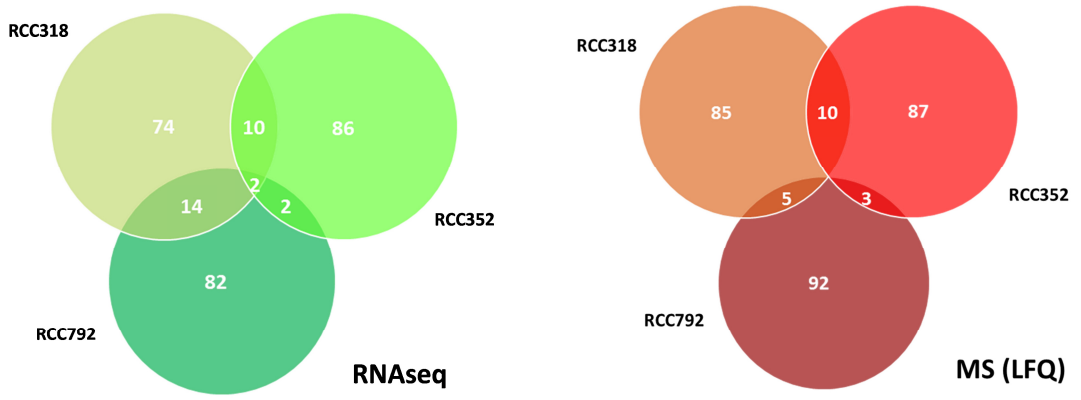

Figure 31: Patient individuality in RCC. Overlap analysis of the top 100 overexpressed gene products as identified by RNAseq (left, green) in three individual RCC samples. Overlap analysis of the top 100 LiTAAs as identified by LFQ MS (right, red) in three individual RCC samples.

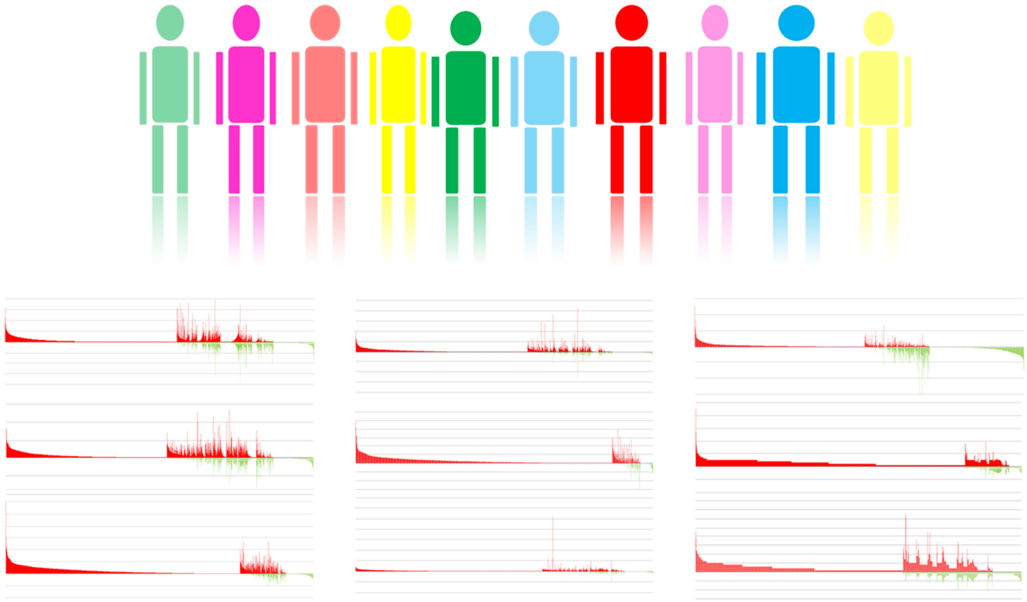

Figure 32: Design of peptide vaccines should account for tumor individuality. Each patient's tumor will exhibit different top-ranking LiTAAs. After MS analysis, peptides derived from the individual top-ranking LiTAAs are selected from the warehouse to design a tailored peptide vaccine.

4.4 HLA class II ligands for peptide vaccination

HLA ligandomics for class II generated no results in many of the samples. This raises the question why, especially when analysis of class I preparations yielded good results. The preparation is conducted simultaneously, so that general failure of preparation can be excluded for most of the samples. One explanation might be that HLA class II molecules are differentially expressed on tumor cells and expression is much more variable than for

HLA class I [317]. Another, more likely explanation might be that HLA class II molecules are not expressed on tumor cells but rather on tumor-infiltrating leukocytes like DCs and macrophages [305]. If this was the case, the amounts of identified HLA class II ligands should correlate with leukocyte infiltrates in the respective tumor samples and would reflect an inflamed phenotype in benign tissues in which HLA class II ligands could be identified. In general, addition of HLA class II-restricted peptides to peptide vaccines against RCC would be feasible however the database for LiTAAs should be extended in the RCC cohort to reach saturation of the identifiable source proteome. Analysis of the HLA class II ligandomes of healthy tissues would be a second prerequisite to obtain reliable results from comparative profiling, especially data from PBMC are of high importance if one assumes that most HLA class II ligands from bulk tumor samples are derived from immune cell infiltrates. One drawback of HLA class II ligands is a more elaborate immunogenicity testing. Production of HLA class II monomers with refolded peptides is not possible and classical priming experiments with dendritic cells are cost-intensive and time-consuming. These facts aggravate high-throughput priming screenings for immunogenicity testing of HLA class II ligands. However, antigen-specific CD4+ T cells can have beneficial effects on tumor therapy as they provide help for other immune cells and were in some cases also shown to have cytotoxic capabilities [318-320]. Additionally, cytokine secretion responses of such cells were shown to induce senescence in tumor cells whereby tumor outgrowth and metastasis may be prevented [321].

4.5 Immunogenicity analysis

As shown in chapter 3.4, all selected HLA-A*02- and –B*07-restricted peptides proved to be immunogenic, while the immunogenicity of the HLA-A*03- and -B*44:03-restricted could not be documented yet. Priming should at least be performed in five donors before peptides are discarded as non-immunogenic. Especially for the peptide KIKSPAKMAEK it would be worth continuing immunogenicity testing. At the time of experiment performance, inclusion bodies for HLA-A*03 were not optimized yet, which might explain negative priming results. For both HLA-A*03-restricted peptides, the background in negative controls of tetramer stainings was quite high. In case of the HLA-B*44:03-restricted peptide, testing could be performed only once due to low frequencies of HLA-

B*44 positive blood donors. Another problem might be that HLA subtyping is not available for blood donors. In case of HLA-B*44, the subtyping influences peptide binding motifs, therefore priming of cells from subtype-mismatched donors may be impaired.

Immunogenicity analyses have to be performed for the newly defined RCC LiTAA-derived peptides to set up a peptide warehouse for off-the-shelf design of peptide vaccines. The ability of a HLA ligand to induce peptide-specific T cell responses *in vitro* and *in vivo* is essential for selection of peptide vaccine candidates. However, as it was seen in the experiments at hand, high-throughput priming with aAPCs identified peptides as immunogenic that were derived from proteins that were later discarded from the LiTAA list due to representation in several normal tissues. This indicates that negative selection of peptide-specific naïve T cells in the thymus is not absolute and priming against ubiquitous antigens is, at least *in vitro*, possible. For more representative analyses of immunogenicity *in vivo*, RCC patients should be screened for spontaneous T cell responses against LiTAA-derived, HLA-matched peptides. Such existing memory T cell responses in patients can be easily detected by ELISPOT analyses and were already shown to correlate with better outcome of patients in chronic lymphatic leukemia (CLL) [292].

4.6 *Mtb*-derived HLA ligands

Identification of *Mtb*-derived HLA ligands was successful in the cell line JY infected with MVA-TBF. This model proved useful for HLA ligandome analysis and may provide HLA ligands of the encoded mycobacterial antigens for additional HLA allotypes if the vector would be used for infection of additional cell lines or primary cells. As this vector is already in clinical trials, the identified peptides may serve as important tools for T cell immunomonitoring to assess the efficacy and immunogenicity of such a subunit / booster vaccine. However, it remains questionable if these HLA ligands would constitute good candidates for a peptide vaccine against TB. To assess this question, further experiments concerning the efficacy and reactivity of peptide-specific T cells need to be performed. In fact, some of the peptides were already shown to be immunogenic and specific memory T cell responses are present in BCG-vaccinated individuals [288]. The peptides might furthermore prove useful to detect latent infections in asymptomatic individuals to provide more reliable screening assays than the currently used ones.

Identification of *Mtb*-derived HLA ligands from primary cells (macrophages) proved to be a difficult task. Experimental outcomes were extremely variable, which was probably due to the complicated experimental setup. Transfer of cells between laboratories probably had an impact on outcomes. Additionally, cell lysates had to be tested for sterility after cell infection and lysis. Therefore, cell lysates had to be frozen until sterility testing was completed and HLA immunoaffinity purification could ensue. Interference of such an intermittent freezing step with HLA precipitation should be ruled out as a cause of experimental variance. A second issue was data processing, as MS raw data had to be processed against two protein databases of different size (*Mtb* and human). FDR values and ion scores are dependent on search database size, therefore spectral annotation features are not reliable in this case, demanding for manual fragment spectrum evaluation. One possibility would be the use of mycobacteria that were cultured in medium with stable isotope-labelled amino acids. This technique would allow to distinguish peptide origin in MS experiments producing more reliable results on the one hand and to reduce the necessity to validate any candidate peptide by comparison to synthetic peptide fragment spectra (as performed in this work) on the other hand [322]. Usage of live mycobacteria might further aggravate identification of *Mtb*-derived HLA ligands, as mycobacteria have evolved a multitude of immune evasion mechanisms on cellular level. After phagocytosis, they are residual in phagosomes and avoid digestion and destruction by ROS. They prevent phagosome maturation and fusion with lysosomes. Thus, presentation of mycobacterial HLA class II ligands is probably impeded as MIIC compartments containing mycobacteria will probably not form in infected cells. Entry of mycobacteria into the cytosol and therefore to MHC class I processing pathways is usually excluded in early infection states and only takes place in dissemination events, accompanied by apoptosis of the host cells. Thus, for effective identification of *Mtb*-derived HLA ligands, the protocol should be adapted to circumvent these shortcomings. MHC preparation should be performed to the step of peptide purification in a S3 laboratory. Ready-to-use MS samples could await measurement in frozen condition until sterility testing was performed. Furthermore, infection with attenuated *Mtb* or loading of macrophages with *Mtb* lysates may enhance processing of mycobacterial antigens for HLA presentation by avoidance of immune escape mechanisms of live mycobacteria.

Annex

A Fragment spectra of selected peptides for immunogenicity testing

Eleven peptides were synthesized and fragment spectra of synthetic peptides were compared to fragment spectra of naturally presented peptides to validate peptide identifications. Fragment spectra of naturally presented peptides are derived from complex HLA ligand extraction samples from primary tissues. Thus, those fragment spectra may contain unexplained mass peaks due to co-elution of different peptide species. Verification of peptide identities was performed by matching of mass peaks from synthetic peptide spectra to those of naturally presented peptides. Some of the peptides were synthesized with a heavy isotope-labelled amino acid (indicated by *).

SLDVSAPKV (*V4)

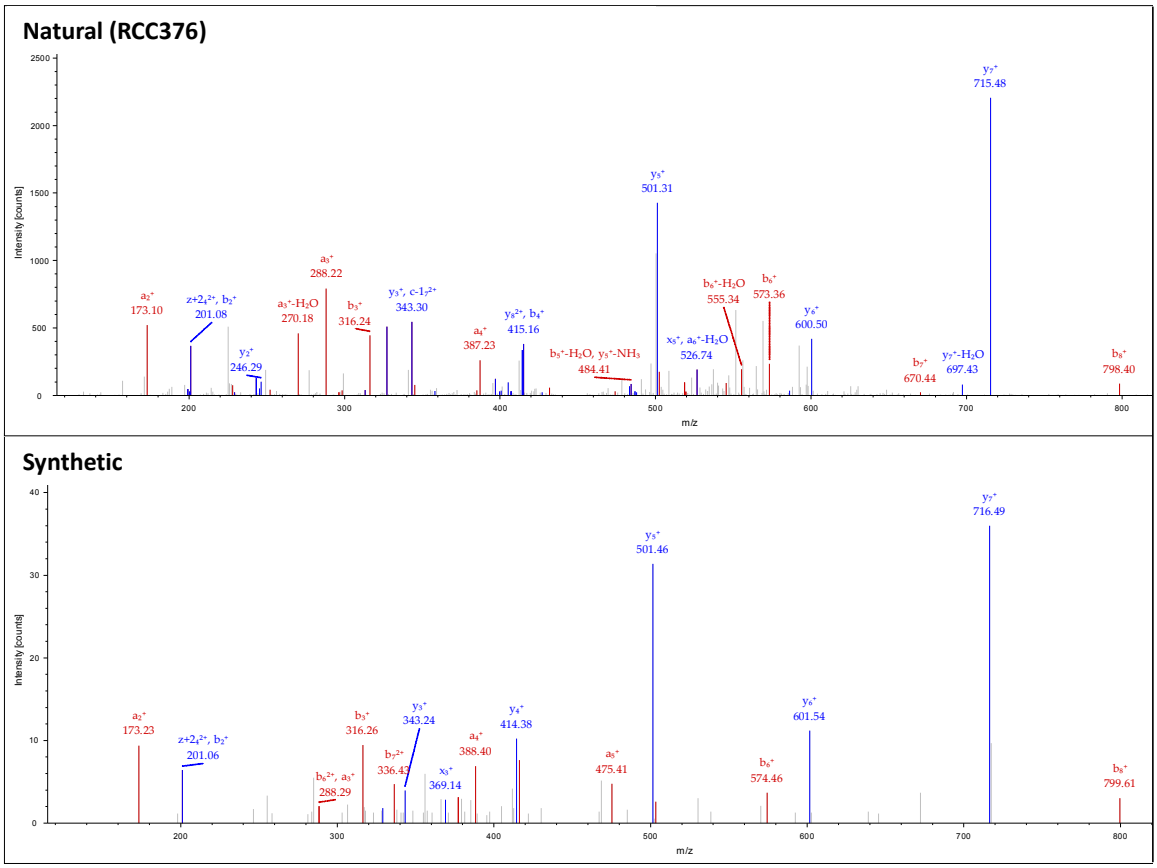

AEIEIVKDL (*V6)

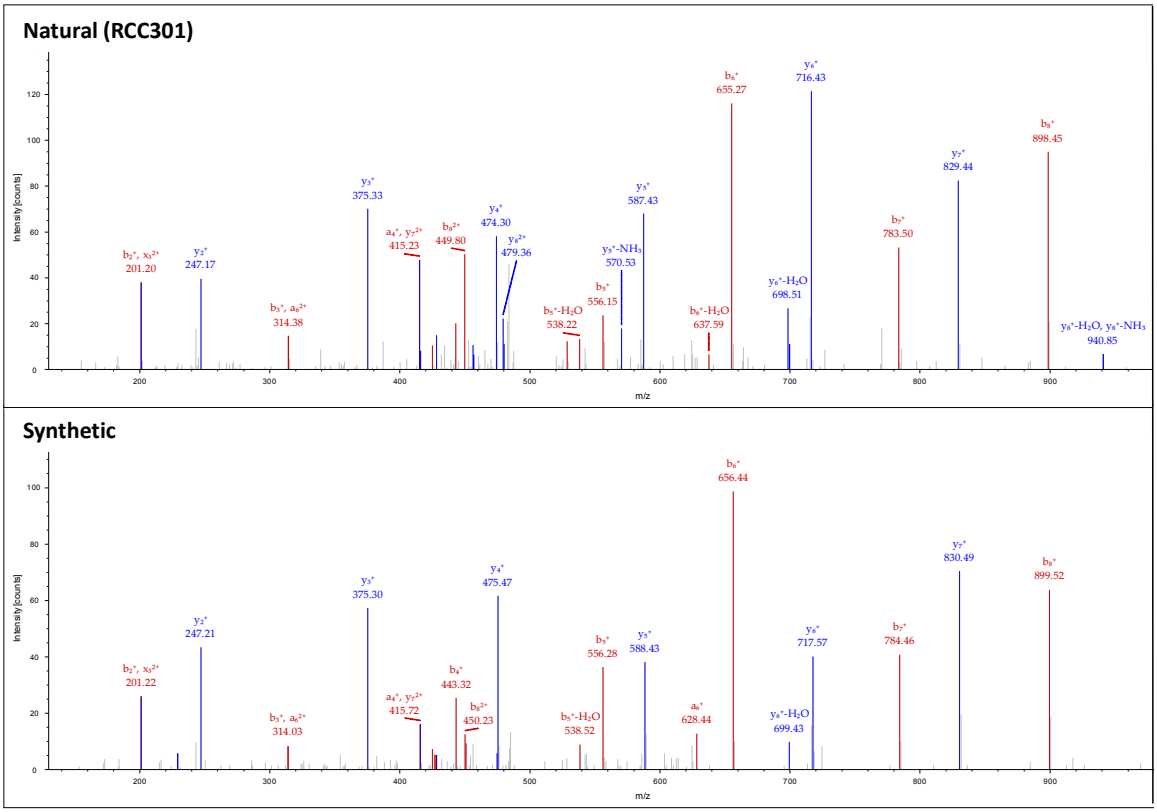

GLADASLLKKV

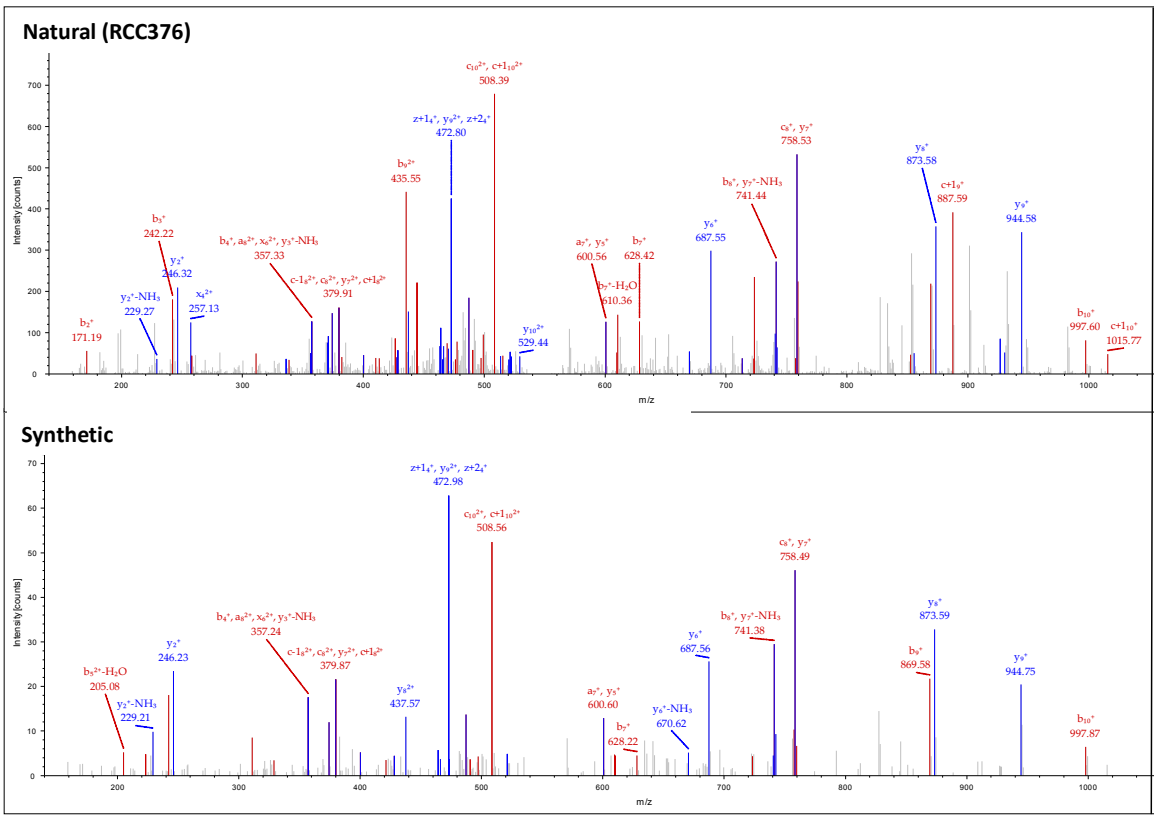

MPSASMTRL

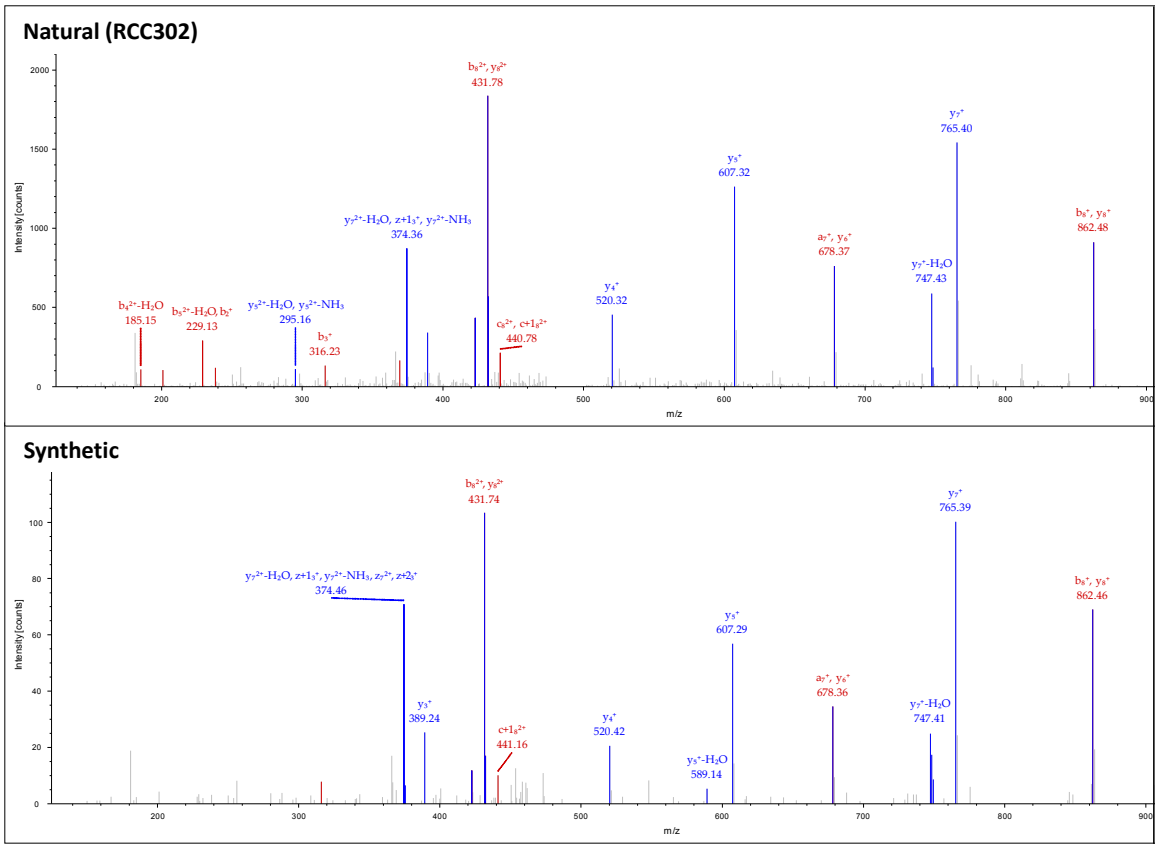

SMTLAIHEI

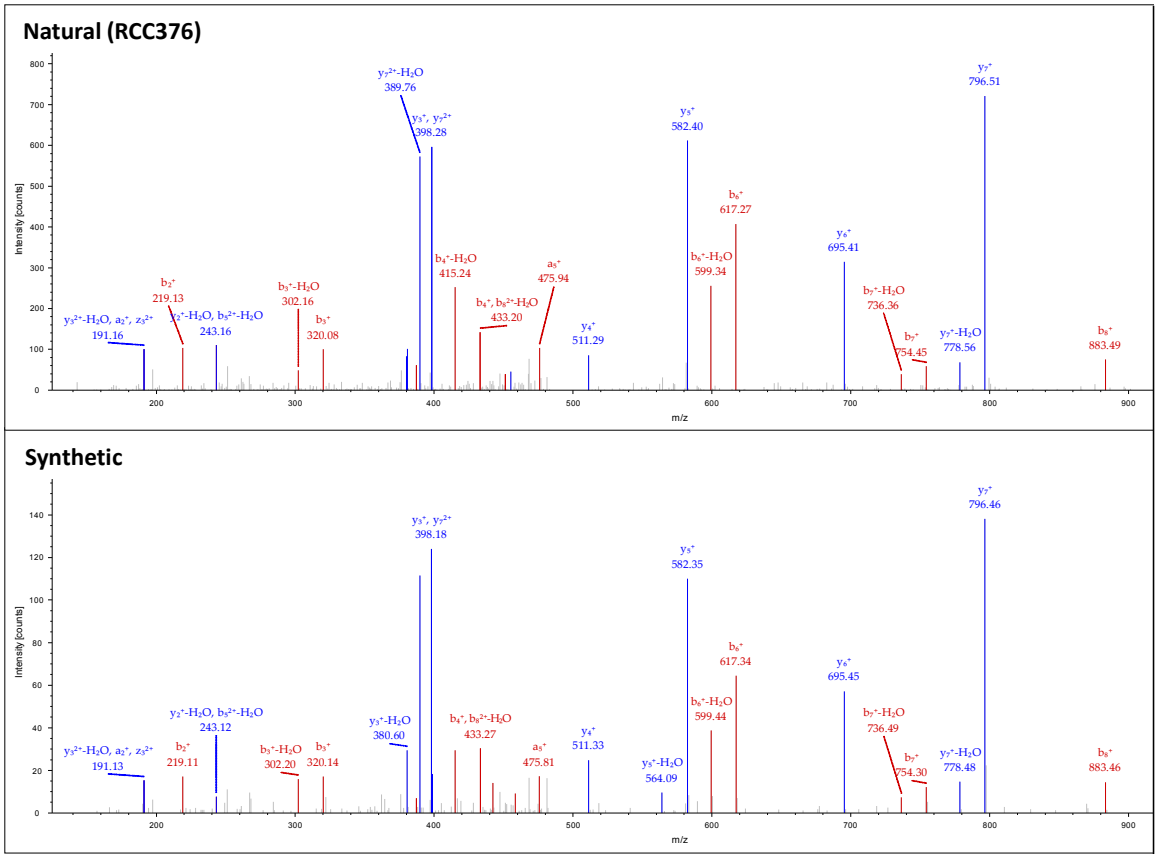

APGVGKSAL (*V4)

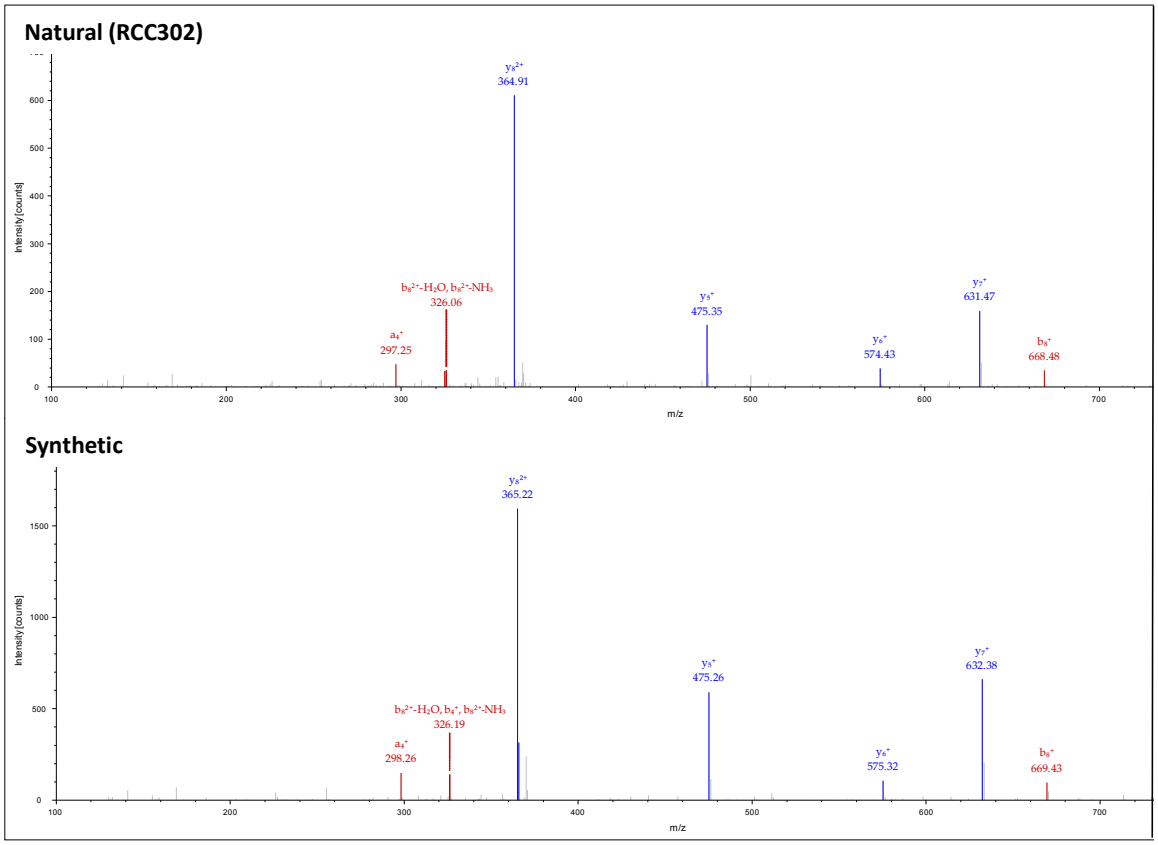

RTAFTLKQK

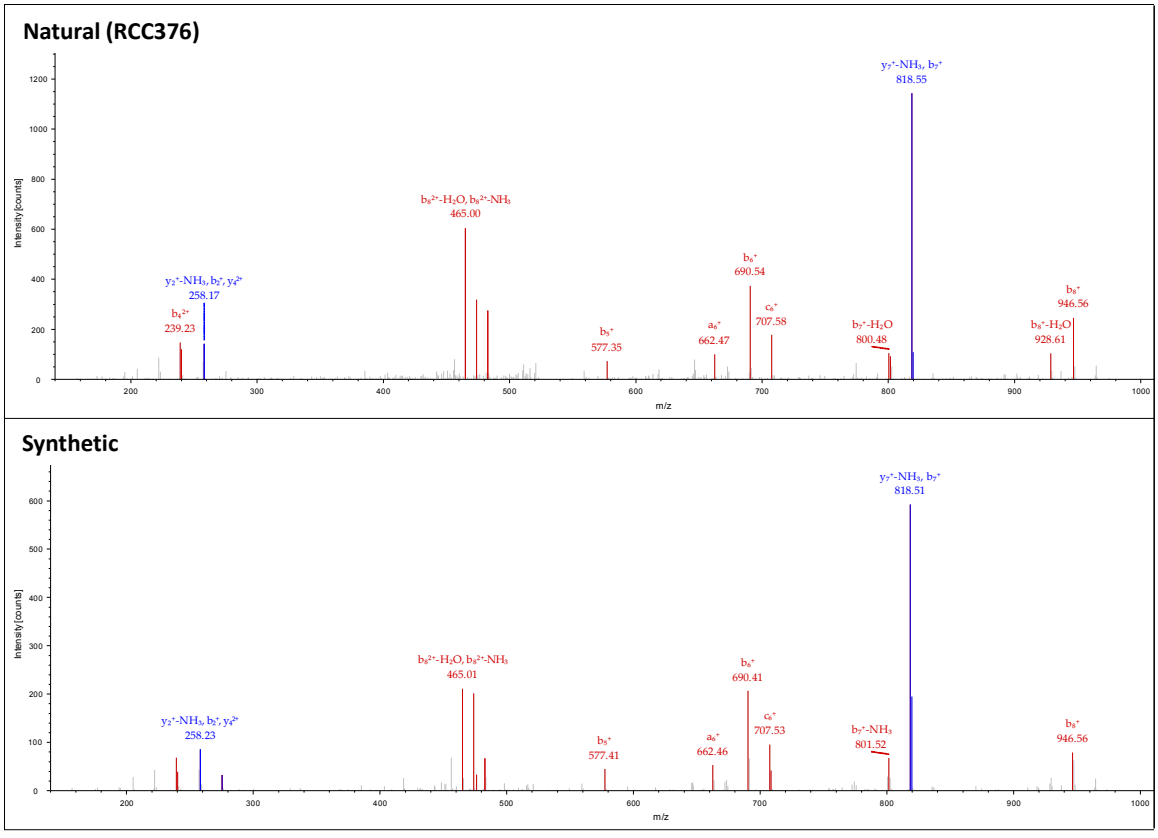

IQAKKALDL

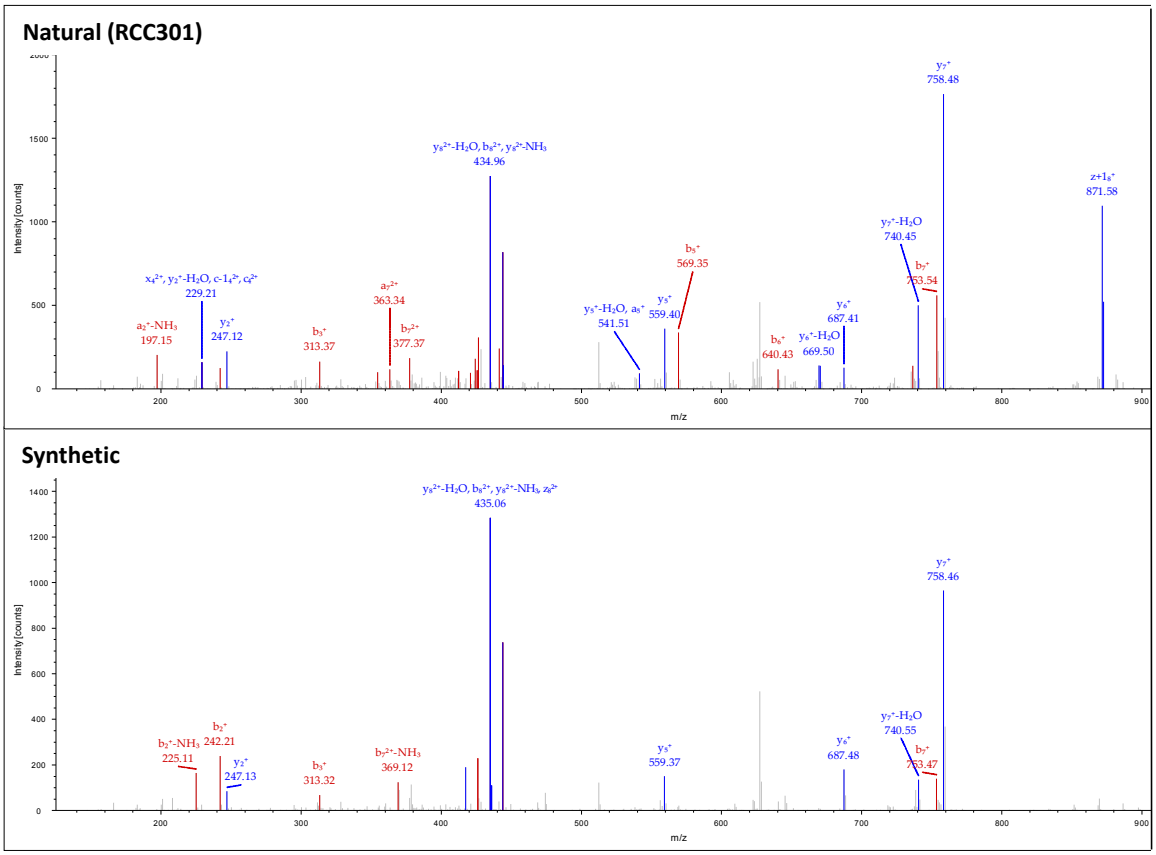

NPNLRIISL

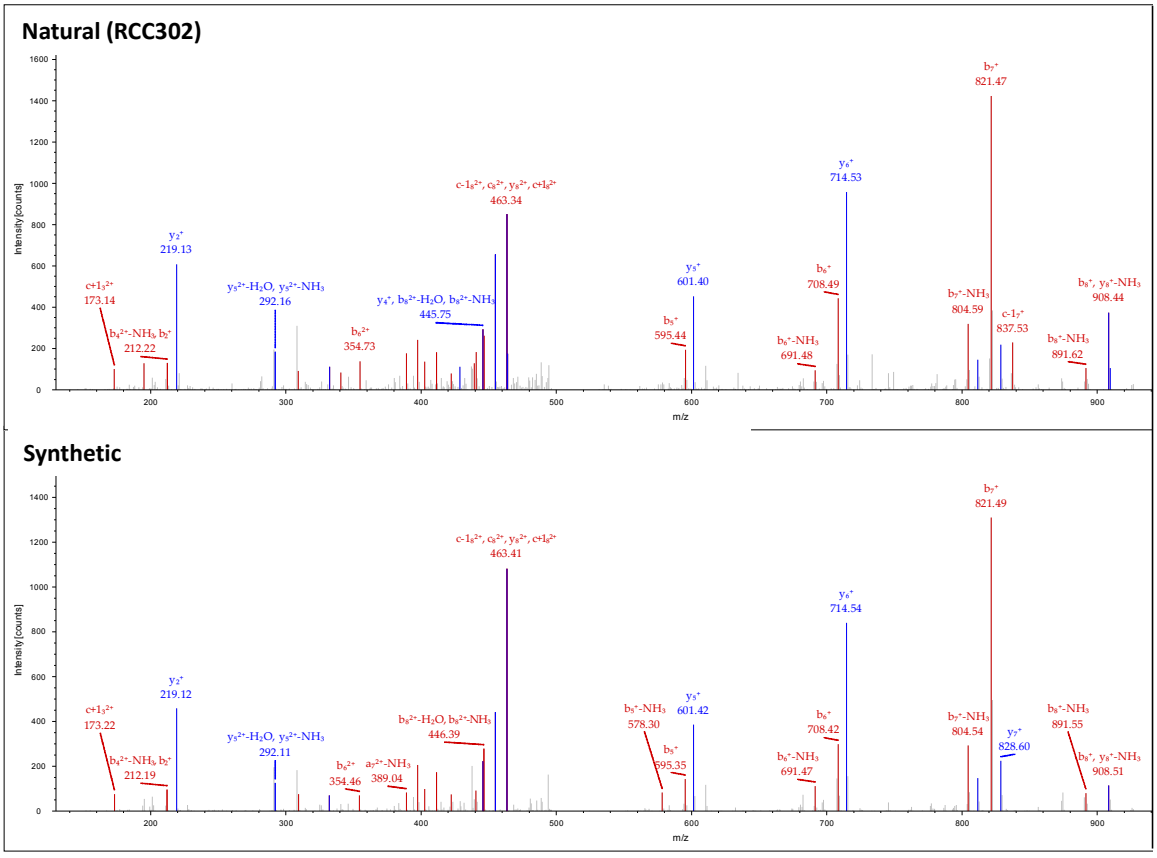

KIKSPAKMAEK

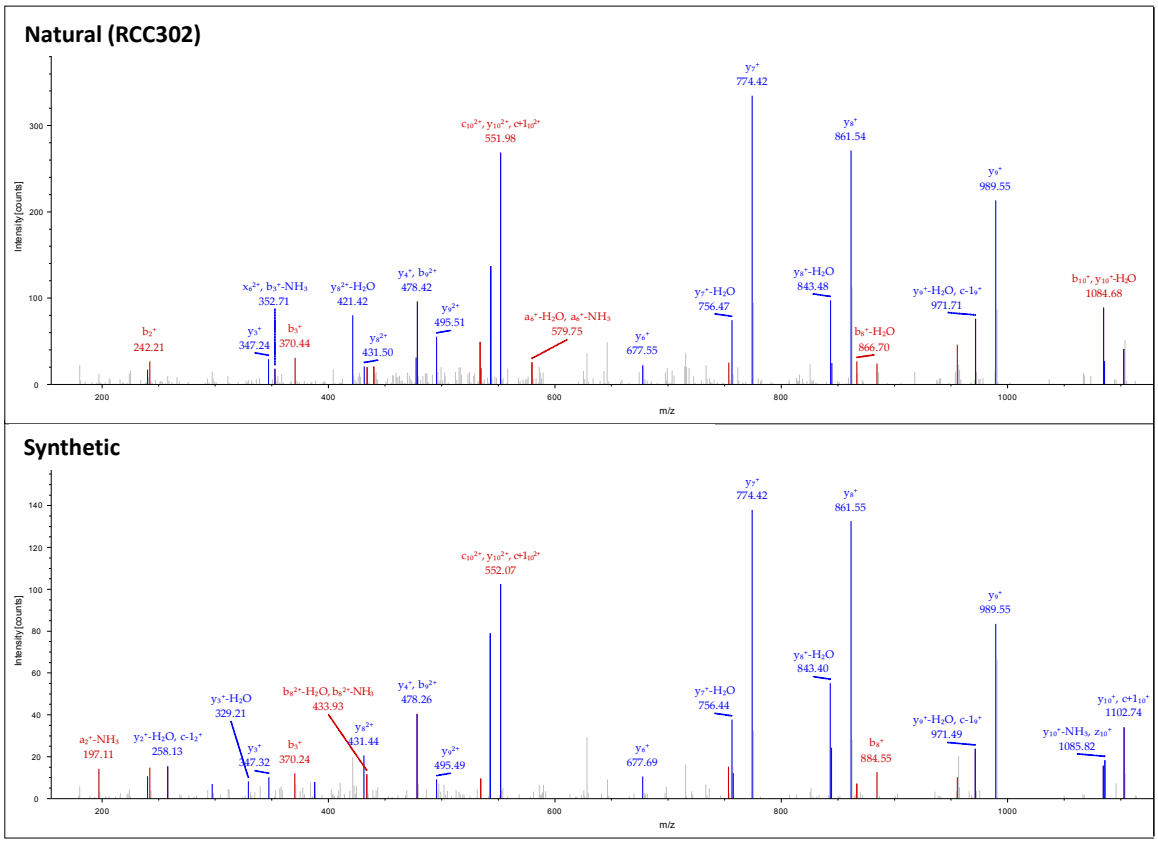

MPLLRQEEL

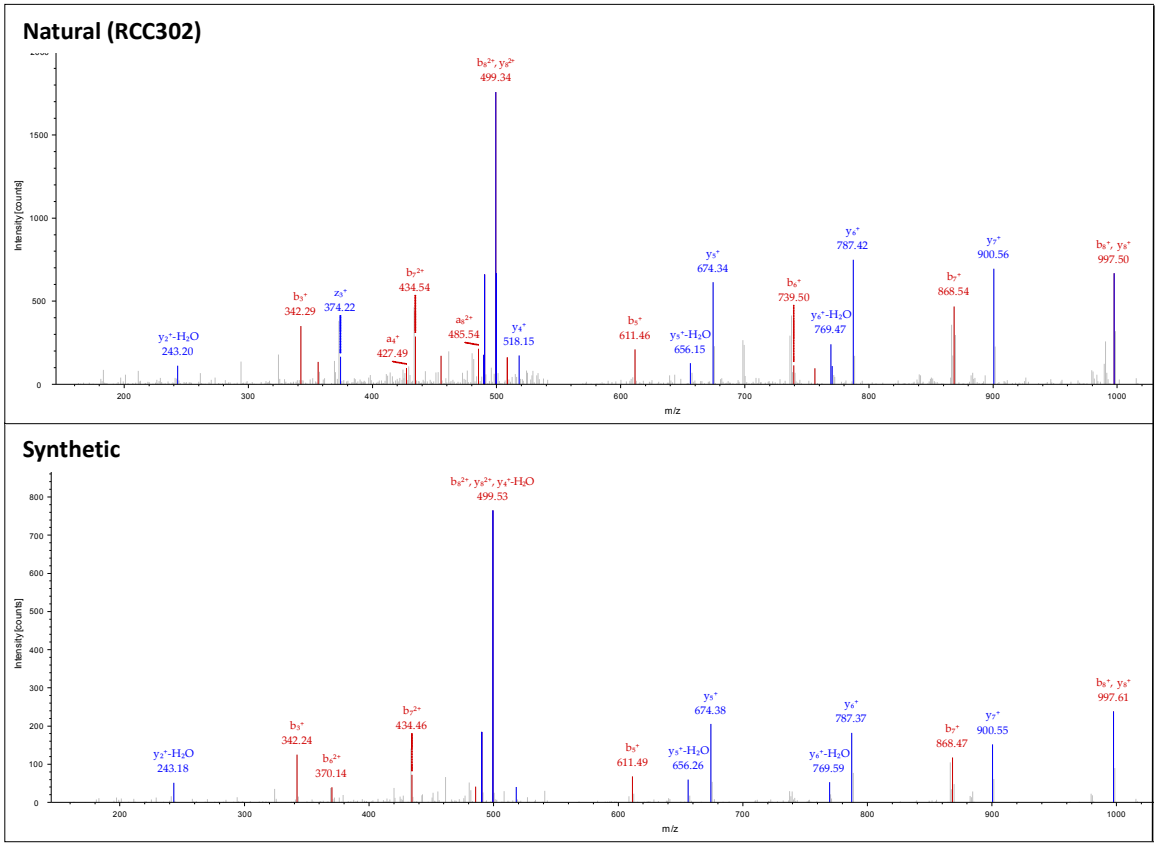

B Fragment spectra of putative *Mtb*–derived HLA class I ligands

Fourteen peptides were synthesized and fragment spectra of synthetic peptides were compared to fragment spectra of naturally presented peptides to validate peptide identifications. Fragment spectra of naturally presented peptides are derived from complex HLA ligand extraction samples from primary tissues. Thus, those fragment spectra may contain unexplained mass peaks due to co-elution of different peptide species. Verification of peptide identities was performed by matching of mass peaks from synthetic peptide spectra to those of naturally presented peptides. Some of the peptides were synthesized with a heavy isotope-labelled amino acid (indicated by *).

LIAVPTGIK (*V4)

Natural

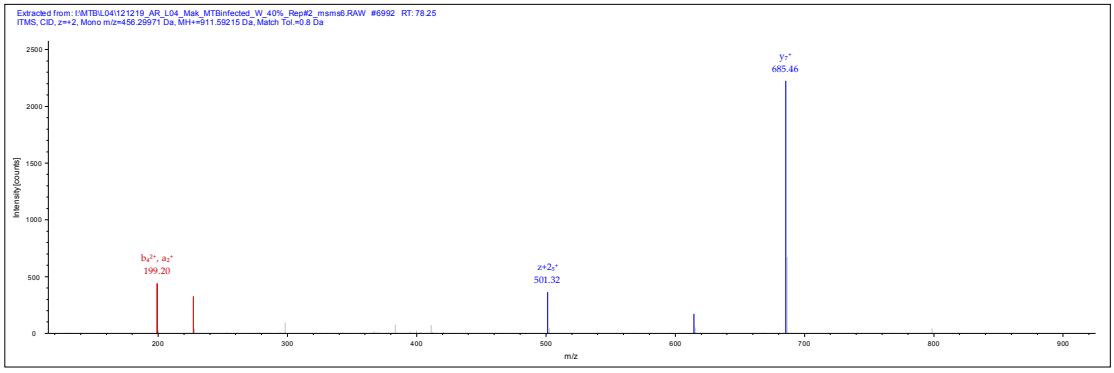

Synthetic

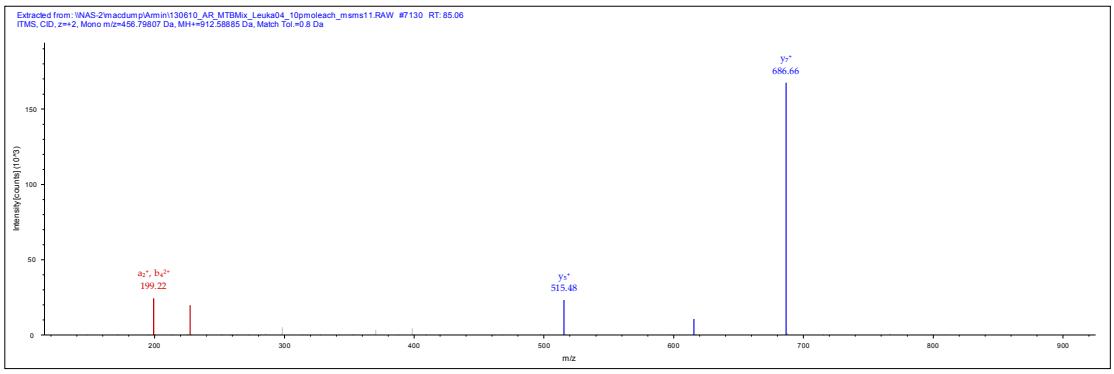

KTTTAEALGK (*L8)

Natural

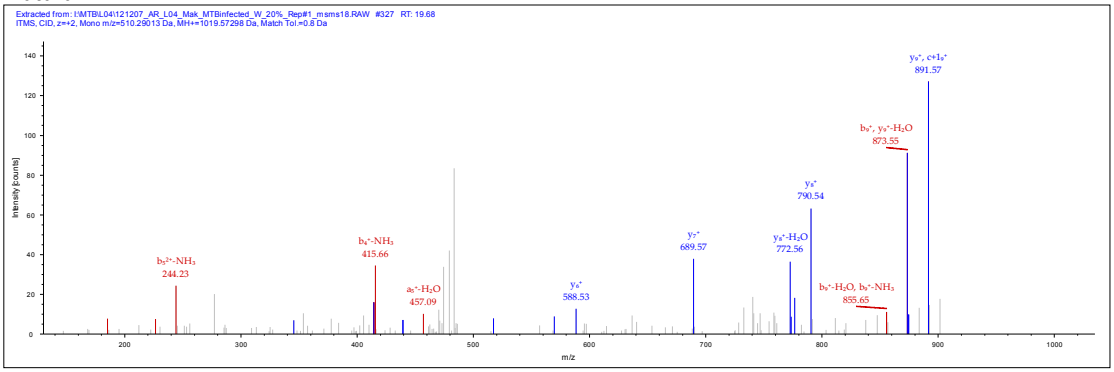

Synthetic

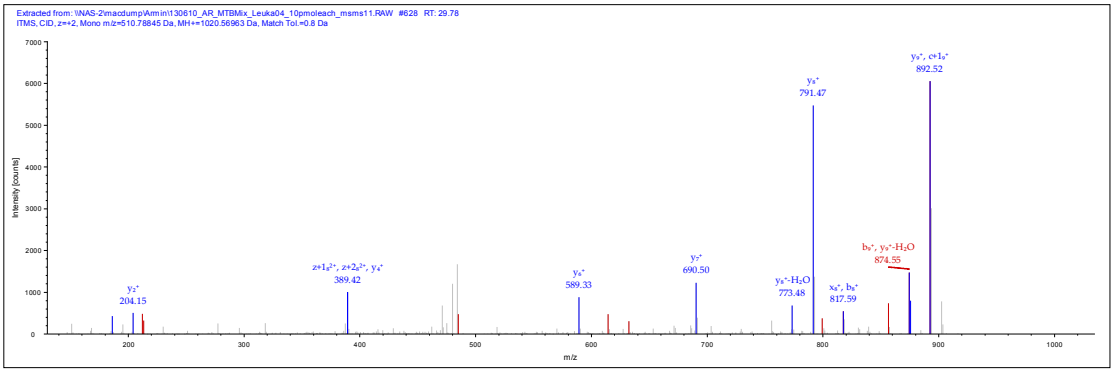

TMEIVGRLR (*V5)

Natural

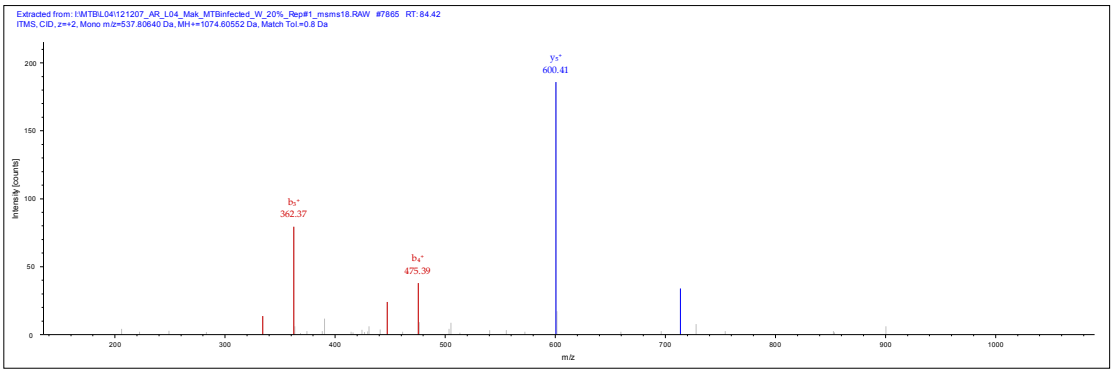

Synthetic

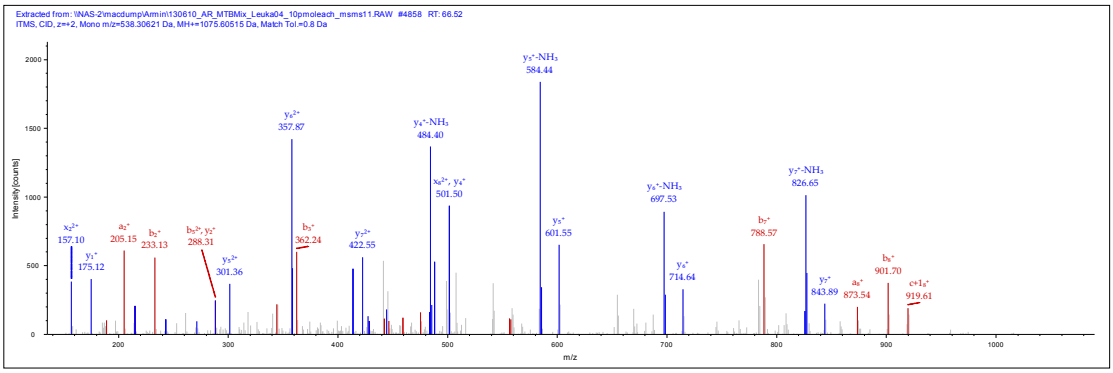

LVDAAVHSY (*V6)

Natural

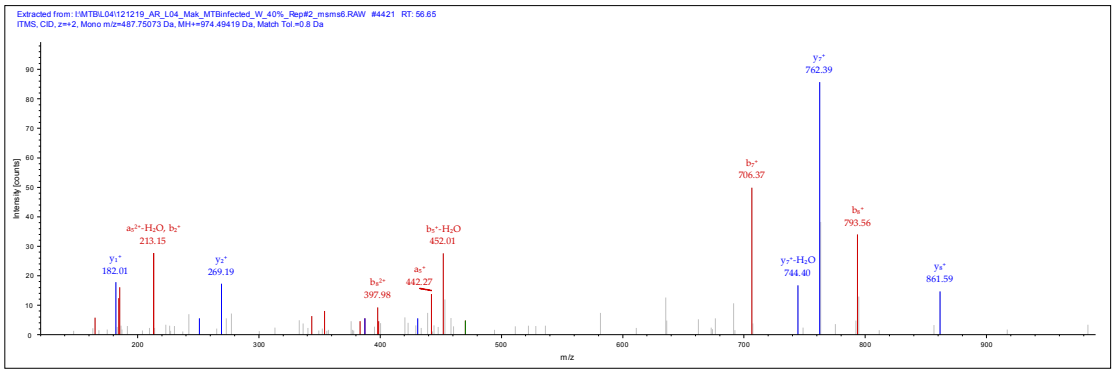

Synthetic

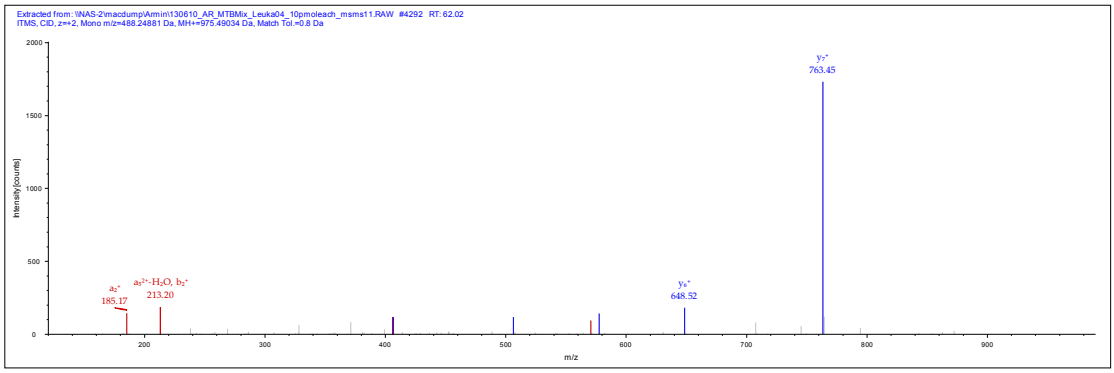

DVLGLLRDAY (*V2)

Natural

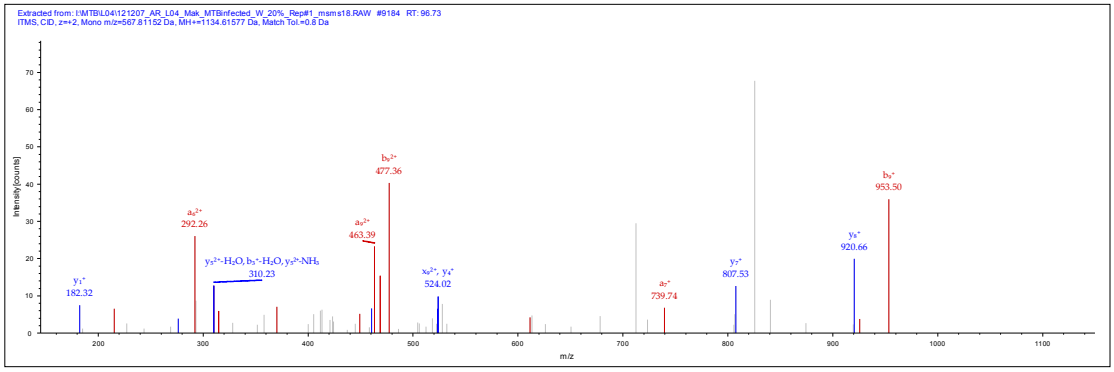

Synthetic

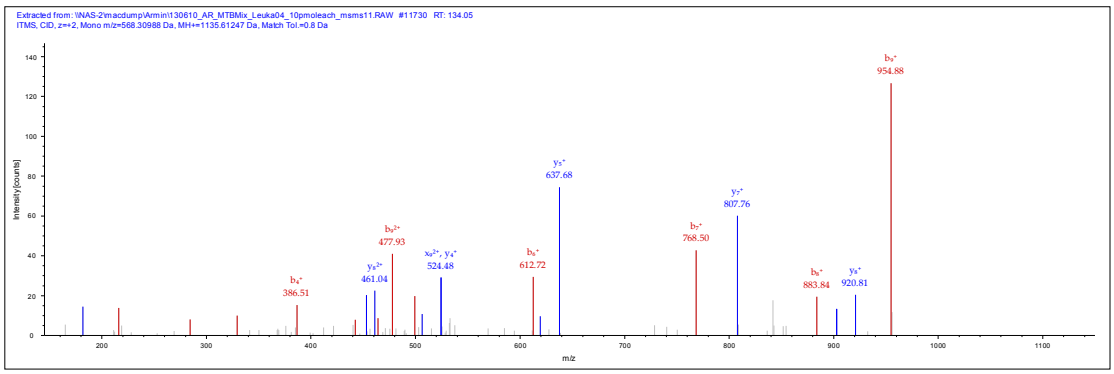

MVASGVVSVY (*V9)

Natural

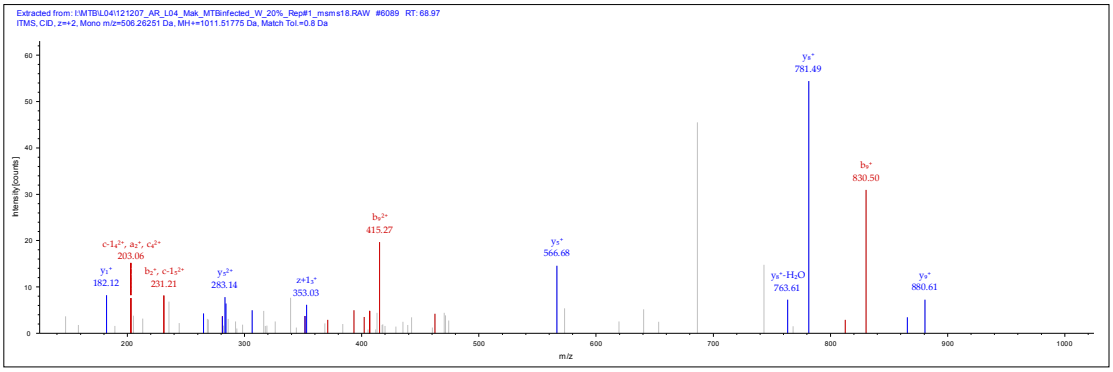

Synthetic

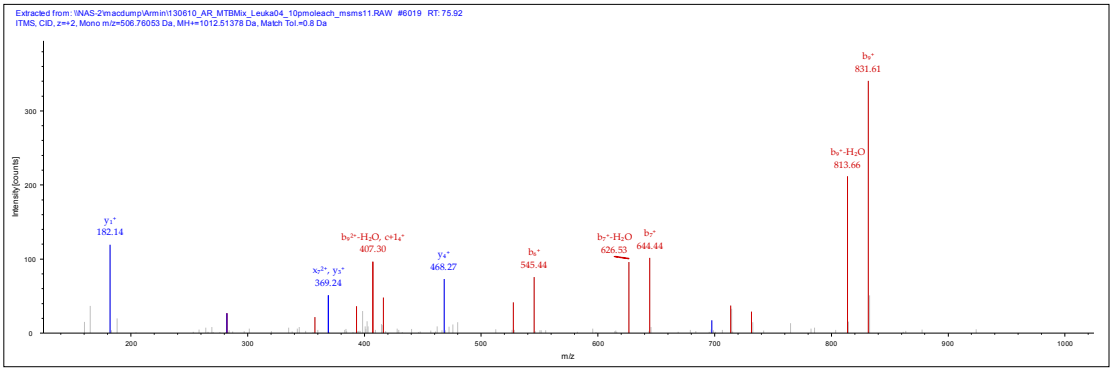

LPPGVVNVV (*V8)

Natural

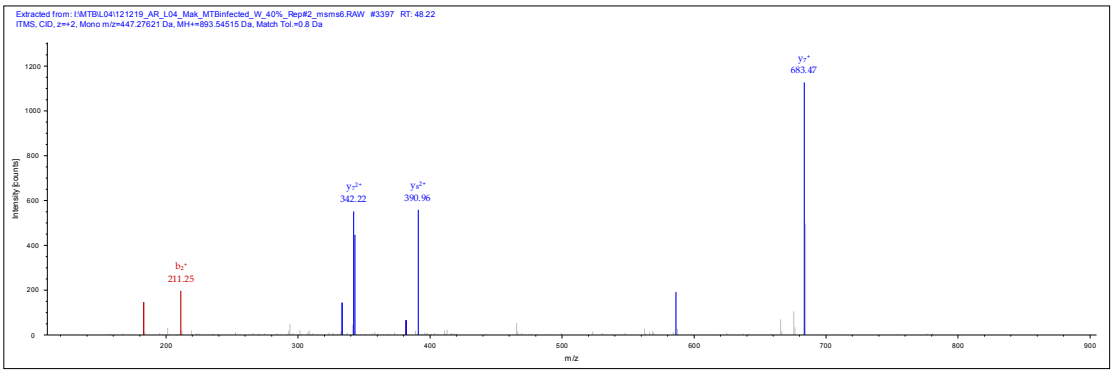

Synthetic

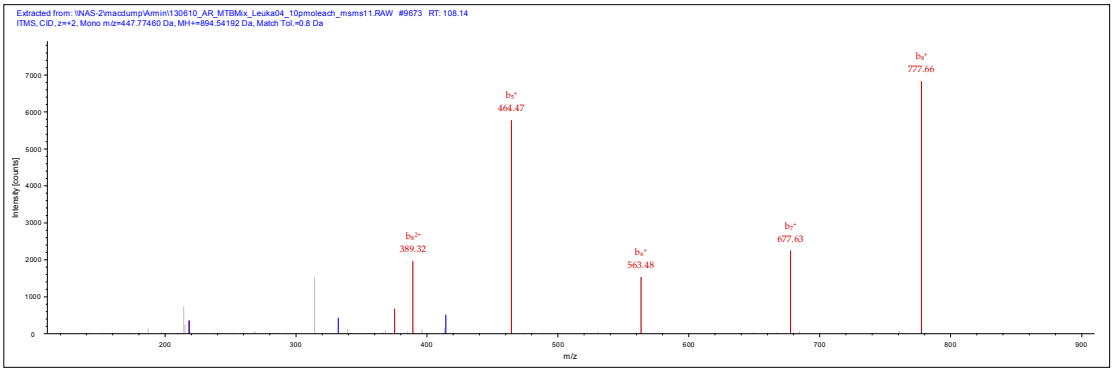

DARNELAPV

Natural

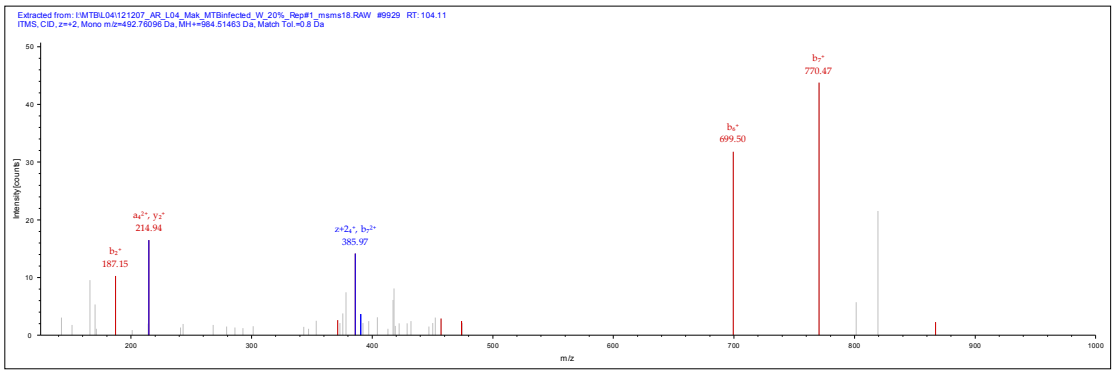

Synthetic

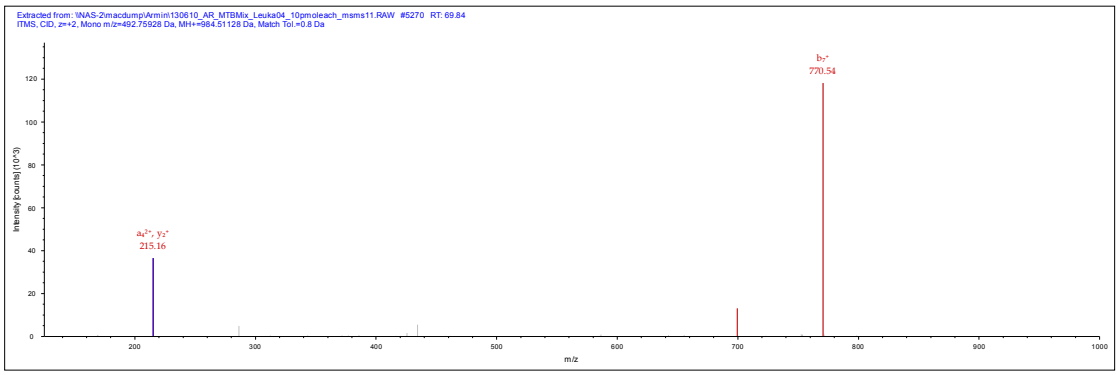

EALVRTDI (*V4)

Natural

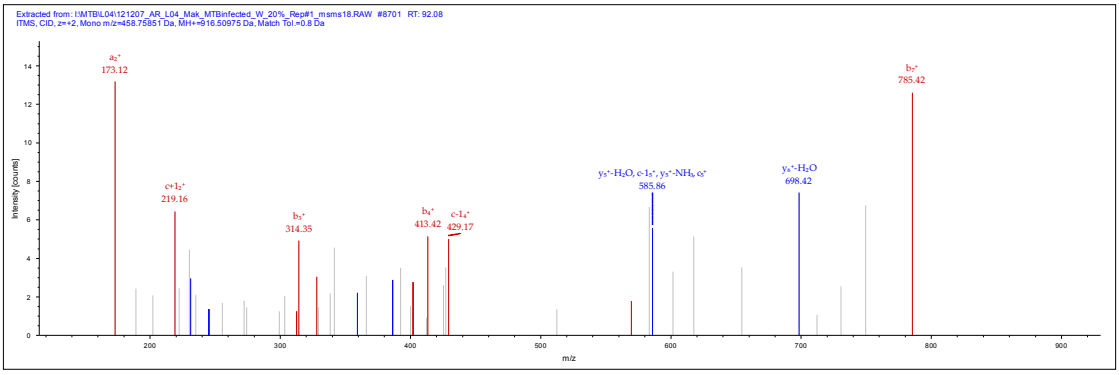

Synthetic

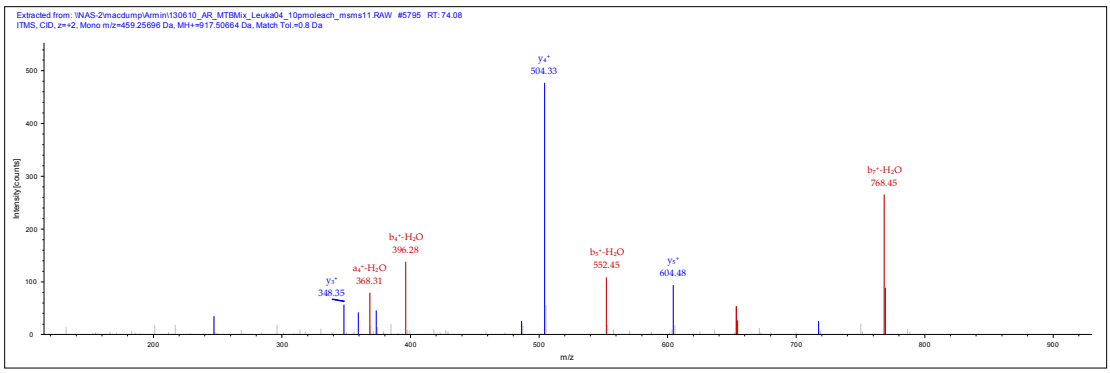

LAQLPITI (*L4)

Natural

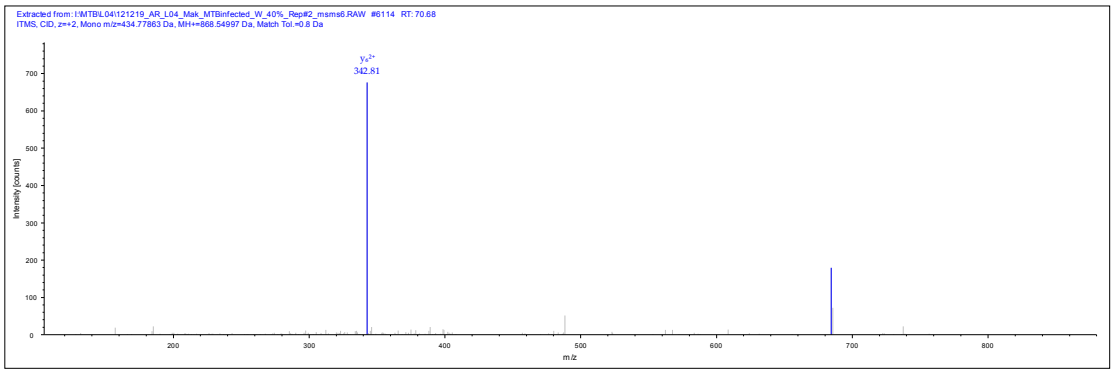

Synthetic

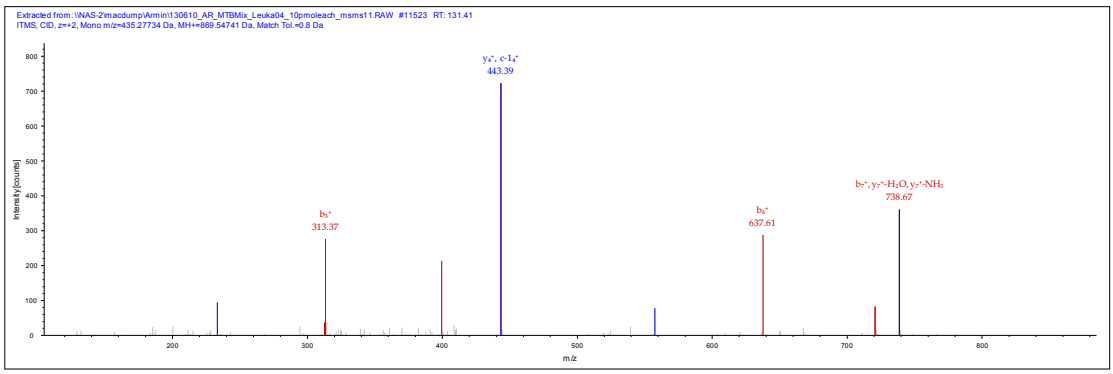

DAIRSAAL

Natural

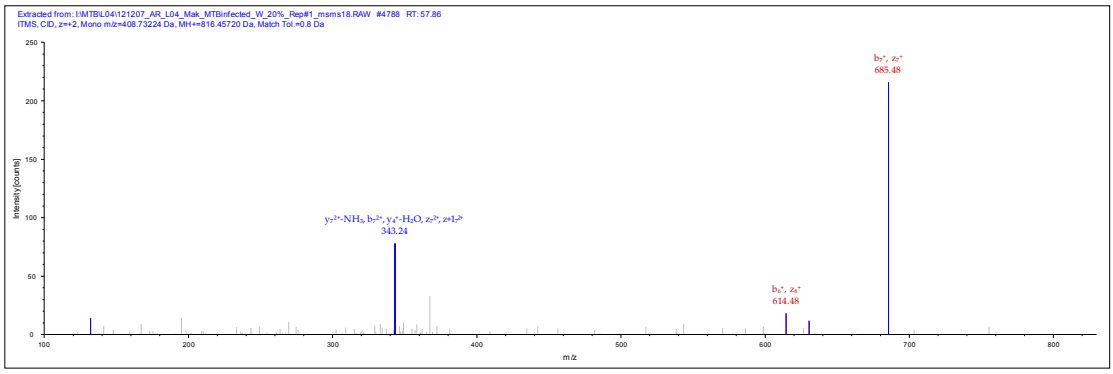

Synthetic

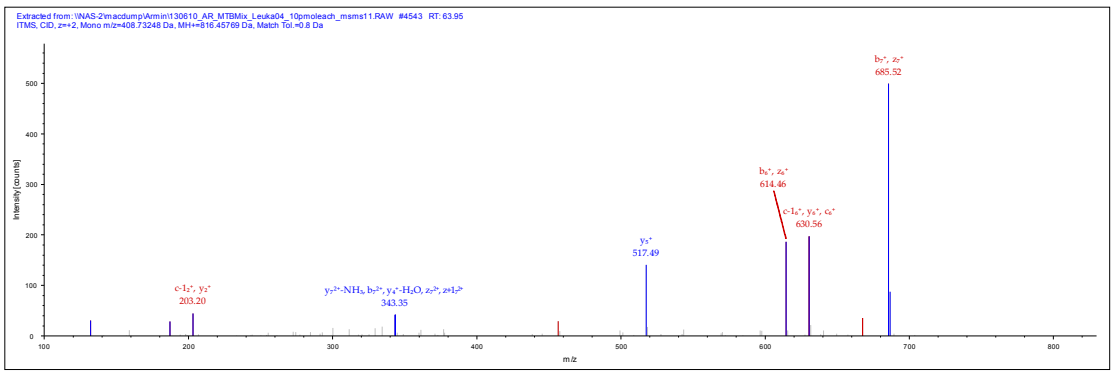

FSISEGLEEY

Natural

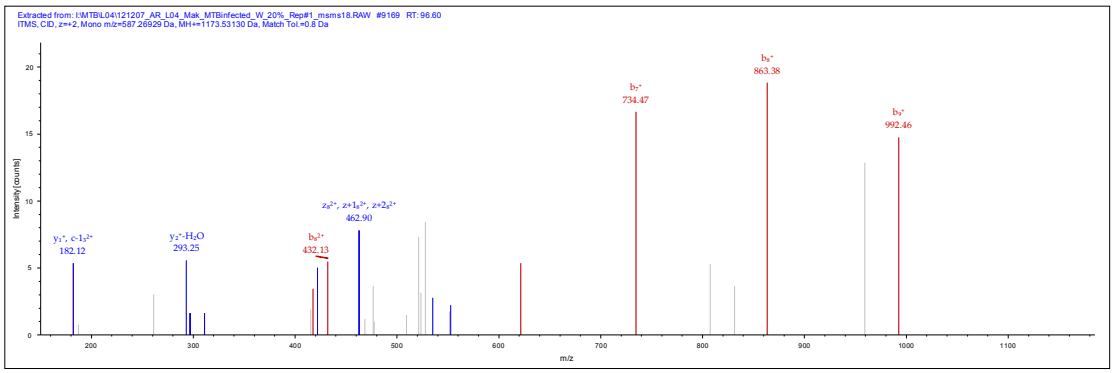

Synthetic

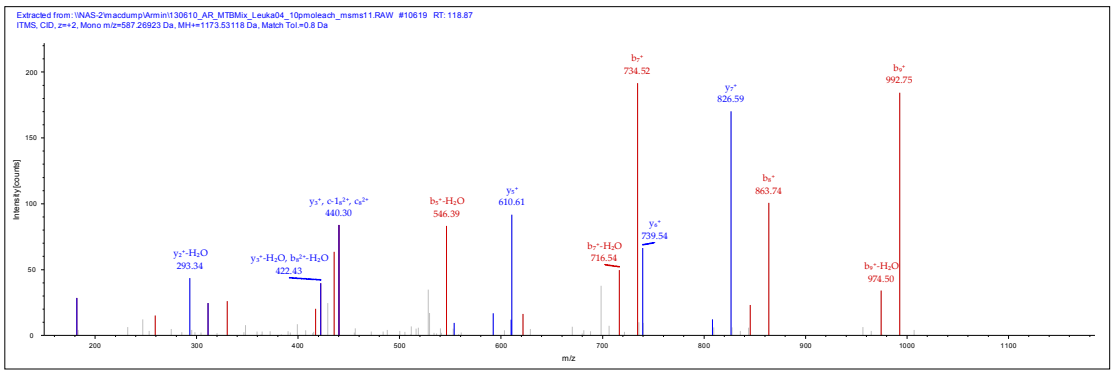

ALTDRVAGTLREW (*V6)

Natural

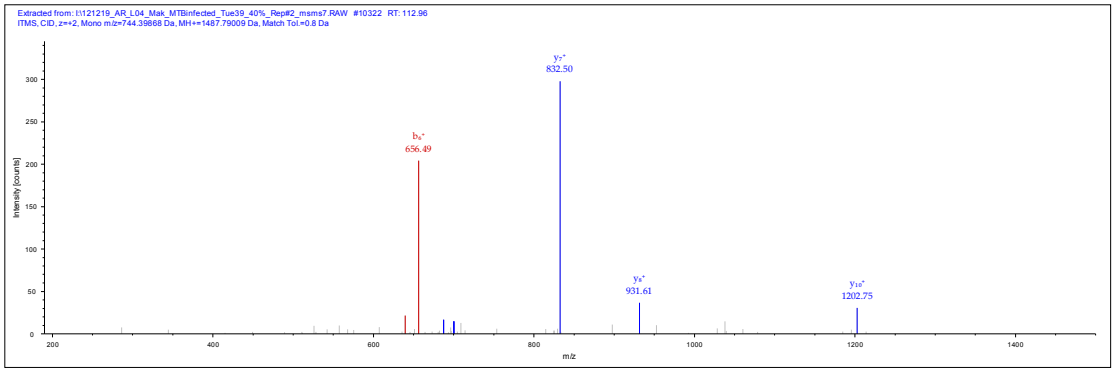

Synthetic

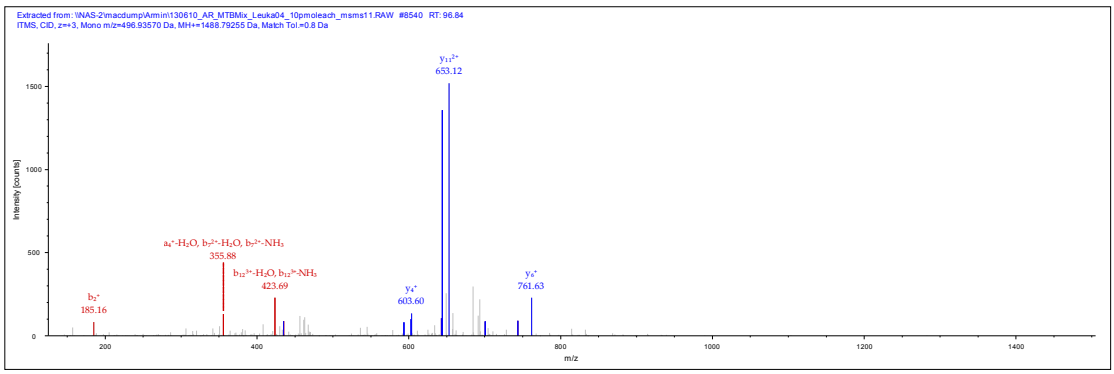

KSASTMLMVDNATGVKAL (*V15)

Natural

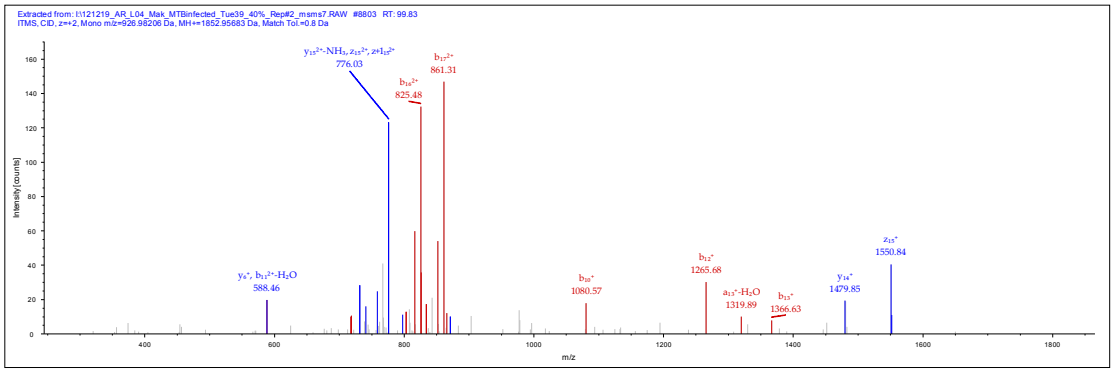

Synthetic

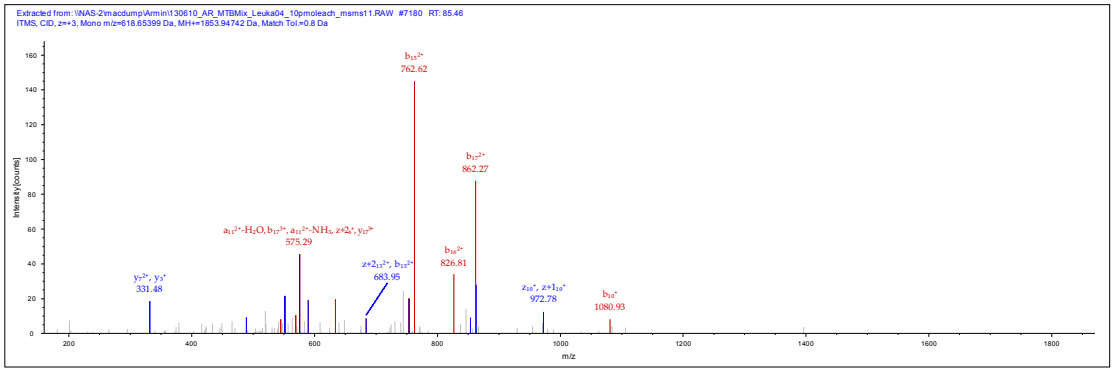

References

1. Sagan, L. *On the origin of mitosing cells.* J Theor Biol, 1967. **14**(3): p. 255-74.

2. Proksch, E., Brandner, J.M., and Jensen, J.M. *The skin: an indispensable barrier.* Exp Dermatol, 2008. **17**(12): p. 1063-72.

3. Rippke, F., Schreiner, V., and Schwanitz, H.J. *The acidic milieu of the horny layer: new findings on the physiology and pathophysiology of skin pH.* Am J Clin Dermatol, 2002. **3**(4): p. 261-72.

4. Selsted, M.E., Tang, Y.Q., Morris, W.L., McGuire, P.A., Novotny, M.J., Smith, W., Henschen, A.H., and Cullor, J.S. *Purification, primary structures, and antibacterial activities of beta-defensins, a new family of antimicrobial peptides from bovine neutrophils.* J Biol Chem, 1993. **268**(9): p. 6641-8.

5. Ridley, F. *Lysozyme: An Antibacterial Body present in Great Concentration in Tears, and its Relation to Infection of the Human Eye.* Proc R Soc Med, 1928. **21**(9): p. 1495-506.

6. Medzhitov, R. *Recognition of microorganisms and activation of the immune response.* Nature, 2007. **449**(7164): p. 819-26.

7. Anderson, K.V., Bokla, L., and Nüsslein-Volhard, C. *Establishment of dorsal-ventral polarity in the Drosophila embryo: the induction of polarity by the Toll gene product.* Cell, 1985. **42**(3): p. 791-8.

8. Lemaitre, B., Nicolas, E., Michaut, L., Reichhart, J.M., and Hoffmann, J.A. *The dorsoventral regulatory gene cassette spatzle/Toll/cactus controls the potent antifungal response in Drosophila adults.* Cell, 1996. **86**(6): p. 973-83.

9. Medzhitov, R., Preston-Hurlburt, P., and Janeway, C.A., Jr. *A human homologue of the Drosophila Toll protein signals activation of adaptive immunity.* Nature, 1997. **388**(6640): p. 394-7.

10. Yokoyama, W.M. and Seaman, W.E. *The Ly-49 and NKR-P1 gene families encoding lectin-like receptors on natural killer cells: the NK gene complex.* Annu Rev Immunol, 1993. **11**: p. 613-35.

11. Lanier, L.L. *Follow the leader: NK cell receptors for classical and nonclassical MHC class I.* Cell, 1998. **92**(6): p. 705-7.

12. Karre, K., Ljunggren, H.G., Piontek, G., and Kiessling, R. *Selective rejection of H-2-deficient lymphoma variants suggests alternative immune defence strategy.* Nature, 1986. **319**(6055): p. 675-8.

13. Trinchieri, G. and Valiante, N. *Receptors for the Fc fragment of IgG on natural killer cells.* Nat Immun, 1993. **12**(4-5): p. 218-34.

14. Schiffmann, E., Corcoran, B.A., and Wahl, S.M. *N-formylmethionyl peptides as chemoattractants for leucocytes.* Proc Natl Acad Sci U S A, 1975. **72**(3): p. 1059-62.

15. Huber, H., Polley, M.J., Linscott, W.D., Fudenberg, H.H., and Muller-Eberhard, H.J. *Human monocytes: distinct receptor sites for the third component of complement and for immunoglobulin G.* Science, 1968. **162**(3859): p. 1281-3.

16. Cagan, R.H. and Karnovsky, M.L. *Enzymatic Basis of the Respiratory Stimulation during Phagocytosis.* Nature, 1964. **204**: p. 255-7.

17. Cline, M.J., Hanifin, J., and Lehrer, R.I. *Phagocytosis by human eosinophils.* Blood, 1968. **32**(6): p. 922-34.

18. Matzinger, P. *Tolerance, danger, and the extended family.* Annu Rev Immunol, 1994. **12**: p. 991-1045.

19. Van Voorhis, W.C., Valinsky, J., Hoffman, E., Luban, J., Hair, L.S., and Steinman, R.M. *Relative efficacy of human monocytes and dendritic cells as accessory cells for T cell replication.* J Exp Med, 1983. **158**(1): p. 174-91.

20. Banchereau, J. and Steinman, R.M. *Dendritic cells and the control of immunity.* Nature, 1998. **392**(6673): p. 245-52.

21. Townsend, A.R., Rothbard, J., Gotch, F.M., Bahadur, G., Wraith, D., and McMichael, A.J. *The epitopes of influenza nucleoprotein recognized by cytotoxic T lymphocytes can be defined with short synthetic peptides.* Cell, 1986. **44**(6): p. 959-68.

22. Shahinian, A., Pfeffer, K., Lee, K.P., Kundig, T.M., Kishihara, K., Wakeham, A., Kawai, K., Ohashi, P.S., Thompson, C.B., and Mak, T.W. *Differential T cell costimulatory requirements in CD28-deficient mice.* Science, 1993. **261**(5121): p. 609-12.

23. Harding, F.A., McArthur, J.G., Gross, J.A., Raulet, D.H., and Allison, J.P. *CD28-mediated signalling co-stimulates murine T cells and prevents induction of anergy in T-cell clones.* Nature, 1992. **356**(6370): p. 607-9.

24. Curtsinger, J.M., Schmidt, C.S., Mondino, A., Lins, D.C., Kedl, R.M., Jenkins, M.K., and Mescher, M.F. *Inflammatory cytokines provide a third signal for activation of naive CD4+ and CD8+ T cells.* J Immunol, 1999. **162**(6): p. 3256-62.

25. Abbas, A.K., Murphy, K.M., and Sher, A. *Functional diversity of helper T lymphocytes.* Nature, 1996. **383**(6603): p. 787-93.

26. Mosmann, T.R., Cherwinski, H., Bond, M.W., Giedlin, M.A., and Coffman, R.L. *Two types of murine helper T cell clone. I. Definition according to profiles of lymphokine activities and secreted proteins.* J Immunol, 1986. **136**(7): p. 2348-57.

27. Stout, R.D. and Bottomly, K. *Antigen-specific activation of effector macrophages by IFN-gamma producing (TH1) T cell clones. Failure of IL-4-producing (TH2) T cell clones to activate effector function in macrophages.* J Immunol, 1989. **142**(3): p. 760-5.

28. Croft, M. and Swain, S.L. *B cell response to fresh and effector T helper cells. Role of cognate T-B interaction and the cytokines IL-2, IL-4, and IL-6.* J Immunol, 1991. **146**(12): p. 4055-64.

29. de Vries, J.E., Carballido, J.M., Sornasse, T., and Yssel, H. *Antagonizing the differentiation and functions of human T helper type 2 cells.* Curr Opin Immunol, 1995. **7**(6): p. 771-8.

30. Harrington, L.E., Hatton, R.D., Mangan, P.R., Turner, H., Murphy, T.L., Murphy, K.M., and Weaver, C.T. *Interleukin 17-producing CD4+ effector T cells develop via a lineage distinct from the T helper type 1 and 2 lineages.* Nat Immunol, 2005. **6**(11): p. 1123-32.

31. Fontenot, J.D., Gavin, M.A., and Rudensky, A.Y. *Foxp3 programs the development and function of CD4+CD25+ regulatory T cells.* Nat Immunol, 2003. **4**(4): p. 330-6.

32. Sakaguchi, S., Sakaguchi, N., Asano, M., Itoh, M., and Toda, M. *Immunologic self-tolerance maintained by activated T cells expressing IL-2 receptor alpha-chains (CD25). Breakdown of a single mechanism of self-tolerance causes various autoimmune diseases.* J Immunol, 1995. **155**(3): p. 1151-64.

33. Monks, C.R., Freiberg, B.A., Kupfer, H., Sciaky, N., and Kupfer, A. *Three-dimensional segregation of supramolecular activation clusters in T cells.* Nature, 1998. **395**(6697): p. 82-6.

34. Podack, E.R. and Konigsberg, P.J. *Cytolytic T cell granules. Isolation, structural, biochemical, and functional characterization.* J Exp Med, 1984. **160**(3): p. 695-710.

35. Heusel, J.W., Wesselschmidt, R.L., Shresta, S., Russell, J.H., and Ley, T.J. *Cytotoxic lymphocytes require granzyme B for the rapid induction of DNA fragmentation and apoptosis in allogeneic target cells.* Cell, 1994. **76**(6): p. 977-87.

36. Rouvier, E., Luciani, M.F., and Golstein, P. *Fas involvement in Ca(2+)-independent T cell-mediated cytotoxicity.* J Exp Med, 1993. **177**(1): p. 195-200.

37. Kriegler, M., Perez, C., DeFay, K., Albert, I., and Lu, S.D. *A novel form of TNF/cachectin is a cell surface cytotoxic transmembrane protein: ramifications for the complex physiology of TNF.* Cell, 1988. **53**(1): p. 45-53.

38. Wheelock, E.F. *Interferon-Like Virus-Inhibitor Induced in Human Leukocytes by Phytohemagglutinin.* Science, 1965. **149**(3681): p. 310-1.

39. Billings, P., Burakoff, S., Dorf, M.E., and Benacerraf, B. *Cytotoxic T lymphocytes specific for I region determinants do not require interactions with H-2K or D gene products.* J Exp Med, 1977. **145**(5): p. 1387-92.

40. Mackaness, G.B. *The influence of immunologically committed lymphoid cells on macrophage activity in vivo.* J Exp Med, 1969. **129**(5): p. 973-92.

41. Schoenberger, S.P., Toes, R.E., van der Voort, E.I., Offringa, R., and Melief, C.J. *T-cell help for cytotoxic T lymphocytes is mediated by CD40-CD40L interactions.* Nature, 1998. **393**(6684): p. 480-3.

42. Stevens, T.L., Bossie, A., Sanders, V.M., Fernandez-Botran, R., Coffman, R.L., Mosmann, T.R., and Vitetta, E.S. *Regulation of antibody isotype secretion by subsets of antigen-specific helper T cells.* Nature, 1988. **334**(6179): p. 255-8.

43. Crotty, S. *A brief history of T cell help to B cells.* Nat Rev Immunol, 2015. **15**(3): p. 185-9.

44. Bernard, O., Hozumi, N., and Tonegawa, S. *Sequences of mouse immunoglobulin light chain genes before and after somatic changes.* Cell, 1978. **15**(4): p. 1133-44.

45. Murphy, K., Travers, P., Walport, M. and Janeway, C.A., Jr., *Janeway's Immunobiology*. 2008, New York: Garland Science.

46. Gotch, F., Rothbard, J., Howland, K., Townsend, A., and McMichael, A. *Cytotoxic T lymphocytes recognize a fragment of influenza virus matrix protein in association with HLA-A2.* Nature, 1987. **326**(6116): p. 881-2.

47. Rowen, L., Koop, B.F., and Hood, L. *The complete 685-kilobase DNA sequence of the human beta T cell receptor locus.* Science, 1996. **272**(5269): p. 1755-62.

48. Oettinger, M.A., Schatz, D.G., Gorka, C., and Baltimore, D. *RAG-1 and RAG-2, adjacent genes that synergistically activate V(D)J recombination.* Science, 1990. **248**(4962): p. 1517-23.

49. Ma, Y., Schwarz, K., and Lieber, M.R. *The Artemis:DNA-PKcs endonuclease cleaves DNA loops, flaps, and gaps.* DNA Repair (Amst), 2005. **4**(7): p. 845-51.

50. Komori, T., Okada, A., Stewart, V., and Alt, F.W. *Lack of N regions in antigen receptor variable region genes of TdT-deficient lymphocytes.* Science, 1993. **261**(5125): p. 1171-5.

51. Hozumi, N. and Tonegawa, S. *Evidence for somatic rearrangement of immunoglobulin genes coding for variable and constant regions.* Proc Natl Acad Sci U S A, 1976. **73**(10): p. 3628-32.

52. Weigert, M., Gatmaitan, L., Loh, E., Schilling, J., and Hood, L. *Rearrangement of genetic information may produce immunoglobulin diversity.* Nature, 1978. **276**(5690): p. 785-90.

53. Westermann, J. and Pabst, R. *Distribution of lymphocyte subsets and natural killer cells in the human body.* Clin Investig, 1992. **70**(7): p. 539-44.

54. Davis, M.M. and Bjorkman, P.J. *T-cell antigen receptor genes and T-cell recognition.* Nature, 1988. **334**(6181): p. 395-402.

55. Jorgensen, J.L., Esser, U., Fazekas de St Groth, B., Reay, P.A., and Davis, M.M. *Mapping T-cell receptor-peptide contacts by variant peptide immunization of single-chain transgenics.* Nature, 1992. **355**(6357): p. 224-30.

56. Lafaille, J.J., DeCloux, A., Bonneville, M., Takagaki, Y., and Tonegawa, S. *Junctional sequences of T cell receptor gamma delta genes: implications for gamma delta T cell lineages and for a novel intermediate of V-(D)-J joining.* Cell, 1989. **59**(5): p. 859-70.

57. Tonegawa, S., Berns, A., Bonneville, M., Farr, A.G., Ishida, I., Ito, K., Itohara, S., Janeway, C.A., Jr., Kanagawa, O., Kubo, R., and et al. *Diversity, development, ligands, and probable functions of gamma delta T cells.* Adv Exp Med Biol, 1991. **292**: p. 53-61.

58. Legut, M., Cole, D.K., and Sewell, A.K. *The promise of gammadelta T cells and the gammadelta T cell receptor for cancer immunotherapy.* Cell Mol Immunol, 2015. **12**(6): p. 656-68.

59. Garboczi, D.N., Ghosh, P., Utz, U., Fan, Q.R., Biddison, W.E., and Wiley, D.C. *Structure of the complex between human T-cell receptor, viral peptide and HLA-A2.* Nature, 1996. **384**(6605): p. 134-41.

60. Call, M.E., Pyrdol, J., Wiedmann, M., and Wucherpfennig, K.W. *The organizing principle in the formation of the T cell receptor-CD3 complex.* Cell, 2002. **111**(7): p. 967-79.

61. Borst, J., Jacobs, H., and Brouns, G. *Composition and function of T-cell receptor and B-cell receptor complexes on precursor lymphocytes.* Curr Opin Immunol, 1996. **8**(2): p. 181-90.

62. Cammarota, G., Scheirle, A., Takacs, B., Doran, D.M., Knorr, R., Bannwarth, W., Guardiola, J., and Sinigaglia, F. *Identification of a CD4 binding site on the beta 2 domain of HLA-DR molecules.* Nature, 1992. **356**(6372): p. 799-801.

63. Leahy, D.J. *A structural view of CD4 and CD8.* FASEB J, 1995. **9**(1): p. 17-25.

64. Salter, R.D., Benjamin, R.J., Wesley, P.K., Buxton, S.E., Garrett, T.P., Clayberger, C., Krensky, A.M., Norment, A.M., Littman, D.R., and Parham, P. *A binding site for the T-cell co-receptor CD8 on the alpha 3 domain of HLA-A2.* Nature, 1990. **345**(6270): p. 41-6.

65. Janeway, C.A., Jr. *The T cell receptor as a multicomponent signalling machine: CD4/CD8 coreceptors and CD45 in T cell activation.* Annu Rev Immunol, 1992. **10**: p. 645-74.

66. Bach, F.H., Bach, M.L., and Sondel, P.M. *Differential function of major histocompatibility complex antigens in T-lymphocyte activation.* Nature, 1976. **259**(5541): p. 273-81.

67. Zinkernagel, R.M. and Doherty, P.C. *Major transplantation antigens, viruses, and specificity of surveillance T cells.* Contemp Top Immunobiol, 1977. **7**: p. 179-220.

68. Stephens, R., Horton, R., Humphray, S., Rowen, L., Trowsdale, J., and Beck, S. *Gene organisation, sequence variation and isochore structure at the centromeric boundary of the human MHC.* J Mol Biol, 1999. **291**(4): p. 789-99.

69. *Nomenclature for factors of the HLA system.* Bull World Health Organ, 1975. **52**(3): p. 261-5.

70. Robinson, J., Malik, A., Parham, P., Bodmer, J.G., and Marsh, S.G. *IMGT/HLA database--a sequence database for the human major histocompatibility complex.* Tissue Antigens, 2000. **55**(3): p. 280-7.

71. Robinson, J., Halliwell, J.A., Hayhurst, J.D., Flicek, P., Parham, P., and Marsh, S.G. *The IPD and IMGT/HLA database: allele variant databases.* Nucleic Acids Res, 2015. **43**(Database issue): p. D423-31.

72. Bjorkman, P.J., Saper, M.A., Samraoui, B., Bennett, W.S., Strominger, J.L., and Wiley, D.C. *Structure of the human class I histocompatibility antigen, HLA-A2.* Nature, 1987. **329**(6139): p. 506-12.

73. Madden, D.R., Garboczi, D.N., and Wiley, D.C. *The antigenic identity of peptide-MHC complexes: a comparison of the conformations of five viral peptides presented by HLA-A2.* Cell, 1993. **75**(4): p. 693-708.

74. Bouvier, M. and Wiley, D.C. *Importance of peptide amino and carboxyl termini to the stability of MHC class I molecules.* Science, 1994. **265**(5170): p. 398-402.

75. Rammensee, H.G., Friede, T., and Stevanovic, S. *MHC ligands and peptide motifs: first listing.* Immunogenetics, 1995. **41**(4): p. 178-228.

76. Falk, K., Rötzschke, O., Stevanovic, S., Jung, G., and Rammensee, H.G. *Allele-specific motifs revealed by sequencing of self-peptides eluted from MHC molecules.* Nature, 1991. **351**(6324): p. 290-6.

77. Rammensee, H., Bachmann, J., Emmerich, N.P., Bachor, O.A., and Stevanovic, S. *SYFPEITHI: database for MHC ligands and peptide motifs.* Immunogenetics, 1999. **50**(3-4): p. 213-9.

78. Nielsen, M., Lundegaard, C., Worning, P., Lauemoller, S.L., Lamberth, K., Buus, S., Brunak, S., and Lund, O. *Reliable prediction of T-cell epitopes using neural networks with novel sequence representations.* Protein Sci, 2003. **12**(5): p. 1007-17.

79. Germain, R.N. and Margulies, D.H. *The biochemistry and cell biology of antigen processing and presentation.* Annu Rev Immunol, 1993. **11**: p. 403-50.

80. Stock, D., Nederlof, P.M., Seemuller, E., Baumeister, W., Huber, R., and Lowe, J. *Proteasome: from structure to function.* Curr Opin Biotechnol, 1996. **7**(4): p. 376-85.

81. Beninga, J., Rock, K.L., and Goldberg, A.L. *Interferon-gamma can stimulate post-proteasomal trimming of the N terminus of an antigenic peptide by inducing leucine aminopeptidase.* J Biol Chem, 1998. **273**(30): p. 18734-42.

82. Stoltze, L., Schirle, M., Schwarz, G., Schröter, C., Thompson, M.W., Hersh, L.B., Kalbacher, H., Stevanovic, S., Rammensee, H.G., and Schild, H. *Two new proteases in the MHC class I processing pathway.* Nat Immunol, 2000. **1**(5): p. 413-8.

83. Neefjes, J.J., Momburg, F., and Hämmerling, G.J. *Selective and ATP-dependent translocation of peptides by the MHC-encoded transporter.* Science, 1993. **261**(5122): p. 769-71.

84. Serwold, T., Gonzalez, F., Kim, J., Jacob, R., and Shastri, N. *ERAAP customizes peptides for MHC class I molecules in the endoplasmic reticulum.* Nature, 2002. **419**(6906): p. 480-3.

85. Saric, T., Chang, S.C., Hattori, A., York, I.A., Markant, S., Rock, K.L., Tsujimoto, M., and Goldberg, A.L. *An IFN-gamma-induced aminopeptidase in the ER, ERAP1, trims precursors to MHC class I-presented peptides.* Nat Immunol, 2002. **3**(12): p. 1169-76.

86. Benham, A.M. and Neefjes, J.J. *Antigen processing by the class I pathway.* Biochem Soc Trans, 1995. **23**(3): p. 664-9.

87. Vyas, J.M., Van der Veen, A.G., and Ploegh, H.L. *The known unknowns of antigen processing and presentation.* Nat Rev Immunol, 2008. **8**(8): p. 607-18.

88. Stern, L.J., Brown, J.H., Jardetzky, T.S., Gorga, J.C., Urban, R.G., Strominger, J.L., and Wiley, D.C. *Crystal structure of the human class II MHC protein HLA-DR1 complexed with an influenza virus peptide.* Nature, 1994. **368**(6468): p. 215-21.

89. Dessen, A., Lawrence, C.M., Cupo, S., Zaller, D.M., and Wiley, D.C. *X-ray crystal structure of HLA-DR4 (DRA*0101, DRB1*0401) complexed with a peptide from human collagen II.* Immunity, 1997. **7**(4): p. 473-81.

90. Rammensee, H.G. *Chemistry of peptides associated with MHC class I and class II molecules.* Curr Opin Immunol, 1995. **7**(1): p. 85-96.

91. Biddison, W.E. and Martin, R. *Peptide binding motifs for MHC class I and II molecules.* Curr Protoc Immunol, 2001. **36**: p. A.1I.1-A.1I.7.

92. Hammer, J., Valsasnini, P., Tolba, K., Bolin, D., Higelin, J., Takacs, B., and Sinigaglia, F. *Promiscuous and allele-specific anchors in HLA-DR-binding peptides.* Cell, 1993. **74**(1): p. 197-203.

93. Lennon-Dumenil, A.M., Bakker, A.H., Wolf-Bryant, P., Ploegh, H.L., and Lagaudriere-Gesbert, C. *A closer look at proteolysis and MHC-class-II-restricted antigen presentation.* Curr Opin Immunol, 2002. **14**(1): p. 15-21.

94. Hiltbold, E.M. and Roche, P.A. *Trafficking of MHC class II molecules in the late secretory pathway.* Curr Opin Immunol, 2002. **14**(1): p. 30-5.

95. Purcell, A.W., McCluskey, J., and Rossjohn, J. *More than one reason to rethink the use of peptides in vaccine design.* Nat Rev Drug Discov, 2007. **6**(5): p. 404-14.

96. Wölfel, T., Schneider, J., Meyer Zum Buschenfelde, K.H., Rammensee, H.G., Rötzschke, O., and Falk, K. *Isolation of naturally processed peptides recognized by cytolytic T lymphocytes (CTL) on human melanoma cells in association with HLA-A2.1.* Int J Cancer, 1994. **57**(3): p. 413-8.

97. Akiyama, K., Kagawa, S., Tamura, T., Shimbara, N., Takashina, M., Kristensen, P., Hendil, K.B., Tanaka, K., and Ichihara, A. *Replacement of proteasome subunits X and Y by LMP7 and LMP2 induced by interferon-gamma for acquirement of the functional diversity responsible for antigen processing.* FEBS Lett, 1994. **343**(1): p. 85-8.

98. Kloetzel, P.M. and Ossendorp, F. *Proteasome and peptidase function in MHC-class-I-mediated antigen presentation.* Curr Opin Immunol, 2004. **16**(1): p. 76-81.

99. Dengjel, J., Schoor, O., Fischer, R., Reich, M., Kraus, M., Müller, M., Kreymborg, K., Altenberend, F., Brandenburg, J., Kalbacher, H., Brock, R., Driessen, C., Rammensee, H.G., and Stevanovic, S. *Autophagy promotes MHC class II presentation of peptides from intracellular source proteins.* Proc Natl Acad Sci U S A, 2005. **102**(22): p. 7922-7.

100. Kurts, C., Robinson, B.W., and Knolle, P.A. *Cross-priming in health and disease.* Nat Rev Immunol, 2010. **10**(6): p. 403-14.

101. Rabsteyn, A., *Massenspektrometrische Analyse der HLA-Liganden im gesunden Nierengewebe*. 2011, Diplomarbeit der Eberhard-Karls-Universität Tübingen.

102. Hasserjian, R.P., Aster, J.C., Davi, F., Weinberg, D.S., and Sklar, J. *Modulated expression of notch1 during thymocyte development.* Blood, 1996. **88**(3): p. 970-6.

103. Levelt, C.N., Carsetti, R., and Eichmann, K. *Regulation of thymocyte development through CD3. II. Expression of T cell receptor beta CD3 epsilon and maturation to the CD4+8+ stage are highly correlated in individual thymocytes.* J Exp Med, 1993. **178**(6): p. 1867-75.

104. Scott, B., Bluthmann, H., Teh, H.S., and von Boehmer, H. *The generation of mature T cells requires interaction of the alpha beta T-cell receptor with major histocompatibility antigens.* Nature, 1989. **338**(6216): p. 591-3.

105. Anderson, M.S., Venanzi, E.S., Klein, L., Chen, Z., Berzins, S.P., Turley, S.J., von Boehmer, H., Bronson, R., Dierich, A., Benoist, C., and Mathis, D. *Projection of an immunological self shadow within the thymus by the aire protein.* Science, 2002. **298**(5597): p. 1395-401.

106. Marusic-Galesic, S., Stephany, D.A., Longo, D.L., and Kruisbeek, A.M. *Development of CD4-CD8+ cytotoxic T cells requires interactions with class I MHC determinants.* Nature, 1988. **333**(6169): p. 180-3.

107. Liston, A., Lesage, S., Wilson, J., Peltonen, L., and Goodnow, C.C. *Aire regulates negative selection of organ-specific T cells.* Nat Immunol, 2003. **4**(4): p. 350-4.

108. Egerton, M., Scollay, R., and Shortman, K. *Kinetics of mature T-cell development in the thymus.* Proc Natl Acad Sci U S A, 1990. **87**(7): p. 2579-82.

109. Guerder, S., Meyerhoff, J., and Flavell, R. *The role of the T cell costimulator B7-1 in autoimmunity and the induction and maintenance of tolerance to peripheral antigen.* Immunity, 1994. **1**(2): p. 155-66.

110. Ferlay, J., Soerjomataram, I., Dikshit, R., Eser, S., Mathers, C., Rebelo, M., Parkin, D.M., Forman, D., and Bray, F. *Cancer incidence and mortality worldwide: sources, methods and major patterns in GLOBOCAN 2012.* Int J Cancer, 2015. **136**(5): p. E359-86.

111. Global Burden of Disease Risk Factors Collaborators. *Global, regional, and national comparative risk assessment of 79 behavioural, environmental and occupational, and metabolic risks or clusters of risks, 1990-2015: a systematic analysis for the Global Burden of Disease Study 2015.* Lancet, 2016. **388**(10053): p. 1659-1724.

112. Torre, L.A., Bray, F., Siegel, R.L., Ferlay, J., Lortet-Tieulent, J., and Jemal, A. *Global cancer statistics, 2012.* CA Cancer J Clin, 2015. **65**(2): p. 87-108.

113. Coley, W.B. *The treatment of malignant tumors by repeated inoculations of erysipelas. With a report of ten original cases. 1893.* Clin Orthop Relat Res, 1991(262): p. 3-11.

114. Ehrlich, P. *Über den jetzigen Stand der Karzinomforschung.* Ned. Tijdschr. Geneeskd, 1909. **5**: p. 18.

115. Old, L.J. and Boyse, E.A. *Immunology of Experimental Tumors.* Annu Rev Med, 1964. **15**: p. 167-86.

116. Burnet, F.M. *Immunological aspects of malignant disease.* Lancet, 1967. **1**(7501): p. 1171-4.

117. Dunn, G.P., Old, L.J., and Schreiber, R.D. *The immunobiology of cancer immunosurveillance and immunoediting.* Immunity, 2004. **21**(2): p. 137-48.

118. Croce, C.M. *Oncogenes and cancer.* N Engl J Med, 2008. **358**(5): p. 502-11.

119. Kawakami, Y., Eliyahu, S., Delgado, C.H., Robbins, P.F., Sakaguchi, K., Appella, E., Yannelli, J.R., Adema, G.J., Miki, T., and Rosenberg, S.A. *Identification of a human melanoma antigen recognized by tumor-infiltrating lymphocytes associated with in vivo tumor rejection.* Proc Natl Acad Sci U S A, 1994. **91**(14): p. 6458-62.

120. Adema, G.J., de Boer, A.J., Vogel, A.M., Loenen, W.A., and Figdor, C.G. *Molecular characterization of the melanocyte lineage-specific antigen gp100.* J Biol Chem, 1994. **269**(31): p. 20126-33.

121. Mandelcorn-Monson, R.L., Shear, N.H., Yau, E., Sambhara, S., Barber, B.H., Spaner, D., and DeBenedette, M.A. *Cytotoxic T lymphocyte reactivity to gp100, MelanA/MART-1, and tyrosinase, in HLA-A2-positive vitiligo patients.* J Invest Dermatol, 2003. **121**(3): p. 550-6.

122. Hegde, P.S., Wallin, J.J., and Mancao, C. *Predictive markers of anti-VEGF and emerging role of angiogenesis inhibitors as immunotherapeutics.* Semin Cancer Biol, 2017.

123. Martiny-Baron, G. and Marme, D. *VEGF-mediated tumour angiogenesis: a new target for cancer therapy.* Curr Opin Biotechnol, 1995. **6**(6): p. 675-80.

124. Yang, J.C., Haworth, L., Sherry, R.M., Hwu, P., Schwartzentruber, D.J., Topalian, S.L., Steinberg, S.M., Chen, H.X., and Rosenberg, S.A. *A randomized trial of bevacizumab, an anti-vascular endothelial growth factor antibody, for metastatic renal cancer.* N Engl J Med, 2003. **349**(5): p. 427-34.

125. zur Hausen, H., Meinhof, W., Scheiber, W., and Bornkamm, G.W. *Attempts to detect virus-secific DNA in human tumors. I. Nucleic acid hybridizations with complementary RNA of human wart virus.* Int J Cancer, 1974. **13**(5): p. 650-6.

126. zur Hausen, H. *Biochemical approaches to detection of Epstein-Barr virus in human tumors.* Cancer Res, 1976. **36**(2 pt 2): p. 678-80.

127. zur Hausen, H. *Condylomata acuminata and human genital cancer.* Cancer Res, 1976. **36**(2 pt 2): p. 794.

128. zur Hausen, H. *Papillomaviruses and cancer: from basic studies to clinical application.* Nat Rev Cancer, 2002. **2**(5): p. 342-50.

129. Joura, E.A., Leodolter, S., Hernandez-Avila, M., Wheeler, C.M., Perez, G., Koutsky, L.A., Garland, S.M., Harper, D.M., Tang, G.W., Ferris, D.G., Steben, M., Jones, R.W., Bryan, J., Taddeo, F.J., Bautista, O.M., Esser, M.T., Sings, H.L., Nelson, M., Boslego, J.W., Sattler, C., Barr, E., and Paavonen, J. *Efficacy of a quadrivalent prophylactic human papillomavirus (types 6, 11, 16, and 18) L1 virus-like-particle vaccine against high-grade vulval and vaginal lesions: a combined analysis of three randomised clinical trials.* Lancet, 2007. **369**(9574): p. 1693-702.

130. van der Bruggen, P., Traversari, C., Chomez, P., Lurquin, C., De Plaen, E., Van den Eynde, B., Knuth, A., and Boon, T. *A gene encoding an antigen recognized by cytolytic T lymphocytes on a human melanoma.* Science, 1991. **254**(5038): p. 1643-7.

131. Zajac, P., Schultz-Thater, E., Tornillo, L., Sadowski, C., Trella, E., Mengus, C., Iezzi, G., and Spagnoli, G.C. *MAGE-A Antigens and Cancer Immunotherapy.* Front Med (Lausanne), 2017. **4**: p. 18.

132. Christensen, K.L., Patrick, A.N., McCoy, E.L., and Ford, H.L. *The six family of homeobox genes in development and cancer.* Adv Cancer Res, 2008. **101**: p. 93-126.

133. Wirth, T.C. and Kuhnel, F. *Neoantigen Targeting-Dawn of a New Era in Cancer Immunotherapy?* Front Immunol, 2017. **8**: p. 1848.

134. Matsushita, H., Vesely, M.D., Koboldt, D.C., Rickert, C.G., Uppaluri, R., Magrini, V.J., Arthur, C.D., White, J.M., Chen, Y.S., Shea, L.K., Hundal, J., Wendl, M.C., Demeter, R., Wylie, T., Allison, J.P., Smyth, M.J., Old, L.J., Mardis, E.R., and Schreiber, R.D. *Cancer exome analysis reveals a T-cell-dependent mechanism of cancer immunoediting.* Nature, 2012. **482**(7385): p. 400-4.

135. Jäger, E., Jäger, D., and Knuth, A. *Antigen-specific immunotherapy and cancer vaccines.* Int J Cancer, 2003. **106**(6): p. 817-20.

136. Jäger, E., Ringhoffer, M., Altmannsberger, M., Arand, M., Karbach, J., Jäger, D., Oesch, F., and Knuth, A. *Immunoselection in vivo: independent loss of MHC class I and melanocyte differentiation antigen expression in metastatic melanoma.* Int J Cancer, 1997. **71**(2): p. 142-7.

137. Ventura, A., Kirsch, D.G., McLaughlin, M.E., Tuveson, D.A., Grimm, J., Lintault, L., Newman, J., Reczek, E.E., Weissleder, R., and Jacks, T. *Restoration of p53 function leads to tumour regression in vivo.* Nature, 2007. **445**(7128): p. 661-5.

138. Natali, P.G., Nicotra, M.R., Bigotti, A., Venturo, I., Marcenaro, L., Giacomini, P., and Russo, C. *Selective changes in expression of HLA class I polymorphic determinants in human solid tumors.* Proc Natl Acad Sci U S A, 1989. **86**(17): p. 6719-23.

139. Ljunggren, H.G. and Karre, K. *In search of the 'missing self': MHC molecules and NK cell recognition.* Immunol Today, 1990. **11**(7): p. 237-44.

140. Draghi, M., Yawata, N., Gleimer, M., Yawata, M., Valiante, N.M., and Parham, P. *Single-cell analysis of the human NK cell response to missing self and its inhibition by HLA class I.* Blood, 2005. **105**(5): p. 2028-35.

141. Menon, A.G., Fleuren, G.J., Alphenaar, E.A., Jonges, L.E., Janssen van Rhijn, C.M., Ensink, N.G., Putter, H., Tollenaar, R.A., van de Velde, C.J., and Kuppen, P.J. *A basal membrane-like structure surrounding tumour nodules may prevent intraepithelial leucocyte infiltration in colorectal cancer.* Cancer Immunol Immunother, 2003. **52**(2): p. 121-6.

142. Tada, T., Ohzeki, S., Utsumi, K., Takiuchi, H., Muramatsu, M., Li, X.F., Shimizu, J., Fujiwara, H., and Hamaoka, T. *Transforming growth factor-beta-induced inhibition of T cell function. Susceptibility difference in T cells of various phenotypes and functions and its relevance to immunosuppression in the tumor-bearing state.* J Immunol, 1991. **146**(3): p. 1077-82.

143. Gabrilovich, D., Ishida, T., Oyama, T., Ran, S., Kravtsov, V., Nadaf, S., and Carbone, D.P. *Vascular endothelial growth factor inhibits the development of dendritic cells and dramatically affects the differentiation of multiple hematopoietic lineages in vivo.* Blood, 1998. **92**(11): p. 4150-66.

144. Strauss, L., Bergmann, C., Szczepanski, M., Gooding, W., Johnson, J.T., and Whiteside, T.L. *A unique subset of CD4+CD25highFoxp3+ T cells secreting interleukin-10 and transforming growth factor-beta1 mediates suppression in the tumor microenvironment.* Clin Cancer Res, 2007. **13**(15 Pt 1): p. 4345-54.

145. Ferretti, G., Felici, A., Pino, M.S., and Cognetti, F. *Does CTLA4 influence the suppressive effect of CD25+CD4+ regulatory T cells?* J Clin Oncol, 2006. **24**(34): p. 5469-70; author reply 5470-1.

146. Prendergast, G.C. *Immune escape as a fundamental trait of cancer: focus on IDO.* Oncogene, 2008. **27**(28): p. 3889-900.

147. Hoffmann, T.K., Dworacki, G., Tsukihiro, T., Meidenbauer, N., Gooding, W., Johnson, J.T., and Whiteside, T.L. *Spontaneous apoptosis of circulating T lymphocytes in patients with head and neck cancer and its clinical importance.* Clin Cancer Res, 2002. **8**(8): p. 2553-62.

148. Dong, H., Zhu, G., Tamada, K., and Chen, L. *B7-H1, a third member of the B7 family, co-stimulates T-cell proliferation and interleukin-10 secretion.* Nat Med, 1999. **5**(12): p. 1365-9.

149. Sheppard, K.A., Fitz, L.J., Lee, J.M., Benander, C., George, J.A., Wooters, J., Qiu, Y., Jussif, J.M., Carter, L.L., Wood, C.R., and Chaudhary, D. *PD-1 inhibits T-cell receptor induced phosphorylation of the ZAP70/CD3zeta signalosome and downstream signaling to PKCtheta.* FEBS Lett, 2004. **574**(1-3): p. 37-41.

150. Hanahan, D. and Weinberg, R.A. *Hallmarks of cancer: the next generation.* Cell, 2011. **144**(5): p. 646-74.

151. Galon, J., Pages, F., Marincola, F.M., Thurin, M., Trinchieri, G., Fox, B.A., Gajewski, T.F., and Ascierto, P.A. *The immune score as a new possible approach for the classification of cancer.* J Transl Med, 2012. **10**: p. 1.

152. Copelan, E.A. *Hematopoietic stem-cell transplantation.* N Engl J Med, 2006. **354**(17): p. 1813-26.

153. Bleakley, M. and Riddell, S.R. *Molecules and mechanisms of the graft-versus-leukaemia effect.* Nat Rev Cancer, 2004. **4**(5): p. 371-80.

154. Rosenberg, S.A., Packard, B.S., Aebersold, P.M., Solomon, D., Topalian, S.L., Toy, S.T., Simon, P., Lotze, M.T., Yang, J.C., Seipp, C.A., Simpson, C., Carter, C., Bock, S., Schwartzentruber, D., Wei, J.P., and White, D.E. *Use of tumor-infiltrating lymphocytes and interleukin-2 in the immunotherapy of patients with metastatic melanoma. A preliminary report.* N Engl J Med, 1988. **319**(25): p. 1676-80.

155. Gattinoni, L., Powell, D.J., Jr., Rosenberg, S.A., and Restifo, N.P. *Adoptive immunotherapy for cancer: building on success.* Nat Rev Immunol, 2006. **6**(5): p. 383-93.

156. Rosenberg, S.A., Restifo, N.P., Yang, J.C., Morgan, R.A., and Dudley, M.E. *Adoptive cell transfer: a clinical path to effective cancer immunotherapy.* Nat Rev Cancer, 2008. **8**(4): p. 299-308.

157. Gill, S. and June, C.H. *Going viral: chimeric antigen receptor T-cell therapy for hematological malignancies.* Immunol Rev, 2015. **263**(1): p. 68-89.

158. Coccoris, M., Swart, E., de Witte, M.A., van Heijst, J.W., Haanen, J.B., Schepers, K., and Schumacher, T.N. *Long-term functionality of TCR-transduced T cells in vivo.* J Immunol, 2008. **180**(10): p. 6536-43.

159. Porter, D.L., Levine, B.L., Kalos, M., Bagg, A., and June, C.H. *Chimeric antigen receptor-modified T cells in chronic lymphoid leukemia.* N Engl J Med, 2011. **365**(8): p. 725-33.

160. Kochenderfer, J.N. and Rosenberg, S.A. *Treating B-cell cancer with T cells expressing anti-CD19 chimeric antigen receptors.* Nat Rev Clin Oncol, 2013. **10**(5): p. 267-76.

161. Mellman, I., Coukos, G., and Dranoff, G. *Cancer immunotherapy comes of age.* Nature, 2011. **480**(7378): p. 480-9.

162. Dougan, M. and Dranoff, G. *Immune therapy for cancer.* Annu Rev Immunol, 2009. **27**: p. 83-117.

163. Beck, A., Wurch, T., Bailly, C., and Corvaia, N. *Strategies and challenges for the next generation of therapeutic antibodies.* Nat Rev Immunol, 2010. **10**(5): p. 345-52.

164. Adams, G.P. and Weiner, L.M. *Monoclonal antibody therapy of cancer.* Nat Biotechnol, 2005. **23**(9): p. 1147-57.

165. Topp, M.S., Kufer, P., Gokbuget, N., Goebeler, M., Klinger, M., Neumann, S., Horst, H.A., Raff, T., Viardot, A., Schmid, M., Stelljes, M., Schaich, M., Degenhard, E., Kohne-Volland, R., Bruggemann, M., Ottmann, O., Pfeifer, H., Burmeister, T., Nagorsen, D., Schmidt, M., Lutterbuese, R., Reinhardt, C., Baeuerle, P.A., Kneba, M., Einsele, H., Riethmuller, G., Hoelzer, D., Zugmaier, G., and Bargou, R.C. *Targeted therapy with the T-cell-engaging antibody blinatumomab of chemotherapy-refractory minimal residual disease in B-lineage acute lymphoblastic leukemia patients results in high response rate and prolonged leukemia-free survival.* J Clin Oncol, 2011. **29**(18): p. 2493-8.

166. Brassard, D.L., Grace, M.J., and Bordens, R.W. *Interferon-alpha as an immunotherapeutic protein.* J Leukoc Biol, 2002. **71**(4): p. 565-81.

167. Hervas-Stubbs, S., Mancheno, U., Riezu-Boj, J.I., Larraga, A., Ochoa, M.C., Alignani, D., Alfaro, C., Morales-Kastresana, A., Gonzalez, I., Larrea, E., Pircher, H., Le Bon, A., Lopez-Picazo, J.M., Martin-Algarra, S., Prieto, J., and Melero, I. *CD8 T cell priming in the presence of IFN-alpha renders CTLs with improved responsiveness to homeostatic cytokines and recall antigens: important traits for adoptive T cell therapy.* J Immunol, 2012. **189**(7): p. 3299-310.

168. Beatty, G.L. and Paterson, Y. *Regulation of tumor growth by IFN-gamma in cancer immunotherapy.* Immunol Res, 2001. **24**(2): p. 201-10.

169. Fyfe, G., Fisher, R.I., Rosenberg, S.A., Sznol, M., Parkinson, D.R., and Louie, A.C. *Results of treatment of 255 patients with metastatic renal cell carcinoma who received high-dose recombinant interleukin-2 therapy.* J Clin Oncol, 1995. **13**(3): p. 688-96.

170. Mullard, A. *2011 FDA drug approvals.* Nat Rev Drug Discov, 2012. **11**(2): p. 91-4.

171. Hodi, F.S., O'Day, S.J., McDermott, D.F., Weber, R.W., Sosman, J.A., Haanen, J.B., Gonzalez, R., Robert, C., Schadendorf, D., Hassel, J.C., Akerley, W., van den Eertwegh, A.J., Lutzky, J., Lorigan, P., Vaubel, J.M., Linette, G.P., Hogg, D., Ottensmeier, C.H., Lebbe, C., Peschel, C., Quirt, I., Clark, J.I., Wolchok, J.D., Weber, J.S., Tian, J., Yellin, M.J., Nichol, G.M., Hoos, A., and Urba, W.J. *Improved survival with ipilimumab in patients with metastatic melanoma.* N Engl J Med, 2010. **363**(8): p. 711-23.

172. Pardoll, D.M. *The blockade of immune checkpoints in cancer immunotherapy.* Nat Rev Cancer, 2012. **12**(4): p. 252-64.

173. Topalian, S.L., Drake, C.G., and Pardoll, D.M. *Targeting the PD-1/B7-H1(PD-L1) pathway to activate anti-tumor immunity.* Curr Opin Immunol, 2012. **24**(2): p. 207-12.

174. Dong, H., Strome, S.E., Salomao, D.R., Tamura, H., Hirano, F., Flies, D.B., Roche, P.C., Lu, J., Zhu, G., Tamada, K., Lennon, V.A., Celis, E., and Chen, L. *Tumor-associated B7-H1 promotes T-cell apoptosis: a potential mechanism of immune evasion.* Nat Med, 2002. **8**(8): p. 793-800.

175. Keir, M.E., Liang, S.C., Guleria, I., Latchman, Y.E., Qipo, A., Albacker, L.A., Koulmanda, M., Freeman, G.J., Sayegh, M.H., and Sharpe, A.H. *Tissue expression of PD-L1 mediates peripheral T cell tolerance.* J Exp Med, 2006. **203**(4): p. 883-95.

176. Wolchok, J.D., Kluger, H., Callahan, M.K., Postow, M.A., Rizvi, N.A., Lesokhin, A.M., Segal, N.H., Ariyan, C.E., Gordon, R.A., Reed, K., Burke, M.M., Caldwell, A., Kronenberg, S.A., Agunwamba, B.U., Zhang, X., Lowy, I., Inzunza, H.D., Feely, W., Horak, C.E., Hong, Q., Korman, A.J., Wigginton, J.M., Gupta, A., and Sznol, M. *Nivolumab plus ipilimumab in advanced melanoma.* N Engl J Med, 2013. **369**(2): p. 122-33.

177. Rotte, A., Bhandaru, M., Zhou, Y., and McElwee, K.J. *Immunotherapy of melanoma: present options and future promises.* Cancer Metastasis Rev, 2015. **34**(1): p. 115-28.

178. Lawrence, M.S., Stojanov, P., Polak, P., Kryukov, G.V., Cibulskis, K., Sivachenko, A., Carter, S.L., Stewart, C., Mermel, C.H., Roberts, S.A., Kiezun, A., Hammerman, P.S., McKenna, A., Drier, Y., Zou, L., Ramos, A.H., Pugh, T.J., Stransky, N., Helman, E., Kim, J., Sougnez, C., Ambrogio, L., Nickerson, E., Shefler, E., Cortes, M.L., Auclair, D., Saksena, G., Voet, D., Noble, M., DiCara, D., Lin, P., Lichtenstein, L., Heiman, D.I., Fennell, T., Imielinski, M., Hernandez, B., Hodis, E., Baca, S., Dulak, A.M., Lohr, J., Landau, D.A., Wu, C.J., Melendez-Zajgla, J., Hidalgo-Miranda, A., Koren, A., McCarroll, S.A., Mora, J., Crompton, B., Onofrio, R., Parkin, M., Winckler, W., Ardlie, K., Gabriel, S.B., Roberts, C.W.M., Biegel, J.A., Stegmaier, K., Bass, A.J., Garraway, L.A., Meyerson, M., Golub, T.R., Gordenin, D.A., Sunyaev, S., Lander, E.S., and Getz, G. *Mutational heterogeneity in cancer and the search for new cancer-associated genes.* Nature, 2013. **499**(7457): p. 214-218.

179. Bassani-Sternberg, M., Braunlein, E., Klar, R., Engleitner, T., Sinitcyn, P., Audehm, S., Straub, M., Weber, J., Slotta-Huspenina, J., Specht, K., Martignoni, M.E., Werner, A., Hein, R., D, H.B., Peschel, C., Rad, R., Cox, J., Mann, M., and Krackhardt, A.M. *Direct identification of clinically relevant neoepitopes presented on native human melanoma tissue by mass spectrometry.* Nat Commun, 2016. **7**: p. 13404.

180. Gubin, M.M., Zhang, X., Schuster, H., Caron, E., Ward, J.P., Noguchi, T., Ivanova, Y., Hundal, J., Arthur, C.D., Krebber, W.J., Mulder, G.E., Toebes, M., Vesely, M.D., Lam, S.S., Korman, A.J., Allison, J.P., Freeman, G.J., Sharpe, A.H., Pearce, E.L., Schumacher, T.N., Aebersold, R., Rammensee, H.G., Melief, C.J., Mardis, E.R., Gillanders, W.E., Artyomov, M.N., and Schreiber, R.D. *Checkpoint blockade cancer immunotherapy targets tumour-specific mutant antigens.* Nature, 2014. **515**(7528): p. 577-81.

181. Snyder, A., Makarov, V., Merghoub, T., Yuan, J., Zaretsky, J.M., Desrichard, A., Walsh, L.A., Postow, M.A., Wong, P., Ho, T.S., Hollmann, T.J., Bruggeman, C., Kannan, K., Li, Y., Elipenahli, C., Liu, C., Harbison, C.T., Wang, L., Ribas, A., Wolchok, J.D., and Chan, T.A. *Genetic basis for clinical response to CTLA-4 blockade in melanoma.* N Engl J Med, 2014. **371**(23): p. 2189-2199.

182. Rizvi, N.A., Hellmann, M.D., Snyder, A., Kvistborg, P., Makarov, V., Havel, J.J., Lee, W., Yuan, J., Wong, P., Ho, T.S., Miller, M.L., Rekhtman, N., Moreira, A.L., Ibrahim, F., Bruggeman, C., Gasmi, B., Zappasodi, R., Maeda, Y., Sander, C., Garon, E.B., Merghoub, T., Wolchok, J.D., Schumacher, T.N., and Chan, T.A. *Cancer immunology. Mutational landscape determines sensitivity to PD-1 blockade in non-small cell lung cancer.* Science, 2015. **348**(6230): p. 124-8.

183. Gubin, M.M. and Schreiber, R.D. *CANCER. The odds of immunotherapy success.* Science, 2015. **350**(6257): p. 158-9.

184. Lahn, M., Kohler, G., Schmoor, C., Dengler, W., Veelken, H., Brennscheidt, U., Mackensen, A., Kulmburg, P., Hentrich, I., Jesuiter, H., Rosenthal, F.M., Fiebig, H.H., Sommerkamp, H., Farthmann, E.H., Hasse, J., Mertelsmann, R., and Lindemann. *Processing of tumor tissues for vaccination with autologous tumor cells.* Eur Surg Res, 1997. **29**(4): p. 292-302.

185. Simons, J.W., Mikhak, B., Chang, J.F., DeMarzo, A.M., Carducci, M.A., Lim, M., Weber, C.E., Baccala, A.A., Goemann, M.A., Clift, S.M., Ando, D.G., Levitsky, H.I., Cohen, L.K., Sanda, M.G., Mulligan, R.C., Partin, A.W., Carter, H.B., Piantadosi, S., Marshall, F.F., and Nelson, W.G. *Induction of immunity to prostate cancer antigens: results of a clinical trial of vaccination with irradiated autologous prostate tumor cells engineered to secrete granulocyte-macrophage colony-stimulating factor using ex vivo gene transfer.* Cancer Res, 1999. **59**(20): p. 5160-8.

186. Geiger, C., Regn, S., Weinzierl, A., Noessner, E., and Schendel, D.J. *A generic RNA-pulsed dendritic cell vaccine strategy for renal cell carcinoma.* J Transl Med, 2005. **3**: p. 29.

187. Nestle, F.O., Farkas, A., and Conrad, C. *Dendritic-cell-based therapeutic vaccination against cancer.* Curr Opin Immunol, 2005. **17**(2): p. 163-9.

188. Brossart, P., Wirths, S., Stuhler, G., Reichardt, V.L., Kanz, L., and Brugger, W. *Induction of cytotoxic T-lymphocyte responses in vivo after vaccinations with peptide-pulsed dendritic cells.* Blood, 2000. **96**(9): p. 3102-8.

189. Kantoff, P.W., Higano, C.S., Shore, N.D., Berger, E.R., Small, E.J., Penson, D.F., Redfern, C.H., Ferrari, A.C., Dreicer, R., Sims, R.B., Xu, Y., Frohlich, M.W., Schellhammer, P.F., and Impact Study Investigators. *Sipuleucel-T immunotherapy for castration-resistant prostate cancer.* N Engl J Med, 2010. **363**(5): p. 411-22.

190. Melief, C.J. and van der Burg, S.H. *Immunotherapy of established (pre)malignant disease by synthetic long peptide vaccines.* Nat Rev Cancer, 2008. **8**(5): p. 351-60.

191. Nagorsen, D. and Thiel, E. *HLA typing demands for peptide-based anti-cancer vaccine.* Cancer Immunol Immunother, 2008. **57**(12): p. 1903-10.

192. Feyerabend, S., Stevanovic, S., Gouttefangeas, C., Wernet, D., Hennenlotter, J., Bedke, J., Dietz, K., Pascolo, S., Kuczyk, M., Rammensee, H.G., and Stenzl, A. *Novel multi-peptide vaccination in Hla-A2+ hormone sensitive patients with biochemical relapse of prostate cancer.* Prostate, 2009. **69**(9): p. 917-27.

193. Legat, A., Maby-El Hajjami, H., Baumgaertner, P., Cagnon, L., Abed Maillard, S., Geldhof, C., Iancu, E.M., Lebon, L., Guillaume, P., Dojcinovic, D., Michielin, O., Romano, E., Berthod, G., Rimoldi, D., Triebel, F., Luescher, I., Rufer, N., and Speiser, D.E. *Vaccination with LAG-3Ig (IMP321) and Peptides Induces Specific CD4 and CD8 T-Cell Responses in Metastatic Melanoma Patients--Report of a Phase I/IIa Clinical Trial.* Clin Cancer Res, 2016. **22**(6): p. 1330-40.

194. Brayer, J., Lancet, J.E., Powers, J., List, A., Balducci, L., Komrokji, R., and Pinilla-Ibarz, J. *WT1 vaccination in AML and MDS: A pilot trial with synthetic analog peptides.* Am J Hematol, 2015. **90**(7): p. 602-7.

195. Azmi, F., Ahmad Fuaad, A.A., Skwarczynski, M., and Toth, I. *Recent progress in adjuvant discovery for peptide-based subunit vaccines.* Hum Vaccin Immunother, 2014. **10**(3): p. 778-96.

196. Walter, S., Weinschenk, T., Stenzl, A., Zdrojowy, R., Pluzanska, A., Szczylik, C., Staehler, M., Brugger, W., Dietrich, P.Y., Mendrzyk, R., Hilf, N., Schoor, O., Fritsche, J., Mahr, A., Maurer, D., Vass, V., Trautwein, C., Lewandrowski, P., Flohr, C., Pohla, H., Stanczak, J.J., Bronte, V., Mandruzzato, S., Biedermann, T., Pawelec, G., Derhovanessian, E., Yamagishi, H., Miki, T., Hongo, F., Takaha, N., Hirakawa, K., Tanaka, H., Stevanovic, S., Frisch, J., Mayer-Mokler, A., Kirner, A., Rammensee, H.G., Reinhardt, C., and Singh-Jasuja, H. *Multipeptide immune response to cancer vaccine IMA901 after single-dose cyclophosphamide associates with longer patient survival.* Nat Med, 2012. **18**(8): p. 1254-61.

197. Schumacher, T., Bunse, L., Pusch, S., Sahm, F., Wiestler, B., Quandt, J., Menn, O., Osswald, M., Oezen, I., Ott, M., Keil, M., Balss, J., Rauschenbach, K., Grabowska, A.K., Vogler, I., Diekmann, J., Trautwein, N., Eichmuller, S.B., Okun, J., Stevanovic, S., Riemer, A.B., Sahin, U., Friese, M.A., Beckhove, P., von Deimling, A., Wick, W., and Platten, M. *A vaccine targeting mutant IDH1 induces antitumour immunity.* Nature, 2014. **512**(7514): p. 324-7.

198. Ott, P.A., Hu, Z., Keskin, D.B., Shukla, S.A., Sun, J., Bozym, D.J., Zhang, W., Luoma, A., Giobbie-Hurder, A., Peter, L., Chen, C., Olive, O., Carter, T.A., Li, S., Lieb, D.J., Eisenhaure, T., Gjini, E., Stevens, J., Lane, W.J., Javeri, I., Nellaiappan, K., Salazar, A.M., Daley, H., Seaman, M., Buchbinder, E.I., Yoon, C.H., Harden, M., Lennon, N., Gabriel, S., Rodig, S.J., Barouch, D.H., Aster, J.C., Getz, G., Wucherpfennig, K., Neuberg, D., Ritz, J., Lander, E.S., Fritsch, E.F., Hacohen, N., and Wu, C.J. *An immunogenic personal neoantigen vaccine for patients with melanoma.* Nature, 2017. **547**(7662): p. 217-221.

199. Sahin, U., Derhovanessian, E., Miller, M., Kloke, B.P., Simon, P., Lower, M., Bukur, V., Tadmor, A.D., Luxemburger, U., Schrors, B., Omokoko, T., Vormehr, M., Albrecht, C., Paruzynski, A., Kuhn, A.N., Buck, J., Heesch, S., Schreeb, K.H., Muller, F., Ortseifer, I., Vogler, I., Godehardt, E., Attig, S., Rae, R., Breitkreuz, A., Tolliver, C., Suchan, M., Martic, G., Hohberger, A., Sorn, P., Diekmann, J., Ciesla, J., Waksmann, O., Bruck, A.K., Witt, M., Zillgen, M., Rothermel, A., Kasemann, B., Langer, D., Bolte, S., Diken, M., Kreiter, S.,

Nemecek, R., Gebhardt, C., Grabbe, S., Holler, C., Utikal, J., Huber, C., Loquai, C., and Tureci, O. *Personalized RNA mutanome vaccines mobilize poly-specific therapeutic immunity against cancer.* Nature, 2017. **547**(7662): p. 222-226.

200. Zitvogel, L., Apetoh, L., Ghiringhelli, F., and Kroemer, G. *Immunological aspects of cancer chemotherapy.* Nat Rev Immunol, 2008. **8**(1): p. 59-73.

201. Ott, P.A., Hodi, F.S., Kaufman, H.L., Wigginton, J.M., and Wolchok, J.D. *Combination immunotherapy: a road map.* J Immunother Cancer, 2017. **5**: p. 16.

202. Seton-Rogers, S. *Immunotherapy: Powerful combinations.* Nat Rev Cancer, 2016. **16**(12): p. 757.

203. Siegel, R.L., Miller, K.D., and Jemal, A. *Cancer statistics, 2016.* CA Cancer J Clin, 2016. **66**(1): p. 7-30.

204. *Krebs in Deutschland 2011/2012*. 2015, Robert Koch Institut und die Gesellschaft der epidemiologischen Krebsregister in Deutschland e.V., Berlin.

205. Petejova, N. and Martinek, A. *Renal cell carcinoma: Review of etiology, pathophysiology and risk factors.* Biomed Pap Med Fac Univ Palacky Olomouc Czech Repub, 2016. **160**(2): p. 183-94.

206. Patil, S., Manola, J., Elson, P., Negrier, S., Escudier, B., Eisen, T., Atkins, M., Bukowski, R., and Motzer, R.J. *Improvement in overall survival of patients with advanced renal cell carcinoma: prognostic factor trend analysis from an international data set of clinical trials.* J Urol, 2012. **188**(6): p. 2095-100.

207. Rini, B.I., Rathmell, W.K., and Godley, P. *Renal cell carcinoma.* Curr Opin Oncol, 2008. **20**(3): p. 300-6.

208. Van den Hove, L.E., Van Gool, S.W., Van Poppel, H., Baert, L., Coorevits, L., Van Damme, B., and Ceuppens, J.L. *Phenotype, cytokine production and cytolytic capacity of fresh (uncultured) tumour-infiltrating T lymphocytes in human renal cell carcinoma.* Clin Exp Immunol, 1997. **109**(3): p. 501-9.

209. Lokich, J. *Spontaneous regression of metastatic renal cancer. Case report and literature review.* Am J Clin Oncol, 1997. **20**(4): p. 416-8.

210. Negrier, S., Escudier, B., Lasset, C., Douillard, J.Y., Savary, J., Chevreau, C., Ravaud, A., Mercatello, A., Peny, J., Mousseau, M., Philip, T., and Tursz, T. *Recombinant human interleukin-2, recombinant human interferon alfa-2a, or both in metastatic renal-cell carcinoma. Groupe Francais d'Immunotherapie.* N Engl J Med, 1998. **338**(18): p. 1272-8.

211. Rini, B.I. and Atkins, M.B. *Resistance to targeted therapy in renal-cell carcinoma.* Lancet Oncol, 2009. **10**(10): p. 992-1000.

212. Motzer, R.J. and Bukowski, R.M. *Targeted therapy for metastatic renal cell carcinoma.* J Clin Oncol, 2006. **24**(35): p. 5601-8.

213. Motzer, R.J., Hutson, T.E., Tomczak, P., Michaelson, M.D., Bukowski, R.M., Oudard, S., Negrier, S., Szczylik, C., Pili, R., Bjarnason, G.A., Garcia-del-Muro, X., Sosman, J.A., Solska, E., Wilding, G., Thompson, J.A., Kim, S.T., Chen, I., Huang, X., and Figlin, R.A. *Overall survival and updated results for sunitinib compared with interferon alfa in patients with metastatic renal cell carcinoma.* J Clin Oncol, 2009. **27**(22): p. 3584-90.

214. Escudier, B., Eisen, T., Stadler, W.M., Szczylik, C., Oudard, S., Siebels, M., Negrier, S., Chevreau, C., Solska, E., Desai, A.A., Rolland, F., Demkow, T., Hutson, T.E., Gore, M., Freeman, S., Schwartz, B., Shan, M., Simantov, R., Bukowski, R.M., and Target Study Group. *Sorafenib in advanced clear-cell renal-cell carcinoma.* N Engl J Med, 2007. **356**(2): p. 125-34.

215. Sternberg, C.N. *Pazopanib in renal cell carcinoma.* Clin Adv Hematol Oncol, 2010. **8**(4): p. 232-3.

216. Escudier, B., Pluzanska, A., Koralewski, P., Ravaud, A., Bracarda, S., Szczylik, C., Chevreau, C., Filipek, M., Melichar, B., Bajetta, E., Gorbunova, V., Bay, J.O., Bodrogi, I., Jagiello-Gruszfeld, A., Moore, N., and Avoren Trial Investigators. *Bevacizumab plus interferon alfa-2a for treatment of metastatic renal cell carcinoma: a randomised, double-blind phase III trial.* Lancet, 2007. **370**(9605): p. 2103-11.

217. Hudes, G., Carducci, M., Tomczak, P., Dutcher, J., Figlin, R., Kapoor, A., Staroslawska, E., Sosman, J., McDermott, D., Bodrogi, I., Kovacevic, Z., Lesovoy, V., Schmidt-Wolf, I.G., Barbarash, O., Gokmen, E., O'Toole, T., Lustgarten, S., Moore, L., Motzer, R.J., and Global Arcc Trial. *Temsirolimus, interferon alfa, or both for advanced renal-cell carcinoma.* N Engl J Med, 2007. **356**(22): p. 2271-81.

218. Motzer, R.J., Escudier, B., Oudard, S., Hutson, T.E., Porta, C., Bracarda, S., Grunwald, V., Thompson, J.A., Figlin, R.A., Hollaender, N., Urbanowitz, G., Berg, W.J., Kay, A., Lebwohl, D., Ravaud, A., and Record Study Group. *Efficacy of everolimus in advanced renal cell carcinoma: a double-blind, randomised, placebo-controlled phase III trial.* Lancet, 2008. **372**(9637): p. 449-56.

219. Choueiri, T.K., Escudier, B., Powles, T., Mainwaring, P.N., Rini, B.I., Donskov, F., Hammers, H., Hutson, T.E., Lee, J.L., Peltola, K., Roth, B.J., Bjarnason, G.A., Geczi, L., Keam, B., Maroto, P., Heng, D.Y., Schmidinger, M., Kantoff, P.W., Borgman-Hagey, A., Hessel, C., Scheffold, C., Schwab, G.M., Tannir, N.M., Motzer, R.J., and Meteor Investigators. *Cabozantinib versus Everolimus in Advanced Renal-Cell Carcinoma.* N Engl J Med, 2015. **373**(19): p. 1814-23.

220. Motzer, R.J., Escudier, B., McDermott, D.F., George, S., Hammers, H.J., Srinivas, S., Tykodi, S.S., Sosman, J.A., Procopio, G., Plimack, E.R., Castellano, D., Choueiri, T.K., Gurney, H., Donskov, F., Bono, P., Wagstaff, J., Gauler, T.C., Ueda, T., Tomita, Y., Schutz, F.A., Kollmannsberger, C., Larkin, J., Ravaud, A., Simon, J.S., Xu, L.A., Waxman, I.M., Sharma, P., and CheckMate Investigators. *Nivolumab versus Everolimus in Advanced Renal-Cell Carcinoma.* N Engl J Med, 2015. **373**(19): p. 1803-13.

221. Quinn, D.I. and Lara, P.N., Jr. *Renal-Cell Cancer--Targeting an Immune Checkpoint or Multiple Kinases.* N Engl J Med, 2015. **373**(19): p. 1872-4.

222. Lawn, S.D. and Zumla, A.I. *Tuberculosis.* Lancet, 2011. **378**(9785): p. 57-72.

223. Armstrong, J.A. and Hart, P.D. *Response of cultured macrophages to Mycobacterium tuberculosis, with observations on fusion of lysosomes with phagosomes.* J Exp Med, 1971. **134**(3 Pt 1): p. 713-40.

224. Barry, C.E., 3rd, Boshoff, H.I., Dartois, V., Dick, T., Ehrt, S., Flynn, J., Schnappinger, D., Wilkinson, R.J., and Young, D. *The spectrum of latent tuberculosis: rethinking the biology and intervention strategies.* Nat Rev Microbiol, 2009. **7**(12): p. 845-55.

225. Niederweis, M., Danilchanka, O., Huff, J., Hoffmann, C., and Engelhardt, H. *Mycobacterial outer membranes: in search of proteins.* Trends Microbiol, 2010. **18**(3): p. 109-16.

226. Brennan, P.J. and Nikaido, H. *The envelope of mycobacteria.* Annu Rev Biochem, 1995. **64**: p. 29-63.

227. Jackson, M. *The mycobacterial cell envelope-lipids.* Cold Spring Harb Perspect Med, 2014. **4**(10).

228. Houben, E.N., Nguyen, L., and Pieters, J. *Interaction of pathogenic mycobacteria with the host immune system.* Curr Opin Microbiol, 2006. **9**(1): p. 76-85.

229. Philips, J.A., Rubin, E.J., and Perrimon, N. *Drosophila RNAi screen reveals CD36 family member required for mycobacterial infection.* Science, 2005. **309**(5738): p. 1251-3.

230. Warner, D.F. and Mizrahi, V. *The survival kit of Mycobacterium tuberculosis.* Nat Med, 2007. **13**(3): p. 282-4.

231. Vergne, I., Chua, J., Lee, H.H., Lucas, M., Belisle, J., and Deretic, V. *Mechanism of phagolysosome biogenesis block by viable Mycobacterium tuberculosis.* Proc Natl Acad Sci U S A, 2005. **102**(11): p. 4033-8.

232. Walburger, A., Koul, A., Ferrari, G., Nguyen, L., Prescianotto-Baschong, C., Huygen, K., Klebl, B., Thompson, C., Bacher, G., and Pieters, J. *Protein kinase G from pathogenic mycobacteria promotes survival within macrophages.* Science, 2004. **304**(5678): p. 1800-4.

233. Voskuil, M.I., Schnappinger, D., Visconti, K.C., Harrell, M.I., Dolganov, G.M., Sherman, D.R., and Schoolnik, G.K. *Inhibition of respiration by nitric oxide induces a Mycobacterium tuberculosis dormancy program.* J Exp Med, 2003. **198**(5): p. 705-13.

234. Orme, I.M., Robinson, R.T., and Cooper, A.M. *The balance between protective and pathogenic immune responses in the TB-infected lung.* Nat Immunol, 2015. **16**(1): p. 57-63.

235. Davis, J.M. and Ramakrishnan, L. *The role of the granuloma in expansion and dissemination of early tuberculous infection.* Cell, 2009. **136**(1): p. 37-49.

236. O'Garra, A., Redford, P.S., McNab, F.W., Bloom, C.I., Wilkinson, R.J., and Berry, M.P. *The immune response in tuberculosis.* Annu Rev Immunol, 2013. **31**: p. 475-527.

237. Mancuso, J.D., Bernardo, J., and Mazurek, G.H. *The elusive "gold" standard for detecting Mycobacterium tuberculosis infection.* Am J Respir Crit Care Med, 2013. **187**(2): p. 122-4.

238. Gandhi, N.R., Nunn, P., Dheda, K., Schaaf, H.S., Zignol, M., van Soolingen, D., Jensen, P., and Bayona, J. *Multidrug-resistant and extensively drug-resistant tuberculosis: a threat to global control of tuberculosis.* Lancet, 2010. **375**(9728): p. 1830-43.

239. Trunz, B.B., Fine, P., and Dye, C. *Effect of BCG vaccination on childhood tuberculous meningitis and miliary tuberculosis worldwide: a meta-analysis and assessment of cost-effectiveness.* Lancet, 2006. **367**(9517): p. 1173-80.

240. Roy, A., Eisenhut, M., Harris, R.J., Rodrigues, L.C., Sridhar, S., Habermann, S., Snell, L., Mangtani, P., Adetifa, I., Lalvani, A., and Abubakar, I. *Effect of BCG vaccination against Mycobacterium tuberculosis infection in children: systematic review and meta-analysis.* BMJ, 2014. **349**: p. g4643.

241. Houghton, B.B., Chalasani, V., Hayne, D., Grimison, P., Brown, C.S., Patel, M.I., Davis, I.D., and Stockler, M.R. *Intravesical chemotherapy plus bacille Calmette-Guerin in non-muscle invasive bladder cancer: a systematic review with meta-analysis.* BJU Int, 2013. **111**(6): p. 977-83.

242. McShane, H. *Tuberculosis vaccines: beyond bacille Calmette-Guerin.* Philos Trans R Soc Lond B Biol Sci, 2011. **366**(1579): p. 2782-9.

243. Kaufmann, S.H. *Future vaccination strategies against tuberculosis: thinking outside the box.* Immunity, 2010. **33**(4): p. 567-77.

244. Kaufmann, S.H.E., Dockrell, H.M., Drager, N., Ho, M.M., McShane, H., Neyrolles, O., Ottenhoff, T.H.M., Patel, B., Roordink, D., Spertini, F., Stenger, S., Thole, J., Verreck, F.A.W., Williams, A., and Consortium, T. *TBVAC2020: Advancing Tuberculosis Vaccines from Discovery to Clinical Development.* Front Immunol, 2017. **8**: p. 1203.

245. Cole, S.T., Brosch, R., Parkhill, J., Garnier, T., Churcher, C., Harris, D., Gordon, S.V., Eiglmeier, K., Gas, S., Barry, C.E., 3rd, Tekaia, F., Badcock, K., Basham, D., Brown, D., Chillingworth, T., Connor, R., Davies, R., Devlin, K., Feltwell, T., Gentles, S., Hamlin, N., Holroyd, S., Hornsby, T., Jagels, K., Krogh, A., McLean, J., Moule, S., Murphy, L., Oliver, K., Osborne, J., Quail, M.A., Rajandream, M.A., Rogers, J., Rutter, S., Seeger, K., Skelton, J., Squares, R., Squares, S., Sulston, J.E., Taylor, K., Whitehead, S., and Barrell, B.G. *Deciphering the biology of Mycobacterium tuberculosis from the complete genome sequence.* Nature, 1998. **393**(6685): p. 537-44.

246. Ottenhoff, T.H., Verreck, F.A., Hoeve, M.A., and van de Vosse, E. *Control of human host immunity to mycobacteria.* Tuberculosis (Edinb), 2005. **85**(1-2): p. 53-64.

247. Aguilo, N., Gonzalo-Asensio, J., Alvarez-Arguedas, S., Marinova, D., Gomez, A.B., Uranga, S., Spallek, R., Singh, M., Audran, R., Spertini, F., and Martin, C. *Reactogenicity to major tuberculosis antigens absent in BCG is linked to improved protection against Mycobacterium tuberculosis.* Nat Commun, 2017. **8**: p. 16085.

248. Groschel, M.I., Sayes, F., Shin, S.J., Frigui, W., Pawlik, A., Orgeur, M., Canetti, R., Honore, N., Simeone, R., van der Werf, T.S., Bitter, W., Cho, S.N., Majlessi, L., and Brosch, R. *Recombinant BCG Expressing ESX-1 of Mycobacterium marinum Combines Low Virulence with Cytosolic Immune Signaling and Improved TB Protection.* Cell Rep, 2017. **18**(11): p. 2752-2765.

249. Wallis, R.S. and Hafner, R. *Advancing host-directed therapy for tuberculosis.* Nat Rev Immunol, 2015. **15**(4): p. 255-63.

250. Queval, C.J., Brosch, R., and Simeone, R. *The Macrophage: A Disputed Fortress in the Battle against Mycobacterium tuberculosis.* Front Microbiol, 2017. **8**: p. 2284.

251. Bifani, P., Moghazeh, S., Shopsin, B., Driscoll, J., Ravikovitch, A., and Kreiswirth, B.N. *Molecular characterization of Mycobacterium tuberculosis H37Rv/Ra variants: distinguishing the mycobacterial laboratory strain.* J Clin Microbiol, 2000. **38**(9): p. 3200-4.

252. McShane, H., Pathan, A.A., Sander, C.R., Keating, S.M., Gilbert, S.C., Huygen, K., Fletcher, H.A., and Hill, A.V. *Recombinant modified vaccinia virus Ankara expressing antigen 85A boosts BCG-primed and naturally acquired antimycobacterial immunity in humans.* Nat Med, 2004. **10**(11): p. 1240-4.

253. Tameris, M.D., Hatherill, M., Landry, B.S., Scriba, T.J., Snowden, M.A., Lockhart, S., Shea, J.E., McClain, J.B., Hussey, G.D., Hanekom, W.A., Mahomed, H., McShane, H., and Mva A Trial Study Team. *Safety and efficacy of MVA85A, a new tuberculosis vaccine, in infants previously vaccinated with BCG: a randomised, placebo-controlled phase 2b trial.* Lancet, 2013. **381**(9871): p. 1021-8.

254. Ndiaye, B.P., Thienemann, F., Ota, M., Landry, B.S., Camara, M., Dieye, S., Dieye, T.N., Esmail, H., Goliath, R., Huygen, K., January, V., Ndiaye, I., Oni, T., Raine, M., Romano, M., Satti, I., Sutton, S., Thiam, A., Wilkinson, K.A., Mboup, S., Wilkinson, R.J., McShane, H., and Mva A Trial Investigators. *Safety, immunogenicity, and efficacy of the candidate tuberculosis vaccine MVA85A in healthy adults infected with HIV-1: a randomised, placebo-controlled, phase 2 trial.* Lancet Respir Med, 2015. **3**(3): p. 190-200.

255. Huygen, K., Content, J., Denis, O., Montgomery, D.L., Yawman, A.M., Deck, R.R., DeWitt, C.M., Orme, I.M., Baldwin, S., D'Souza, C., Drowart, A., Lozes, E., Vandenbussche, P., Van Vooren, J.P., Liu, M.A., and Ulmer, J.B. *Immunogenicity and protective efficacy of a tuberculosis DNA vaccine.* Nat Med, 1996. **2**(8): p. 893-8.

256. McShane, H., Behboudi, S., Goonetilleke, N., Brookes, R., and Hill, A.V. *Protective immunity against Mycobacterium tuberculosis induced by dendritic cells pulsed with both CD8(+)- and CD4(+)-T-cell epitopes from antigen 85A.* Infect Immun, 2002. **70**(3): p. 1623-6.

257. Hawkridge, T., Scriba, T.J., Gelderbloem, S., Smit, E., Tameris, M., Moyo, S., Lang, T., Veldsman, A., Hatherill, M., Merwe, L., Fletcher, H.A., Mahomed, H., Hill, A.V., Hanekom, W.A., Hussey, G.D., and McShane, H. *Safety and immunogenicity of a new tuberculosis vaccine, MVA85A, in healthy adults in South Africa.* J Infect Dis, 2008. **198**(4): p. 544-52.

258. Corr, M., Slanetz, A.E., Boyd, L.F., Jelonek, M.T., Khilko, S., al-Ramadi, B.K., Kim, Y.S., Maher, S.E., Bothwell, A.L., and Margulies, D.H. *T cell receptor-MHC class I peptide interactions: affinity, kinetics, and specificity.* Science, 1994. **265**(5174): p. 946-9.

259. Altman, J.D., Moss, P.A., Goulder, P.J., Barouch, D.H., McHeyzer-Williams, M.G., Bell, J.I., McMichael, A.J., and Davis, M.M. *Phenotypic analysis of antigen-specific T lymphocytes.* Science, 1996. **274**(5284): p. 94-6.

260. Sturm, T., Leinders-Zufall, T., Macek, B., Walzer, M., Jung, S., Pommerl, B., Stevanovic, S., Zufall, F., Overath, P., and Rammensee, H.G. *Mouse urinary peptides provide a molecular basis for genotype discrimination by nasal sensory neurons.* Nat Commun, 2013. **4**: p. 1616.

261. Woolley, D.W. and Merrifield, R.B. *Anomalies of the structural specificity of peptides.* Ann N Y Acad Sci, 1963. **104**: p. 161-71.

262. Kohn, J. and Wilchek, M. *Procedures for the analysis of cyanogen bromide-activated Sepharose or Sephadex by quantitative determination of cyanate esters and imidocarbonates.* Anal Biochem, 1981. **115**(2): p. 375-82.

263. Whitehouse, C.M., Dreyer, R.N., Yamashita, M., and Fenn, J.B. *Electrospray interface for liquid chromatographs and mass spectrometers.* Anal Chem, 1985. **57**(3): p. 675-9.

264. Fenn, J.B., Mann, M., Meng, C.K., Wong, S.F., and Whitehouse, C.M. *Electrospray ionization for mass spectrometry of large biomolecules.* Science, 1989. **246**(4926): p. 64-71.

265. Kebarle, P. and Verkerk, U.H. *Electrospray: from ions in solution to ions in the gas phase, what we know now.* Mass Spectrom Rev, 2009. **28**(6): p. 898-917.

266. Nguyen, S. and Fenn, J.B. *Gas-phase ions of solute species from charged droplets of solutions.* Proc Natl Acad Sci U S A, 2007. **104**(4): p. 1111-7.

267. Clegg, G.A. and Dole, M. *Molecular beams of macroions. 3. Zein and polyvinylpyrrolidone.* Biopolymers, 1971. **10**(5): p. 821-6.

268. McLafferty, F.W. *Tandem mass spectrometry.* Science, 1981. **214**(4518): p. 280-7.

269. Scigelova, M. and Makarov, A. *Orbitrap mass analyzer--overview and applications in proteomics.* Proteomics, 2006. **6 Suppl 2**: p. 16-21.

270. Hu, Q., Noll, R.J., Li, H., Makarov, A., Hardman, M., and Graham Cooks, R. *The Orbitrap: a new mass spectrometer.* J Mass Spectrom, 2005. **40**(4): p. 430-43.

271. Gierlich, H.H., Heinen, H.J., and Beckey, H.D. *The application of quadrupole mass filters in field desorption mass spectrometry.* Biomed Mass Spectrom, 1975. **2**(1): p. 31-5.

272. Douglas, D.J., Frank, A.J., and Mao, D. *Linear ion traps in mass spectrometry.* Mass Spectrom Rev, 2005. **24**(1): p. 1-29.

273. Biemann, K. *Sequencing of peptides by tandem mass spectrometry and high-energy collision-induced dissociation.* Methods Enzymol, 1990. **193**: p. 455-79.

274. Choudhary, C. and Mann, M. *Decoding signalling networks by mass spectrometry-based proteomics.* Nat Rev Mol Cell Biol, 2010. **11**(6): p. 427-39.

275. Olsen, J.V., Schwartz, J.C., Griep-Raming, J., Nielsen, M.L., Damoc, E., Denisov, E., Lange, O., Remes, P., Taylor, D., Splendore, M., Wouters, E.R., Senko, M., Makarov, A., Mann, M., and Horning, S. *A dual pressure linear ion trap Orbitrap instrument with very high sequencing speed.* Mol Cell Proteomics, 2009. **8**(12): p. 2759-69.

276. Perkins, D.N., Pappin, D.J., Creasy, D.M., and Cottrell, J.S. *Probability-based protein identification by searching sequence databases using mass spectrometry data.* Electrophoresis, 1999. **20**(18): p. 3551-67.

277. Pappin, D.J., Hojrup, P., and Bleasby, A.J. *Rapid identification of proteins by peptide-mass fingerprinting.* Curr Biol, 1993. **3**(6): p. 327-32.

278. Bairoch, A. and Apweiler, R. *The SWISS-PROT protein sequence data bank and its supplement TrEMBL in 1999.* Nucleic Acids Res, 1999. **27**(1): p. 49-54.

279. Kall, L., Canterbury, J.D., Weston, J., Noble, W.S., and MacCoss, M.J. *Semi-supervised learning for peptide identification from shotgun proteomics datasets.* Nat Methods, 2007. **4**(11): p. 923-5.

280. Roepstorff, P. and Fohlman, J. *Proposal for a common nomenclature for sequence ions in mass spectra of peptides.* Biomed Mass Spectrom, 1984. **11**(11): p. 601.

281. Biemann, K. *Mass spectrometry of peptides and proteins.* Annu Rev Biochem, 1992. **61**: p. 977-1010.

282. Keller, B.O., Sui, J., Young, A.B., and Whittal, R.M. *Interferences and contaminants encountered in modern mass spectrometry.* Anal Chim Acta, 2008. **627**(1): p. 71-81.

283. Peper, J.K., *Identification and characterization of naturally presented, immunogenic HLA ligands for establishing a peptide-based anti-tumor vaccination in ovarian cancer*. 2015, Dissertation der Eberhard-Karls-Universität Tübingen.

284. Fulwyler, M.J. *Electronic separation of biological cells by volume.* Science, 1965. **150**(3698): p. 910-1.

285. Kowalewski, D.J., *Massenspektrometrische Analyse von Nierenzellkarzinomen zur Entwicklung neuer Tumorvakzine*. 2011, Diplomarbeit der Eberhard-Karls-Universität Tübingen.

286. Schmidt, J., Neumann-Haefelin, C., Altay, T., Gostick, E., Price, D.A., Lohmann, V., Blum, H.E., and Thimme, R. *Immunodominance of HLA-A2-restricted hepatitis C virus-specific CD8+ T cell responses is linked to naive-precursor frequency.* J Virol, 2011. **85**(10): p. 5232-6.

287. Alanio, C., Lemaitre, F., Law, H.K., Hasan, M., and Albert, M.L. *Enumeration of human antigen-specific naive CD8+ T cells reveals conserved precursor frequencies.* Blood, 2010. **115**(18): p. 3718-25.

288. Christ, C., *Identifikation von natürlich prozessierten HLA-Liganden des Mycobacterium tuberculosis mittels massenspektrometrischer Analyse*. 2014, Dissertation der Eberhard-Karls-Universität Tübingen.

289. Wilhelm, M., Schlegl, J., Hahne, H., Gholami, A.M., Lieberenz, M., Savitski, M.M., Ziegler, E., Butzmann, L., Gessulat, S., Marx, H., Mathieson, T., Lemeer, S., Schnatbaum, K., Reimer, U., Wenschuh, H., Mollenhauer, M., Slotta-Huspenina, J., Boese, J.H., Bantscheff, M., Gerstmair, A., Faerber, F., and Kuster, B. *Mass-spectrometry-based draft of the human proteome.* Nature, 2014. **509**(7502): p. 582-7.

290. Kim, M.S., Pinto, S.M., Getnet, D., Nirujogi, R.S., Manda, S.S., Chaerkady, R., Madugundu, A.K., Kelkar, D.S., Isserlin, R., Jain, S., Thomas, J.K., Muthusamy, B., Leal-Rojas, P., Kumar, P., Sahasrabuddhe, N.A., Balakrishnan, L., Advani, J., George, B., Renuse, S., Selvan, L.D., Patil, A.H., Nanjappa, V., Radhakrishnan, A., Prasad, S., Subbannayya, T., Raju, R., Kumar, M., Sreenivasamurthy, S.K., Marimuthu, A., Sathe, G.J., Chavan, S., Datta, K.K., Subbannayya, Y., Sahu, A., Yelamanchi, S.D., Jayaram, S., Rajagopalan, P., Sharma, J., Murthy, K.R., Syed, N., Goel, R., Khan, A.A., Ahmad, S., Dey, G., Mudgal, K., Chatterjee, A., Huang, T.C., Zhong, J., Wu, X., Shaw, P.G., Freed, D., Zahari, M.S., Mukherjee, K.K., Shankar, S., Mahadevan, A., Lam, H., Mitchell, C.J., Shankar, S.K., Satishchandra, P., Schroeder, J.T., Sirdeshmukh, R., Maitra, A., Leach, S.D., Drake, C.G., Halushka, M.K., Prasad, T.S., Hruban, R.H., Kerr, C.L., Bader, G.D., Iacobuzio-Donahue, C.A., Gowda, H., and Pandey, A. *A draft map of the human proteome.* Nature, 2014. **509**(7502): p. 575-81.

291. Berlin, C., Kowalewski, D.J., Schuster, H., Mirza, N., Walz, S., Handel, M., Schmid-Horch, B., Salih, H.R., Kanz, L., Rammensee, H.G., Stevanovic, S., and Stickel, J.S. *Mapping the HLA ligandome landscape of acute myeloid leukemia: a targeted approach toward peptide-based immunotherapy.* Leukemia, 2015. **29**(3): p. 647-59.

292. Kowalewski, D.J., Schuster, H., Backert, L., Berlin, C., Kahn, S., Kanz, L., Salih, H.R., Rammensee, H.G., Stevanovic, S., and Stickel, J.S. *HLA ligandome analysis identifies the underlying specificities of spontaneous antileukemia immune responses in chronic lymphocytic leukemia (CLL).* Proc Natl Acad Sci U S A, 2015. **112**(2): p. E166-75.

293. Hassan, C., Kester, M.G., de Ru, A.H., Hombrink, P., Drijfhout, J.W., Nijveen, H., Leunissen, J.A., Heemskerk, M.H., Falkenburg, J.H., and van Veelen, P.A. *The human leukocyte antigen-presented ligandome of B lymphocytes.* Mol Cell Proteomics, 2013. **12**(7): p. 1829-43.

294. Heemskerk, B., Kvistborg, P., and Schumacher, T.N. *The cancer antigenome.* EMBO J, 2013. **32**(2): p. 194-203.

295. Schuster, H., Peper, J.K., Bosmuller, H.C., Röhle, K., Backert, L., Bilich, T., Ney, B., Löffler, M.W., Kowalewski, D.J., Trautwein, N., Rabsteyn, A., Engler, T., Braun, S., Haen, S.P., Walz, J.S., Schmid-Horch, B., Brucker, S.Y., Wallwiener, D., Kohlbacher, O., Fend, F., Rammensee, H.G., Stevanovic, S., Staebler, A., and Wagner, P. *The immunopeptidomic landscape of ovarian carcinomas.* Proc Natl Acad Sci U S A, 2017. **114**(46): p. E9942-E9951.

296. Kuznetsov, V.A., Knott, G.D., and Bonner, R.F. *General statistics of stochastic process of gene expression in eukaryotic cells.* Genetics, 2002. **161**(3): p. 1321-32.

297. Mann, M., Kulak, N.A., Nagaraj, N., and Cox, J. *The coming age of complete, accurate, and ubiquitous proteomes.* Mol Cell, 2013. **49**(4): p. 583-90.

298. Schuster, H., *Durchflusscytometrische Dissektion renaler Tumore*. 2010, Diplomarbeit der Eberhard-Karls-Universität Tübingen.

299. Kageyama, S., Tsomides, T.J., Sykulev, Y., and Eisen, H.N. *Variations in the number of peptide-MHC class I complexes required to activate cytotoxic T cell responses.* J Immunol, 1995. **154**(2): p. 567-76.

300. Stevanovic, S. and Schild, H. *Quantitative aspects of T cell activation--peptide generation and editing by MHC class I molecules.* Semin Immunol, 1999. **11**(6): p. 375-84.

301. Stickel, J.S., Stickel, N., Hennenlotter, J., Klingel, K., Stenzl, A., Rammensee, H.G., and Stevanovic, S. *Quantification of HLA class I molecules on renal cell carcinoma using Edman degradation.* BMC Urol, 2011. **11**: p. 1.

302. Saenz-Lopez, P., Gouttefangeas, C., Hennenlotter, J., Concha, A., Maleno, I., Ruiz-Cabello, F., Cozar, J.M., Tallada, M., Stenzl, A., Rammensee, H.G., Garrido, F., and Cabrera, T. *Higher HLA class I expression in renal cell carcinoma than in autologous normal tissue.* Tissue Antigens, 2010. **75**(2): p. 110-8.

303. Gerlinger, M., Rowan, A.J., Horswell, S., Math, M., Larkin, J., Endesfelder, D., Gronroos, E., Martinez, P., Matthews, N., Stewart, A., Tarpey, P., Varela, I., Phillimore, B., Begum, S., McDonald, N.Q., Butler, A., Jones, D., Raine, K., Latimer, C., Santos, C.R., Nohadani, M., Eklund, A.C., Spencer-Dene, B., Clark, G., Pickering, L., Stamp, G., Gore, M., Szallasi, Z., Downward, J., Futreal, P.A., and Swanton, C. *Intratumor heterogeneity and branched evolution revealed by multiregion sequencing.* N Engl J Med, 2012. **366**(10): p. 883-892.

304. Geissler, K., Fornara, P., Lautenschlager, C., Holzhausen, H.J., Seliger, B., and Riemann, D. *Immune signature of tumor infiltrating immune cells in renal cancer.* Oncoimmunology, 2015. **4**(1): p. e985082.

305. Chevrier, S., Levine, J.H., Zanotelli, V.R.T., Silina, K., Schulz, D., Bacac, M., Ries, C.H., Ailles, L., Jewett, M.A.S., Moch, H., van den Broek, M., Beisel, C., Stadler, M.B., Gedye, C., Reis, B., Pe'er, D., and Bodenmiller, B. *An Immune Atlas of Clear Cell Renal Cell Carcinoma.* Cell, 2017. **169**(4): p. 736-749 e18.

306. Weinzierl, A.O., Lemmel, C., Schoor, O., Müller, M., Krüger, T., Wernet, D., Hennenlotter, J., Stenzl, A., Klingel, K., Rammensee, H.G., and Stevanovic, S. *Distorted relation between mRNA copy number and corresponding major histocompatibility complex ligand density on the cell surface.* Mol Cell Proteomics, 2007. **6**(1): p. 102-13.

307. Dong, D., Jia, L., Zhou, Y., Ren, L., Li, J., and Zhang, J. *Serum level of ANGPTL4 as a potential biomarker in renal cell carcinoma.* Urol Oncol, 2017. **35**(5): p. 279-285.

308. Zhang, J., Cao, J., Weng, Q., Wu, R., Yan, Y., Jing, H., Zhu, H., He, Q., and Yang, B. *Suppression of hypoxia-inducible factor 1alpha (HIF-1alpha) by tirapazamine is dependent on eIF2alpha phosphorylation rather than the mTORC1/4E-BP1 pathway.* PLoS One, 2010. **5**(11): p. e13910.

309. Türeci, O., Sahin, U., Vollmar, E., Siemer, S., Gottert, E., Seitz, G., Parkkila, A.K., Shah, G.N., Grubb, J.H., Pfreundschuh, M., and Sly, W.S. *Human carbonic anhydrase XII: cDNA cloning, expression, and chromosomal localization of a carbonic anhydrase gene that is overexpressed in some renal cell cancers.* Proc Natl Acad Sci U S A, 1998. **95**(13): p. 7608-13.

310. Bastid, J., Cottalorda-Regairaz, A., Alberici, G., Bonnefoy, N., Eliaou, J.F., and Bensussan, A. *ENTPD1/CD39 is a promising therapeutic target in oncology.* Oncogene, 2013. **32**(14): p. 1743-51.

311. Uemura, H., Fujimoto, K., Tanaka, M., Yoshikawa, M., Hirao, Y., Uejima, S., Yoshikawa, K., and Itoh, K. *A phase I trial of vaccination of CA9-derived peptides for HLA-A24-positive patients with cytokine-refractory metastatic renal cell carcinoma.* Clin Cancer Res, 2006. **12**(6): p. 1768-75.

312. Hase, H., Jingushi, K., Ueda, Y., Kitae, K., Egawa, H., Ohshio, I., Kawakami, R., Kashiwagi, Y., Tsukada, Y., Kobayashi, T., Nakata, W., Fujita, K., Uemura, M., Nonomura, N., and Tsujikawa, K. *LOXL2 status correlates with tumor stage and regulates integrin levels to promote tumor progression in ccRCC.* Mol Cancer Res, 2014. **12**(12): p. 1807-17.

313. Zhao, Q., Kun, D., Hong, B., Deng, X., Guo, S., Tang, X., Yang, Y., Gong, K., Li, Q., Ye, L., Jiang, W.G., and Zhang, N. *Identification of Novel Proteins Interacting with Vascular Endothelial Growth Inhibitor 174 in Renal Cell Carcinoma.* Anticancer Res, 2017. **37**(8): p. 4379-4388.

314. Li, J., Wei, K., Yu, H., Jin, D., Wang, G., and Yu, B. *Prognostic Value of Ezrin in Various Cancers: A Systematic Review and Updated Meta-analysis.* Sci Rep, 2015. **5**: p. 17903.

315. Altobelli, E., Marzioni, D., Lattanzi, A., and Angeletti, P.M. *HtrA1: Its future potential as a novel biomarker for cancer.* Oncol Rep, 2015. **34**(2): p. 555-66.

316. Minamida, S., Iwamura, M., Kodera, Y., Kawashima, Y., Ikeda, M., Okusa, H., Fujita, T., Maeda, T., and Baba, S. *Profilin 1 overexpression in renal cell carcinoma.* Int J Urol, 2011. **18**(1): p. 63-71.

317. Gastl, G., Ebert, T., Finstad, C.L., Sheinfeld, J., Gomahr, A., Aulitzky, W., and Bander, N.H. *Major histocompatibility complex class I and class II expression in renal cell carcinoma and modulation by interferon gamma.* J Urol, 1996. **155**(1): p. 361-7.

318. Kreiter, S., Vormehr, M., van de Roemer, N., Diken, M., Lower, M., Diekmann, J., Boegel, S., Schrors, B., Vascotto, F., Castle, J.C., Tadmor, A.D., Schoenberger, S.P., Huber, C., Tureci, O., and Sahin, U. *Mutant MHC class II epitopes drive therapeutic immune responses to cancer.* Nature, 2015. **520**(7549): p. 692-6.

319. Haabeth, O.A., Lorvik, K.B., Hammarstrom, C., Donaldson, I.M., Haraldsen, G., Bogen, B., and Corthay, A. *Inflammation driven by tumour-specific Th1 cells protects against B-cell cancer.* Nat Commun, 2011. **2**: p. 240.

320. Takeuchi, A. and Saito, T. *CD4 CTL, a Cytotoxic Subset of CD4(+) T Cells, Their Differentiation and Function.* Front Immunol, 2017. **8**: p. 194.

321. Braumüller, H., Wieder, T., Brenner, E., Assmann, S., Hahn, M., Alkhaled, M., Schilbach, K., Essmann, F., Kneilling, M., Griessinger, C., Ranta, F., Ullrich, S., Mocikat, R., Braungart, K., Mehra, T., Fehrenbacher, B., Berdel, J., Niessner, H., Meier, F., van den Broek, M., Haring, H.U., Handgretinger, R., Quintanilla-Martinez, L., Fend, F., Pesic, M., Bauer, J., Zender, L., Schaller, M., Schulze-Osthoff, K., and Röcken, M. *T-helper-1-cell cytokines drive cancer into senescence.* Nature, 2013. **494**(7437): p. 361-5.

322. Chen, X., Wei, S., Ji, Y., Guo, X., and Yang, F. *Quantitative proteomics using SILAC: Principles, applications, and developments.* Proteomics, 2015. **15**(18): p. 3175-92.

Danksagung

Ich danke…

…Prof. Dr. Stefan Stevanović für die Aufnahme in seine Arbeitsgruppe, die ausgezeichnete Betreuung während der Doktorarbeit und die gute und angenehme Atmosphäre, die in seiner Arbeitsgruppe immer herrschte.

…Prof. Dr. Hans-Georg Rammensee für die einzigartige Abteilung für Immunologie, die es ohne ihn nicht gäbe. Die Elche bieten ein familiäres Arbeitsumfeld und nehmen jeden neuen Kollegen herzlich auf.

…Jörg Hennelotter und Arnulf Stenzl, die die Gewebeproben für diese Arbeit zur Verfügung gestellt haben.

…Patricia, Nicole, Beate, Claudia, Franziska und Salman, die die Abteilung am Laufen halten und allen die Arbeit ungemein erleichtern.

…den Jungs aus dem MS-Büro, Daniel, Nico und Heiko, für die stets gute Stimmung.

…Chris, CC, Thomas, Christina, Janet, Steffi, Marlene, Moni, Mathias, Markus, Benni, Ralf, die besten Kollegen (und Freunde) die man sich wünschen kann.

…allen anderen Elchen für das tolle Arbeitsklima in der Abteilung.

…Lea, die mich immer unterstützt und an meiner Seite steht.

…meiner Familie, besonders meinen Eltern für die Unterstützung während Studium und Doktorarbeit.